Functional analysis of conserved microRNAs in *Arabidopsis thaliana*

Yanjiao Li

April 2015

A thesis submitted for the degree of Doctor of Philosophy of

The Australian National University

Statement of Authorship

The research carried out in this thesis was conducted at The Australian National University (ANU) between April 2011 and April 2015. I declare that I am the sole author of this thesis, and I have fully acknowledged and referenced the ideas and the work of others, whether published or unpublished in my thesis. My thesis does not contain work extracted from a thesis, dissertation or research paper previously presented for another degree or diploma at this or any other university, except for the data presented in section 3.2.2 and 3.2.5, which was extracted from the thesis for the degree of Masters of Biotechnology (Honours, ANU), and the work presented in section 4.2.2 and 4.2.3 was performed with the help of Rob Allen.

Yanjiao Li

Acknowledgements

Since the first day I came to ANU on 11 February 2009, I've been deeply impressed by not only the awesome study environment, but also the amicable smile on everyone's face, which truly made me feel at home. After conducting a two-year study for Master of Biotechnology, I started my PhD in 2011. Pursuing this PhD has been a life-changing experience for me, and completion of this thesis represents a milestone in my full six-year journey at ANU, which would not have been possible without the support and guidance that I received from many genuine caring people. I would like to express my sincere gratitude to them.

First of all, I am extremely grateful to my supervisor Dr. Tony Millar, for providing me opportunity to do the PhD program under his guidance and to learn from his research expertise. In fact, it was a big surprise for me to receive the IPRS scholarship as I know how competitive it could be to get that, but what really moved me is how excited Tony were when he knew the panel's decision, his strong faith in me is one of the major motivations I remain committed to this long and tough PhD life. From him, I learned how to think logically and critically, how to present in a concise yet attractive manner. Because of his encouragement, I took the job as a casual demonstrator in the teaching lab and attended several international conferences, both of which enriched me in many ways. Whenever I had doubts, Tony always made himself available for a discussion. When I became too serious or frustrated, his humour and friendly sarcasm always allowed me to laugh and fired me up. Like my labmate Mary said, his caring and positive personality set an example of a great man besides an excellent scientist, I cannot agree more! I'd also like to give a heartfelt thanks to my co-supervisor Dr.

Ming-bo Wang. His wisdom and passion for science, especially the miRNA biology, impressed me immediately the first time we met, and his flexibility in scheduling, valuable advice and constant encouragement made the impetus for me throughout these years. Also, a big thank to my co-supervisor Dr. Iain Searle, for his support and suggestion whenever we had the chance to talk.

Next, my sincere thanks go to all the lab members, you are the ones proved me that the great team dynamic makes people feel good about coming to work. To start with, I would like to express my special thanks to Maria Alonso, the former postdoctoral fellow. She was one of the first friendly faces to greet me when I started as an honour student, and has been my mentor and friend ever since. She is such an organized, critical and lovely person, who has been tough on me as has been caring and supportive. Her patient guidance and unconditional support secured my ticket into the PhD journey, it was tremendous. Many thanks go to Rob Allen and Mary (Junyan) Li, the former PhD students who made the lab nothing short of fun and enjoyment. Their academic support and personal cheering are greatly appreciated. I've learned so much from both of them and will always be grateful for their friendship. Thanks to the fellow students Linda Lin, Marlene Reichel, Amber (Zihui) Zheng, Ira Deveson and Gigi Wong, they are the persons with many admirable qualities. We've laughed and cursed, travelled and played, planned and discussed together, I cherish all those warm and beautiful memories. Thank you to the visiting fellow Allan Lohe, for being always willing to help and give constructive suggestions, and also for the weird and funny plants he brought to us, which definitely changed our office into a more energizing and inspiring workplace. Lastly, I would like to thank the former technician Eric (Cheng) Sun and the summer

student Lucia Du, for not only helping with experiments and getting the lab so well-organized, but also keeping things light and me smiling.

My gratitude also extends to everyone who has ever helped, encouraged and befriended me. Thank you to Susan Cosetto, for clarifying all my doubts throughout the period of Master study, without you I would be totally lost and confused back then. Thank you to Spencer Whitney, for providing guidance of completing every milestone in my PhD years, and for giving the provoking questions on the panel meeting and annual student conferences, which allowed me to review my project from different angles. Thank you to Hector Rodriguez and Graham Hick, for keeping all the machines running smoothly in RSB, and cheering us up with many funny stories. Thank you to Erin Pugh, Gagan Bhardwaj and Panit Thamsongsana for their kind administrative help, I couldn't have completed all the required paperwork and sent it to the right place without them. Thank you to Peta Moisis and Yiming Li from teaching lab for providing the research support throughout these years. I would also like to thank everyone from Barry Pogson's lab, your guys are the excellent neighbours who are willing to help or lend equipment to me all the time. Thank you to Nazia Nisar and Diep Ganguly for sparing us the growth chambers to perform stress tests. Thank you to Kai Chan and Su Yin Phua for teaching me how to use the Lemna Tec Scanalyzer for plant screening and phenotyping. Thank you to the bioinformatics expert Riyan Cheng, for teaching me to do statistical analysis of my messy data. Thank you to Postdoctoral fellows Deyun Qiu and Weihua Chen, for sharing your experience on choosing a career path. My heartfelt thanks also go to several other friends, Yikai Lai, Jackie (Yi) Huang, Wil (Wei) Hee, Jiahui Du, Jing Gao, Haiyi Yu, Alice Burgess, Ashley Jones, for being around, inspiring

and understanding, my life would not have so much fun without all your companions and caring.

Lastly, I'd like to give special thanks to my parents, who encouraged and helped me at every stage of my personal and academic life. They've taught me about hard work, self-respect, and persistence. Thank you for boosting my self-confidence with your unconditional love. Through your eyes I've seen myself as a capable, intelligent girl who could do anything once I made up my mind, which was really important for me in these oversea years. Thank you for being my biggest fans, and always expressing how proud you are of me and how much you love me. Here, I'd like to say, Dad and Mum, I am proud of you too and love you for ever. Thank you with all my heart and soul!

Publications and Presentations

Li, J., Reichel, M., **Li, Y.** & Millar, A. A. (2014). The functional scope of plant microRNA-mediated silencing. *Trends Plant Sci* **19**, 750–6.

Reichel, M. *, **Li, Y.** *, Li, J. & Millar, A. A. (2015). Inhibiting plant microRNA activity: molecular SPONGEs, Target Mimics and STTMs all display variable efficacies against target microRNAs. *Plant Biotechnol J* **13**, 915-26..

Li, Y., Allen, R. S. & Millar, A. A. An EMS-based revertant screen to elucidate the function of miR159 in *Arabidopsis*. 24th International Conference on *Arabidopsis* Research (ICAR); Sydney Convention and Exhibition Centre Australia, 24th – 28th June 2013 (Poster/Abstract)

Li, Y., Alonso-Peral, M. M. & Millar, A. A. Functional analysis of the miR159-*MYB* module in the *Arabidopsis* rosette. CSHL Meeting: Regulatory & Non-coding RNAs, Cold Spring Harbor Laboratory USA, 26th–30th August 2014 (Poster/Abstract)

*: Those authors contributed the same to the work.

Abstract

MicroRNAs (miRNAs) are non-coding RNAs of approximately 21 nucleotides that negatively regulate gene expression. In plants, many miRNAs target key regulatory genes, such as transcription factors, which play critical roles in plant developmental processes and stress responses. Underscoring their importance, many of these miRNA-target relationships are highly conserved, such as the miR159-*MYB* regulatory module that appears present in all land plants. This regulatory relationship has been extensively studied in *Arabidopsis*. In seeds and flowers, where miR159 activity is weak, MYB activity promotes programmed cell death (PCD), facilitating seed germination and anther development respectively. Moreover, the generation of a loss-of-function *mir159* mutant has been shown to result in pleiotropic vegetative defects (e.g. curled/rounded leaves and stunted growth), indicating a critical role of miR159 in controlling rosette development. However, what the functional role of this regulatory module in rosettes remains unknown.

Via transcript analysis, I found that miR159 was strongly and ubiquitously expressed throughout the rosette development, where it appeared to constitutively silence *MYB* activity, suggesting the miR159-*MYB* module is not developmentally responsive. However, constant miR159 activity is required for normal rosette growth, as an inducible inhibition of miR159 resulted in morphological abnormalities of the rosette. This led to the hypothesis that miR159 could be stress responsive, where if repressed under a particular condition this would enable MYB expression. However, under what environmental condition this occurs remains unclear, because miR159 silencing was found to be extremely robust: neither biotic stresses known to inhibit miRNA activity (a

virus containing a silencing suppressor), nor a range of abiotic stresses was able to inhibit miR159 function sufficiently to activate MYB-related phenotypic defects.

As a complementary approach to gain insights into the function of the *MYB33/65* pathway, an ethyl methanesulfonate (EMS) mutagenesis screen of *mir159* suppressor was undertaken. Interestingly, a high frequency of *mir159* revertants was obtained, in which *MYB* expression was attenuated, suggesting the existence of multiple regulators of MYB expression, and that possibly the miR159-*MYB* module is extensively networked. The eventual identification of these repressor alleles may shed light on function of the miR159-*MYB* module in rosettes.

Owing to the fact that most miRNAs belong to multigene families, to which traditional loss-of-function approaches cannot be applied due to genetic redundancy, the transgenic approach of using miRNA "*SPONGE*s (*SP*s)" was explored to determine their ability in generating loss-of-function *mirna* outcomes. *SP*s are transgenes that harbor multiple target sites complementary to miRNAs, leading to their sequestration, an approach that has been effective in animal systems, but not tested in plants. Here, ten miRNA *SP*s were designed to target different conserved plant miRNA families. Their efficacies in inhibiting the respective miRNAs varied dramatically, where some *SP*s induced a strong loss-of-function outcome, whereas others did not. What underpins this variability is unclear; neither *SP* expression level, the free energy (ΔG) of the miRNA-*SP* interaction or the predicted target accessibility correlated with inhibition efficacies. This likely highlights the complexity of miRNA-target interactions and that when a *SP* cannot induce any obvious phenotypic impact, alternative approaches will be required.

Abbreviations

The following abbreviations have been used throughout this thesis.

Abbreviation	Definition
ABA	Abscisic acid
BC	Backcrossing
BSS	Bacterial silencing suppressor
bp	Base pair
CaMV	Cauliflower Mosaic Virus
DNA	Deoxyribonucleic acid
dNTP	Deoxynucleoside triphosphate
dsRNA	Double stranded RNA
EMS	Ethyl methanesulfonate
GA	Gibberellin
GUS	β-glucuronidase
h	Hour(s)
kb	Kilobase-pair
LB	Luria Broth
LNA	Lock-nucleic acid
min	Minute(s)
MIR	MIRNA gene
miRNA	microRNA
mRNA	Messenger RNA
nt	Nucleotide
PCD	Programmed cell death
PCR	Polymerase chain reaction
Pre-miRNA	MIRNA precursor transcript
Pri-miRNA	Primary MIRNA transcript
qRT-PCR	Quantitative real time polymerase chain reaction
Pst	Pseudomonas syringae pv. tomato
RACE	Rapid amplification of cDNA ends
RISC	RNA-induced silencing complex
RNA	Ribonucleic acid
RNAi	RNA interference
RNase	Ribonuclease
RT primer	Reverse transcription primer
RT-PCR	Reverse transcriptase polymerase chain reaction
SAM	Shoot apical meristem
SD	Standard Deviation

The following abbreviations have been used throughout this thesis.

Abbreviation	Definition
SDN	SMALL RNA DEGRADING NUCLEASE
sec	Second(s)
SEM	Standard Error of the Mean
siRNA	Small interfering RNA
SNP	Single Nucleotide Polymorphism
SOLiD sequencing	Sequencing by Oligonucleotide Ligation and Detection
sRNA	Small RNA
STTM	Short Tandem Target Mimic
ta-siRNAs	Trans-acting siRNAs
T-DNA	Transferred DNA
TF	Transcription factor
TuMV	Turnip Mosaic Virus
vsiRNA	Virus-derived small interfering RNA
VSS	Viral silencing suppressor
X-gluc	5-bromo-4-chloro-3-indoyl-β-D-glucuronic acid

Table of Contents

Chapter 1

Introduction

1.1 Discovery and conservation of plant miRNAs

1.1.1 Plant miRNA discovery: a new area for investigating plant regulatory systems

MicroRNAs (miRNAs), categorized as a class of regulatory RNA molecules of approximately 21-nucleotides (nts) in length, were first discovered to mediate the juvenile-to-adult transition in *Caenorhabditis elegans* (Lee et al., 1993). Namely, the founding members, *lin-4* and *let-7*, were identified to express late in larval development, repressing the expression of genes mediating the juvenile traits, and therefore promoting adult development (Lee et al., 1993; Reinhart et al., 2000; Pasquinelli and Ruvkun, 2002). Since then, through intensive small RNA (sRNA) profiling, miRNAs have been found to be ubiquitously present in higher eukaryotes (reviewed in Bartel et al., 2004; Xiu-JieWang et al., 2004). Their main function is to mediate the repression of gene expression, via the down-regulation of target mRNAs through specific base-pairing interactions (Pasquinelli and Ruvkun, 2002; Abrahante et al., 2003; Lin et al., 2003). Such miRNA-target interactions have been shown to be involved in a broad range of biological processes, involving development, senescence, metabolism, disease and stress response (Bartel et al., 2004; Voinnet, 2011; Wong et al., 2011), which have revolutionized our understanding of gene regulation in eukaryotes.

The field of plant miRNA discovery started from identifying conserved miRNAs that were present across a diverse range of angiosperms and often represented by multiple loci in sequenced genomes (reviewed by Axtell and Bowman, 2008). Soon after, the number of miRNA sequences discovered in various plant species rapidly increased, mainly driven by the development of high-throughput sRNA sequencing techniques, as well as the completion of whole-genome sequences for more plant species (Nobuta et al., 2010). Besides that, miRNA microarray analysis, a rapid method for detecting and

profiling a large number of miRNAs, had also been successfully applied in *Arabidopsis thaliana*, *Oryza sativa*, *Brassica napus*, *Solanum lycopersicum*, and *Medicago truncatula* (Buhtz et al., 2008; Liu et al., 2008; Meng et al., 2009; Lang et al., 2011; Zhou et al., 2012). Meanwhile, based on the finding that plant miRNAs and their targets frequently show near-perfect complementarity (Rhoades et al., 2002), the computational prediction of miRNA targets by scanning the genomic or cDNA sequences for high complementarity to a potential miRNA was also developed (Rhoades et al., 2002). Since these *in silico* predicted targets are required to be validated, predicted miRNA targets were experimentally verified via combining a modified 5'-rapid amplification of cDNA ends (RACE) with high-throughput deep sequencing and bioinformatic analysis (German et al., 2008). This globally verified miRNA-target RNA pairs in *Arabidopsis thaliana* (German et al., 2008), and has now been applied to many other plant species: *Oryza sativa*, *Physcomitrella patens*, *Glycine max* and *Zea mays* (Addo-Quaye et al., 2009; Li et al., 2010; Song et al., 2011; Zhao et al., 2012). Together, there are now >1000 registered plant miRNAs in miRBase (http://www.mirbase.org/), the most widely used database for miRNA genomics (Meyers et al., 2008; Ivashuta et al., 2011; Meng et al., 2012), and these miRNAs are predicted to regulate hundreds of genes that involve diverse aspects of plant biology, such as development (Baker et al., 2005), metabolism (Bonnet et al., 2004), hormone signaling (Liu et al., 2007) and biotic and abiotic stress responses (Shukla et al., 2008; Kozomara and Griffiths-jones, 2014). As a result, this tremendous miRNA-target resource provides a great opportunity to understand the miRNA regulatory layer underlying plant development and/or the response to a wide range of environmental stimuli and stresses, making the functional analysis of these miRNA-target pathways a rapidly growing interest of current plant science.

1.1.2 Plant miRNA conservation: an indication of the critical roles plant miRNAs play in development

To date, *Arabidopsis thaliana* has been the most widely used plant for miRNA studies. According to the miRBase (Release 21, http://www.mirbase.org/), there are more than 400 miRNAs that have been predicted and cloned from *Arabidopsis*. This number continues to increase with advances in sRNA deep-sequencing analysis (Rajagopalan et al., 2014), identifying a large pool of miRNAs that potentially play many roles in the plant. It appears that many miRNAs in *Arabidopsis* correspond to single young genes that have arisen from recent evolutionary processes (Rajagopalan et al., 2006; Fahlgren et al., 2007; Fahlgren et al., 2010; Ma et al., 2010), in which miRNAs are thought to be frequently spawned and then mostly lost (Fahlgren et al., 2007). Consistent with this, most of these young miRNAs are non-conserved, having no identifiable orthologues in other plant species (Rajagopalan et al., 2006). Interestingly, a high proportion of these non-conserved miRNAs do not have any identifiable target genes, hence they do not appear to be in clearly identifiable plant regulatory networks (Axtell, 2008; Fahlgren et al., 2007). Furthermore, when Todesco et al. (2010) applied miRNA *Target Mimic*ry to knockdown the activities of 71 different *Arabidopsis* miRNA families, none of the recently evolved miRNAs were found to have any impact on plant growth. This suggests that either they affect processes other than development (e.g. adaptation to a certain abiotic or biotic stress), or potentially have no discernible function at all. Thus, it is still unclear whether these recently evolved miRNAs have a relevant biological function (Axtell, 2008; Todesco et al., 2010)

In contrast to the single young miRNAs, many other miRNAs belong to families of related genes. They appear to be ancient, being present in all land plants with

conservation extending even to mosses (> 400 million years; Bartel, 2004; Floyd and Bowman 2004; Arazi et al. 2005; Axtell, 2008). For example, Fahlgren et al. (2007) had found 22 and 20 *Arabidopsis* miRNA families being conserved in Poplar and Rice respectively, among which several miRNA families (e.g. miR159 and miR390) were also identified in mosses (Arazi et al. 2005; Axtell and Bartel, 2005; Li et al., 2011). Thereby, these miRNA families appear to have become fixed early on during evolution, acquired an indispensable role in plant development (Rajagopalan et al., 2006; Fahlgren et al., 2007). Supporting this, at least 21 miRNA families in *Arabidopsis*, have been predicted or demonstrated to target genes encoding transcription factors required in specific developmental processes, including organ polarity determination, meristem formation, floral patterning, vascular development, lateral root development and hormone response (Baulcombe, 2004; Chen, 2005; Mallory and Vaucheret, 2006; Ha et al., 2008). The functional analysis of these miRNA-target interactions has underpinned the interest in miRNA biology in plants.

1.2 miRNA biogenesis and action

Such a critical role for miRNAs in plant development was first alluded to from mutations in genes encoding the machinery that is required for miRNA biogenesis and action (Vaucheret et al., 2004). This includes loss-of-function mutants in genes encoding the ribonuclease III DICERLIKE1(DCL1) (i.e. *dcl1-7*, *dcl1-8* and *dcl1-9*, Schauer et al. 2002), HUA ENHANCER1(HEN1) (i.e. *hen1-1* and *hen1-2*, Park et al. 2002), HASTY (HST, the orthologue of nucleocytoplasmic transport receptor exportin 5) (i.e. *hst-1*, Bollman et al., 2003) and ARGONAUTE1 (AGO1) (e.g. mutants carrying *ago1-null* or hypomorphic alleles, Bohmert et al. 1998; Fagard et al. 2000; Morel et al.2002; Vaucheret et al., 2004), all of which displayed pleiotropic developmental defects that

partially overlap with each other, highlighting the critical roles plant miRNAs play in development (Vaucheret et al., 2004).

Through the extensive analyses of above components, the plant miRNA biogenesis pathway has been well characterized. It is commonly accepted that the biogenesis of most of the conserved miRNAs are derived from a common pathway. In the nucleus, *MIRNA* genes (*MIR*s) are mostly transcribed by RNA polymerase II (Kurihara and Watanabe, 2004; Lee et al., 2004; Xie et al., 2005), to produce noncoding primary *MIRNA* transcripts (pri-miRNAs) of varying lengths (some extending up to 300 nts; Wang et al., 2004). These pri-miRNAs can then form into imperfect hairpin *MIRNA* precursors (pre-miRNA) and are subjected to further DCL1-mediated cleavage, generating 20-24 nt miRNA/miRNA* duplexes (Kurihara and Watanabe, 2004; Jones-Rhoades et al., 2006). After this nuclear processing, the resulting sRNA duplexes are 2'-O methylated at the 3' end of each strand by HEN1, and exported to the cytoplasm, probably via HST (Lund et al. 2004; Park et al., 2005; Yu et al., 2005). Finally, in the cytoplasm, the strand of the miRNA duplex that has the thermodynamically less stable 5′ end (the mature miRNA) is preferentially loaded into the AGO1 of the RNA-induced silencing complex (RISC), where the passenger miRNA strand (miRNA*) gets degraded (Hibio et al., 2012). However, the ARGONAUTE protein family comprises 10 members in *Arabidopsis* (Morel et al., 2002), and exceptions to the miRNA-AGO1 loading exist, such as AGO7 and AGO10 that show a preferential association with miR390 and miR165/166 respectively, achieving specific regulatory outcomes regarding plant development (Montgomery et al., 2008; Zhu et al., 2011).

Upon miRNA-AGO1 assembly, the miRNA guides the RISC complex to highly complementary mRNA targets, negatively regulating their expression. This was demonstrated by the overexpression of *MIR* precursor transcripts (pre-miRNA) in transgenic plants followed by transcript profiling: genes containing motifs of high sequence complementary, with perfect central matches (nt positions 10–11 relative to the 5' end of the miRNA sequence) were strongly repressed by a mechanism that included miRNA-mediated mRNA cleavage (Schwab et al., 2005; Jones-Rhoades et al., 2006). Such mRNA cleavage is catalyzed by the ribonucleolytic activity of the plant AGO1 protein, opposite nt 10 of the sRNA (Baumberger and Baulcombe 2005; Filipowicz, 2005; Kim, 2005), and the cleaved target mRNAs can be detected via 5' RACE analysis (Llave et al., 2002). To date, target mRNA cleavage has been accepted as one of the principal modes of plant miRNA action (Llave et al., 2002; Jones-Rhoades et al., 2006). Consistent with this, in strong loss-of-function *ago1 Arabidopsis* mutants, target mRNA levels strongly increase (Vaucheret et al., 2004; Baumberger and Baulcombe, 2005; Qi et al., 2005).

In addition to the cleavage-based miRNA regulation of target gene expression, miRNA-directed translational inhibition also occurs in plants. For example, the near-perfect complementarity of miR172 and its binding sequence in target *APETALA2* (*AP2*) mRNA supports both cleavage-based and translation-based miRNA inhibitory mechanisms. For the latter, it was shown that expression of a *35S::AP2* transgene and expression of a miR172-resistant *AP2* transgene (35S::*AP2m1*) displayed comparable *AP2* mRNA levels, however, only the latter plant displayed elevated AP2 protein level, indicating the occurrence of translational inhibition on *AP2* mRNA mediated by miR172 action (Chen, 2004). Then, in a viral-stress experiment, Va ŕallyay et al. (2010)

found that the virus-induced elevation of miR168 level was associated with an increased *AGO1* mRNA level but a reduced AGO1 protein level, indicating a miR168-mediated translational inhibition mechanism might also be responsible for AGO1 expression. Moreover, by analysing the *miRNA action deficient* (*mad*) *Arabidopsis* mutants, *mad1* to *mad6,* translational inhibition by miRNAs was suggested to be widespread in plants (Brodersen et al., 2008). Providing supporting biochemical evidence for this, many *Arabidopsis* miRNAs are found on polysomes in association with AGO1, suggesting the miRNA-AGO1 is potentially blocking the target mRNA translation (Lanet et al., 2009). Thus, many miRNAs may regulate their targets through a combination of cleavage-based and translation-based inhibitory mechanisms (Brodersen et al., 2008), whose respective prevalence is currently unknown.

The reversible nature of translational inhibition has been shown to occur in animal cells (Bhattacharyya et al., 2006), and it has been suggested that this mechanism may coordinate stress-responsive gene expression, enabling a rapid response and avoid the metabolic costs associated with new target mRNA synthesis when the stress dissipates (Brodersen et al., 2008). By comparison, miRNA cleavage will likely result in irreversible target degradation, and such a mechanism may play crucial roles in plant development when transcripts need to be cleared to enable cellular differentiation (Vionnet, 2009). Supporting this, several *ago1* hypomorphic mutants exhibit compromised cleavage activity and consequent developmental defects regarding to plant stature, leaf shape, and flower phenotypes (Vaucheret et al., 2004). However, whether these *ago1* mutants also become hypersensitive to environmental stresses has not been addressed.

Finally, with respect to the miRNA turnover, several exonucleases have been suggested to participate in miRNA degradation, such as SMALL RNA DEGRADING NUCLEASE (SDN), a family of 3' to 5' exonucleases that have been shown to degrade 3' methylated miRNAs in *Arabidopsis* (Ramachandran and Chen, 2008). Besides this, nucleotidyl transferases, such as URT1 and HEN1 SUPPRESSOR1 (HESO1) have been found to uridylate AGO1-bound miRNAs *in vitro* (Allen et al., 2005, Mullen and Marzluff, 2008). Hence, it is suggested that AGO1 probably recruits HESO1 and URT1 to ensure the degradation of damaged or even intact miRNAs that need to be eliminated (Mullen and Marzluff, 2008). However, since AGO1 presumably protects both ends of a miRNA from degradation by making the ends inaccessible to nucleases (Shen and Goodman, 2004), and the activities of HESO1 and URT1 can be completely inhibited by 3'methylation on the substrate miRNA (Allen et al., 2005; Qi et al., 2006; Vaucheret 2006), the degradation mechanism regarding AGO1-loaded 3' methlylated miRNAs remains unclear. For this, the recent discovery that the expression of "*Target Mimics*" leads to the degradation of miRNAs in *Arabidopsis* may provide a plausible explanation (see section 1.4 for details).

1.3 Features of miRNA target genes in plants

As determined by both bioinformatics prediction and experimental verification, most plant miRNA targets are found to carry a single miRNA-complementary motif in the coding region with few or no mismatches (Rhoades et al., 2002; Rajewsky and Socci, 2004; Wang et al., 2004; Schwab et al., 2005). It is distinctly different from the scenario in animal systems, where most miRNAs mainly base-pair with their mRNA targets via a sequence between 2-8 nucleotides of 5′ ends of miRNAs (Lewis et al., 2005), while the additional complementarity is not nesesary, eventhough the interaction between 9-20

nucleotides of the miRNA and its targets is also required (Tóreault and De Guire, 2013). This difference of complementarity requirement is probably the cause of different regulation outcomes, namely a single animal miRNA usually simultaneously inhibit the expression of hundreds of different mRNAs (Lim et al., 2005; Selbach et al., 2008; Baek et al., 2008), while the target number of a plant miRNA is at least an order of magnitude lower (Schwab et al., 2005, Jones-Rhoades et al., 2006; Palatnik et al., 2007).

In support of the high complementarity between plant miRNAs and their cognate targets, Rhoades et al. (2002) performed a conservation analysis of miRNA target sites in two distantly related species, *Arabidopsis* and rice, and found that high complementarity between miRNAs and their targets was a conserved feature among different plant species. More specifically, the complementarity requirement adopted by most, if not all the prediction methods, is that a potential target site carries no more than 3.5 mismatches (counting G:U pairs as 0.5 mismatches; Jones-Rhoades and Bartel, 2004) to the corresponding miRNA (Aukerman and Sakai, 2003; Xie et al., 2003; Achard et al., 2004; Chen, 2004; Laufs et al., 2004; Vaucheret et al., 2004). Then, Schwab et al. (2005) defined the empirical parameters of plant miRNA recognition of target genes via the overexpression of different miRNAs in transgenic *Arabidopsis*, followed by transcript profiling. Namely, relative to the 5' end of the miRNA sequence, most genuine target mRNAs have long stretches of perfectly matching nucleotides, with no mismatch at positions 10 and 11, no more than one mismatch at positions 2–12, and no more than two consecutive mismatches downstream of position 13 (Schwab et al., 2005). These findings defined the requirement of high complementarity in plant miRNA-target interactions, underpinning the notion of a much narrower and more specific target range

in plants than in animals (Schwab et al., 2005; Jones-Rhoades et al., 2006). Additionally, Schwab et al. (2005) found that a preferential (low) free energy cost of miRNA-target hybridization is required for strong plant miRNA-target interaction, namely at least 72% of free energy compared to a perfectly complementary target should be satisfied.

Finally, underscoring the roles plant miRNAs have in regulatory networks, many known miRNA targets were predicted and/or experimentally verified as transcription factors, which coordinate crucial steps during plant development (Rhoades et al., 2002; Jones-Rhoades and Bartel, 2004; Jones-Rhoades et al., 2006; Chen et al., 2010). In *Arabidopsis*, it has been suggested that more than half of the known conserved miRNA targets genes encoding transcription factors (TF, Jones-Rhoades et al., 2006), where each plant miRNA family targets a single paralogous family of TF genes. For instance, targets of miR171 correspond to a small gene family encoding SCARECROW-like (SCL) TFs, involved in radial patterning of roots, as well as gibberellin and light signaling pathways (Ma et al., 2014); targets of miR396 correspond to a small gene family encoding GROWTH REGULATING FACTORs (GRFs) TFs, with a demonstrated role in controlling cell proliferation during leaf development (Jones-Rhoades et al., 2006; Rodriguez et al., 2010; Wang et al., 2011); targets of miR156 correspond to ten members of a gene family encoding SQUAMOSA PROMOTER BINDING PROTEIN LIKE (SPL) TFs, while targets of miR172 correspond to six members of a gene family encoding APETALA2-LIKE (AP2-like) TFs. In each case, functional redundancy between members within each TF family has been found, with the latter two target families displaying sequential actions in controlling the stability of juvenile and adult phases (Wu and Poethig, 2006; Guo et al., 2008; Wu et al., 2009). More examples can also be found in many good reviews (Chen,

2010; Nag and Jack 2010; Xie et al., 2010; Wang et al., 2011). These strongly support evolutionary studies that suggest these miRNA-regulated TFs have underpinned land plant development (Liu et al., 2014).

1.4 Additional regulatory layers, *MIMIC*s and possible feedback loops

Plant miRNA-target interactions have been shown to be modulated by subtle regulatory mechanisms. For instance, a functional non-coding RNAs with a non-cleavable miRNA binding site has been reported by Franco-Zorrilla et al. (2007). The non-protein coding gene *INDUCED BY PHOSPHATE STARVATION1* (*IPS1*) contains a motif with high sequence complementary to the phosphate (Pi) starvation-induced miR399, but a 3 nt mismatched bulge at the miR399 cleavage site prevents the miR399-guided cleavage of *IPS1* RNA. This results in fine tuning of miR399 levels that impact another target, *PHO2*, which encodes an E2 ubiquitin conjugase–related protein that negatively affects shoot Pi content and Pi remobilization, achieving precise control of Pi starvation response (Fujii et al., 2005; Aung et al., 2006; Franco-Zorrilla et al., 2007). This so-called "*Target Mimic*ry" phenomenon has been further investigated via genome-wide computational prediction methods and found to be potentially widespread, at least in *Arabidopsis* and rice (Meng et al., 2012), but currently *IPS1* is the only functionally determined target mimic. Interestingly, in *Arabidopsis* transformants expressing various artificial target *MIMICs* the levels of the cognate miRNAs were found to be reduced (Todesco et al., 2010; Ivashuta et al., 2011; Wu et al., 2013), suggesting that the expression of target *MIMIC*s might lead to miRNA degradation. Further investigation by Yan et al. (2012) found that SDN1 and SDN2 were required for the *MIMIC*-induced reduction of miRNA levels. This is in line with the hypothesis that recognition of target *MIMIC*s by plant miRISCs might dislodge miRNA 3' ends from the PAZ domain of the

AGO protein, rendering miRNAs susceptible to the 3’ truncation, which is mediated perhaps by SDN1, resulting in unmethylated miRNAs that are susceptible to 3’ tailing by nucleotidyl transferases (e.g. URT1 and HESO1) and their final degredation. (Sanei and Chen, 2015). Therefore, it is likely that the widespread “*Target Mimic*ry” phenomenon may be attributable to a regulatory layer of miRNA turnover at least in some plant species.

In addition, the feedback control of miRNA abundance via the miRNA target expression has been brought up. First, it is known that miR162 can regulate the expression of DCL1, which is the predominant miRNA Dicer that is required for most plant miRNAs (Xie et al., 2003); and that miR168 can regulate the expression of AGO1, which can protect and stabilize miRNAs from degradation in plants (Vaucheret et al., 2004; Vaucheret et al., 2006; Diederichs and Haber, 2007). Additionally, an *MIR* gene, miR838, has been found to be located in intron 14 of *DCL1*, which may limit DCL1 expression, as the processing of *DCL1* pre-mRNA to release pre-miR838 probably generates truncated transcripts that cannot give rise to *DCL1* mRNA and protein (Rajagopalan et al., 2006). Together, these findings strongly suggest that the biogenesis and fucntion of plant miRNAs are regulated at global levels by miR162-DCL1, miR168-AGO1, and possibly the miR838-DCL1 feedback loops.

More than that, complex feedback loops in which a miRNA target gene encodes a protein that in turn regulates the abundance of the corresponding miRNA have also been found in plants. For instance, miR172 abundance is reduced in the loss-of-function double mutant of its corresponding target, *TOE1/TOE2* [*APETALA2-LIKE* (*AP2*-like) transcription factors], while the abundance of miR156 is elevated in transgenic plants

overexpressing its target genes, *SPL3, SPL4* and *SPL5* (Wu et al., 2009). This indicates the abundance of some miRNAs are positively correlated to their target proteins, hence possible feedback loops may exist, where the miRNAs can regulate the expression of target genes, and the target proteins can in turn regulate the abundance of miRNAs. Supporting this notion, miR396 abundance was found significantly increased in the triple knockout mutant of its target *GRF1/GRF2/GRF3* (Hewezi and Baum, 2012). Similarly, the abundance of miR167 and miR160 were found to be negatively regulated by their respective target *ARF8* and *ARF17* (*AUXIN RESPONSE FACTORs*; Gutierrez et al., 2009), which suggests the possible negative regulation of miRNA abundance by their corresponding targets. Regarding to the importance of these possible feedback loops, Martinez et al. (2008) suggest that negative feedback loops buffer small changes in the expression of proteins with important regulatory functions. Such a concept may also be applicable to these possible miRNA-target feedback loops: namely through the feedback loop, a small change of target protein expression can trigger a corresponding change of miRNA abundance, adjusting the miRNA-regulation of the target expression, so that in turn the target protein is maintained at certain levels for desired biological outcome.

1.5 The role of miRNAs in plant development

As mentioned, since genetic screens for developmental defects identified many proteins required for miRNA biogenesis and functions, the role of miRNAs in controlling developmental processes has been a focus of plant miRNA biology (Lu and Federoff, 2000; McConnell et al., 2001; Park, et al., 2002; Schauer et al., 2002; Vaucheret et al., 2004; Lobbes et al., 2006; Sunkar et al., 2007). To investigate, gain-of-function experiments were performed by the overexpression of miRNAs or miRNA-resistant

transgenes (Palatnik et al., 2003; Achard et al., 2004; Chen, 2004; Wu et al., 2006; Wu et al., 2009; Rodriguez et al., 2010), or the loss-of-function *mirna* mutants were generated (Allen et al., 2007; Sieber et al., 2007; Nag et al., 2009). Such experiments resulted in varying developmental abnormalities, and have found that plant miRNAs are involved in developmental processes ranging from establishment of meristem identity, cell proliferation, to developmental timing and patterning, for which several excellent reviews provide a comprehensive description (Bartel, 2004; Dugas and Bartel, 2004; Kidner and Martienssen, 2005; Mallory and Vaucheret, 2006; Jones-Rhoades et al., 2006).

Complementing such functional analysis has been expression analysis. For instance, via using the *pMIR390b:GUS* transgene, the promoter activity of the *MIR390b* was monitored to investigate how miR390 abundance is regulated by auxin in *Arabidopsis* (Yoon et al., 2009). It was found that the GUS signal in the lateral root (LR) primordia of *pMIR390b:GUS* seedlings positively correlated with *DR5:GUS* expression in the *DR5:GUS* seedlings (DR5, an auxin-responsive synthetic promoter), implying expression of the *MIR390b* gene may correlate with a putative auxin gradient present in the LR primordium (Yoon et al., 2009). Hence this miR390 expression pattern supports the role of miR390 in lateral root development (Yoon et al., 2009; Marin et al., 2010). In other examples, using the lock-nucleic acid (LNA)-based *in situ* hybridization, *Arabidopsis* miR165/166 was found to accumulate at high levels in the abaxial domain and low levels in adaxial domain of cotyledons, and accumulate in the peripheral domain of hypocotyls in torpedo and subsequent stages (Liu et al., 2009). This observation implied an expression pattern of miR165/166 that supports its role in establishing the leaf polarity in *Arabidopsis* (Nogueira et al., 2006; Liu et al., 2009).

Also, LNA-based *in situ* hybridization of plant miRNAs performed by Vá óczi and colleagues (2006), revealed the presence of six conserved miRNAs in vascular bundles of developing organs, suggesting that miRNAs could be phloem-mobile and hence coordinating developmental processes. Taken together, both functional and expression analyses help to define the roles of miRNAs in plants.

1.6 The involvement of plant miRNAs in response to stresses

1.6.1 The involvement of plant miRNAs in response to abiotic stresses

In addition to development, plant miRNAs are also likely to play roles in stress response, given that stresses can alter their expression patterns, and targets of several miRNAs are stress-associated genes (reviewed in Sunkar et al., 2007; Sunkar et al., 2012). Additionally, functional analysis has found that several plant miRNAs might play vital roles in plant resistance to abiotic as well as biotic stresses (Fujii et al., 2005; Aung et al., 2006; Sunkar et al., 2006; Kawashima et al., 2011; Maunoury and Vaucheret 2011; Li et al., 2012c; Shivaprasad et al., 2012).

Firstly, as previously reviewed by Sunkar et al. (2007), abiotic stress conditions such as drought, cold, salinity, high light and heavy metals usually results in the accumulation of excess reactive oxygen species (ROS) in plant cells, which requires immediate scavenging, a process that is achieved through down-regulated miR398 under oxidative stress and consequent expression of its two target superoxide dismutase (*CSD1* and *CSD2*) genes (Sunkar et al. 2006). Other examples include miR399 (Fujii et al., 2005; Aung et al., 2006; Franco-Zorrilla et al., 2007) and miR395 (Jones-Rhoades and Bartel, 2004; Kawashima et al., 2011), that have been identified as potent regulators of inorganic phosphate and sulfur homeostasis respectively, hence were implicated to be

crucial for plant growth under low-nutrient conditions. Nevertheless, the evidence suggesting broader miRNA function in stress response continues to increase, such as an observation that plants overexpressing miR168a and the loss-of-function *ago1* mutant displayed hypersensitivity to abscisic acid (ABA) and drought tolerance, hence miRNAs were also suggested to play important and conserved roles in signal transduction during stress response (Li et al., 2012). Moreover, the recent discovery of miR319 induction during cold stress in sugarcane (Thiebaut et al., 2012) and miR408 induction during drought stress in *Medicago truncatula* (Trindade et al., 2010), also suggests that the role of these miRNAs in these abiotic stresses may be conserved in wide range of plant species. However, altered miRNA abundance in response to a stress is only the first step in determining whether that miRNA is important for the stress response. Functional evidence is required, ideally by demonstrating a loss-of-function *mirna* mutant can display an altered tolerance to the stress.

1.6.2 The involvement of plant miRNAs in response to biotic stresses

Next, the impact of viral stress on plant miRNA biogenesis/functions has also been found, which may suggest the possible involvement of plant miRNAs in response to biotic stresses. This is largely based on the discoveries about plant-virus interaction. On one hand, the plant RNAi mechanism plays a key role in antiviral defense: the DCL proteins generate virus-derived small interfering RNAs (vsiRNAs) upon viral infections, these vsiRNA can then direct the silencing of virus RNA through the similar biogenesis and action as that of miRNAs (Blevins et al., 2006; Fusaro et al., 2006). Supporting this, the AGO1 protein, has been found to bind vsiRNAs, and suggested to mediate cleavage of virus RNAs (Zhang et al., 2006); whereas the *ago1* mutants are found hyper-susceptible to viral infections, such as infections of *Cucumber Mosaic Virus*

(CMV; Morel et al., 2002), and *Turnip Crinkle Virus* (TCV; Qu et al., 2008). On the other hand, to counteract the plant RNAi defence, viruses have evolved viral silencing suppressor (VSS) proteins, to obstruct the biogenesis/action of vsiRNAs (Chapman et al., 2004; Voinnet, 2005). For example, the coat protein (P38) of TCV can inhibit DCL-mediated vsiRNA duplex processing through its RNA binding activity (Ding and Voinnet, 2007), and the Polerovirus F-box protein P0 can prevent the assembly of vsiRNA-containing RISC complexes and promote degradation of AGO1 effector (Bortolamiol et al., 2007; Csorba et al., 2010). Since plant miRNAs and vsiRNAs share common biogenesis steps at the cytoplasmic level and both mediate gene silencing through AGO1 protein, the VSS activities may inadvertently perturb plant miRNA functions. This was supported by the transgenic *Arabidopsis* overexpressing distinct types of VSSs: in many cases, the transgenic plants displayed morphological abnormalities resembling defects exhibited by hypomorphic miRNA mutants and alterations of miRNA/target levels had been identified in these VSS transgenic plants (Mallory et al., 2002; Dunoyer et al., 2004; Chapman et al., 2004; Chellappan et al., 2005a). However, no strong evidence has shown that the miRNA pathway is important for plant antiviral defence, as experiments over-expressing miRNAs or generation of loss-of-function *mirna* mutants have not found any phenotypic/molecular evidence suggesting that miRNAs strongly contribute to the antiviral response. Additionally, Jay et al. (2011) found that expression of three unrelated VSSs (i.e. Hc-Pro, P19 and P15) has comparable, yet modest effects on the mRNA levels of known miRNA targets. In contrast, only the up-regulated expression of the AUXIN RESPONSE FACTOR 8 (ARF8, a target of miR167) was identified a major trigger of the morphological abnormalities exhibited by VSS transgenic plants, but whether this is due to the VSS-disruption of miR167-mediated regulation of *ARF8* is unclear. Therefore, the

majority of conserved miRNAs do not appear to have strong contribution to the VSS-induced abnormalities

In addition, the antiviral role of the AGO2 protein was recently revealed by the reports showing that *ago2* mutants are hyper-susceptible to viral infections (Harvey et al., 2011), and a *Nicotiana benthamiana* AGO (NbAGO) with similarity to *Arabidopsis AGO2* is involved in antiviral defence through direct association with vsiRNAs in the case of *Tomato Bushy Stunt Virus* infection (TBSV; Scholthof et al., 2011). Due to the regulation of *AGO2* mRNA by miR403-AGO1 repression (Allen et al., 2005), multiple layers of *AGO1*/miRNA contributing to plant antiviral defence mechanism have been proposed. AGO1 represents a first layer to target the vsiRNAs, if this layer is overcome by viral effectors that can inhibit AGO1 function, a second layer involving AGO2 can take place to limit further virus accumulation, because the expression of AGO2 can then be released from miR403-AGO1 repression (Harvey et al., 2011). However no solid evidence has been shown for this hypothesis, thus to what extent is this conserved miR403 involved in the plant antiviral response requires further investigation. Perhaps by generating the loss-of-function *mir403 Arabidopsis* mutant, and analyzing if this mutant has enhanced AGO2 expression accompanied with enhanced resistance to several viral infections, the above hypothesis can be examined.

Besides viral stresses, bacterial infection may be another biotic stress that can influence the biogenesis and/or function of plant miRNAs. As supporting evidence, Navarro et al, (2006 & 2008) have found that the bacterial elicitor flg22 could trigger miR393 induction in *Arabidopsis* seedlings, and that effectors of *Pseudomonas syringae* pv. *tomato* (*Pst*) could suppress the transcriptional activation of some PAMP-responsive

miRNAs (i.e. miR393 and miR396) (PAMP: pathogen-associated molecular patterns), without affecting PAMP-insensitive miRNAs (e.g. miR166a and miR173). Following this, Zhang et al. (2011) performed deep-sequencing profiling on *Arabidopsis* infected by different strains of *Pst*, and identified more bacterial-responsive miRNA families, the targets of which are genes involved in plant hormone biosynthesis and signaling pathways, including auxin, abscisic acid, and jasmonic acid pathways. Hence, it has been suggested that there were bacterial silencing suppressor (BSS) that can interfere miRNA biogenesis and/or function in plants; and plant miRNAs may play a role in antibacterial defense. However, it has not been elucidated which step or effector of miRNA biogenesis/function does the BSS effect, thus the critical evidence for supporting the above suggestion is still missing,

1.7 Approaches for functional analysis of plant miRNAs

Many of the above hypotheses have been generated via the observation of alterations to miRNA abundances in response to particular stresses. However, the functional significance of these changes largely remains to be determined, as functional analysis of plant miRNAs is still problematic.

To elucidate the biological role of a plant miRNA family, theoretically the generation of loss-of-function *mirna* mutants should be the most precise and ideal approach. However, this is complicated by the presence of extensive miRNA redundancy in plants. Plant miRNA families frequently contain many related genes that can produce near-identical or identical mature miRNA members, many of which have overlapping expression domains, resulting in functional redundancy to buffer against the loss of any single miRNA locus (Nogueira et al., 2006; Sieber et al., 2007; Yan et al., 2012). Moreover,

MIR genes are small in size (Ma et al., 2010; Todesco et al., 2010), making the generations of loss-of-function alleles of *MIR* genes infrequent events, and to date only a few loss-of-function *mirna* mutants have been identified (Aukerman and Sakai, 2003; Palatnik et al., 2003; Guo et al., 2005; Kim et al., 2005; Williams et al., 2005; Allen et al., 2007; Sieber et al., 2007; Nag et al., 2009; Li et al., 2012). Hence, the generation and characterization of genetic mutants may not be easily put into practice.

To circumvent the potential complexity of plant miRNA redundancy, generation of gain-of-function *mirna* mutants (Palatnik et al., 2003) or transgenic plants overexpressing miRNAs (Schwab et al., 2005) has been utilized. Such experiments have indicated developmental roles for several miRNAs. For example, the generation of gain-of-function mutations for miR156, miR159, miR160, miR164, miR172, and miR319 lead to defects in vegetative and floral organ development, meristem function and flowering, suggesting their potential development roles (reviewed in Jones-Rhoades et al. 2006). However, these developmental defects induced by miRNA overexpression normally resembles the defects of knockout mutants of major miRNA target genes, which generally present the phenotypes that are the opposite of what is seen in plants with reduced miRNA activity (Todesco et al., 2010). Thus this approach may not accurately define the role of plant miRNAs.

Complementing such approaches is the transgenic method to express miRNA-resistant versions of the target gene(s). Here, a number of synonymous mutations are introduced into the miRNA binding sites of the target gene, resulting in a gene resistant to miRNA regulation, but coding for an identical protein to the wild-type gene. Hence, comparison of the miRNA-resistant target version to a wild-type target version will be able to define

the importance of miRNA regulation for this target gene. This approach has been widely used in functional analysis of the conserved miRNAs in *Arabidopsis* (Palatnik et al., 2003; Mallory et al., 2004a; Mallory et al, 2004b; Hunter et al., 2006; Wu et al., 2006; Nag et al., 2009; Wu et al., 2009; Hewezi and Baum, 2012), and in several instances the miRNA-resistant transgenes have caused morphological defects that are highly similar to the corresponding loss-of-function *mirna* phenotypes (Palatnik et al., 2003; Mallory et al., 2004a; Mallory et al., 2004b; Allen et al., 2007; Sieber et al., 2007).

However, this transgenic approach also has shortcomings. For instance, most of the conserved miRNAs appear to have multiple target genes that correspond to a single paralogous family (reviewed by Li et al., 2014). Such target genes of a miRNA family may potentially have similar functions in a particular tissue or biological process. Therefore, the expression of a single miRNA-resistant target may not reflect all the functions of a particular miRNA family. In addition, this transgenic method may result in the high expression, or mis-expression of the miRNA-resistant transgene due to position effect (Li and Millar, 2013). This misrepresentation of expression compared to the corresponding endogenous target, may lead to an exaggeration of the importance of miRNA-mediated target regulation (Li and Millar, 2013). Hence, to what extent the phenotypes conferred by expressing a miRNA-resistant target can reflect the functions of a plant miRNA family should always be questioned when using this method.

Perhaps a better approach for the functional analysis of plant miRNAs, is to generate a transgene that simultaneously inactivates all members of a plant miRNA family, so as to generate a loss-of-function *mirna* outcome. The generation of so called “miRNA decoys” was initially put into practice in plants with the discovery of ‘*Target Mimic*ry’ in *Arabidopsis* (Franco-Zorrilla et al., 2007). Here, the non-protein coding gene *IPS1*

was found to contains a sequence complementary to miR399, but with a central 3 nt bulge that is predicted to prevent miR399 cleavage, but rather resulting in the sequestration of miR399. Based on this *IPS1* gene, the miR399 binding site was altered with other 3 nt-bulged miRNA binding sites (*MIM*) so to sequester many other miRNA families and generate loss-of-function *mirna* phenotypes (termed *Target Mimic*, Todesco et al., 2010). Expression of these *Mimic* decoys could result in obvious morphological defects, demonstrating their potential application in generating loss-of-function *mirna* outcomes. However, since not all these *Mimic* transgenes could result in detectable morphological outcomes (Todesco et al., 2010), their efficacies in inhibiting different plant miRNAs should be questioned: whether the failure of a *Mimic* to confer any phenotypic defect is due to its incompetence in inhibiting the miRNA activity, or it is because the respective miRNA cannot make discernable contribution to the plant morphology? Moreover, some of these *Mimic* decoys were then demonstrated to confer only weak inhibitions of some miRNAs, when compared with a modified "*Short Tandem Target Mimic*" method (*STTM*; Yan et al., 2012). This *STTM* is designed to have two 3 nt-bulged *MIM* sites for miRNA sequestration, and linked by an AT-rich spacer with an optimal length of 48~88 nts (Yan et al., 2012). As the strong inhibition effects of *STTM* decoys were only demonstrated for three miRNAs in comparison with the original *Mimic* decoys (i.e. miR165/166, miR156/157, miR160; Yan et al., 2012), the inhibition effects of *STTM*s on many other miRNAs requires further investigations.

Taken together, it appeared that *Target Mimic* and *STTM* transgenes were designed with a similar principle: namely, insert one or two *MIM* target sites into certain backbones to sequester miRNAs from their endogenous targets. This may effectively inhibit the activities of some plant miRNA families, but apparently another transgenic method (or

miRNA decoy) is required to complement and verify the *Mimic* inhibitory effect. To realize that, in this thesis the miRNA *SPONGE* (*SP*), another miRNA decoy developed in mammalian cells to carry many targets sites with simple 4 nt linkers (Ebert et al., 2007, refer to chapter 5 for details), was investigated for its inhibition efficacies against different miRNAs in *Arabidopsis*. By doing this, the questions regarding if the *SP* approach could be widely used to efficiently inhibit different miRNAs in plants, and could it be an alternative to the currently used *Mimic* approaches would be addressed.

1.8 The *Arabidopsis* miR159-*MYB* pathway

1.8.1 miR159 regulation of *MYB33/65* in *Arabidopsis*

The miR159 family represents one of the most ancient miRNA families, being identified as one of only eight highly conserved miRNA families present in all embryophytes (Axtell and Bartel, 2005, Axtell and Bowman, 2008; Cuperus et al., 2011). In *Arabidopsis*, miR159 is consistently the most abundant miRNAs as determined by deep-sequencing analysis (Nakano et al., 2006; Rajagopalan et al., 2006; Kasschau et al., 2007). There are three distinct *MIR159* genes in *Arabidopsis*: *MIR159a*, *MIR159b*, and *MIR159c*, located in different regions of the genome and generate their respective mature 21-nt miR159a, miR159b and miR159c isoforms (Table1.1, Allen et al., 2010). As determined by both deep sequencing (Rajagopalan et al., 2006) and TaqMan miRNA quantitative assays (Allen et al., 2010), miR159a and miR159b are highly expressed compared with miR159c (Backman et al., 2007). Moreover, miR159a and miR159b only differ in sequence at one nucleotide, and were demonstrated to function redundantly in regulating gene expression, upon the observation that neither loss-of-function *mir159a* nor *mir159b* single mutants displayed a mutant phenotype, but

a *mir159ab* double mutant displayed pleiotropic development defects, such as curled/rounded leaves, stunted growth, and altered apical dominance (Figure 1.1 B, Allen et al., 2007). These defects indicated the critical role of miR159a/b in the control of plant development. By contrast, miR159c is expressed at an extremely low level, and currently no functional role has been identified, even though a comprehensive functional analysis on the *MIR159c* gene has been performed (Allen et al., 2010).

A

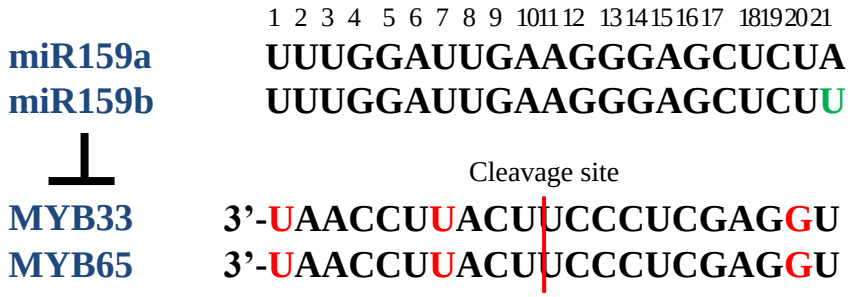

B

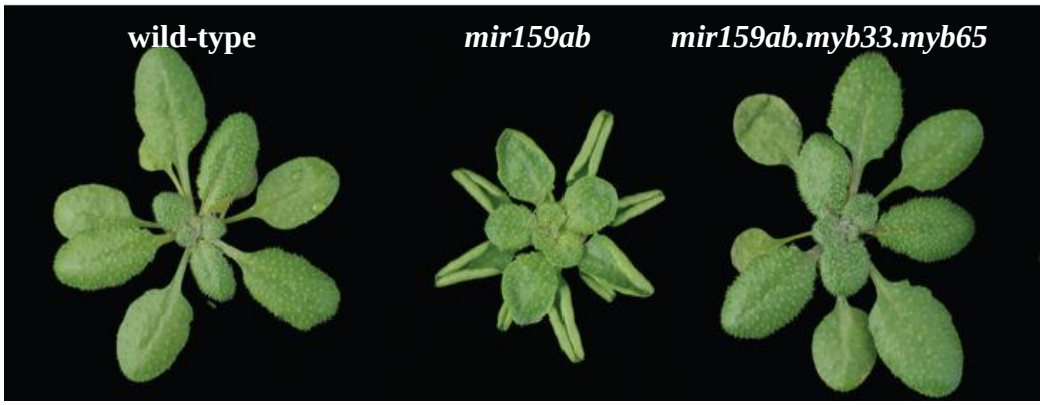

Figure 1.1: The miR159-*MYB* module appears as a genetic futile cycle in *Arabidopsis* rosettes. (Figure courtesy of Rob Allen et al., 2007) (A) Sequence alignment between miR159a, miR159b and their two redundant targets, *MYB33* and *MYB65*. The miR159b is different from miR159a at one nucleotide on the 3' end (green coloured). They redundantly target *MYB33* and *MYB65* mRNA through near-perfect sequence complementarity, the mismatches in target sites of *MYBs* transcripts are marked in red colour. The miR159-cleavage site in *MYB* mRNAs are indicated by red line. (B) Aerial views of rosettes of 5-week-old plants of wild-type, *mir159ab* double mutant, and *mir159ab.myb33.myb65* quadruple mutant.

Via bioinformatics and overexpression strategies, the *Arabidopsis* miR159 family has been predicted to regulate 20 potential target genes, seven of which belong to the *GAMYB*-like family of transcription factors (Table 1.1, Allen et al., 2010). Supporting this, miR159-mediated regulation of five of these *GAMYB-like* members have been validated by 5'-RACE (i.e. *MYB33*/*65*/*101*/*120*/*81*) (Allen et al., 2010). However, in a loss-of-function *mir159ab*, the *MYB33* and *MYB65* were the only two de-regulated targets as judged by increases in their mRNA levels (Allen et al., 2007; Alonso-Peral et al., 2010). This specificity is likely due to the finding that many of the other targets have mutually exclusive transcriptional domains when compared to that of *MIR159a* and*MIR159b* (Allen et al., 2007; Allen et al., 2010). More specifically, using the *MIR159a*:*GUS* and *MIR159b*:*GUS* reporter genes, the *MIR159a* and *MIR159b* were found ubiquitously expressed but were absent in anthers (Allen et al., 2007); such an expression domain strongly overlaps with the broad transcriptional domain of *MYB33* and *MYB65* (Zimmermann et al., 2004; Millar and Gubler, 2005; Zhang et al., 2009), whereas the other potential targets were found to be transcribed predominantly in anthers/pollens, and hence appeared to be spatially excluded from miR159 regulation (Allen et al., 2007; Slotkin et al., 2009; Allen et al., 2010). Additionally, the miR319 family, another conserved miRNA family closely related in sequence to the miR159 family, has been identified with the ability to regulate *MYB33/MYB65* as well, but due to the expression of miR319 being much lower than that of miR159 in vegetative tissues, miR319 regulation of the *MYB33/65* genes does not make a significant impact on MYB33/65 expression (Palatnik et al., 2007). In further support of this specific miR159a/b-*MYB33/65* regulatory relationship, introducing loss-of-function *myb33/myb65* alleles in *mir159ab* resulted in suppression of all *mir159ab* vegetative defects, as illustrated by a quadruple *mir159ab/myb33/myb65* mutant (Figure 1.1, Allen

et al., 2007). This genetic suppression strongly implies that miR159a/b are functionally specific for only two targets in rosette tissues, *MYB33* and *MYB65*.

Target	At Ident	Sequence vs miR159 (a) AUCUCGAGGGAAGUUAGGUUU (b) UUCUCGAGGGAAGUUAGGUUU (c) UCCUCGAGGGAAGUUAGGUUU	Prediction/ Validation	Anther/ pollen prevalent?
MYB33	At5g06100	UGGAGCUCCCUUCAUUCCAAU	P/M/H/R[d]/D[a-c]	Y
MYB65	At3g11440	UGGAGCUCCCUUCAUUCCAAU	P/M/H/R[d]/D[a-c]	Y
MYB101	At2g32460	UAGAGCUUCCUUCAAACCAAA	P/M/H/R[e-g, 29]/OE[h]	Y
MYB104	At2g26950	UGGAGCUCCCUUCAUUCCAAG	P/M/H	Y
MYB97	At4g26930	AUGAGCUCUCUUCAAACCAAA	P/M/H	Y
MYB120	At5g55020	AGCAGCUCCCUUCAAGCCAAA	P/M/H/OE[h]	Y
MYB81	At2g26960	UCGAGUUCCCUUCAUUCCAAU	M/H	Y
DUO1(MYB125)	At3g60460	UGGAGCUCCAUUCGAUCCAAA	P/M/R[e,g]	Y
TCP2	At4g18390	AGGGGGACCCUUCAGUCCAAU	M(159c)	N
ACS8	At4g37770	UCGAGUUUCUUUCAAUCCAAA	P/M/R[g]/OE[h]	N
OPT1	At5g55930	UAGAGCUUUCUUCAUUCCAAC	M/H/R/OE[h]	Y
Zinc/Cu SODM	At5g18100	UGGACCUCACUUCAAUCCAUU	D[c]	N
MRG1	At2g34010	UAGAGCCCCCUUCAAACCAAA	P/H/R[g]/D[c]	n/a
MRG-similar	At1g29010	UAGAGCCUCCUUCAAGCCAAA	P/M	n/a
PHD(ATX3)	At3g61740	UAGAGCUCUCUUAAGUCUAAA	P/M	Y
Anion/ExProt	At3g06450	AAGAGCUCCGUUCAGUCCACG	M	N
NPH3 Prot	At5g17580	AAAAGCUUCCUACGAUCCAAG	M(159b)	N
NAS2	At5g56080	UAGAGCUUUCUUGUAUCCAAU	M	N
SPL	At4g27330	U AUGAGCUCUCUUCAAUCCAAA	H	Y
PPDK	At4g15530	G AAGAGUUUCCUUCAAUCCAAA	P	Y

Table 1.1: miR159 targets predicted by bioinformatics, validated by 5'-RACE or miR159 over-expression (Table courtesy of Rob Allen et al., 2010)**.** All predicted miR159 targets from three different plant bioinformatics programs and verified miR159 targets from published 5'-RACE and overexpression studies; overexpression describes targets shown to have lower RNA levels than wild-type in *35S:MIR159a* transgenic plants. Mature miR159 members are shown 3'- 5'. Target mismatches with miR159a are bold. Bioinformatically identified targets specific for miR159b or miR159c are indicated with brackets. Anther/pollen expression data is compiled from Genevestigator (Hruz et al., 2008). Not all genes were available on the dataset (shown as n/a). Key: P = psRNA target (Zhang et al., 2005), M = miRU (Dai and Zhao, 2011), H = RNAhybM (Alves-Junior et al., 2009). R= 5'-RACE; OE = Overexpression, D=degradome. a. Gregory et al., 2008; b. Addo-Quaye et al., 2008; c. German et al., 2008; d. Palatnik et al., 2003; e. Palatnik et al., 2007; f. Reyers and Chua, 2007; g. Alves-Junior et al., 2009; h. Schwab et al., 2005.

MiR159 regulates *MYB33* and *MYB65* mRNAs through AGO1-mediated cleavage of their mRNAs (Figure 1.1, A). This is experimentally determined by the detection of miR159-specific cleavage products of *MYB33* and *MYB*65 (Palatnik et al., 2003; Allen et al., 2010). However, a translational repression mechanism is also in operation based on the observation that *MYB33* mRNAs can accumulate to high levels, but is not translated into protein (Alonso-Peral et al., 2010; Li et al., 2014). With these mechanisms, the expression of *MYB33* and *MYB65* is efficiently and completely silenced by miR159a/b in vegetative tissues. This is a notion supported by several lines of evidence. First, from genetic analysis, it is estimated that less than 10% of wild-type miR159 levels are sufficient to completely silence *MYB33* and *MYB65* in vegetative tissues (Allen et al., 2007; Allen et al., 2010). Secondly, loss-of-function *myb33.myb65* mutant plants display a wild-type phenotype at the vegetative stage, and microarray analyses found that the transcriptome of *myb33.myb65* was indistinguishable from that of wild-type (Alonso-Peral et al., 2010). Together, these data supports the idea that miR159 acts as a molecular switch, fully suppressing *MYB33/MYB65* expression in vegetative tissues, and that *MYB* expression is silenced everywhere but in seeds and anthers (Millar and Gubler, 2005; Alonso-Peral et al., 2010).

1.8.2 The confirmed and proposed functions of the miR159-*MYB33/65* pathway

Recent progress of understanding the role of the miR159-*MYB* pathway is mostly based on the functional analysis of *MYB33* and *MYB65* in the seeds and anthers. First, an loss-of-function *myb33.myb65 Arabidopsis* double mutant did not display widespread developmental defects, but was defective in anthers development, where the tapetum failed to undergo programmed cell death (PCD) and degenerate (Figure 1.2 B, Millar

and Gubler, 2005; Aya et al., 2009). Additionally, in a *myb33.myb65.myb101* triple mutant, there was a defect in seed germination, where there was slower vacuolation in

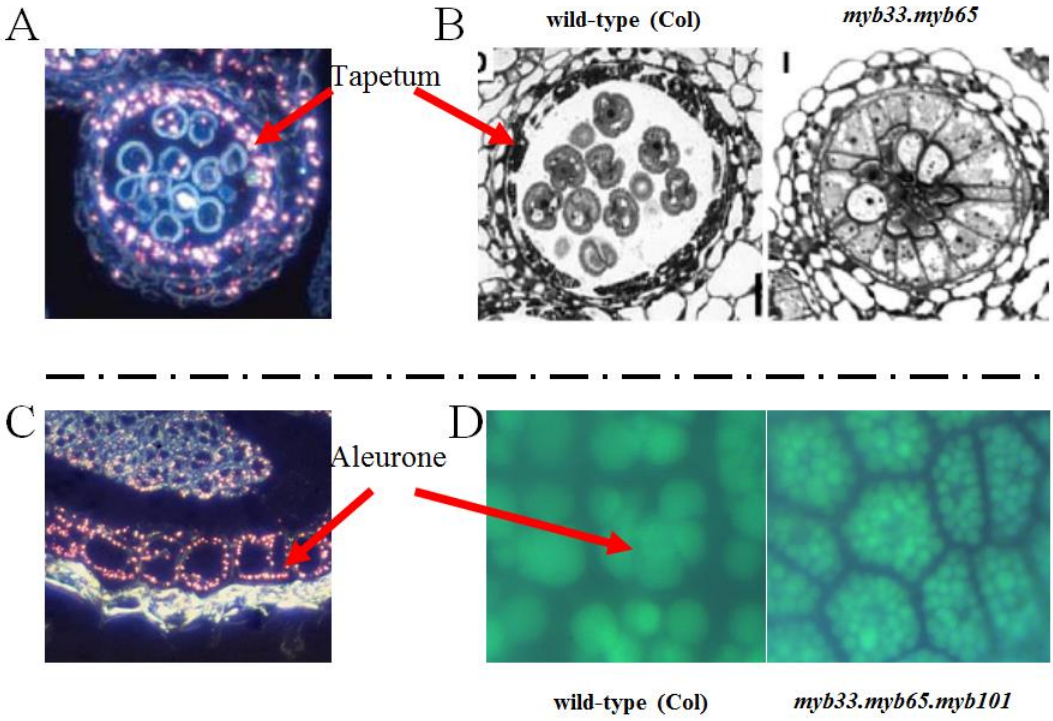

Figure 1.2: Evidence supporting a role for *MYB33/65* expression in the PCD of the tapetum of anthers and the aleurone of seeds in *Arabidopsis* (Figures courtesy of Millar and Gubler, 2005; Alonso-Peral et al., 2010). (A) And (C) reporter gene analysis demonstrating the *MYB* could only be expressed in tissues undergoing PCD. The stained cells showed pink fluorescence under dark field optics (Millar and Gubler, 2005; Alonso-Peral et al., 2010). (B) and (D) phenotypic analysis showing the deletion of MYB expression will lead to compromised cell degeneration in tapetum (Millar and Gubler, 2005), and slower vacuolation in aleurone cells (Alonso-Peral et al., 2010), which are essential steps of PCD in these tissues. The wild-type plant (Col) is used as a control. *myb33.myb65*: loss-of-function *MYB33* and *MYB65* double mutant, with a T-DNA insertion in each *MYB* gene. *myb33.myb65.myb101*: loss-of-function *MYB33*, *MYB65* and *MYB101* triple mutant, with a T-DNA insertion in every *MYB* gene. *MYB101*: another *GAMYB-like* family member highly expressed in seeds.

the aleurone cells (Figure 1.2 D), a process which is again PCD-related and is required for seed germination in *Arabidopsis* (Guo and Ho, 2008; Alonso-Peral et al., 2010). This PCD-related function of *MYB33/65* is consistent with the transcript profiling analysis performed on *mir159ab* (Alonso-Peral et al. 2010). Here, de-regulated expression of *MYB33* and *MYB65* is accompanied with up-regulation of a number of genes associated with PCD, including proteinases (e.g. *CYSTEINE PROTEINASES*, *CP* and *CP1*), hydrolases (e.g. *BETA-XYLOSIDASES*, *BXL1* and *BXL2*), and transporters (e.g. *OLIGOPEPTIDE TRANSPORTER*, *OPT*). Annotated functions of these genes are consistent with the degradation and transportation of cellular plant components, processes which are associated with PCD (Lee et al., 2004; Li et al., 2006; Lee et al., 2007). Moreover, this PCD-related function of the *GAMYB-like* genes appears to be conserved, as *GAMYB* expression has been identified in the aleurone and tapetum of barley (Gubler et al., 1995; Murray et al., 2003) and in the anthers of rice (Tsuji et al., 2006; Aya et al., 2009). In rice, *GAMYB* is required for PCD in the tapetum, which undergoes hypertrophy in the rice *gamyb* mutant, expanding to occupy the entire locule, causing the microspores to degenerate and causing male sterility (Kaneko et al., 2004, Aya et al., 2009).

In contrast to seeds and anthers, no clear role is known for the miR159-*MYB* module in vegetative tissues. From a cellular analysis of the *mir159ab* mutant, in which the *MYB33/65* genes are strongly expressed, it was found that this *MYB* activity antagonises cell proliferation in rosette tissues (Alonso-Peral et al., 2010), but no evidence of altered PCD was detected in the *mir159ab* rosette. Thus, the question remains: what role is the miR159-*MYB* pathway playing in the rosette tissue?

Considering the metabolic cost associated with *MYB33/MYB65* transcription and the subsequent miR159-guided silencing, it would seem unlikely that the miR159-*MYB* pathway is a futile process in plant rosettes. The abundance of miR159 has been found to be positively associated with the plant hormone gibberellin (GA, Achard et al. 2004) and abscisic acid (ABA, Reyes and Chua, 2007; Kim et al., 2008), but whether these associations have any biological role is not clear (details can be referred to the introduction of chapter four). Additionally, the involvement of miR159 activity in a control of plant floral transition from the vegetative phase has also been suggested (Achard et al., 2004; Tsuji et al., 2006; Li et al., 2013b), but this notion is not well supported as there are several conflicting lines of evidence (reviewed by Teotia and Tang, 2014, also refer to chapter 6 for detailed discussion). Therefore, what is the role of miR159-mediated silencing of MYB expression in plants is still an intriguing question that is poorly answered. With this respect, this PhD programme focused on performing the functional analysis of miR159-*MYB* module in *Arabidopsis* rosettes, and this thesis aimed to provide new phenotypic and molecular data, to develop our understanding of this module in plant vegetative tissues.

Chapter 2

Materials and Methods

2.1 Plant materials

Arabidopsis thaliana ecotype Columbia-0 (Col-0) was used in all experiments and is referred to as wild type. The following mutants were described previously and represent T-DNA insertional loss-of-function mutants: *mir159a* (Allen et al., 2007), *mir159ab* (Allen et al., 2007), *myb33.myb65* (Millar and Gubler, 2005), *ago7-1* (Adenot et al., 2006) and *rdr6-15* (Fahlgren et al., 2006). The *rdr6-15* and *ago7-1* mutants were kindly donated by Iain Searle. All mutants were in the Col-0 background, except the double mutant *myb33.myb65, which* was in a mixed Col-6 (*myb33*) and Col-0 (*myb65-2*) background (Millar and Gubler, 2005). The transgenic lines *MIR159b:GUS* and *mMYB33:GUS* were previously generated in the Col-0 background respectively by Allen et al. (2007) and Millar and Gubler (2005). The LhG4 enhancer line HET:59a was previously generated in the Col background by Rutherford et al. (2005). The *mir159ab.myb33.myb65* quadruple mutant and the other *mir159ab* mutants carrying different combinations of *myb33* and *myb65* T-DNA insertional alleles were generated by crossing the above double mutants *mir159ab* and *myb33.myb65*. The *mir159ab.cp1* triple mutant was generated by crossing the *mir159ab* double mutant with the T-DNA insertional *cp1* mutant from the SALK collection (SALK_051510). The genotypes were confirmed by PCR genotyping experiments (see section 2.8).

2.2 Plant Growth conditions

For plant growth, all seeds were sterilized using a vapour-phase method. Seeds were placed into a desiccator jar and exposing them to chlorine gas for 3-6 hours, and the chlorine gas was generated by mixing 100 mL of commercial bleach with 3 mL of concentrated HCl. Sterilized seeds were either sown on soil (Debco Plugger soil mixed with Osmocote Extra Mini fertilizer at 3.5 g/L), or on agar plates containing 0.5X *MS*

(Murashige and Skoog, 2.2g/L), and stratified at 4℃ overnight in the dark. Seeds were then washed once with 70% ethanol followed by three washes with sterilized water and then sown on plates. Plants were grown in 21℃ growth cabinets under long day (LD) photoperiod (16 h light/8 h dark, fluorescent illumination of 150 μmol m^{-2} s^{-1}). For the purpose of phenotypic verification, the plants were placed in a 21℃ growth chamber under short day (SD) photoperiod (8 h light/16 h dark, fluorescent illumination of 150 μmol/m^2/sec), to delay flowering and facilitate vegetative development.

For stress treatments, Col, *mir159a*, *mir159ab*, *mir159ab.myb33.myb65* plants were grown side by side in soil, for three weeks in a 21℃ growth chamber (a LD photoperiod was applied throughout the treatment if not otherwise specified), and then transferred into a 4ºC growth room with constant light at 80~90 μmol m^{-2} s^{-1} (low-temperature treatment), or a growth chamber with high temperatures (32℃ day/28℃ night, high-temperature treatment), or a growth chamber with high light intensity (~500 μmol m^{-2} s^{-1}, high light intensity stress), or provided with ~800 mL tap water per two weeks (drought stress). Plant phenotypes were examined every three days, in order to assess whether morphological differences could be induced among the plants of different genotypes.

2.3 EMS mutagenesis and *mir159ab* revertant screening

Approximately 5000 seed of the *mir159ab* mutant were immersed in 0.025% ethyl methanesulfonate (Sigma) overnight with gentle agitation. Approximately 1200 EMS treated seeds were planted in soil and grown (LD photoperiod was applied for all screen processes), and were then screen for M1 revertants which will have rosettes with larger sizes and reduced leaf curl in comparison with the non-mutagenized *mir159ab* rosette.

The M1 plants displaying a *mir159ab* phenotype were allowed to self-pollinate so to generate M2 progenies. For the M2 screen, initially ~30 M2 seeds per M1 line were planted in soil and scrutinized for M2 revertants with larger rosette sizes and reduced leaf curl. Then, because of the high frequency of *mir159ab* reversion events, seeds of 15 M1 lines were grouped into a M2 pool, from which ~1000 M2 plants per pool were screened for revertants. This approach maximized the number of mutagenized seeds screened, which in turn maximizes the chances of identifying mutants that were complete revertants.

2.4 Design of miRNA decoys

SP transgenes were designed for ten miRNA families: miR159, miR164, miR167, miR168, miR169, miR170/171, miR319, miR390, miR396 and miR403. They were designed to contain binding sites that are complementary to the respective miRNA, with two mismatches at the cleavage site, which are opposite nucleotides 10 and 11 of the miRNA. Modifications of these *SP* transgenes regarding the miRNA binding sites were as specified in chapter five (Figure 5.11, Table 5.2and5.3). Every *SP* is composed 15 miRNA binding sites, separated by 4 nt DNA spacers of random sequence and contains identical primer binding sequences that can be used to measure *SP* RNA levels by quantitative real-time PCR (qRT-PCR). The MIM binding sites of miR159 and miR156 were also respectively placed into either a *TuD* or predicted *stem-loop* backbone as specified in chapter five (Figure 5.9). All the sequences of *SP, TuD, stem-loop* transgenes could be referred in the Appendix file 1.

2.5 Bioinformatics

The free energy (ΔG) of each miRNA-target site hybridization was calculated by two independent web servers: Mfold web server (http://mfold.rna.albany.edu//?q=DINAMelt/Two-state-melting; Zuker, 2003) and RNAhybrid web server (http://bibiserv.techfak.uni-bielefeld.de/rnahybrid/submission.html, Rehmsmeier et al., 2004). Secondary structures were predicted by the RNAfold web server (http://rna.tbi.univie.ac.at/cgi-bin/RNAfold.cgi). Thermodynamic stabilities were illustrated by free energies of the thermodynamic ensemble [ΔG(s)], which were calculated by RNAfold web server (http://rna.tbi.univie.ac.at/cgi-bin/RNAfold.cgi).

2.6 Generation of expression vectors

Dr. Craig Wood from CSIRO kindly provided Gateway compatible entry vectors harbouring the viral silencing suppressors (VSS) P0, P19 and V2. All miRNA inhibitor sequences were synthesized and cloned into the Gateway donor vector pDONR/Zeo (Invitrogen) by GenScript (USA). The VSSs and miRNA inhibitors were sequenced with the BigDye Terminator v3.1 Cycle Sequencing Kit (Applied Biosystems, USA), to verify their integrity. For constitutive gene expression, the transgenes were sub-cloned into the Gateway compatible destination vector pMDC32 harboring the *Cauliflower Mosaic Virus* (CaMV) 35S promoter (Curtis and Grossniklaus, 2003), using the Gateway LR Clonase II enzyme mix (Invitrogen) according to the manufacturer's instructions. For inducible gene expression, the destination vector pMDC7 contains a chimeric transcription activator, XVE, which can efficiently activate the expression of gene fused downstream of it, upon induction by 17-β-estradiol (Zuo et al., 2000) was adopted for the sub-cloning making use of the same Gateway LR approach described

above. For tissue specific expression, the MultiSite Gateway entry vectors: pEN-L4-pOP6M2-R1, pEN-L1-S-L2, pEN-R2-F-L3 and destination vector pB7m34GW.0 were obtained online at http://www.psb.ugent.be/gateway/ (Karimi et al., 2007), and the LR reaction containing pDONR/Zeo-*SP165/166*, pEN-L4-pOp6M2-R1, pEN-R2-F-L3 and pB7m34GW.0 was carried out to generate the *pOP6-SP* expression vector; while the LR reaction containing pEN-L1-S-L2, pEN-L4-pOp6M2-R1, pEN-R2-F-L3 and pB7m34GW.0 was carried out to generate the *pOP6-GUS* expression vector, following the methods described by Karimi et al. (2007).

The LR reaction mixture was transformed into *E. coli* Alpha-Select Gold Efficiency competent cells (Bioline) by heat shock. After recovery at 37℃ for one hour, the bacteria were grown overnight at 37℃ on Luria Broth (LB) plates containing the corresponding selection antibiotics (Invitrogen) (50 μg/mL Kanamycin for selection of *E. coli* transformants of 35S-expression vectors; 50 μg/mL spectinomycin for selection of *E. coli* transformants of *XVE*-expression vectors or *pOP6*-expression vectors). Next, single *E. coli* colonies obtained were inoculated into 4 mL of liquid LB medium containing the appropriate antibiotics as mentioned for selection. After 18~20 hours growth at 37℃, the plasmids were extracted using AxyPrep^{TM} Plasmid Miniprep Kit (Axygen), and the desired expression vectors were screened by diagnostic restriction enzyme digestion, for which two restriction endonuclease enzymes were selected to digest each plasmid extraction. All restriction enzyme digestion reactions were incubated at 37℃ for 1 hour, and then analysed on 1% agarose gels by electrophoresis.

2.7 Generation of transgenic *Arabidopsis*

All expression vectors were transformed into *Agrobacterium tumefaciens* strain GV3101 by electroporation (Hellens et al., 2000), and incubated on LB plates containing Rifamycin (50 μg/mL), Gentamicin (25 μg/mL), and either Kanamycin (50 μg/mL, for selection of *Agrobacterium* transformants of 35S-expression vectors) or spectinomycin (50 μg/mL, for selection of *Agrobacterium* transformants of *XVE*-expression vectors or *pOP6*-expression vectors). All plates were incubated at 28℃ for two days until the colonies appeared. Single *Agrobacterium* colonies obtained were then subcultured in a 10 mL liquid LB medium containing the same antibiotics for selection. After growth at 28℃ overnight, plasmid was extracted from the culture using AxyPrep^{TM} Plasmid Miniprep Kit (Axygen), following the protocol provided by the manufacturer, but the volume of each reagent used was increased by 50%. The structure of the vector was confirmed by performing the diagnostic restriction enzyme digestion on the plasmid extracted. Then 1 mL of the remaining culture was inoculated into a 500 mL liquid LB culture containing again the same antibiotics as mentioned, and incubated overnight at 28℃ with constant shaking at 220 rpm. Next, *Agrobacterium* was harvested by a 15 min centrifugation at 5,000 r.p.m, and resuspended in 500 mL infiltration medium containing 5% sucrose and 0.03% surfactant Silwet L-77 (Clough and Bent, 1998), which was *Agrobacterium* infiltration medium ready for transforming the plants.

To prepare Col-0, *myb33.myb65*, *rdr6-15* and HET:59a plants for transformation, they were grown in a 21℃ growth chamber with LD photoperiod. The primary flowering bolts of all plants were clipped to promote the production of multiple secondary bolts. When secondary bolts began to produce flowers, the aerial parts of the plants including

rosettes were dipped into the *Agrobacterium* solution for 30~45 sec, ensuring all the floral organs were submerged. Plants were then placed back into the growth chamber and covered with a plastic membrane for 24 hours to maintain high humidity. Seeds were harvested later and sterilized using a vapour-phase method as described. Transformants were selected by growing seeds on agar plates containing 0.5X MS and antibiotics for selection (30 μg/mL Hygromycin for Col-0, *myb33.myb65* and *rdr6-15* transformants of 35S-transgenes or *XVE*-transgenes; 30 μg/mL Kanamycin and 25 μg/mL Basta for HET:59a transformants of *pOP6*-transgenes). After 7-10 days growth, transformants were identified and transplanted onto soil.

2.8 Estradiol induction of *XVE-MIM159* transgene

The primary *XVE-MIM159* transgenic plants were germinated on 0.5X MS plates with 30 μg/mL Hygromycin for seven days in a 21ºC growth chamber with LD photoperiod, and then transplanted onto soil. After another two-week growth on the soil, the rosettes of *XVE-MIM159* transformants were sprayed with either 10 μM 17-β-estradiol (inducer) or 10 μM dimethyl sulfoxide (DMSO, solution to dissolve 17-β-estradiol). The treatment was done *once every three days* till the leaf-curling phenotype appeared on the estradiol-treated rosettes.

2.9 PCR genotyping and identification of T-DNA Insertional alleles

The DNA extraction was performed on one to two newly initiated rosette leaves, according to the Edward preparation method (Edwards et al., 1991). Then, PCR was carried out using Platinum® Taq DNA Polymerase (Invitrogen) in a 20 μL reaction volume. 2 μL of Edward prep purified genomic DNA was used for each PCR, with final primer concentration at 0.2 μM. PCR conditions used were one cycle of 94℃/ 2 min;

30 cycles of 95 ℃/30 sec, 60 ℃/30 sec, 72 ℃/1-2 min; one cycle of 72 ℃ for 5 min. 10 μL of each PCR reaction was analysed on a 1% agarose gel by electrophoresis.

Amplification using the following pairs of gene-specific primers (Appendix file 2) detected the wild-type alleles: 159a-5 and 159b-3 to give an 884 bp fragment (*MIR159a* wild-type allele); 159b-5 and 159b-3 to give a 707 bp fragment (*MIR159b* wild-type allele); MYB33-5 and MYB33-3 to give a 1086 bp fragment (*MYB33* wild-type allele); MYB65-5 and MYB65-3 give a 1440 bp fragment (*MYB65* wild-type allele); CP1-5 and CP1-3 to give a 1032 bp fragment (*CP1* wild-type allele). To detect the mutant T-DNA alleles, gene-specific primers were combined with the T-DNA-specific primers as follows: 159a-5 and LB3 to give a 210 bp fragment (*mir159a* mutant allele); 159b-5 and LB3 to give a 530 bp fragment (*mir159b* mutant allele); MYB33-5 and JL202 to give a 462 bp fragment (*myb33* mutant allele); MYB65-5 and LBb1 to give a 1200 bp fragment (*myb65* mutant allele); CP1-5 and LBb1 to give a 786 bp fragment (*cp1* mutant allele).

2.10 RNA extraction

TRIzol® (Invitrogen) was used for RNA extraction of tissues from seedlings or rosettes at different growth stages. The extraction procedure was carried out following manufacturer's instructions with some modifications: (1) ~500 mg of plant material per 1ml Trizol reagent was applied for each extraction; (2) grinding the plant material in liquid nitrogen with a mortar and pestle; (3) The chloroform extraction step was done twice; (4) RNA precipitation was carried out 24h~48h at -20 ℃ to maximize the recovery of small RNAs.

2.11 DNase treatment and purification of RNA samples

The RNA samples were further treated with RQ1 RNase-Free DNase (Promega) to eliminate genomic DNA contamination and prepare for qRT-PCR, except those for Taqman sRNA assays (see section 2.13). For each sample, 30-50 μg of total RNA was treated with 25 μL of RQ1 DNase in a 100 μL reaction volume following the protocol provided, with the addition of 2.5 μL of RNaseOut™ Recobinant RNase Inhibitor (Invitrogen) to protect the RNA from degradation. The digested samples were purified with the Spectrum™ plant Total RNA Kit (Sigma Aldrich) following the kit protocol to remove digest DNA fragments. The concentration of each sample was measured using a nanodrop spectrophotometer. The quality of purified RNA was then examined by denaturing 1 μg sample with RNA loading buffer at 65℃ for 5 min, followed by 1% agarose gel electrophoresis.

2.12 cDNA synthesis

cDNA synthesis was carried out using SuperScript® III Reverse Transcriptase (Invitrogen) and oligo dT primers according to the manufacturer's instructions. As a modification, for each sample, 250 ng – 2.5 μg of total RNA was prepared with nuclease free distilled water in a final volume of 5 μL; and the volume of each reagent used was reduced by 50%, so that the half reaction (10 μL reaction volume instead of 20 μL) was performed. The 10 μL cDNA product was then diluted 50 times in nuclease free distilled water and used for subsequent qRT-PCR.

2.13 Quantitative Real-time PCR (qRT-PCR) analysis

For qRT-PCR, Platinum® Taq DNA Polymerase (Invitrogen) with SYB Green (Sigma) and dNTPs (Fisher Biotec) added was used as a master mix. 10 μL of each cDNA

sample was added to 9.6 µL of SYB/Taq master mix with 0.4 µL of forward and reverse primers at 10 µmol each, for a final reaction volume of 20 µL. All qRT-PCR reactions were carried out on a Corbett Rotor-Gene Q real time PCR machine (Qiagen), in triplicate under the following cycling conditions: one cycle of 95 ℃/5 min; 45 cycles of 95 ℃/15 sec, 60 ℃/15 sec, 72 ℃/20 sec, and the fluorescence was acquired at the 72 ℃ step; one melting cycle from 55 ℃ to 90 ℃, rising by 1 degree(s) each step, 15 sec for the first step, and 5 sec for each step afterward. *CYCLOPHILIN* (At2g29960) was used to normalize mRNA levels using the comparative quantitation program in the Rotor-Gene 6 software provided by Qiagen. The value for each gene represents the average of triplicate assays (the mean), and the standard deviation was calculated to appraise how widely the triplicate results are dispersed from the mean.

2.14 Taqman sRNA assays for mature miRNAs

For determining the mature miR159 levels, the RNA samples from TRIzol® (Invitrogen) extraction were directly subjected to TaqMan MicroRNA Assays (Applied Biosystems) following the protocol described by Allen et al. (2010). Different from the above qRT-PCR protocol, this assay used 10 ng of each RNA sample to perform the retro-transcription, with the use of a TaqMan MicroRNA Reverse Transcription kit (Applied Biosystems), and each reaction included the stem-loop RT primers for both the miR159a (or mir159b) and the normalization sRNA *sno101*. Then, each cDNA was assayed in triplicate using the Corbett Rotor-Gene 2000 real time PCR machine (Corbett) under the cycling conditions described above. The Expression of miR159a (or miR159b) were normalized with *sno101* using again the comparative quantitation analysis program in the Rotor-Gene 6 software (Corbett), and the standard deviation was calculated.

2.15 GUS staining

In situ GUS staining was performed on rosette tissues at different growth stages, using the method described by Jefferson (1987) with the following modifications: 1) Rosette tissues were collected and fixed with 90% acetone for 20 minutes at room temperature, followed by a 30min vacuum infiltration with GUS staining buffer 1 (50 mM Na phosphate buffer, pH 7.2, 0.2% Triton X-100, 2mM potassium ferricyanide and 2mM potassium ferrocyanide). 2) Histochemical reactions were performed by a 30~60 min vacuum infiltration with staining buffer 2 (staining buffer 1 plus 2 mM X-gluc, which is 5-bromo-4-chloro-3-indolyl-β-D-glucuronide), and then an overnight incubation at 37℃. The staining buffer was removed by successive washes with 20%, 50%, 70% and 90% ethanol (1h per wash), and the cleared tissues were photographed using either a Olympus Dissecting Microscope OLYMPUS SZX2-ILLK (Tokyo, Japan) (for 10~20-day-old seedlings) or a normal camera and a light box (for older and bigger rosettes).

2.16 Trypan blue staining

This staining was performed basically as described in Van Wees (2008). First, freshly harvested leaves were submerged into a 2.5 mg/mL Trypan blue solution and heated in boiling water for 1 min, followed by 2 h incubation at room temperature. Next, these tissues were incubated in a chloral hydrate solution for 2h at room temperature, followed by replacement of the chloral hydrate solution and an overnight incubation at room temperature. To detect the dead or dying cells, which is supposed to be stained in dark blue, the leaf tissues were covered with 70% glycerol, and observed under the bright-field microscopy OLYMPUS SZX2-ILLK (Tokyo, Japan).

Chapter 3

Functional analysis of the miR159-*MYB* module in the *Arabidopsis* rosette

3.1 Introduction

The miR159 family represents one of the most ancient miRNA families identified not only widely in both monocots and dicots (Axtell and Bartel, 2005; Axtell and Bowman, 2008), but is present in lycopods, and even moss the earliest-branching clade in land plants (> 400 million years, Bartel, 2004; Arazi et al. 2005; Li et al., 2011b). Via bioinformatic prediction and experimental validation in different species, such as barley (*Hordeum vulgare*), rice (*Oryza sativa*), *Arabidopsis*, potato and strawberry, miR159 has been found to specifically regulate the expression of several *GAMYB* or *GAMYB*-like genes, which are also ancient (Achard et al. 2004; Tsuji et a., 2006; Allen et al., 2007; Csukasi et al., 2012; Yang et al., 2014). As the miR159 binding site in these *MYB*s is highly conserved, despite the considerable evolutionary distance that separates these species from their last common ancestor, the miR159-*MYB* relationship is considered to have a long co-evolutionary history (Rhoades et al., 2002; Achard et al. 2004; Tsuji et al., 2006; Csukasi et al., 2012; Yang et al., 2014). Therefore, it appears that the miR159-*MYB* module is evolutionarily selected to play vital roles in plants.

These *GAMYB* or *GAMYB*-like genes encode R2R3 MYB domain transcription factors, members of the largest plant transcription factor family (Dubos et al., 2010; Li and Lu, 2014). As the name indicates, these *MYB* genes have been implicated in gibberellin (GA) signal transduction, which has shown to be the case in anthers and germinating seeds (Woodger et al., 2003). However, the role of the miR159-*MYB* module in plant vegetative growth is largely unknown. In this chapter, I aim to first characterize the expression patterns of miR159 and the *MYB* target genes during rosette development in

Arabidopsis thaliana, and then investigate the possible role of miR159-*MYB* module in plant development or response to abiotic/biotic stresses.

In *Arabidopsis*, miR159 is the most abundant miRNA family (Nakano et al., 2006; Kasschau et al., 2007), where the two predominantly expressed miR159 isoforms, miR159a and miR159b (miR159a/b, Fahlgren et al., 2007), play redundant roles controlling plant growth. The importance of miR159a/b in plant growth is illustrated by a loss-of-function *mir159ab* double mutant that displays pleiotropic developmental defects (e.g. curled/rounded leaves, stunted growth and altered apical dominance), which are not apparent in either single loss-of-function *mir159a* or *mir159b* mutant (Allen et al., 2007). Although bioinformatic and molecular analyses have identified approximately 20 miR159 target genes in *Arabidopsis* (Allen et al., 2010), only miR159 regulation of two *GAMYB-like* genes, *MYB33* and *MYB65* (*MYB33/65*), appear functionally relevant, because all development defects in a *mir159ab* are fully suppressed in a *mir159ab/myb33/myb65* quadruple mutant (Allen et al., 2007).

One major biological role of the *GAMYB-like* genes is promoting programmed cell death (PCD). This is evidenced by a male sterile phenotype of the rice *gamyb*, and *Arabidopsis myb33.myb65* mutants in which the tapetum fails to undergo PCD (Kaneko et al., 2004; Millar and Gubler, 2005; Aya et al., 2009). Furthermore, Alonso-Peral et al. (2010) found that expression of the *GAMYB-like* genes in the aleurone of *Arabidopsis* also promoted PCD, as the aleurone vacuolation, a GA-mediated PCD process required for seed germination, was impaired in the *myb33.myb65.myb101* mutant seeds (*MYB101*, another 5'-RACE verified target of miR159, which is highly expressed in *Arabidopsis*

seeds, Penfield et al., 2006; Allen et al., 2010). Therefore, it appears that in seeds and flowers, where miR159 activity is weak, these *MYB* genes are expressed, regulating PCD processes of the tapetum and aleurone to promote anther and seed development respectively.

By contrast, in vegetative tissues, where *MYB33*/*65* are transcribed, strong miR159 activity has been demonstrated to mediate complete silencing of *MYB33/65* expression (Allen et al., 2007; Alonso-Peral et al., 2010), making the miR159-*MYB* pathway a seemingly genetic futile cycle. By analyzing the *mir159ab* mutant, Alonso-Peral et al. (2010) discovered that though the *MYB* activity antagonizes cell proliferation in rosette tissues, no altered PCD was detected in the rosette of *mir159ab*. Moreover, by applying GA to loss-of-function *myb33.myb65* mutant and wild-type *Arabidopsis* rosettes, the *MYB33*/65 were found not required for GA-induced rosette growth, as *myb33.myb65* and wild-type plants responded to GA similarly in terms of petiole length of rosette leaves; also, *MYB33*/65 mRNA levels failed to change with GA application in wild-type plant (Alonso-Peral et al. 2010). Therefore, it is still unclear why plant makes a metabolic investment in *MYB33/65* transcription only for these transcripts to be fully silenced by miR159. This raises the fundamental questions of what role is the miR159-*MYB* module playing in these vegetative tissues, and what, if any, developmental or stress-response function is it playing?

To address this, my experiments have focused on answering the following questions:

a. In what developmental stages/tissues/cells of the rosette is miR159 expressed, and in what developmental stages/tissues/cells are *MYB33*/*65* transcribed?

b. Are there conditions in which miR159 activity is suppressed, resulting in the activation of the *MYB33/65* pathway?

c. What is the biological role of miR159-*MYB* module in the *Arabidopsis* rosette?

3.2 Results

3.2.1 Identification of a marker gene for *MYB33*/65 activity: *CP1* transcript level tightly correlates with MYB33/65 expression

To facilitate the functional analysis of the miR159-*MYB* pathway in the *Arabidopsis* rosette, a marker of the MYB33/65 activity is required. Owing to the difficulty in detecting MYB33/65 protein expression by western blotting, the transcript levels of *MYB33/65* are generally used as an indicator of MYB expression/activity (Naqvi et al., 2010; Wu et al., 2010; Du et al., 2014). However, it is clear that miR159 can strongly suppress translation of *MYB33/65* mRNA, and hence *MYB33/65* mRNA levels are not accurate indicators of their expression (Li et al., 2014a).

Potential downstream genes of *MYB33/65* have been reported previously in a microarray study that identified genes up-regulated by MYB33/65 expression (Alonso-Peral et al., 2010). To determine whether one such *MYB33/65* downstream candidate gene, *CYSTEINE PROTEINASE1* (*CP1*; At4g36880, Alonso-Peral et al., 2010), could act as an accurate molecular marker of MYB33/65 expression/activity, it was investigated how tightly *CP1* mRNA level correlated to *MYB33/65* expression. This was performed in a set of *mir159ab* mutants that carry different combinations of *myb33* and *myb65* T-DNA-insertional alleles, and hence different levels of MYB33/65 expression (Figure 3.1, A). These mutants were isolated by firstly crossing *mir159ab* with *myb33.myb65*, and then genotyping the self-fertilized third generation progenies (F3). By measuring *CP1* mRNA levels in these mutants carrying various combinations of *myb33*/*myb65* alleles, the feasibility of using *CP1* mRNA level as a marker of MYB33/65 expression was appraised.

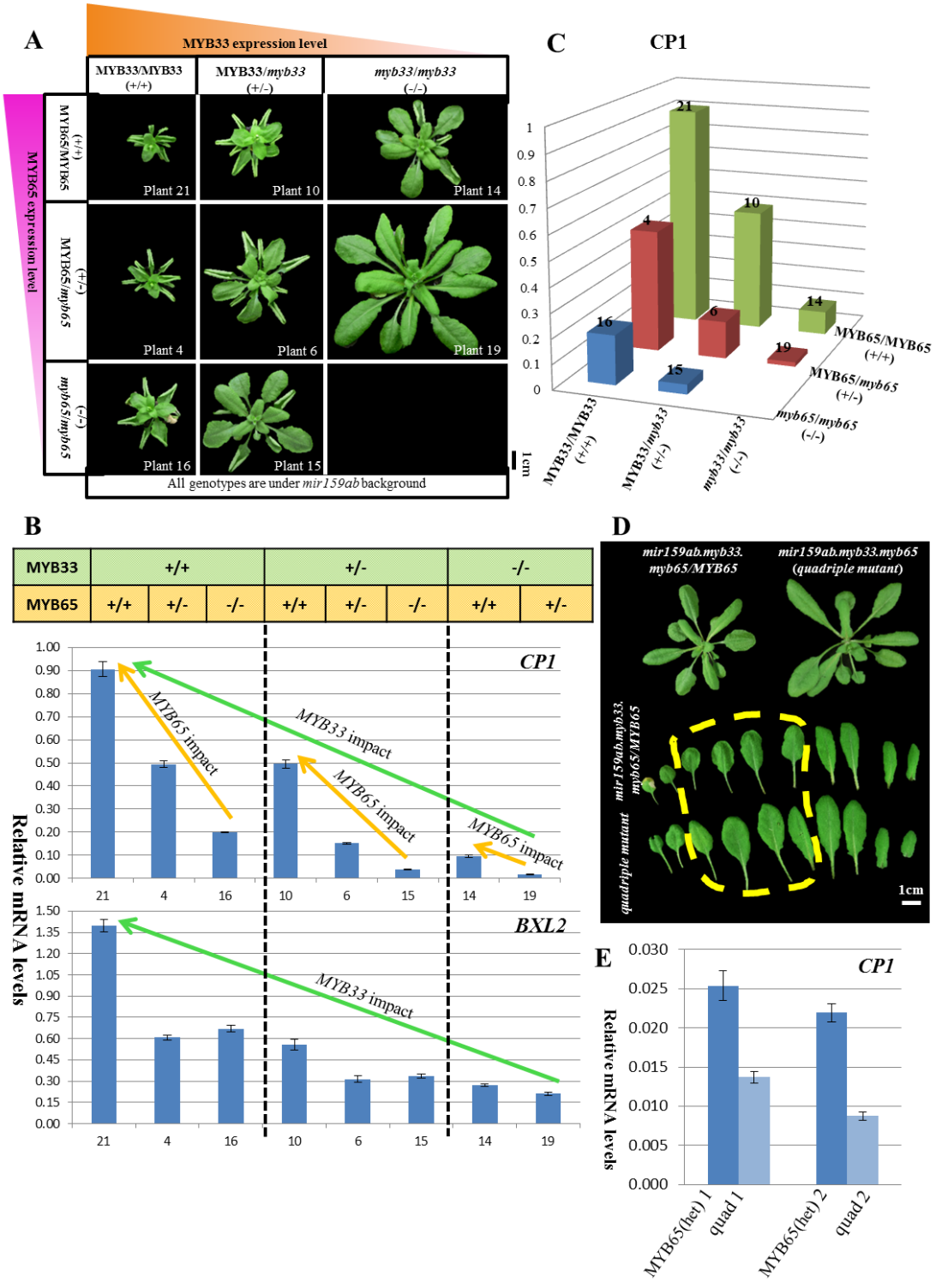

Figure 3.1 *CP1* transcript level tightly correlates with MYB33/65 expression. (A) Representative rosette phenotypes of five-week-old *mir159ab* plants carrying different combinations of heterozygous or homozygous T-DNA insertion *myb33/myb65* alleles. The F3 progenies were numbered in order as the genotyping was performed, and one numbered plant of every confirmed genotype was selected to represent the rosette phenotype. (B) qRT-PCR analysis of *CP1* and *BXL2* mRNAs in five-week-old rosettes of different genotypes. The numbers along the x-axis correspond to the numbered plants

shown in A. Coloured arrows indicate the impact of MYB33/65 expression on *CP1* and *BXL2* mRNA levels. (C) 3D-column presentation of *CP1* mRNA levels, for comparison between the molecular and phenotypic impacts (i.e. phenotypes shown in A). (D) and (E) Phenotypic and molecular impacts of single wild-type *MYB65* allele expression. Analysis was done on five-week-old *mir159ab.myb33.MYB65/myb65* [*myb65* (het)] mutants and *mir159ab.myb33.myb65/myb65* (quad) mutants. All mRNA levels were normalized to that of housekeeping gene *CYCLOPHILIN* (At2g29960). Error bars represent the SD of three technical replicates of this assay.

As predicted, it was found that the number of wild-type *MYB33* or *MYB65* alleles present in the *mir159ab* background strongly correlated with defect severity of rosette morphology; i.e. upwardly curled leaves and reductions in rosette sizes. Even the presence of only one wild-type *MYB33* allele (Figure 3.1, A, plant 15) or one *MYB65* allele (Figure 3.1, D) could induce *mir159ab* phenotypic characteristics of upwardly curled leaves. More importantly, *CP1* mRNA level was tightly correlated to the number of wild-type *MYB33* and *MYB65* alleles. Additionally, this correlation appeared tighter than the correlation of another *MYB33/65* downstream candidate, *BETAXYLOSIDASE2* (*BXL2*) (Figure 3.1, B), whose transcript level correlated strongly with the *MYB33* allele, but less so with the *MYB65* allele.

It was worth noting that the wild-type *MYB33* allele (Figure 3.1, A, plant 16) triggered severer *mir159ab* rosette defects than the wild-type *MYB65* allele (Figure 3.1, A, plant14), which indicated that MYB65 has a weaker activity than that of MYB33. To determine whether the *CP1* mRNA level also reflects this weaker MYB65 activity, *CP1* mRNA levels were compared between the *mir159ab.myb33.myb65/MYB65* (carries one wild-type *MYB65* allele) and the *mir159ab.myb33.myb65* (carries no wild-type *MYB65* allele) plants (Figure 3.1, E). In two biological replicates, significantly higher *CP1* mRNA levels were detected in the *mir159ab.myb33.myb65/MYB65* plants compared to *mir159ab.myb33.myb65* plants (Student's T-test: $P < 0.05$). This supports the notion

that *CP1* mRNA levels are a sensitive and reliable indicator of *MYB33/65* expression/activity in rosette tissues.

3.2.2 The miR159-*MYB* module is constantly and ubiquitously present in *Arabidopsis* rosettes

To begin the characterisation of miR159-*MYB* module in *Arabidopsis* rosettes, two time-course experiments were performed to determine in what developmental stages, tissues or cells of the rosette are the miR159 and its *MYB33/65* target genes expressed (Figure 3.2).

First, a qRT-PCR based transcript profiling experiment was performed on wild-type *Arabidopsis* (Col) rosettes over a 63-day time course, to study the levels of mature miR159a and miR159b abundance, and the mRNA levels of *MYB33*, *MYB65* and *CP1* during rosette development (Figure 3.2, A). It was found that both miR159a and miR159b were expressed strongly throughout rosette development. Both miRNAs had similar developmental profiles, increasing approximately two-fold during the first half of rosette development and then decreasing slightly. Next, the transcript levels of *MYB33* and *MYB65* were measured in the same samples (Figure 3.2, A). The abundances of both transcripts were found to be low. Although fluctuations in their abundances were detected, they did not inversely correlate with the miR159 profile, and so are likely to be independent of miR159 activity.

To determine whether these *MYB33* and *MYB65* mRNA levels reflect MYB33/65 protein expression, the *CP1* mRNA level was measured (Figure 3.2, A). Analysis showed that in three-day-old seedlings, the *CP1* mRNA level was high, which is

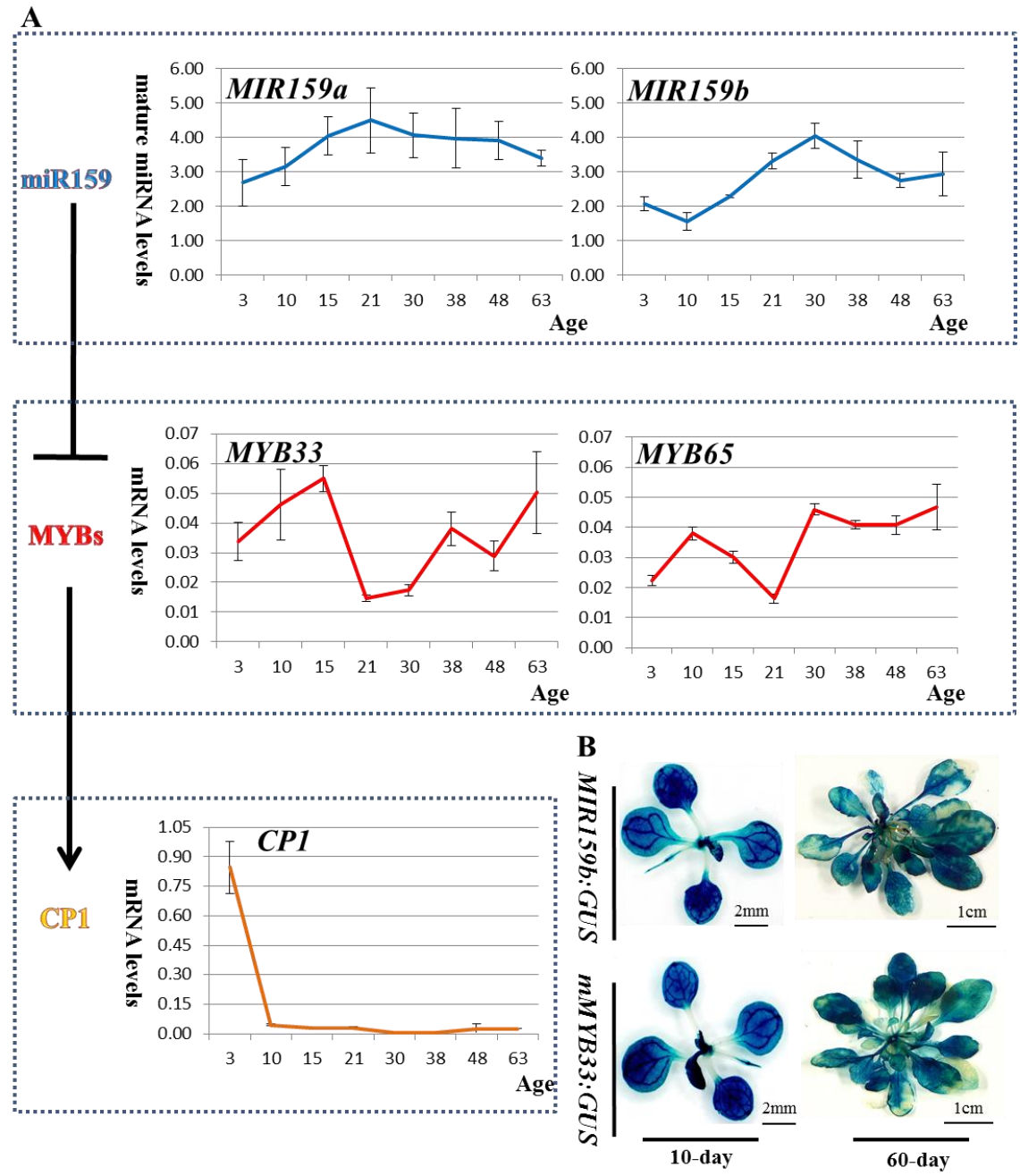

Figure 3.2 miR159 activity constantly represses *MYB33/65* activity throughout rosette development. (A) Time-course transcript profiling of miR159-*MYB* module in rosettes. The relative miRNA and mRNA in rosettes were measured every ~10 days throughout its development. The miR159 levels were normalized to *sno101*, a constitutively and strongly expressed small RNA (Allen et al., 2010; Alonso-Peral et al., 2010). The mRNA levels of *MYB33*, *MYB65* and *CP1* were normalized to that of *CYCLOPHILIN*. Error bars represent the SD of three technical replicates of this assay. (B) Time-course GUS-staining assay for rosettes of *MIR159b:GUS* and *mMYB33:GUS* transgenic lines. The staining was carried out on ten individual rosettes per time point, at ten-day interval during plant growth; the very first and last staining results were shown to represent the consistent staining pattern for all the tested time points.

consistent with the fact that *CP1* is highly expressed in germinating seeds (Alonso-Peral et al., 2010). However, other than this time point, *CP1* mRNA level constantly stayed low throughout rosette development. This suggests *MYB33/65* mRNAs are strongly silenced by miR159 throughout rosette development, and that the fluctuations in *MYB33/65* mRNA levels do not reflect changes in MYB33/65 protein expression.

To determine in what rosette tissues and cells *MIR159* and its target *MYB* genes are transcribed, a β-glucuronidase (GUS)-staining assay was then carried out over a 60-day time course, on two transgenic *Arabidopsis* lines: *MIR159b:GUS* and *mMYB33:GUS*. The *MIR159b:GUS* line was constructed by fusing the *GUS* gene downstream of the *MIR159b* promoter, to visualize the transcriptional domain of *MIR159b* (Allen et al., 2007); while the *mMYB33:GUS* line carries a miR159-resistant version of *MYB33*, which enables visualization of the *MYB33* transcriptional domain (Millar and Gubler, 2005). The rosettes of each line were harvested and stained every ten days.

It was found that the rosettes of both lines could be stained at all the tested time points, from young seedling (10-day-old) to the late reproductive (60-day-old) growth phases (Figure 3.2, B). Moreover, the staining appeared ubiquitous throughout *MIR159b:GUS* and *mMYB33:GUS* rosettes. Patches of unstained cells in the older plants were either dead in those areas or possibly reflects a leaf staining penetration problem (Schieferstein and Loomis, 1956), which did not correspond to a consistent developmental pattern. Hence, the result extends the previous GUS-staining observation showing *MIR159b* and *MYB33* are co-transcribed (Allen et al., 2007), by demonstrating this co-transcription occurs in all cells and developmental stages of the *Arabidopsis* rosette.

Summarizing the data, the overall time-course results revealed the presence of strong constitutive expression of miR159 that suppresses the expression of *MYB33* and *MYB65* throughout *Arabidopsis* rosette development.

3.2.3 miR159 is functionally active in the developing rosette

To test the idea that constant miR159 activity is required for normal rosette development, a *XVE-MIM159* construct was then generated and transformed into *Arabidopsis* (Col, Figure 3.3, A). The transactivator *XVE* can be induced by estrogen (e.g. 17-β-estradiol), resulting in transcriptional activation of the downstream transgene (Zuo et al., 2000); while the *MIM159* carries a non-cleavable miR159 binding site that sequestrates and inhibits miR159 (Todesco et al., 2010). Primary *XVE-MIM159* transformants were selected and grown for 21 days so that rosettes were well established. These transformants were then treated with either 10 μM 17-β-estradiol (inducer) or dimethyl sulfoxide (dissolving solution, control). Two weeks after the treatment, leaves to which the 17-β-estradiol was applied had become upwardly curled (Figure 3.3, B), consistent with the hyponastic leaf phenotype of *mir159ab*. Supporting this were qRT-PCR analyses that found elevated *MYB33*, *MYB65* and *CP1* mRNA levels in 17-β-estradiol treated *XVE-MIM159* plants (Figure 3.3, C)

Therefore, both the phenotypic and molecular data indicate that miR159 function is constantly active in developing rosettes, and perturbation of this function results in derepression of *MYB33/65* expression accompanied with morphological alterations to the rosette. This raises the possibility that the miR159-*MYB* module may be involved in response to environmental stress(es), where inhibition of miR159 activity by a biotic or

abiotic stress will activate *MYB33/65* expression, inducing the morphological alterations accommodating that stress(es).

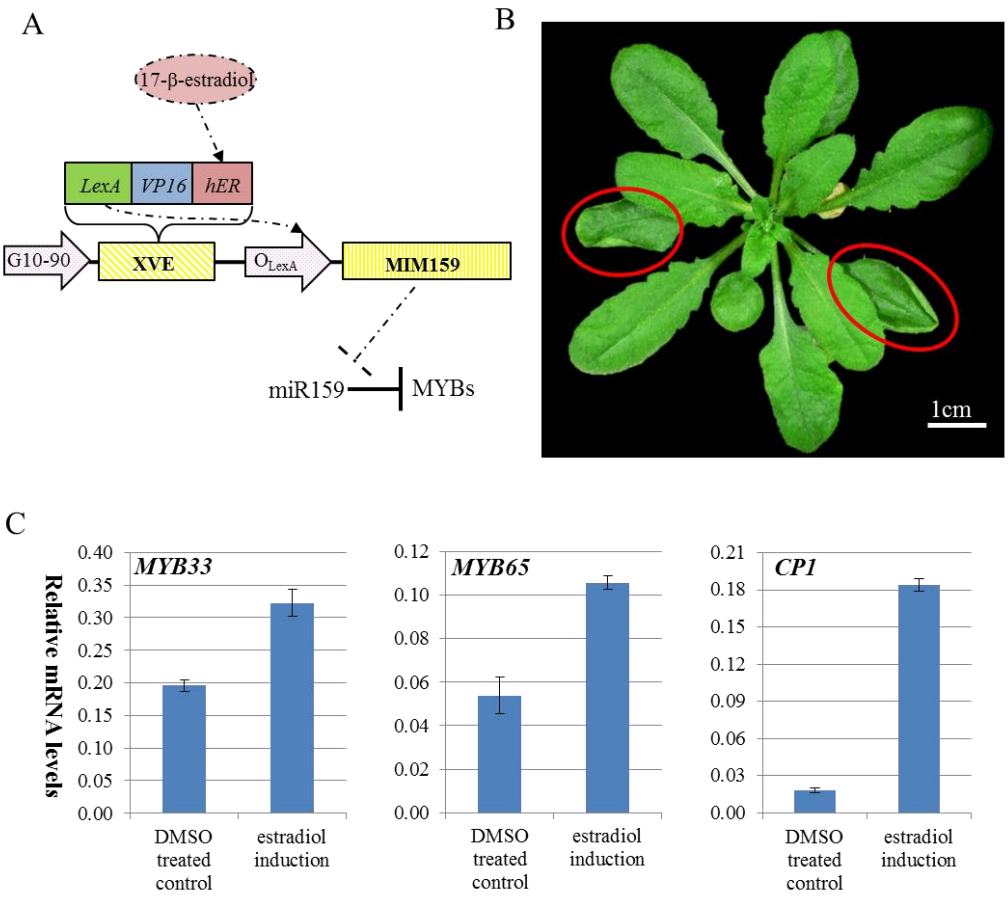

Figure 3.3 Morphological and molecular responses induced by inhibiting miR159 activity during rosette development. (A) Cartoon illustrating the construction of the *XVE-MIM159* inducible system. G10−90, a constitutive promoter controlling the *XVE* fusion gene (Ishige et al., 1999); XVE, chimeric transcription factor containing the DNA-binding domain of LexA, transcription activation domain of VP16 and regulatory region of the human estrogen receptor (Zuo et al., 2000); O_{LexA}, eight copies of the *LexA* operator sequence (Zuo et al., 2000); *MIM159*, DNA sequence complementary to miR159, with a central three-nucleotide bulge to obstruct the miR159-mediated cleavage of *MIM159* transcript (Todesco et al., 2010). Application of 17-β-estradiol promotes the XVE transactivity, leading to the *MIM159* transcription, which can consequently sequester and inhibit the miR159 function. (B) Application of 17-β-estradiol to 21-day-old *XVE-MIM159* transformants induced the leaf-curling defect (red circled). The representative picture was taken when plants were 35-day-old. (C) qRT-PCR of *MYB33*/65 and *CP1* mRNA levels in 35-day-old transformant rosettes with different treatments. DMSO: dimethyl sulfoxide, solution to dissolve 17-β-estradiol, applied as the control treatment. All mRNA levels were normalized to that of *CYCLOPHILIN*. Error bars represent the SD of three technical replicates of this assay.

3.2.4 miR159 silencing in rosettes cannot be inhibited by common abiotic stresses

Recently, the function of miR159 has been implicated in plant response to abiotic stresses, such as to heat stress in wheat (Wang et al., 2012), drought stress in potato (Yang et al., 2014), based on down-regulation of miR159 levels in these species under these respective abiotic stresses. The *Arabidopsis* response to drought stress has also been reported, but with opposing northern blotting data showing increased miR159 accumulation under tested drought conditions (Reyes and Chua, 2007). Here, prior to any further investigation, we searched the GENEVESTIGATOR platform (https://www.genevestigator.com/gv/) and *Arabidopsis* eFP Browser (http://bar.utoronto.ca/efp/cgi-bin/efpWeb.cgi), for growth conditions that may activate *CP1* transcription, based on the assumption that this gene will be activated as shown above if the miR159 activity is compromised under certain stressful conditions. However, *CP1* mRNA levels were found to remain low under all examined growth conditions and stresses. Hence, in *Arabidopsis*, it appeared that the suggested role of miR159 function in plant stress response requires further phenotypic and molecular analyses, which will be addressed by following experiment utilizing the *mir159ab.myb33.myb65* quadruple mutant.

To investigate the effect of a certain stress on the miR159 silencing, the wild-type Col and *mir159ab.myb33.myb65* quadruple mutant were grown under several conditions [i.e. high (32 ℃ day/28 ℃ night) or low (4^{o}C) temperatures, high light intensity (~500 µ mol m^{-2} s^{-1}) and drought (~250mL tap water per 1L soil every two weeks)]. Also included in the analysis were the loss-of-function *mir159a* and *mir159ab* mutants that were grown side-by-side for comparison. As miR159 abundance in *mir159a* is reduced to approximately 10% of wild type, but is morphologically indistinguishable from the

wild-type Col (Allen et al., 2007; Allen et al., 2010), such a genotype would be sensitized to subtle perturbation of miR159 activity which may result in *mir159ab*-like phenotype that may not be manifested in wild-type plants.

None of the tested stress conditions could induce an observable phenotypic difference among the Col, *mir159a* and *mir159ab.myb33.myb65* plants, suggesting no strong disturbance of miR159 activity in the Col or *mir159a* plants under these stresses. Since the low-temperature stress triggered obvious morphological alterations to the rosettes (Figure 3.4, A), further molecular analysis was performed on these plants (Figure 3.4, B). qRT-PCR analysis found that although the *MYB33/65* mRNA levels in *mir159a* were slightly higher than that of Col (Student's Test: $P < 0.005$), the mRNA levels of *CP1* remained unchanged between Col or *mir159a* and *mir159ab.myb33.myb65* plants (Student's Test: $P > 0.05$) (Figure 3.4, B). This indicates miR159-mediated silencing of *MYB33/65* had not been perturbed, which supported the observation that the Col, *mir159a* and *mir159ab.myb33.myb65* plants were morphologically indistinguishable under cold stress.

From these analyses it appears that miR159 activity in rosettes is generally robust under common abiotic stresses, and the activation of *MYB* expression during these stresses did not occur. Therefore, to perturb the miR159 function, a stress that can strongly repress plant miRNA pathways may be required.

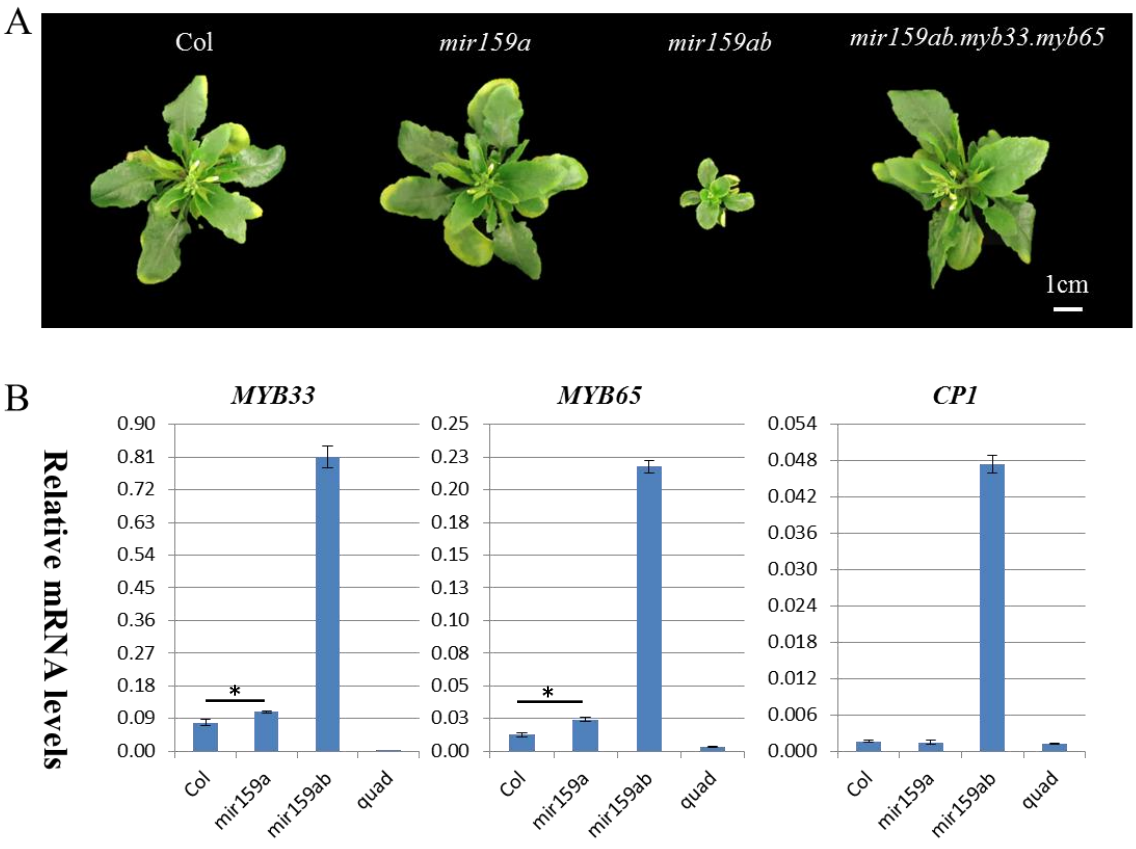

Figure 3.4: Morphological and molecular analysis of low-temperature effect on the *Arabidopsis* miR159-*MYB* module. (A) Phenotypic comparison of rosettes of Col, *mir159a*, *mir159ab* and *mir159ab.myb33.myb65* plants stressed with low-temperature. All plants were grown at 21℃ for three weeks after seed germination, and at 4℃ for another eight weeks. Right after that, the rosettes (~75-day-old) of each genotype were photographed and harvested. (B) qRT-PCR analysis of *MYB33*, *MYB65* and *CP1* mRNA levels in the above rosettes (5~10 rosettes per genotype were randomly picked for analysis). The mRNA levels were normalized to *CYCLOPHILIN*. Error bars represent the SD of three technical replicates of this assay. The symbol * indicates that *MYB33/65* mRNA levels in *mir159a* were significantly higher than that of Col (Student's Test: $P < 0.005$)

3.2.5 The constitutive expression of viral silencing suppressor (VSS) proteins cannot strongly inhibit miR159 activity in *Arabidopsis* rosettes

One potential biotic stress is the expression of viral silencing suppressor (VSS) proteins. Viruses have evolved VSS proteins to counteract plant antiviral RNAi, via interfering with one or more steps of small RNA (sRNA) biogenesis (Chapman et al., 2004; Voinnet, 2005; Li and Ding, 2006; Diaz-Pendon and Ding, 2008). These VSSs include P19 and HC-Pro, which bind and sequester sRNA duplexes with high affinity (Reyes and Chua, 2007; Stav et al., 2010; Wu et al., 2010); and P0, which targets sRNA effector ARGONAUTE1 (AGO1) protein to promote its ubiquitination and subsequent degradation (Pazhouhandeh et al., 2006; Bortolamiol et al., 2007; Csorba et al. 2010). In this study, P19 and P0 were strongly and constitutively expressed in *Arabidopsis* to test if VSSs can inhibit miR159 activity and trigger *mir159ab*-related defects.

First of all, the *P19* and *P0* coding genes were fused downstream of the *Cauliflower Mosaic Virus* (CaMV) 35S promoter to generate *35S-P19* and *35S-P0* transgenes for strong, constitutive expression in transgenic *Arabidopsis* (Col). As a negative control, the VSS protein V2 was used, because its activity inhibits *SUPPRESSOR OF GENE SILENCING3* (*SGS3*), which is required for siRNA amplification, but not miRNA biogenesis or function (Fukunaga and Doudna, 2009). Consistent with this, *35S-V2* transgenic plants [termed *35S-V2*(Col), Figure 3.5, A] displayed no morphological abnormalities. Different from that, the *35S-P19* transformants [termed *35S-P19*(Col), Figure 3.5, A] displayed reduced rosette sizes, indicating that *P19* expression inhibits the growth of *Arabidopsis*. However, despite the smaller size, these rosettes displayed no obvious morphological abnormality and no obvious leaf-curl phenotype, suggesting that *35S-P19* expression could not strongly perturb miR159 activity.

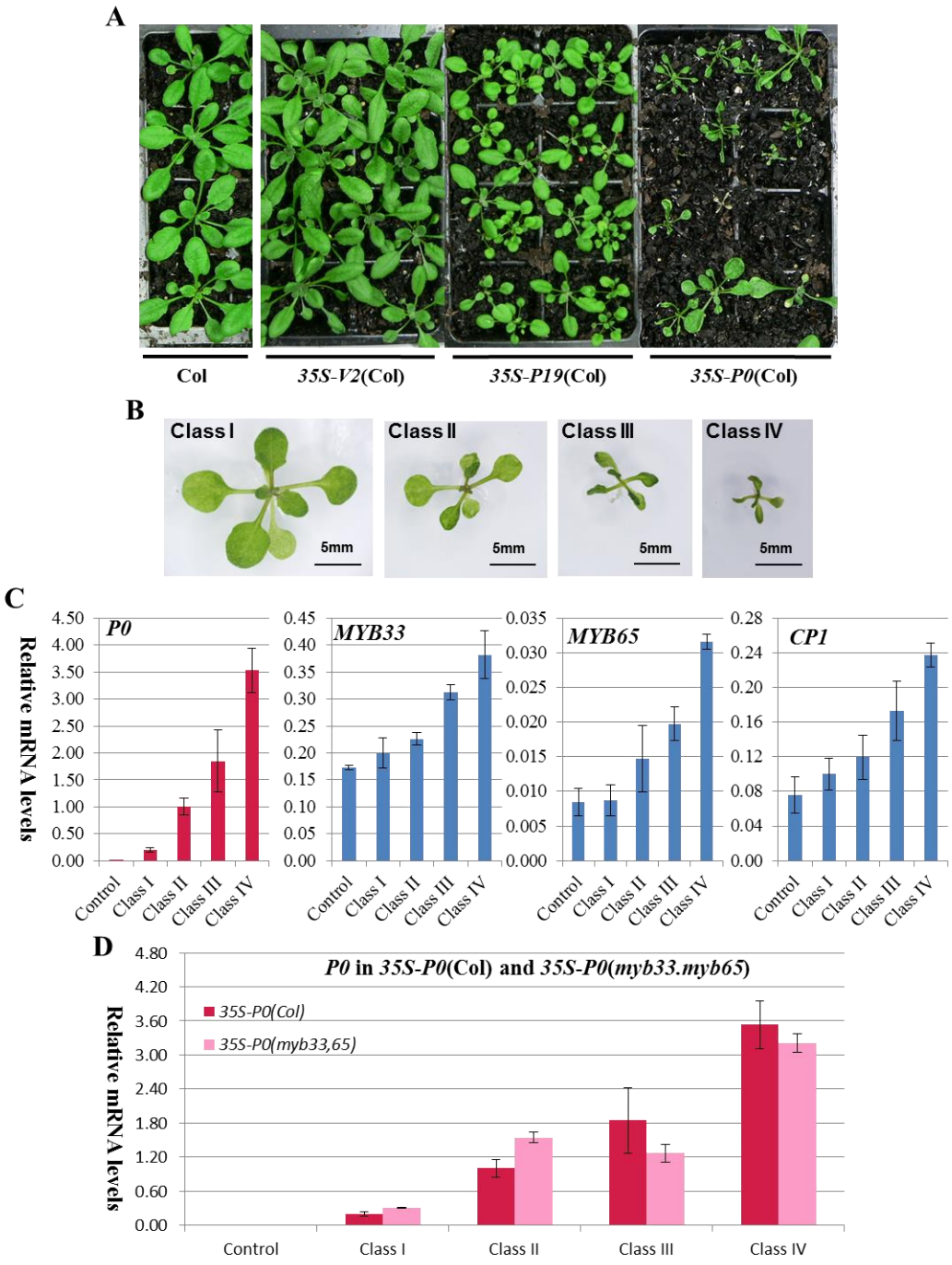

Figure 3.5 Constitutive expression of VSS P19 and P0 could not strongly perturb the miR159 activity to induce *mir159ab* relative defects. (A) Different phenotypes developed in 28-day-old *35S-V2*(Col), *35S-P19*(Col) and *35S-P0*(Col) primary transgenic lines. The wild-type plants (Col) were grown side by side as controls. Each plant has been generated by an individual primary transformation event and thereby together these multiple lines should represent a range of expression levels of respective silencing suppressors. (B) The representative classification of symptom severities among *35S-P0* transgenic plants. Class I: wild-type-looking group; Class II: intermediate group that has mild reduction in rosette size and partially curled leaves; Class III: further reduction in rosettes and all leaves curled group; Class IV: most severe

group that has stunted tiny rosettes and all leaves curled. (C) qRT-PCR analysis of relative mRNA levels in every classified *35S-P0*(Col) group. (D) Comparison of *P0* mRNA levels between *35S-P0*(Col) and *35S-P0*(*myb33.myb65*) with the same classified phenotypes. The RNA samples were extracted from 26-day-old plants, Col and *myb33.myb65* were used as control. The mRNA levels of *P0* were normalized to that of a housekeeping gene *UBIQUITIN* (At4g05320), while those of *MYB* and *CP1* were normalized to that of *CYCLOPHILIN*. Error bars represent the SD of three technical replicates of this assay.

By contrast, *35S-P0* transgenic plants [termed *35S-P0*(Col), Figure 3.5, A] developed severe morphological abnormalities, which were characterized by reduced sizes in rosettes and curled leaves. These abnormalities appeared similar to that of *mir159ab* rosettes and thus were further investigated. First, the *35S-P0*(Col) transgenic plants were grouped into four classes, based on the severity of rosette defects (Figure 3.5, B). Next, the *P0* transcript level was measured in each class, and found to strongly correlate with the severity of morphological abnormalities (Figure 3.5, C), suggesting the P0-induced phenotypes are dose-dependent. To determine whether these phenotypes were potentially due to miR159 inhibition, *MYB33* and *MYB65* transcript levels were measured by qRT-PCR. With the exception of Class I (wild-type looking phenotype), mild increases (1-3 fold) of *MYB33* and *MYB65* transcript levels were observed in all other 35S-*P0* classes, and positively correlated with the abnormality severity and the *P0* transcript level (Figure 3.5, C). This data suggested that P0 expression inhibited miR159 activity in a dose-dependent manner, leading to the corresponding de-regulation of *MYB33/65*. However, although increase in *CP1* mRNA level was observed to positively correlate with both the *P0* and *MYB33/65* transcript levels (Figure 3.5, C), even in the group with the most severe abnormalities, the fold change of *CP1* mRNA level was much lower than that observed in *mir159ab* (~40 fold up-regulation; Alonso-Peral et al., 2010). This suggests that perturbation of miR159 by P0 expression is mild, and

de-regulation of *MYB33/65* may not be strongly impacting the phenotype of the *35S-P0*(Col) plants.

To investigate this possibility, the *35S-P0* transgene was transformed into a loss-of-function *myb33.myb65* T-DNA mutant (Millar and Gubler, 2005). Next, the *35S-P0*(*myb33.myb65*) transformants were selected and grown alongside *35S-P0*(Col) transformants in order to carry out morphological and molecular comparisons. The *35S-P0*(*myb33.myb65*) transformants developed similar phenotypes to those of *35S-P0*(Col) transformants, which could be grouped into the same phenotypic classes (class I, II, III and IV as shown in Figure 3.5, B). Moreover, qRT-PCR data demonstrated that, the *P0* transcript levels were similar in similar *35S-P0*(Col) and *35S-P0*(*myb33,myb65*) phenotypic classes (Figure 3.5, D). This finding indicated that the similar P0 expression levels triggered the similar phenotypic defects in both Col and *myb33.myb65* plants. Hence, these P0-induced phenotypes must be largely *MYB33* and *MYB65* independent, and not related to the mild increase of *MYB33* and *MYB65* mRNA levels in *35S-P0*(Col). This agreed with the weak induction of *CP1* as discussed above (Figure 3.5, C). Therefore, together these data imply that P0 expression is unable to perturb miR159 function to an extent that results in a strong activation of the *MYB33/65* pathway with a detectable MYB-related rosette defect.

3.2.6 TuMV infection does not strongly perturb miR159 function in *Arabidopsis* rosettes

The failure of the VSSs to strongly inhibit miR159 function may relate to expression levels of the VSSs, which can be very high during viral infection (Scholthof et al., 1995, Scholthof et al., 1999). Thus, to further investigate the possibility of perturbing miR159

function with a biotic stress, *Arabidopsis* was infected with the dicot-infecting *Turnip Mosaic Virus* (TuMV) that contains the VSS HC-Pro (HELPER COMPONENT-PROTEINASE) protein, which also sequesters sRNA duplexes, and causes dose-dependent viral symptoms correlated with HC-Pro expression (Bazzini et al., 2007; Shiboleth et al., 2007).

TuMV inoculations were made by infecting two leaves of 21-day-old wild-type (Col) plants. Three weeks post inoculation, the infected rosettes developed symptoms including upwardly-folded and twisted leaves, exaggerated serrations of leaf edges, and accelerated senescence of the older leaves (Figure 3.6, A). To explore the impact of TuMV infection on miR159-*MYB* pathway, transcript levels of *TuMV*, *MYB33/65* and *CP1* were analysed in the TuMV-infected Col rosettes by qRT-PCR (Figure 3.6, B). The results showed that compared with uninfected plants (mock control, inoculated with Na_2PO_4 buffer, Figure 3.6), *MYB33/65* mRNA levels were higher in the TuMV-infected plants (*MYB33*: increased 2-3 fold; *MYB65*: increased 5-9 fold); and moreover the *MYB33/65* mRNA increases strongly correlated with the transcript level of *TuMV* (Figure 3.6, B). Since the higher TuMV transcription indicates higher expression of HC-Pro protein, this strong correlation between *TuMV* and *MYB33/65* transcript levels supports that the disrupting effect of HC-Pro expression on miR159 activity is likely dose dependent. Consistent with their possible de-regulation, *CP1* mRNA level was also increased (4-10 fold) in these infected rosettes. However, the increases in *CP1* mRNA level were not strictly correlated with that of *MYB33/MYB65* or *TuMV* transcript levels (Figure 3.6, B).

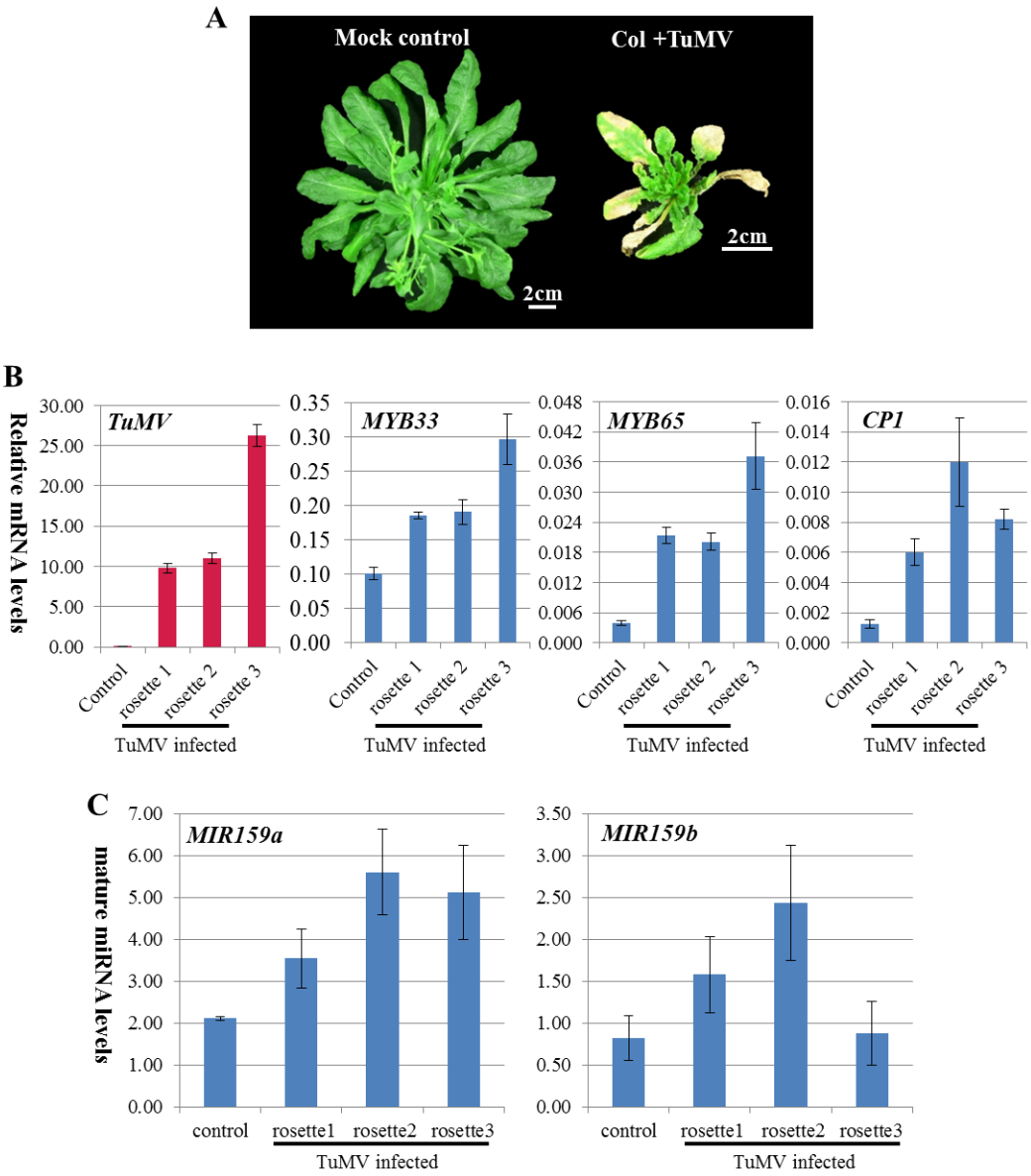

Figure 3.6 TuMV infection perturbed miR159 activity in *Arabidopsis* rosettes. (A) TuMV infection induced clear symptoms on 56-day-old rosettes. 35-day-old plants were inoculated with either Na_2PO_4 (buffer to prepare TuMV solution, mock) or TuMV solution. Representative photos were taken after another three-week incubation (short-day 8h light/16h dark, 21°C). (B) qRT-PCR analysis of relative mRNA accumulations in rosettes with TuMV-symptoms. RNA samples were extracted from individual rosette with control or TuMV-induced phenotypes as presented in (A), control: rosettes of mock plants. All mRNA levels were normalized to *CYCLOPHILIN*. Error bars represent the SD of three technical replicates of this assay. (C) Analysis of mature miR159 levels in TuMV-infected rosettes. miRNA Taqman assays were performed on the same RNA samples used in (B). The miR159 levels were normalized to *sno101*. Error bars represent the SD of three technical replicates of this assay.

Finally, the abundance of mature miR159a/b were measured in the TuMV-infected rosettes by Taqman microRNA Assays (Applied Biosystems), and found to accumulate to higher levels in TuMV-infected rosettes (Figure 3.6, C). As the VSS HC-Pro sequestrates sRNA duplexes, this increase of miR159 steady-state level might reflect an accumulation of inactivated form of miR159 (Reyes and Chua, 2007), and hence could be seen as being consistent with the possible de-regulation of *MYB33/65* in the above analysis. Thus, taken together, these data suggest that viral infection can perturb miR159 activity, leading to activation of the *MYB33/65* pathway.

3.2.7 TuMV infection at lower temperature does not enhance inhibition of miR159 function

There is evidence that low temperature inhibits the plant RNAi defence against viral infections (Szittya et al., 2003; Chellappan et al., 2005b; Várallyay et al., 2010). In *Arabidopsis*, it has also been observed that at 15℃ (instead of 21℃) the activity of siRNA-mediated RNA silencing is attenuated (Szittya et al., 2003), which may facilitate a viral infection. Therefore, it was examined whether incubation of the TuMV infection at a lower temperature can perturb miR159-mediated silencing even further. Accordingly, the viral infection was modified by growing the TuMV-infected plants for seven days at lower temperature (15℃), following two weeks of post-inoculation at the standard temperature (21℃). Again, the infected plants displayed typical TuMV symptoms at varying severity levels, which could be classified as mild or severe with respect to the rosette size (Figure 3.7, A). qRT-PCR analysis found that *TuMV* RNA accumulated to higher levels in the rosettes classified with severe symptoms (Figure 3.7, B). However, this RNA level is comparable to the level which had been achieved in

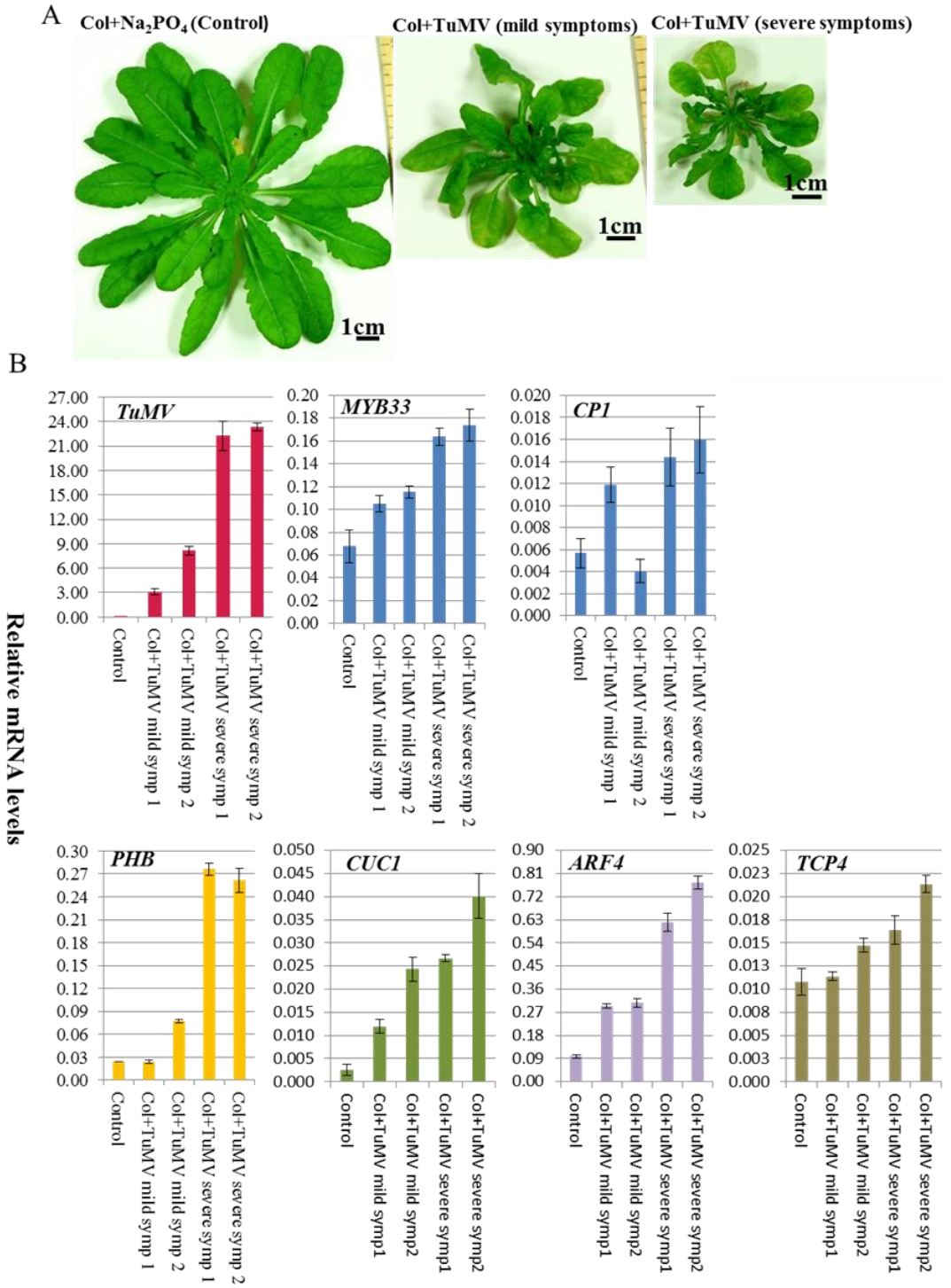

Figure 3.7 Low-temperature incubation does not strongly enhance TuMV infection or inhibition of miR159. (A) Representative classification of symptom severities among TuMV-infected rosettes. (B) Molecular analysis of relative mRNA levels in rosettes with classified symptoms. 29-day-old rosettes were inoculated with either TuMV or Na_2PO_4 solution (mock control), and put back into the growth chamber of 21℃ for 14 days (8h light/16h dark), then were grown under 15℃ for the last week (8h light/16h dark). mRNA levels were normalized to that of *CYCLOPHILIN*. Error bars represent the SD of three technical replicates of this assay.

TuMV infected rosettes under standard conditions (21℃, Figure 3.6, B). Additionally, the fold changes of *MYB33* and *CP1* mRNA levels were no greater than those induced by previous infections carried out under standard conditions. Thus, both the morphological and molecular data indicated that the TuMV infection triggered similar inhibitions of miR159 function under different growth temperatures. This suggests that the impact of TuMV infection on the miR159-MYB pathway is not stronger under a favourable cold-temperature condition.

3.2.8 Other miRNA pathways are possibly strongly disturbed by TuMV infection

To assess the impact of TuMV infection on other miRNA systems, the mRNA levels of canonical miRNA targets: *PHABULOSA* (*PHB*; miR165/166 target), *CUP-SHAPED COTYLEDON 1* (*CUC1*; miR164 target), *AUXIN RESPONSE FACTOR 4* (*ARF4*; miR390 target) and *TCP FAMILY TRANSCRIPTION FACTOR 4* (*TCP4*; miR319 target), were measured by qRT-PCR. Interestingly, the mRNA levels of *PHB*, *CUC1* and *ARF4* were found to increase approximately 8-15 folds in the same rosette samples showing severe TuMV defects (Figure 3.7, B). These were higher fold-increases than that of *MYB33* (~2.5 fold, Figure 3.7, B), suggesting stronger inhibitions of the corresponding miRNAs. Conversely, *TCP4* mRNA level showed a mild increase (~2 fold) similar to that of *MYB33*, which is likely due to the low expression and activity of miR319 in the rosette tissue (Warthmann et al., 2008; Neg et al., 2009), where inhibition of miR319 would not result in a drastic up-regulation of *TCP4*. Therefore, these data together suggested that in comparison with miR159, other miRNA pathways (e.g. miR164, miR165 and miR390) might be more responsive to the TuMV infection and contribute stronger to the observed symptoms.

3.2.9 *MYB33/65* does not strongly impact TuMV viral symptoms

It was worth noting that the increase of *CP1* mRNA level in TuMV-infected rosettes was comparable to that in the rosettes of 17-β-estradiol treated *XVE-MIM159* transformants (Figure 3.3, C). This may indicate similar biological/morphological outcome, where *XVE-MIM159* transformants developed mild curliness on a few well-established leaves (Figure 3.3, B). Thereby, to address the possible involvement of this *MYB* de-regulation in the manifestation of TuMV pathogenesis and symptoms, a comparison of TuMV-infected Col and *myb33.myb65* plants was performed (Figure 3.8). Both TuMV-infected Col and *myb33.myb65* plants developed similar abnormal leaves and rosettes that appeared indistinguishable from one another [Figure 3.8, (1) and (2)]. Considering the expression of *MYB33/65* promotes PCD in the tapetum of anthers and aleurone cells of seeds (Millar and Gubler, 2005; Alonso-Peral et al., 2010), trypan blue staining was performed on TuMV infected leaves to detect whether viral infection could accelerate the cell death process in TuMV-infected Col but not in TuMV-infected *myb33.myb65*, as the latter plant will not express the MYB33/65. However, the results revealed that the dead cells on TuMV-infected Col leaves were only detectable in trace amounts, and did not appear different from that of TuMV-infected *myb33.myb65* leaves [Figure 3.8, (3)]. Therefore, no evidence of enhanced PCD in TuMV-infected Col rosettes could be found, which supports the observation that there were no obvious differences in the symptoms that developed in TuMV-infected Col and *myb33.myb65* plants. Taken together, the suggestion can be made that the expression of MYB33/65 does not strongly contribute to rosette morphological defects induced by TuMV infection.

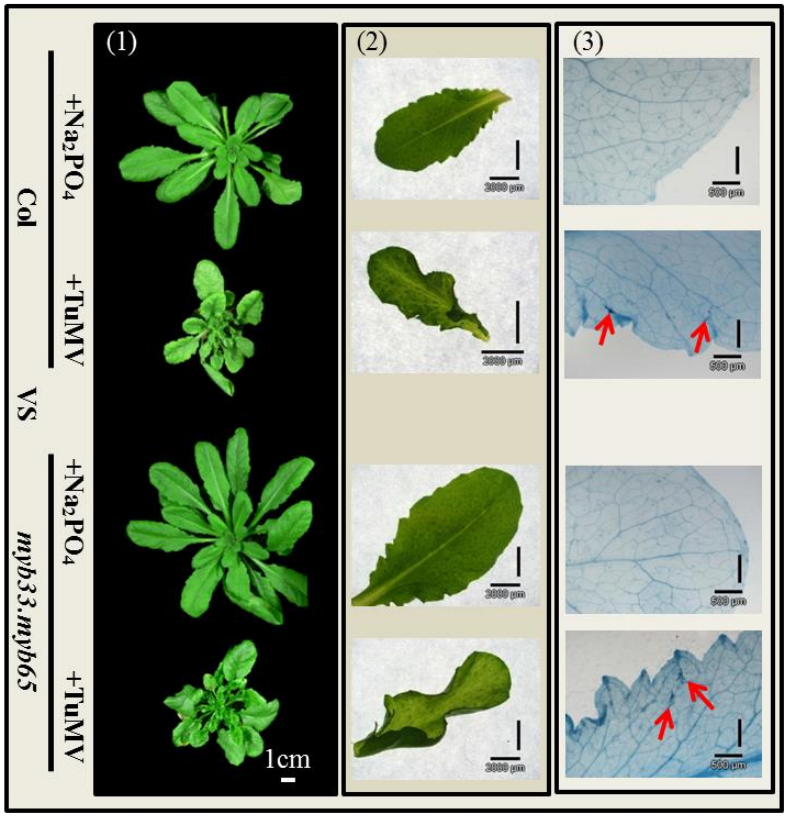

Figure 3.8 *MYB33/65* does not strongly impact TuMV viral symptoms. (1) Morphological comparison between TuMV-infected Col and *myb33.myb65* rosettes of 42-day-old (21-day-post infection). Plants applied with Na_2PO_4 are the mock controls; (2) A close-up of their leaves with same developmental age. (3) Comparison of trypan-blue staining patterns on these leaves. Red arrows indicate the dead or dying cells stained by trypan-blue in dark blue. Similar trace amount of stained cells were detected on both TuMV-infected Col and *myb33.myb65* leaves.

3.3 Discussion

3.3.1 MYB33 and MYB65 are co-regulators with different efficacies in regulating rosette morphology

In this study, *mir159ab* mutants were generated with homozygous or heterozygous combinations of *myb33* and *myb65* alleles (Figure 3.1), and a strict correlation was observed between *MYB* alleles and *mir159ab* rosette defects – the reductions of rosette size and leaf hyponasty. In addition, either one or two alleles of *MYB33* induced more severe rosette defects than either one or two alleles of *MYB65* respectively, indicating that endogenous *MYB33* expression could play a stronger role in the rosette tissue than *MYB65*. This might also explain why the *BXL2* transcription is more tightly correlated to *MYB33* alleles as shown in Figure 3.1. Thus, one suggestion that can be drawn from these data is *MYB33* and *MYB65* have similar functional roles in rosette, but with different efficacies, where *MYB33* appears to be stronger.

3.3.2 miR159-medidated silencing of *MYB33/65* is constitutive, ubiquitous and functionally active during rosette development

It is suggested that the *MYB33/65* expression promotes PCD processes during the anther and seed development (Kaneko et al., 2004; Millar and Gubler, 2005; Aya et al., 2009; Alonso-Peral et al., 2010). It is also reported that the regulation of *TCP* transcription factors by miR319 family, which is highly related to miR159 in sequence (Li et al., 2011b), negatively regulates leaf growth and positively regulates leaf senescence (Schommer et al., 2008). With these facts in mind, one may hypothesize that the miR159-*MYB* pathway in rosette tissues can mediate some PCD-related process during rosette development, such as senescence. If this is the case, the miR159-mediated

silencing of MYB expression maybe assumed to facilitate rosette development by having a specific spatial and temporal expression pattern. This would then be similar to other plant miRNAs that are known to control rosette development (e.g. miR164, miR319, miR396, miR156 and miR172), in which they regulate their targets in specific spatiotemporal manners (Sieber et al., 2007; Poethig, 2009; Wu et al., 2009; Wang et al., 2011b; Schommer et al., 2012).

However, via the time-course transcript profiling and GUS-staining assays, it was revealed that miR159 is strongly and constitutively expressed throughout rosette development, which resulted in constant silencing of MYB33/65 expression. More specifically, the constitutive staining pattern of *MIR159b:GUS* rosettes uncovered the constitutive transcription of *MIR159* throughout rosette development (Figure 3.2); and the constant high levels of mature miR159a/b detected by time-course qRT-PCR supported their constant strong expression (Figure 3.2). Though the abundance of mature miR159b was relatively variable, with the lowest level appearing in ten-day-old rosettes (Figure 3.2), it would not influence the complete inhibition of MYB33/65 expression in rosettes. This is based on the genetic and molecular evidence that *Arabidopsis* miR159 is made in great excess to silence MYB expression (Rajagopalan et al., 2006; Fahlgren et al., 2007); and the predominant forms miR159a and miR159b function redundantly, where either isoform can efficiently silence the MYB33/65 expression to biologically insignificant levels (Allen et al., 2007). Moreover, the *CP1* mRNA levels remained low throughout rosette development, strongly supporting the notion that MYB33/65 expression is constitutively silenced in rosettes. Consequently, one may conclude that at no developmental time point does MYB33/65 expression occur in rosettes. Additionally, it was observed that all rosette cells of *MIR159b:GUS*

plants, at all the tested time points, expressed GUS activity (Figure 3.2). This indicates that miR159 expression is ubiquitous both spatially and temporally throughout rosette development, and so is unlikely to make a contribution to cell differentiation of the rosette tissue. Therefore, in sharp contrast to other miRNAs that control developmental processes, the miR159-mediated silencing of *MYB* expression does not facilitate normal rosette growth or development, at least under normal laboratory growth condition.

Next, via an inducible expression of the *XVE-MIM159* transgene it was proved that the *MYB33/65* had an impact on rosette morphology only when miR159 function was strongly inhibited. This suggests that the constant miR159 activity is functionally active in regulating the rosette morphology. Thus as an alternative hypothesis, the miR159-*MYB* module may be responsive to some environmental stimuli (e.g. biotic/abiotic stress), which if is able to inhibit miR159 activity, the de-regulation of *MYB33/65* expression will be resulted and a functional outcome will be manifested in rosettes. Therefore, finding the stimuli that can inhibit the miR159 activity was the next direction for finding the role of miR159-*MYB* module in the rosette tissue.

3.3.3 The miR159-*MYB* pathway does not strongly contribute to plant symptoms induced by VSS expression or viral infection

Over 30 VSS proteins have been discovered from both RNA and DNA viruses (Li and Ding, 2006), and have been well known for their activities in sequestration of RNA intermediates produced during siRNA/miRNA biogenesis (Lakatos et al., 2006; Ding and Voinnet, 2007). For instance, VSS protein P19 of *Tomato Bushy Stunt Virus* binds to short (19–21 nt) siRNA/miRNA duplexes in a 1:1 stoichiometric ratio (Stav et al.,

2010), and VSS protein HC-Pro of TuMV also sequestrates the siRNA/miRNA duplexes (Wu et al., 2010). Besides that, some VSS proteins inhibit functions of essential RNAi factors, such as the VSS protein P0 that promotes the ubiquitination and subsequent degradation of AGO1 protein (Pazhouhandeh et al., 2006; Bortolamiol et al., 2007; Csorba et al. 2010), and present in several viruses (e.g. *Beet Western Yellows Virus*, *Sugarcane Yellow Leaf Virus* and *Cereal Yellow Dwarf Virus*) (Pazhouhandeh et al., 2006; Bortolamiol et al., 2007; Mangwende et al., 2009). Therefore, by overexpressing the VSS proteins, P19 and P0, the abundance of active miRNAs and AGO1 protein complexes should be reduced respectively, triggering a general perturbation of plant miRNA pathways.

Previous studies reported that P0 expression could perturb miR159 function in *Arabidopsis* rosettes. Bortolamiol et al. (2007) generated *XVE-P0* transgenic *Arabidopsis* plants, which displayed an increase in *MYB65* mRNA levels upon induction of P0 expression. Additionally, Csorba et al. (2010) demonstrated that the P0-mediated destabilization of AGO1 protein could cause the accumulation of miR159 in an AGO1-free fraction, indicating that the assembly of effective miR159-AGO1 complexes was impeded by P0 activity. However, in this thesis, it was found that even in the transgenic plants with the most severe P0-symptoms, the *CP1* up-regulation was markedly milder in comparison with that of *mir159ab* (Figure 3.5). Moreover, similar P0 expression levels in *35S-P0*(Col) and *35S-P0*(*myb33myb65*) plants triggered identical symptoms, indicating that the up-regulated expression of MYB33/65 in *35S-P0*(Col) was not enhancing or alleviating the P0-induced symptoms. Therefore, this study strongly suggests that if P0 expression is perturbing miR159-mediated silencing

of MYB expression in rosettes, this perturbation was probably mild and insufficient to activate the *MYB* pathway to make a discernable contribution to P0-induced symptoms.

This was further supported by the TuMV infection experiment, where the VSS HC-Pro protein of TuMV perturbs the miRNA biogenesis via binding with the sRNA duplexes (Bazzini et al., 2007; Shiboleth et al., 2007). Although TuMV infection resulted in symptoms on rosettes similar to that of *mir159ab* defects (i.e. reduced rosette size and increased leaf curl), TuMV induced defects in Col and *myb33.myb65* plants were phenotypically indistinguishable (Figure 3.8), despite the up-regulation of MYB33/65 expression and the increased *CP1* mRNA levels in Col (Figure 3.6 and 3.7). This again suggests that the perturbation of miR159 activity by VSS-mediated sequestration of sRNA duplexes is not sufficient to be causative of TuMV symptoms.

Regarding previous evidence suggesting perturbation of miR159 function by VSS expression or virus infection (Chellappan et al 2005a; Reyes and Chua, 2007; Ho et al., 2010; Ohshima et al., 2010; Naqvi et al., 2010; Du et al., 2014), the phenotypic and molecular comparison between VSS-transgenic/virus-infected Col and *myb33.myb65* mutants have rarely been made. Results from this thesis imply that if a thorough conclusion on biological importance of miR159 perturbation is to be made, such a comparison is required. Recently, Du et al. (2014) reported a possible causative role of miR159 in disease symptoms induced by a *Cucumber Mosaic Virus* (i.e. Fny-CMV), as they compared the Fny-CMV infected Col and *myb33.myb65*, showing phenotypic evidence that the infected Col plants displayed more deformation of the upper, young systemically infected leaves. Based on this, they concluded that miR159 contributes to

Fny-CMV induced symptoms (Du et al. 2014). However, molecular analysis to verify the phenotypic analysis, by measuring *MYB* and *CP1* mRNA levels would have supported such claims, especially since viral infection is complex that displays a wide variability in symptoms.

3.3.4 miR159 appears less sensitive than other miRNAs to viral infection

As VSS proteins interfere with common effectors/biogenesis steps of miRNA pathways, these pathways will all be equally effected (Chapman et al., 2004; Voinnet, 2005; Dunoyer and Voinnet, 2005; Díaz-Pendón and Ding, 2008). However, given that miR159 is one of the most abundant miRNAs in the rosette tissue, which can efficiently inhibit *MYB* expression even at low levels (Rajagopalan et al., 2006; Allen et al., 2007), it is reasonable to consider that miR159 is less sensitive to VSS activity than many less abundant miRNAs. This is supported by the observation that the function of several other miRNA appeared to be more strongly inhibited under the same TuMV infection (i.e. miR164, miR165, miR390, Figure 3.7), suggesting differences in sensitivities of miRNAs to viral infection. This, as well as the suggestion that many relatively lowly expressed miRNAs can be essential for plant growth of which strong inhibitions would result in plant lethality (Schommer et al., 2012), may imply that the cell may die before miR159 can be strongly inhibited.

However, the possibility cannot be excluded that there is a VSS that preferentially perturbs miR159 function, like the identified viral impact on miR168 accumulation (Várallyay et al., 2010). In addition, the complexity of viral pathogenesis should not be ignored since it is usually accompanied with multifactorial stresses (e.g. combined

drought, heat and viral stress) in the natural environment. These additional stresses may considerably influence the plant-virus interaction (Prasch and Sonnewald, 2013), and possibly miR159 function to result in a morphological outcome. Considering these possibilities, it can only be cautiously concluded that the miR159 silencing of MYB expression is extremely robust in *Arabidopsis* rosettes and is unlikely to be perturbed by viral stress under laboratory condition. Whether there are other stresses that can strongly perturb the miR159 activity to induce a morphological effect still requires more in-depth research.

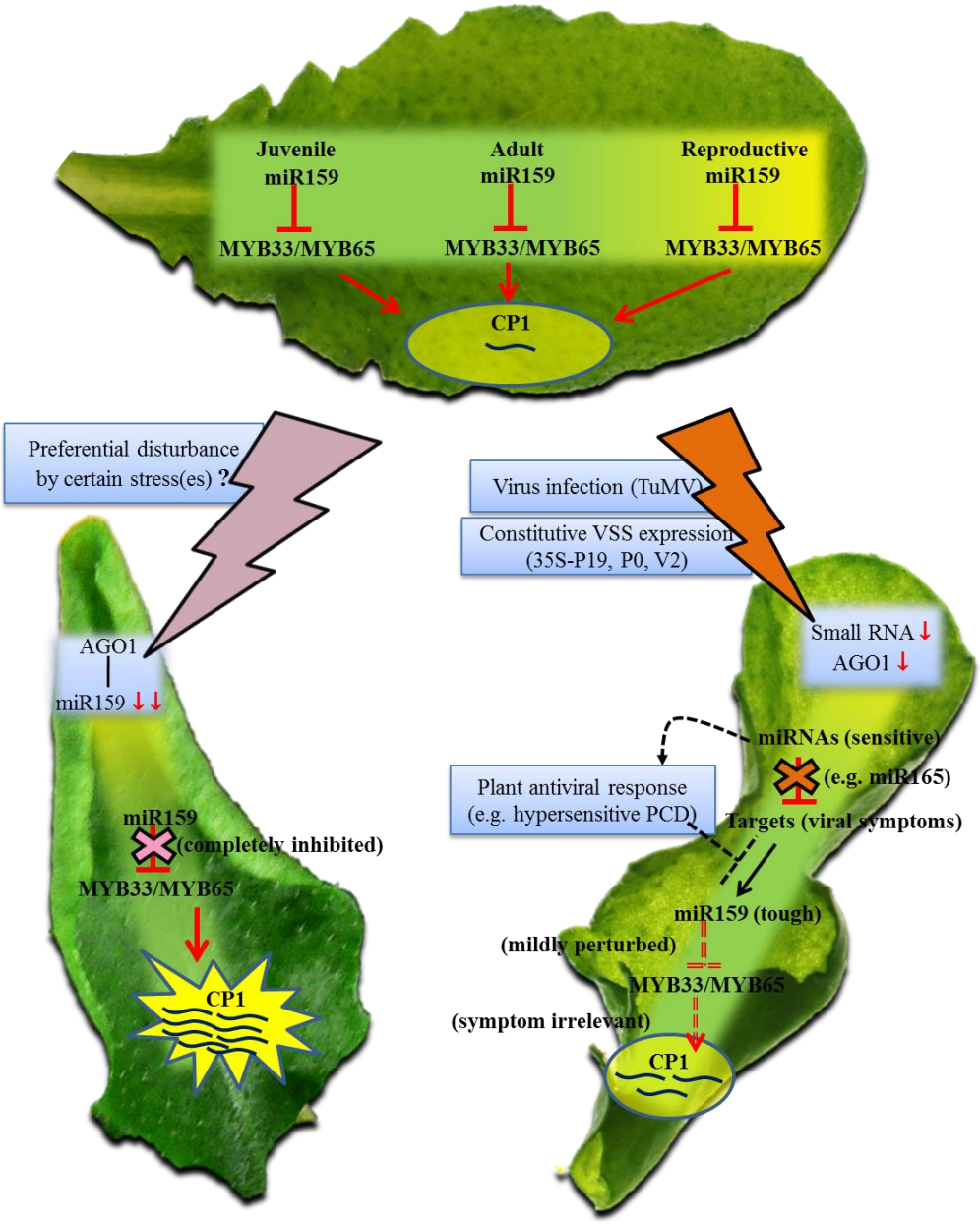

Figure 3.9: Summary diagram of functional analysis of miR159-*MYB* module in *Arabidopsis* rosette. During rosette development under normal growth condition, the miR159 mediates constitutive silencing of MYB33/65 expression, as indicated by the constantly low *CP1* transcription. The viral infection (TuMV) and VSS expression that induce a reduction of either active miRNA or AGO1 abundance, can perturb the function of sensitive miRNAs (e.g. miR165) and trigger the rosette symptoms. However, these viral impacts on miR159 activity appeared mild, likely due to miR159 is less sensitive to the same viral stress. Considering the great abundance and efficiency of miR159 in rosette tissue, it is hypothesized that the perturbation of other less abundant miRNAs may be sufficient to trigger a cell death before the miR159 activity being strongly perturbed. This points out the next research focus, that is if there is any stress(es) that can specifically and strongly perturb the miR159 activity, to trigger the corresponding biological response (i.e. rosette defects and *CP1* up-regulation)

Chapter 4

An EMS-based *mir159ab* revertant screening identified an unusually high frequency of mutations impacting *MYB33/65* expression

4.1 Introduction

It has been known that the number of genes targeted by a plant miRNA is at least an order of magnitude lower than that targeted by an animal miRNA, which is perhaps due to the high complementarity requirement for a plant miRNA-target interaction (Schwab et al., 2005, Jones-Rhoades et al., 2006; Palatnik et al., 2007). More than that, as defined by loss-of-function genetic analysis, the number of targets that are subjected to functionally relevant plant miRNA regulation appears even smaller than the number of plant miRNA targets predicted by complementarity-based bioinformatic programs, which may reflect the existence of other regulatory constrain(s) for modulating the plant miRNA-target relationship (e.g. target mRNA accessibility, or specific RNA-binding protein; reviewed by Li et al., 2014). For instance, most conserved plant miRNAs only appear to regulate a few target genes that correspond to a single paralogous family, and these miRNA-target relationships are usually evolutionarily conserved (Li et al., 2014). Therefore, to gain insight into the functions of these plant miRNAs, analysing the roles of their specific targets may help to elucidate the pathways these miRNAs are involved in and their functional roles.

As one of the most conserved plant miRNA modules, miR159-mediated regulation has been found to be restricted to a family of genes encoding GAMYB or GAMYB-like transcription factors that share a highly conserved miR159-binding site (Rhoades et al., 2002; Achard et al., 2004; Millar and Gubler, 2005; Tsuji et al., 2006). In *Arabidopsis*, two *GAMYB*-like genes, *MYB33* and *MYB65* have been identified as the major functionally relevant targets of miR159, since not only the widespread de-regulation of these two *MYB*s was detected in most tissues of a loss-of-function *mir159* mutant (*i.e. mir159ab*, miR159a and miR159b are the two most abundant forms in *Arabidopsis* as found by deep sequencing,

Fahlgren et al., 2007), but also all the developmental defects of *mir159ab* were suppressed in a *mir159ab.myb33.myb65* quadruple mutant (Allen et al., 2007). However, the functional reason behind why these *MYB* target genes are strongly transcribed in rosette tissues, only to be then fully silenced by miR159 is unknown.

To address this, elucidating the role of *MYB33* and *MYB65* in rosettes can be the first step. The *GAMYB* transcription factor has been implicated in gibberellin (GA) signal transduction in cereal aleurone, as its expression is positively regulated by GA (Gubler et al., 1995; Gubler et al., 2002; Zentella et al., 2002; Woodger et al., 2003). However, in *Arabidopsis*, there have been conflicting reports regarding miR159-*MYB* involvement in GA signal transduction. At first, Achard et al. (2004) have reported that GA enhances both miR159 abundance and *MYB33* transcript level, which appeared important for modulating floral development. By contrast, Alonso-Peral et al. (2010) reported that miR159 abundance and *MYB33* and *MYB65* mRNA levels all remain unchanged after GA application, suggesting this module is not involved in GA-mediated processes for rosette development or for mediating the floral transition. Similarly, Reyes and Chua (2007) could not detect any GA-response of *MYB33* and miR159 RNA levels during seed germination. Instead, the phytohormone abscisic acid (ABA), with antagonistic roles to GA, was shown to induce miR159 abundance during seed germination. Therefore, whether the *Arabidopsis* miR159-*MYB* module interacts with GA and/or ABA signaling pathway remains unclear. Besides that, a miR159-miR167-miR319 regulatory circuit has recently been reported, where the miR159-*MYB* and miR319-*TCP* nodes coordinate to regulate the miR167-*ARF* node, responsible for several checkpoints in floral organ maturation (Rubio-Somoza and Weigel, 2013). However, it has also been found that the miR319 is predominantly expressed in floral organs, but not leaves (Warthmann et al., 2008; Neg et al., 2009). Thus,

the possibility of miR159-*MYB* module interacting with miR319 or other miRNA module(s) in rosettes is tempting but requires supporting evidence.

As a straightforward approach analysing the role(s) of *MYB33/65*, Alonso-Peral et al. (2010) performed a transcriptomic comparison between shoot apex regions (SAR) of loss-of-function *mir159ab* and wild-type *Arabidopsis*. This has found 121 up-regulated genes in *mir159ab* SARs, which were potentially downstream of *MYB33/65*. Many of these genes were annotated hydrolases and proteases, agreeing with the suggested *MYB* function in promoting programmed cell death (PCD) in seeds and flowers (Millar and Gubler, 2005; Alonso-Peral et al., 2010). However, no experiment has verified the causative nature of these genes with regards to the morphological defects of the *mir159ab* rosettes. In addition, no enhanced PCD has been identified in the *mir159ab* rosette tissue. Thereby, it is still unknown can the gene(s) downstream of *MYB33/65* determine the *mir159ab* rosette morphology.

Here, to address above possibilities and investigate the role of *MYB33/65* in rosettes, the commonly used ethyl methanesulfonate (EMS) mutagenesis in *Arabidopsis* (Kim et al., 2006; Uchida et al., 2011) was applied on *mir159ab* seeds, aiming to identify *mir159ab* revertants in a bid to identify the causative gene(s)/pathway(s) mediating MYB33/65 activity (Figure 4.1, A). The EMS mutagen can induce chemical modification of nucleotides, resulting primarily in C/G to T/A substitutions and hence the nonbiased irreversible mutations in plant genome (McCallum et al., 2000; Henikoff and Comai, 2003). In *Arabidopsis*, the EMS-induced mutations are randomly distributed throughout the genome, which generate either loss- or gain-of-function mutants owing to alterations of certain amino acids in the proteins (Kim et al., 2006). Therefore, via screening for

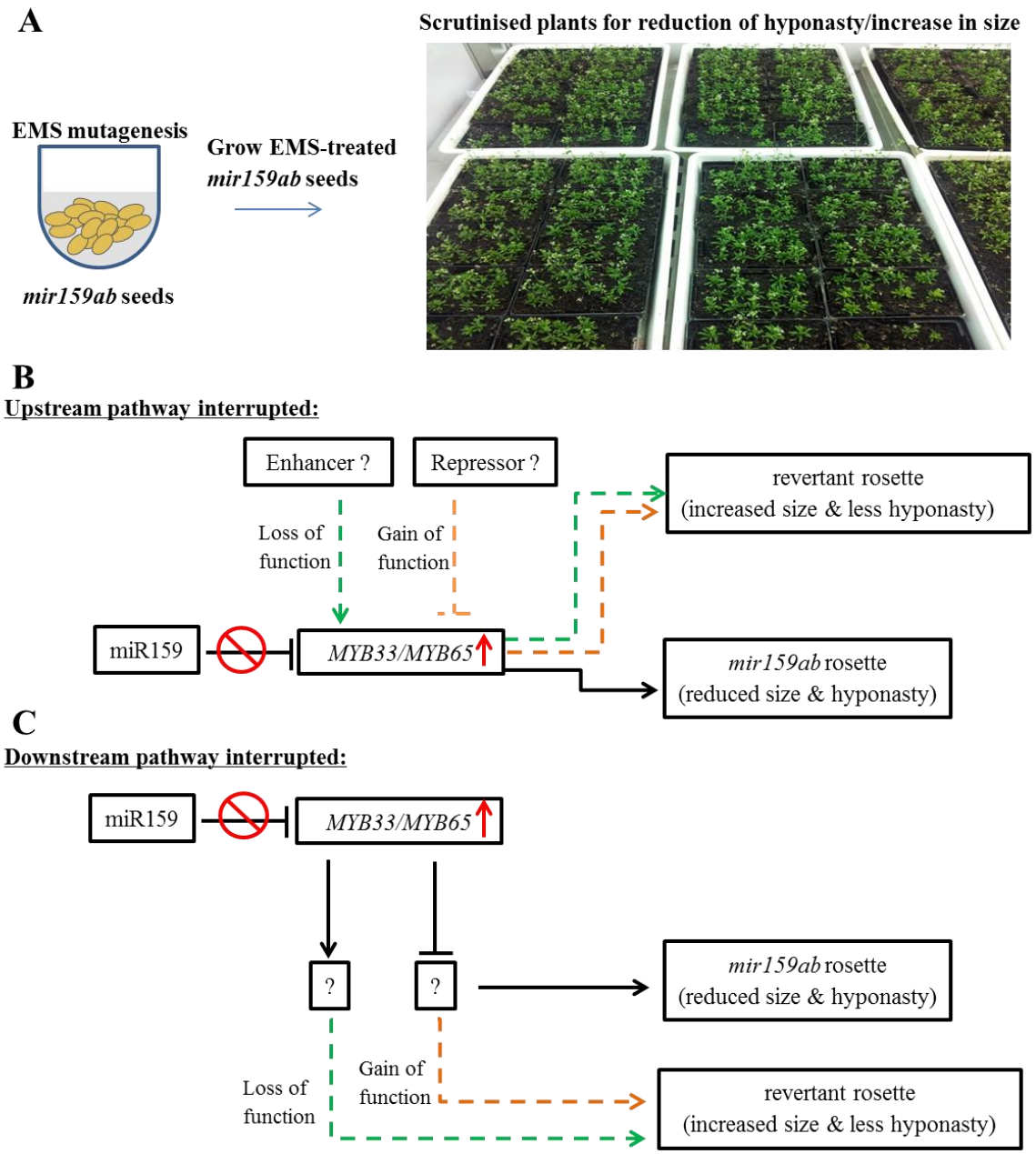

Figure 4.1 Illustration of EMS-based *mir159ab* revertant screening. A: Layout of EMS treatment and revertant screening. B and C: Hypothesized outcomes. In the *mir159ab* mutant, expression of miR159a/b has been knocked out, resulting in up-regulation of *MYB33/65* and consequent stunted rosettes with hyponastic leaves. Via the EMS treatment, both loss-of-function (green coloured) and gain-of-function mutations (orange coloured) can be introduced into genes. If the mutated gene involve in a pathway upstream of *MYB*s (e.g. enhancer or repressor) and causes down-regulation of *MYB33/65* expression (B); or downstream of *MYB33/65* that mediates MYB activity (C), it will induce a revertant rosette phenotype, namely increased size and less hyponasty. Up-arrow: up-regulation; dotted line: potential outcome.

EMS-mutant with a morphological suppression of *mir159ab* defects, the genes either upstream or downstream of *MYB33/65* expression/activity are expected to be identified (Figure 4.1, B and C). Hence, the characterization of such revertants may provide materials that will assist in identifying the pathways and processes the *MYB33/65* genes play in rosette tissues. Identifying the causative mutation(s) in these revertant mapping population via advanced deep-sequencing methods (Austin et al., 2011; Lindner et al., 2012), and elucidating these identified gene(s) should be the next steps to reveal the miR159-*MYB* function in rosettes.

4.2 Results

4.2.1 A *mir159ab.cp1* triple mutant does not suppress the *mir159ab* phenotype

Since the *CYSTEINE PROTEINASE 1* (*CP1*) is the most up-regulated gene in *mir159ab* (Alonso-Peral et al., 2010), and it may be an important protease promoting PCD (Lee et al., 2004; Li et al. 2006), a *mir159ab.cp1* triple mutant was generated to investigate whether *CP1* is a causative gene mediating *mir159ab* rosette defects. First, a *cp1* T-DNA insertional mutant was obtained from the SALK collection (SALK_051510). Verified by sequencing using left border primer of the T-DNA insertion (i.e. LBb1, refer to appendix file 2 for primer sequence), the position of the T-DNA insertion site was located to the third intron, 16 bp downstream of exon 3 of *CP1* gene (Figure 4.2, A). As a partial CP1 protein can still be made, it was critical to assess to what extent the *CP1* transcription was disrupted by the T-DNA insertion via qRT-PCR analysis.

The triple mutant *mir159ab.cp1* was generated by crossing *mir159ab* with the above *cp1* mutant. A homozygous *mir159ab.cp1* triple mutant was identified via genotyping (Figure 4.2, B), and progenies of this *mir159ab.cp1* line were then grown side by side with *mir159ab* and wild-type Col plants to determine the impact of introducing the *cp1* mutation. Based on qRT-PCR analysis, the *CP1* mRNA was in great abundance in the original *mir159ab* mutant, but reduced to an undetectable level in the *mir159ab.cp1* mutant, which is even lower than that in the wild-type Col (Figure 4.2, C). This indicates the severely disrupted *CP1* transcription in the *mir159ab.cp1* mutant, but the limitation of this qRT-PCR result should be acknowledged that the qRT-PCR primer pair is designed around the 3'downstream region of *CP1* (Figure 4.2, A), which cannot tell if the upstream mRNA potion can be made, hence qRT-PCR analysis using other *CP1* primer pairs upstream of the T-DNA insertion site may be required to address this concern.

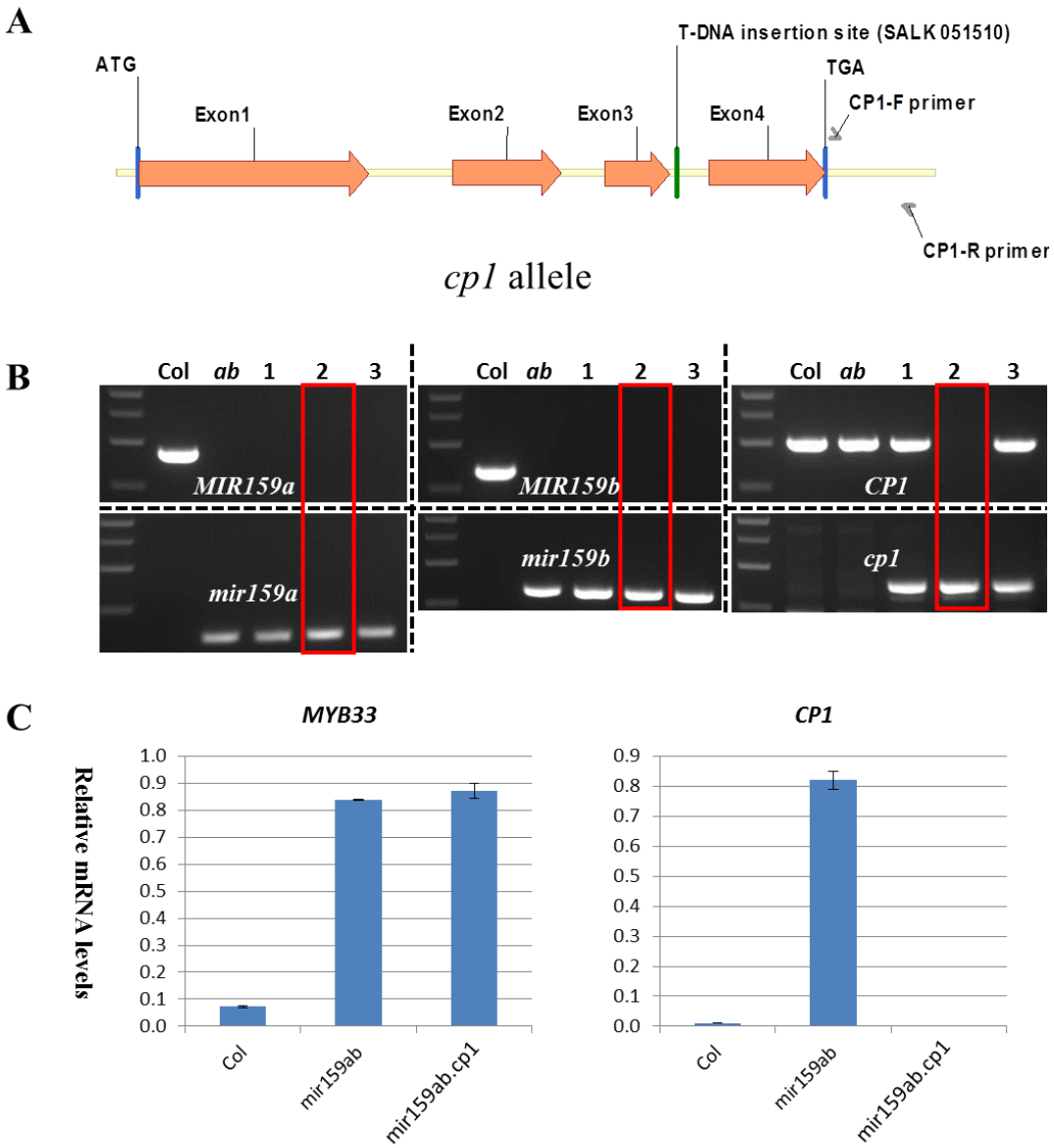

Figure 4.2 Generation and analysis of a *mir159ab.cp1* triple mutant. (A) Illustration of the location of T-DNA insertion in a *cp1* mutant allele (SALK_051510). CP1-F and CP1-R primers were designed around the 3' downstream region of *CP1* to perform qRT-PCR analysis. (B) Identification of *mir159ab.cp1* triple mutant via PCR genotyping. The F2 progenies of a *mir159ab* × *cp1* cross, were genotyped for T-DNA-insertional alleles of *MIR159a*, *MIR159b* and *CP1*. Genomic DNA samples extracted from Col and *mir159ab* were used as controls. The identified homozygous *mir159ab.cp1* triple mutant was marked in red box (i.e. Plant No. 2). DNA bands present on top panel of gels indicate relative wild-type alleles, while those on the bottom panel of gels indicate corresponding T-DNA inserted alleles. (C) Analysis of *MYB33* and *CP1* mRNA levels in the *mir159ab.cp1* triple mutant and control plants. For every genotype, RNA samples were extracted from five rosettes of four-week-old plants. All mRNA levels were normalized with *CYCLOPHILIN* (At2g29960). Measurements are the average of three technical replicates. Error bars represent the SD.

In a phenotypic comparison, *mir159ab.cp1* had a leaf-curl phenotype indistinguishable from that of *mir159ab* (Figure 4.3, A). Moreover, as determined using a Lemna Tec Scanalyzer (Figure 4.3, B), there is no significant difference between *mir159ab* and *mir159ab.cp1* plants in the phenotypic trait of rosette compactness (Student's T-Test: P = 0.44182); though the rosette size of *mir159ab.cp1* was slightly bigger than that of *mir159ab* (Student's T-Test: P = 0.04611), the rosette of Col is more than 10 fold bigger than both of these mutants, suggesting the decreased *CP1* mRNA level cannot induce a major recovery of the *mir159ab* rosette size. Therefore, the results indicate that the up-regulated *CP1* mRNA in *mir159ab* is not the absolute cause of the leaf-curling phenotype.

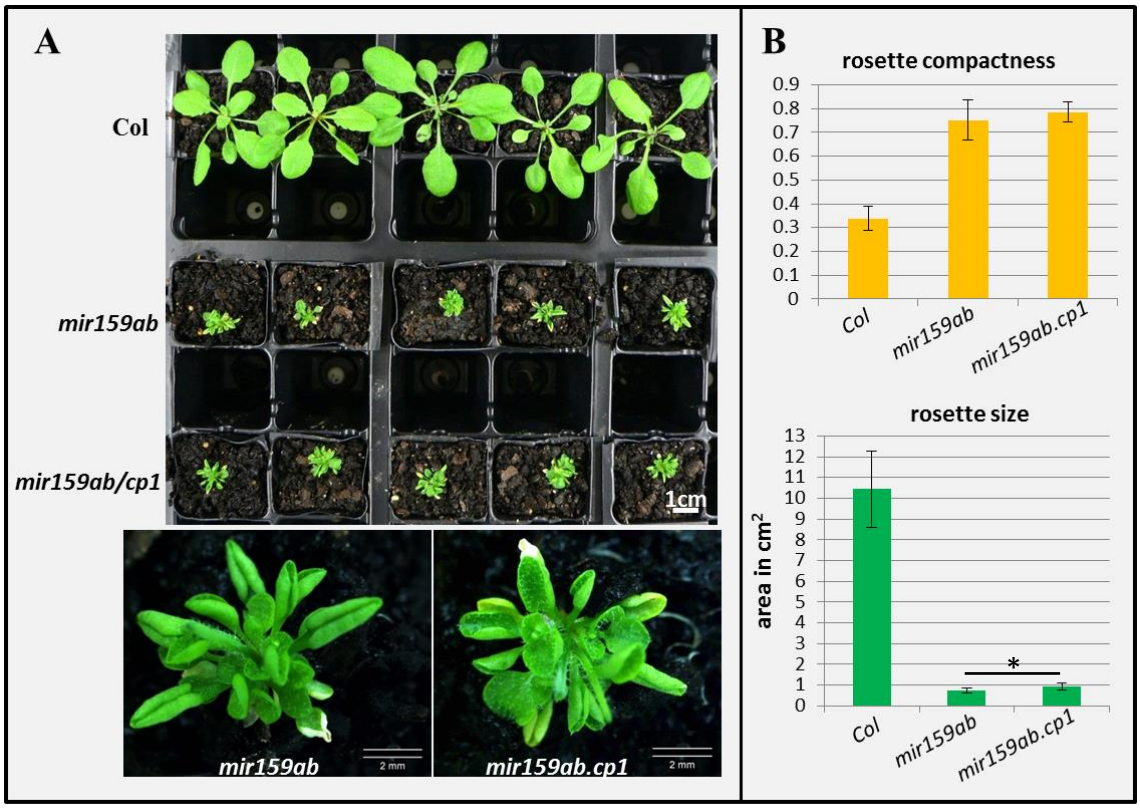

Figure 4.3: Morphological analysis of the *mir159ab.cp1* triple mutant. (A) Aerial view of four-week-old rosettes of wild-type (Col-0), *mir159ab* and *mir159ab.cp1* plants. The close up comparison of *mir159ab* and *mi159ab.cp1* rosettes is shown in the bottom panel. (B) Statistical analysis of rosette compactness and size of wild-type (Col-0), *mir159ab* and *mir159ab.cp1* plants. Plants were grown under long-day condition (16h light/8h dark, 21 ℃) for four weeks. Measurements are the average of five biological replicates. Error bars represent the SEM. The symbol * indicates the significant deference of rosette size between *mir159ab.cp1* and *mir159ab* plants (Student's T-Test: P = 0.04611).

4.2.2 Identification of *mir159ab* suppressor alleles via EMS mutagenesis

To identify potential gene(s) mediating the function of miR159-*MYB* pathway in *Arabidopsis* rosettes, an ethyl methanesulfonate (EMS)-based *mir159ab* revertant screen was performed as shown in Figure 4.1 A. Here, ~5000 *mir159ab* seeds were treated with a 0.025% EMS solution, and approximately 1200 EMS treated seeds were planted in soil, which theoretically should result in a saturation mutagenesis of one mutation for every 100 bp of *Arabidopsis* genome (~ 120,000,000 bp), assuming the EMS treatment will generate ~1000 mutations in one *Arabidopsis* plant (Colbert et al., 2001; Bevan et al., 2001). EMS-mutagenized *mir159ab* seeds (M1) were then planted in soil, followed by screening for revertants which will have rosettes with larger sizes and reduced leaf curl.

Among ~1200 EMS-mutagenized *mir159ab* lines (M1), rosettes of two lines appeared larger and less hyponastic than the parent *mir159ab* (Figure 4.4). As the EMS induced mutations should be heterozygous in this M1 generation (Henikoff and Comai, 2003), M1 plants displaying partially revertant phenotypes would be predicted to carry dominant mutations. These M1 plants were allowed to self-fertilize and seeds (M2) were collected and sown. Resulting plants were screened, and the phenotypic reversions could still be observed in respective M2 generation, confirming that the mutations were inherited to the M2 generation (data not shown).

Figure 4.4: Two M1 plants developed larger and less hyponastic rosettes than *mir159ab*. The plants were photographed to show the obvious phenotypic difference between the revertant candidate and the other *mir159ab*-like M1 plants, which is likely due to a putatively dominant mutation in the revertant plant.

4.2.3 Many semi-revertant lines were identified in the M2 progenies of other M1 lines

As the EMS-mutagenized seeds result in M1 chimeric plants, which then produce the heterozygous or homozygous M2 progenies (Henikoff and Comai, 2003), more revertants were expected to be identified in the M2 generation. Initially, the seeds of M1 mutants were individually harvested and approximately 30 M2 seeds per M1 line were planted in soil. Surprisingly, of 117 individual M1 lines, 45 produced M2 plants that had clear revertant phenotypes (Table 4.1). This observation indicates an extremely high revertant frequency, where greater than one third of M1 lines could produce progenies that appeared partially reverted (termed semi-revertant), which may indicate the *MYB33/65* are extensively networked with many other genes and/or have many downstream effectors that mediate the *mir159ab* defects. Alternatively, it is also a likelihood of *mir159ab* defects being easily masked by many unrelated EMS-mutations that promote the rosette growth. Therefore, the identified phenotypic reversions of *mir159ab* defects require to be further examined by molecular analysis (see section 4.2.5 for details).

Moreover, a comparison between the number of M2s displaying revertant phenotypes and the number of M2s displaying *mir159ab* phenotype, found that at least nine M1 lines have more M2s of revertant phenotypes than the *mir159ab* phenotype (Table 4.1, indicated by red boxes). These observations suggest two possibilities: first, in one such M1 line, there are multiple recessive mutations that could induce suppression of *mir159ab* defects, so that they segregate in the M2 generation and result in revertant phenotypes when they become in homozygous status. Second, mutations in some of these M1 lines are possibly dominant, so that the M2 segregation ratios of these M1

lines are greater than the 1:3 Mendelian ratio for a recessive mutation causing reversion of *mir159ab* rosette defects. To clarify the situation, genetic analysis investigating if the nature of a causative mutation in a revertant is recessive or dominant should be performed (see section 4.2.6 for details).

M2 revertant screening mastertable

M1 line	M2 revert phenotype	# *mir159ab*-like	# revertants
RS1	yes		
RS2	yes		
RS3	no		
RS4	yes	11	18
RS5	yes	24	1
RS6	no		
RS7	yes	21	6
RS8	yes	16	4
RS9	yes	11	5
RS10	yes	7	7
RS11	no		
RS12	yes	10	8
RS13	yes	13	6
RS14	no		
RS15	no		
RS16	yes	4	10
RS17	no		
RS18	no		
RS19	no		
RS20	no		
RS21	no		
RS22/23	yes	16	2
RS24	yes	4	15
RS25	yes	6	12
RS26	no		
RS27	no		
RS28	no		
RS29	yes	14	2
RS30/31	no		
RS32	no		
RS33	no		
RS34	no		
RS35	yes	10	10
RS36	no		
RS37	yes	11	7
RS38	no		
RS39	yes	5	12
RS40/41	yes	16	1
RS42	no		
RS43	yes	28	8
RS44/45	yes	18	3
RS46	no		
RS47/48	no		
RS49	no		
RS50	yes	30	4
RS51	no		
RS52	yes	26	4
RS53	yes	17	9
RS54	yes	7	20
RS56	no		
RS57	no		
RS58	no		
RS59	yes	8	18
RS60	no		
RS61	no		
RS62	yes	4	23
RS63	no		
RS64	no		
RS65	no		
RS66	yes	30	5
RS67	no		
RS68	no		
RS69	yes	20	2
RS70	yes	15	4
RS71	no		
RS72	yes	10	5
RS73	yes	15	6
RS74	no		
RS75	yes	15	6
RS76	yes	20	3
RS77	yes	10	20
RS78	yes	20	3
RS79	no		
RS80	no		
RS81	yes	12	12
RS82	no		
RS90	yes	12	12
RS91	yes	30	1
RS92	no		
RS93	no		
RS94	no		
RS95	no		
RS96	no		
RS97	no		
RS98	no		
RS99	no		
RS100	no		
RS101	no		
RS102	no		
RS103	yes	20	6
RS104	no	30	
RS105	yes	30	2
RS106	yes	25	2
RS107	yes	15	5
RS108	no		
RS109	no		
RS110	no		
RS111	yes	20	6
RS112	no		
RS113	no		
RS114	no		
RS115	no		
RS116	yes	30	1
RS117	yes	30	5
RS118	no		
RS119	yes	20	16
RS120	no		
RS121	yes	20	2
RS122	yes	10	8
RS123	no		
RS124	yes	20	10

Total : 45 out of 117 M1 progenies developed revertant phenotypes

Table 4.1: Summary of the M2 revertant screen for 117 individual M1 lines. M1 lines are termed RS1-124 (courtesy of Rob Allen). RS1 and RS2 are the putative dominant mutations identified from M1 revertant screening. Seeds of RS83-89 lines are not available and not screened. Identified M2 revertant populations are highlighted in green. Among them, there are several lines present majorly the revertant phenotypes (red boxed), which may indicate a dominant trait of the respective mutations.

Due to the high frequency of *mir159ab* revertants, seeds of every 15 M1 lines were grouped into a M2 pool, and a total 70 M2 pools were set up, from which screening was performed on ~1000 M2 plants per pool. In this way, the following screen was aimed to maximize the number of mutagenized seeds screened, which in turn maximizes the chances of identifying revertants that most closely or even fully resemble a wild-type (Col) rosette appearance.

In early development, all the M2 plants developed *mir159ab*-like rosettes, but after two to three-weeks growth, many of the mutant rosettes appeared larger than *mir159ab*, and their younger leaves were less curled. Noticeably, some of the M2 plants even developed rosettes larger than that of wild-type, and had extended periods of vegetative growth (Figure 4.5). Since the delayed transition from vegetative phase to reproductive phase could result in increased sizes of rosettes and numerous leaves (Ding et al., 2013), it is possible that the prolonged-vegetative-growth phenotypes triggered by EMS-mutations had overwritten the *mir159ab* phenotype. Thus, to avoid the ambiguities introduced by additional mutation phenotypes, the screening of M2 pools focused on searching for rosettes that closely resemble wild-type, within a normal period of vegetative growth (4~5 week under long-day growth condition).

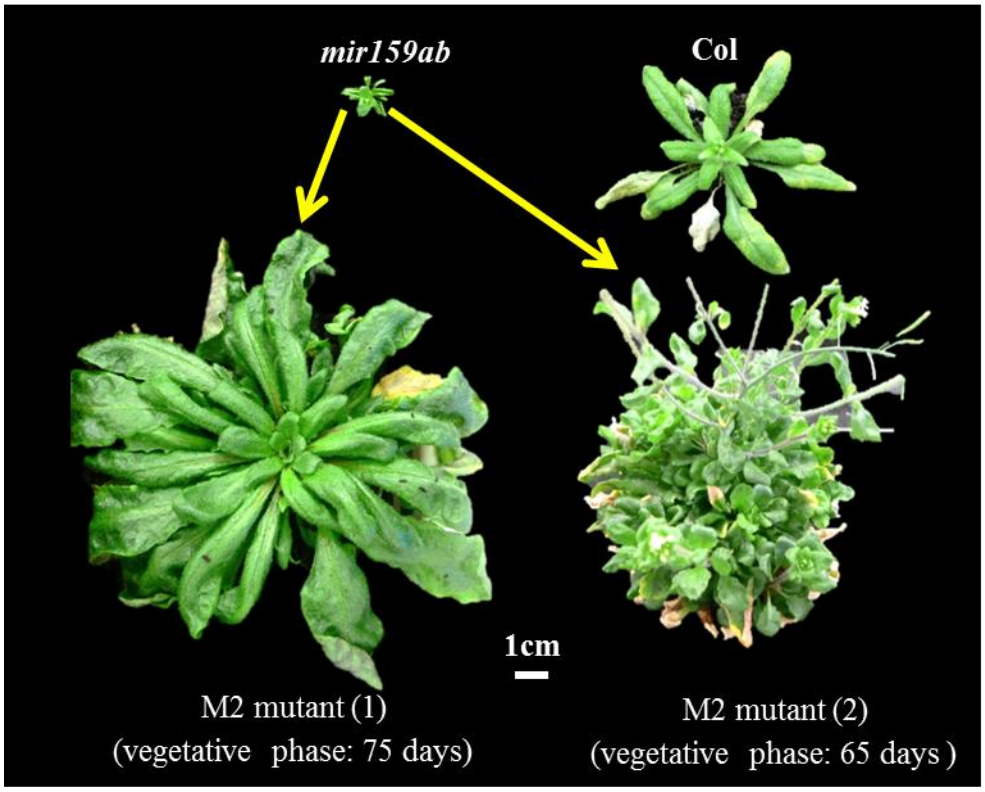

Figure 4.5: M2 mutants identified with extended vegetative growth. All plants were grown under long-day condition (16h light/ 8h dark, 21 ℃). Photos of *mir159ab*, wild-type Col and M2 mutant (1) were taken when plants were 40-day-old. The photo of M2 mutant (2) was taken when it was 80-day-old.

By a series of phenotypic comparisons, a large number of revertants were identified from the M2 pools. In most pools, there were multiple revertants which could be potential siblings, thus only one to two revertants were kept from each pool if the revertants displayed similar phenotype (i.e. rosette size and leaf hyponasty). In total, 104 M2 revertants were identified (Figure 4.6). These revertants all developed larger rosettes with leaves less curled in comparison to *mir159ab* of the same age, but none of the M2 revertants were completely wild-type in appearance. Therefore, only semi-revertants were identified from this screen. Additionally, this ruled out the possibility of these revertants had arisen via wild-type pollen contamination, as *mir159ab*-like traits are only observed when both the *mir159a* and *mir159b* loss-of-function alleles are homozygous (Allen et al., 2007).

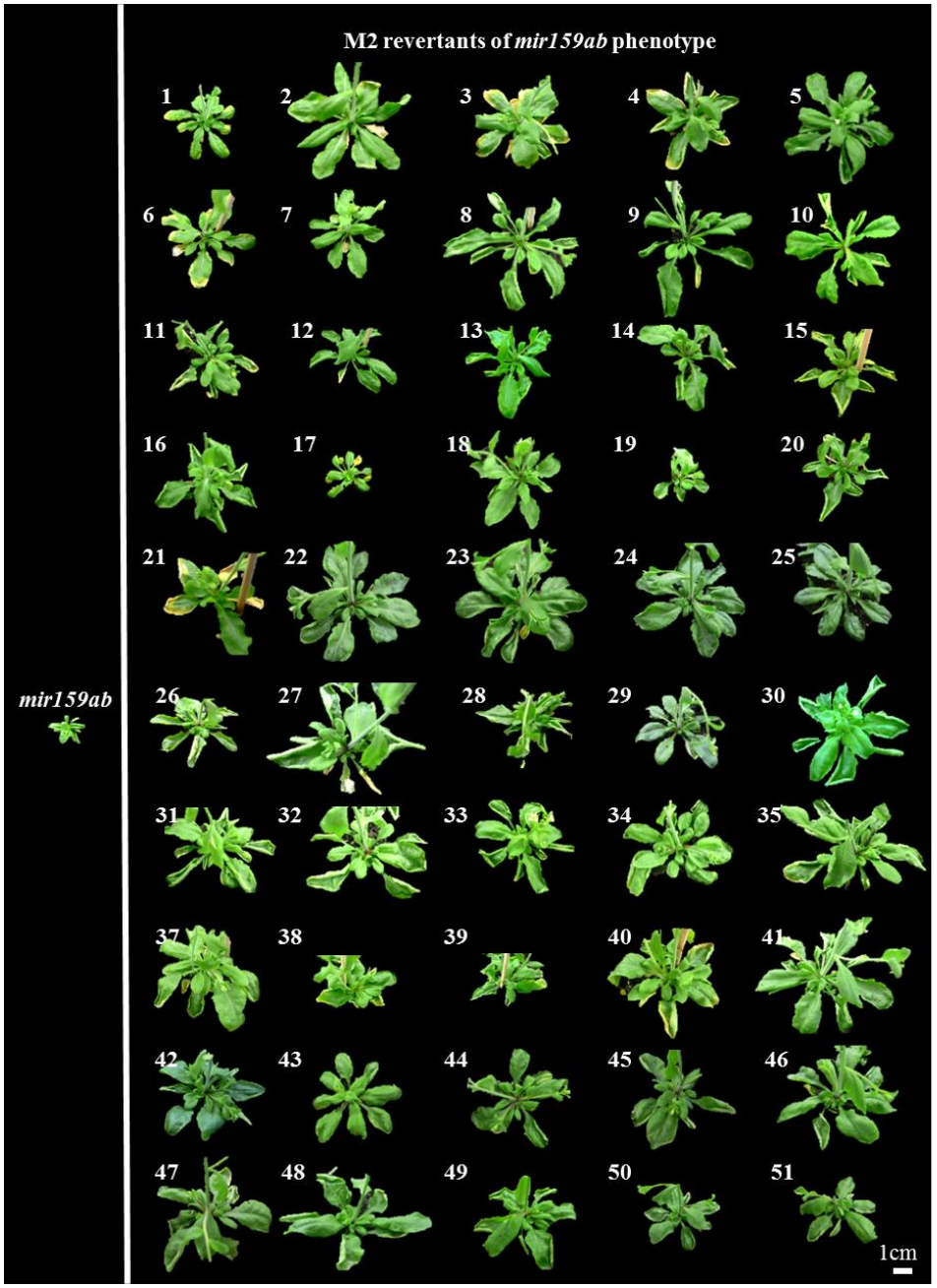

M2 line	pool
1	p5
2	p1
3, 4	p3
5	p13
6, 7	p2
8, 9, 10, 41	p14
11, 12, 13, 14, 15, 16, 17, 18	p7
19, 20, 21	p4
22, 23, 24, 25, 26, 27, 28, 29	p8
30, 31, 32, 33, 34, 35	p11
37, 38, 39, 40	p9
42	p22
43	p35
44, 45, 46, 47	p26
48, 49, 50, 51	p36

Figure 4.6: Identified M2 plants developing semi-revertant phenotypes. Five-week-old plants are shown and compared to parental *mir159ab* (left panel). Rosettes of 104 M2 revertants were larger and developed leaves with reduced curl. Revertants were assigned a number based on the order in which they were identified. The pools from which these revertants were identified are recorded in the table on the right side. The revertants chosen for further phenotypic and molecular analysis were indicated with red-coloured numbers in the table.

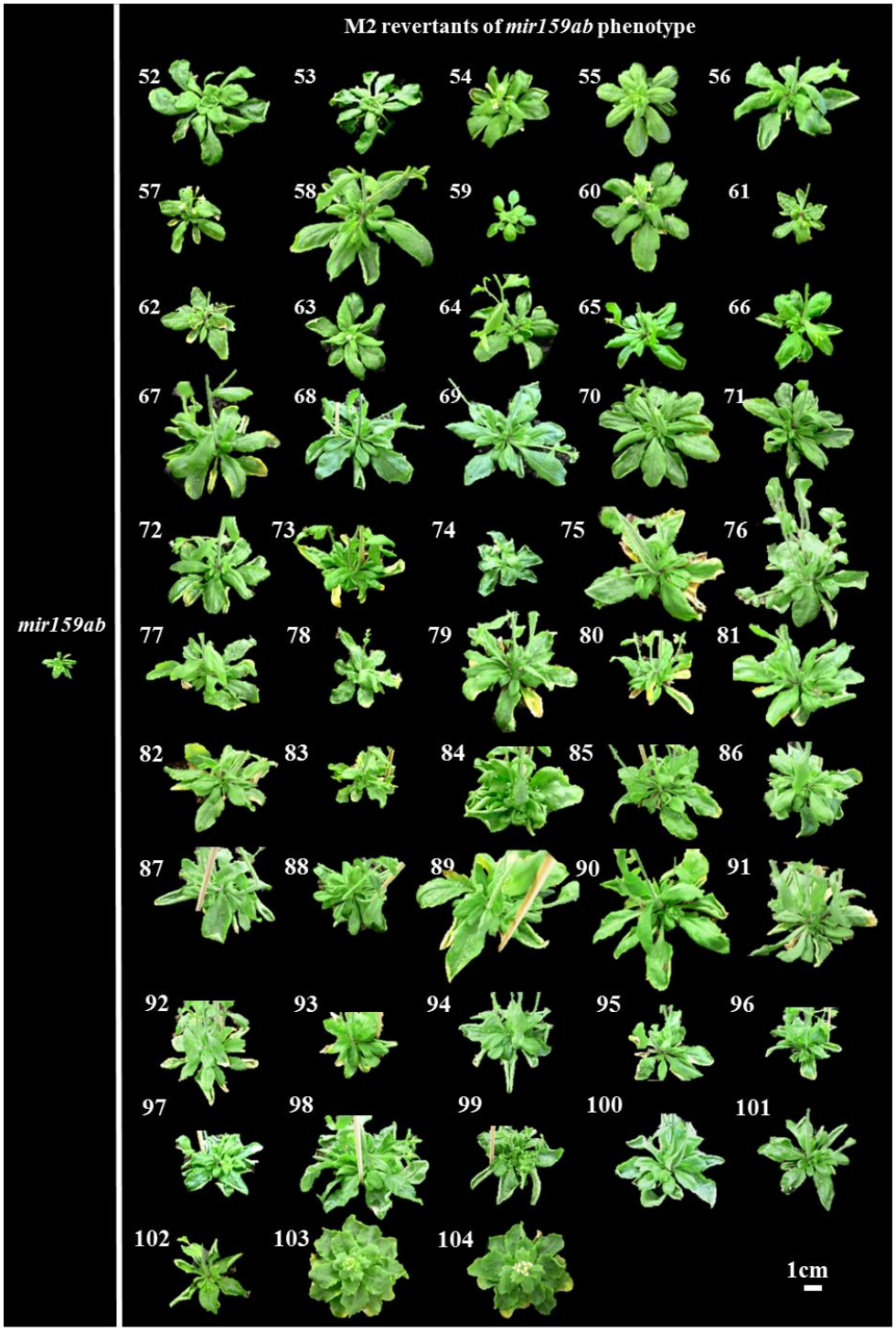

M2 line	pool
52, 53	p27
54, 55, 56, 57, 58, 59, 60, 61, 62, 63, 64, 65, 66	p33
67, 68	p39
69, 70, 71	p40
72	p38
73, 74	p46
75	p45
76	p41
77	p44
78, 79, 80, 81, 82	p52
83, 84	p57
85	p54
86	p60
87, 88, 89, 90, 91, 92	p53
93, 94, 95	p59
96	p67
97, 99	p66
98, 100	p68
101	p62
102	p65
103,104	p57

Figure 4.6 (continued): Identified M2 plants developing semi-revertant phenotypes.

4.2.4 Phenotypic analysis of M3 progenies from self-fertilized M2 revertants

To investigate whether these mutations are in a homozygous or heterozygous state, ~20 M3 self-fertilized seeds of 33 M2 revertants were randomly selected for further phenotypic and molecular analysis (indicated by the red-coloured numbers in Figure 4.6, and the M2s of RS1, RS2, RS8, RS107 shown in Table 4.1).

After four-week growth, most of the M3 progenies developed revertant phenotypes consistent with their corresponding M2 parents (Figure 4.7), confirming that the revertant phenotypes were heritable. Some additional phenotypes were occasionally observed in some M3 plants (e.g. tiny but not curled leaves and short petioles, as shown in Figure 4.7, line 17 and line 42). These possibly resulted from unrelated segregating mutations. In some instances, the revertant phenotypes were not segregating in the M3 progenies (Figure 4.7, e.g. line55 and 60), suggesting the causative mutations were in homozygous status in the selected M2 and M3 generations. In other instances, the revertant phenotypes segregated in the M3 progenies of a few M2 lines (Figure 4.7, e.g. line 73 and 76), suggesting a likelihood of each causative mutation in a heterozygous state in respective parental M2 lines. These suggestions are only made upon phenotypic observation, which requires further genetic analysis as addressed in section 4.2.6.

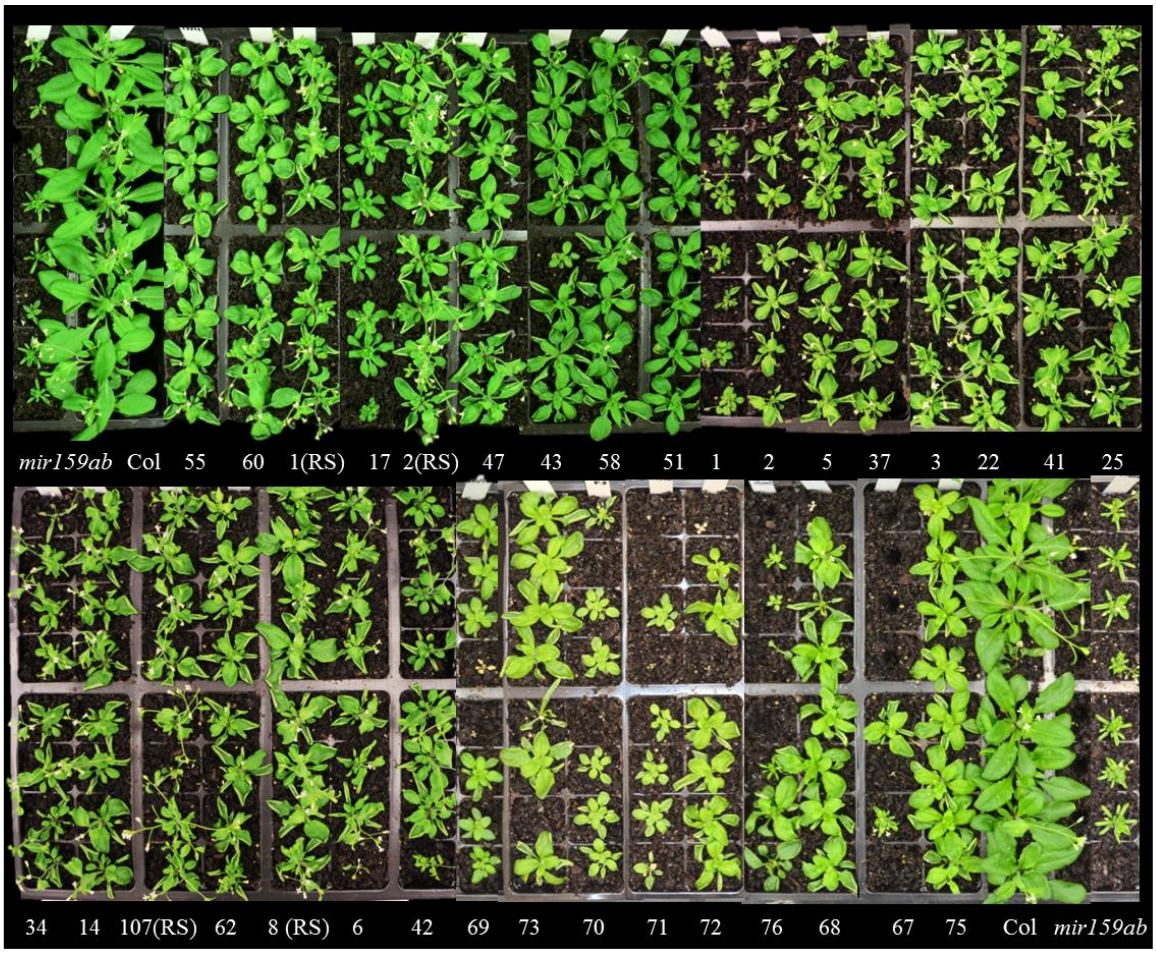

Figure 4.7: Phenotypic verification of M3 revertant progenies. M2 revertant lines were self-fertilized to generate M3 progeny populations, 33 of which were randomly selected for this phenotypic and following molecular analysis. For every line, ~20 M3 seeds were sowed alongside the control plants *mir159ab* and Col. The merged Figure is a representative of the segregation status for each M3 population. Every observation was confirmed by a parallel repeat, except for the line 67 which is partially sterile, generating a few seeds of low viability.

4.2.5 Expression of both *MYB33* and *MYB65* were attenuated in most of the M3 revertant populations

To investigate if the causative mutation is a component of: 1) a pathway upstream of *MYB33/65* expression; or 2) a pathway downstream that does not influence the *MYB33/65* expression but mediate their function, transcript levels of both *MYB33* and *MYB65* in above M3 populations were analysed. Intriguingly, in comparison with the *mir159ab* parent, both *MYB33* and *MYB65* transcript levels were reduced in all revertant rosettes of all these M3 populations (Figure 4.8, A). Moreover, in revertant rosettes of every M3 population, the *CP1* mRNA level was also found lower than that of *mir159ab* (Figure 4.8, B), supporting the expression/activity of *MYB33/65* was compromised in all these lines. Additionally, the observation that mRNA levels of *MYB33*, *MYB65* and *CP1* in these M3 lines were higher than those in wild-type Col, was consistent with these lines being semi-revertants. Note that the M3 line 34 illustrated an intriguing observation that *MYB33* and *MYB65* mRNAs were reduced to undetectable levels (Figure 4.8, A), but the plant is not a full revertant in wild-type appearance. Considering our unpublished data showing there are other *MYB*s that are paralogous to *MYB33/65* and can cause leaf-curl phenotype, it is possible that the mutation in revertant line 34 activated the expression of other *MYB*(s) when the expression of *MYB33/65* were inhibited. Taken together, the reductions of both *MYB33* and *MYB65* mRNA levels supported the phenotypical revertant identification, and moreover indicated the causative mutations being in genes that regulate *MYB33/65* expression, which so would be considered upstream of *MYB33*/*65*. An exception to this was presented by M3 line 69, in which only the *MYB33* mRNA level was reduced, whereas the *MYB65* mRNA level remained unchanged to that of *mir159ab* (Student

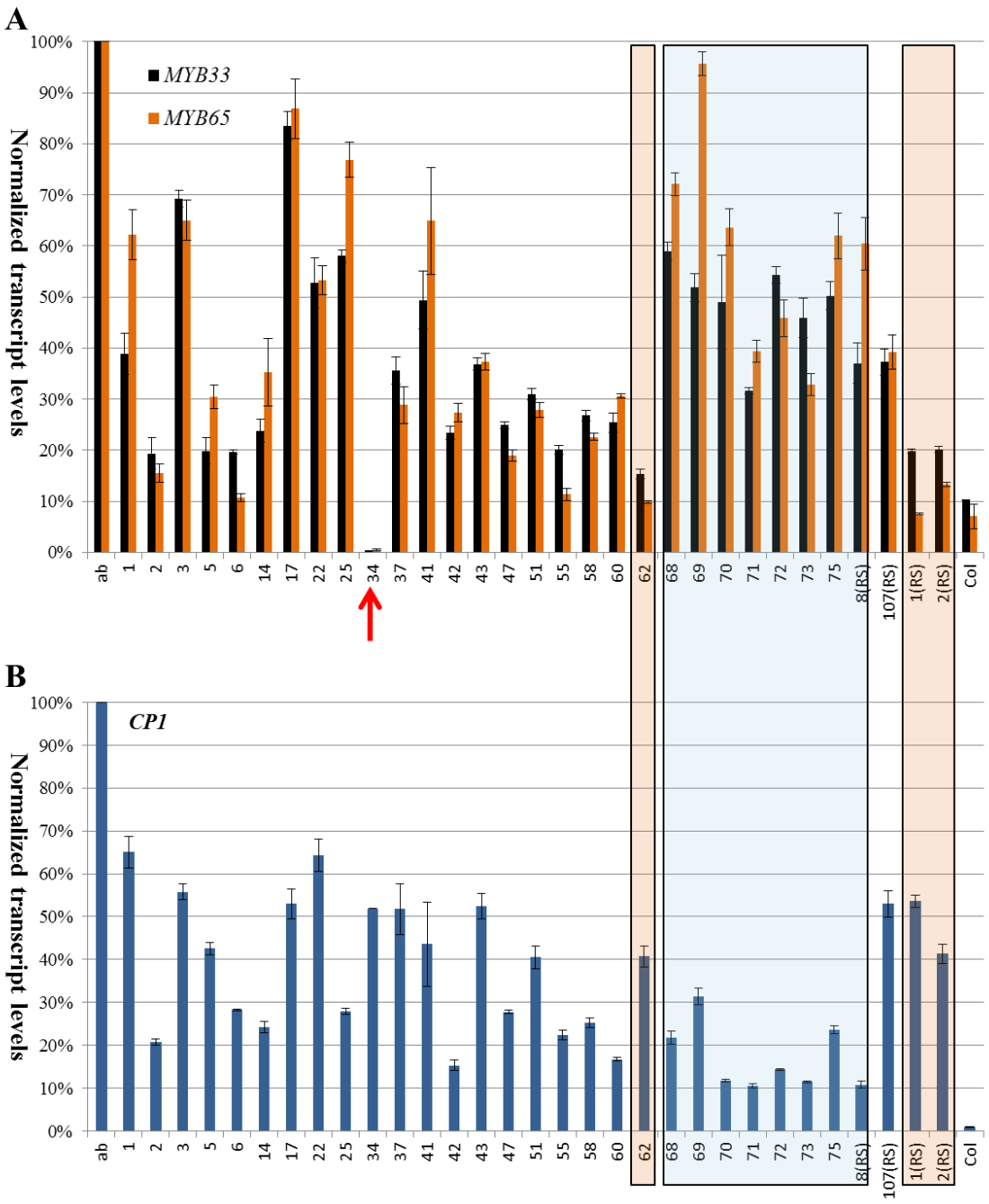

Figure 4.8: Molecular analysis of *MYB33/MYB65* and *CP1* mRNA levels in M3 revertants. (A) *MYB33* and/or *MYB65* mRNA levels reduced in the M3 revertant populations. (B) *CP1* mRNA levels reduced in the M3 revertant populations. RNA samples were harvested from four-week-old rosettes showing revertant phenotypes, and quantified for relative mRNAs by qRT-PCR. *mir159ab* and Col were used as unmutagenized controls. Quantifications were normalized to that of *CYCLOPHILIN*, then to the value of the *mir159ab* plants, which was arbitrarily fixed to 100%. Error bars represent standard deviation of three technical replicates of qRT-PCR analysis. Results were verified by two biological replicates. Pink/blue coloured blocks indicate reduction pattern discrepancies between *MYBs* and *CP1* mRNA levels.

T-test: P = 0.33). Whether it was due to a mutation on the promotor of *MYB33* gene that resulted in a reduction of *MYB33* transcription requires further investigation.

Generally, *CP1* mRNA level strongly correlated with *MYB33/65* mRNA levels in most M3 populations. However, there were some exceptions. First, some M3 populations had relatively high *MYB33/65* mRNA levels but relatively low *CP1* mRNA levels [Figure 4.8, Lines 68-73, 75 and 8(RS)]. A plausible explantation for this is that the translation of MYB protein might be arrested in these mutants, leading to the downregulation of the *CP1* transcription. Conversely, some other M3 populations had relatively low *MYB33/65* mRNA levels but relatively high *CP1* mRNA levels [Figure 4.8, line 62, 1(RS) and 2(RS)]. An explanation for this could be some repressor-operator mutation(s) that resulted in the release of the *CP1* transcription. In addition, we should also acknowledge the possibility that some unknown regulatory factor(s) might exsit and was mutated to intervene in the *MYB33/65* activation of *CP1* transcription. Overall, to clarify the relationship between *MYB33/65* expression and *CP1* transcription in the mutant background, all these possibilities should be cautiously discussed once these causative mutations are identified.

4.2.6 Genetic analysis suggests the dominant nature of these causative mutations in many M3 revertants

As mentioned in section 4.2.4, some of the M2 revertants may carry dominant mutations, because the phenotypic segregation ratio of them are apparently higher than a 1:3 Mendelian ratio for a recessive mutation causing reversion of *mir159ab* rosette defects (Table 4.1, red boxed). This is intriguing with regard to the expectation that the

revertants mutations identified in the M2 generation should be predominantly recessive, if they were not apparent in the M1 generation. To gain deeper insights, further genetic analysis was performed by backcrossing individual M3 revertant from every self-fertilized M2 to the unmutagenized *mir159ab* parent. And the assumption was made that if the causative mutations of M3 revertants inherited from the M2s are recessive, the progenies (BC1) resulted from M3 X *mir159ab* backcrossing should have the causative alleles in heterozygous state and display *mir159ab* phenotype. However, the phenotypic analysis showed that most of the BC1 progenies developed consistent semi-revertant phenotypes after four-week growth, arguing against this assumption (Figure 4.9, A).

Next, to analyse if the inheritance mode of these BC1s' revertant mutations agree with a dominant segregation ratio (Table 4.2), the BC1 plants were self-fertilized to generate the BC2 progeny populations. As shown in every BC2 population (Figure 4.9, B-H), the parental *mir159ab* phenotype reoccurred in some, but not all progeny plants. This verified the causative mutations in the parent BC1s were heterozygous and hence could segregate in the BC2 generation. Moreover, via the chi-square test (Table 4.3), it was found that the segregation ratios of these BC2 populations followed the Mendel's laws, namely a 1:3 ratio of *mir159ab* to revertant phenotypes presents in most of the BC2 generations. These ratios support the dominant nature of these mutations in respective M3 revertant plants, in terms of mediating the suppression of *mir159ab* phenotype. An exception to this is the BC2s produced by the crossing event of RS1 M3 X *mir159ab*, which displayed a segregation ratio (~3:5) greater than 1:3. This is likely due to the M2 of RS1 carries the dominant mutation in a heterozygous status (Table 4.2), thus is still consistent with the dominant trait of this mutation in the RS1 revertant.

Taken together, what has been identified is extremely unusual. Firstly, the EMS-mutagenized *mir159ab* plants developed the phenotypic suppression of *mir159ab* rosette defects at a remarkably high frequency; secondly, the genetic and molecular characterization of at least 30 of these revertant mutants revealed that many of these causative mutations are dominant and are able to mediate the expression of *MYB33/65*. Hence, our results suggest that miR159-*MYB33/65* module is likely extensively networked, and elucidation of these genes that cause reversions may shed light on the role miR159 plays in plants.

	If a dominant mutation of M2 is at homozygous status :	If a dominant mutation of M2 is at heterozygous status	
Backcross (BC)	M3(AA) X *mir159ab*(aa)	*mir159ab*(aa) X M3(Aa)	2:1 M3(AA) X *mir159ab*(aa)
BC1 phenotype	revert (Aa)	revert (Aa) : *mir159ab* (aa) 1:1	revert (Aa)
BC2 phenotype	ab(aa):revert (AA): revert(Aa) 1:1:2	ab(aa):revert (AA): revert(Aa) 5:1:2	ab(aa):revert (AA): revert(Aa) 1:1:2
BC2 segregation ratio	ab:revert 1:3	ab:revert >1:3	

Table 4.2 Expected genetic and phenotypic inheritance modes of revertant mutations upon backcrossing of M3s with *mir159ab*. The phenotypes of backcrossing-resulted progenies are categorised into two groups: ab: *mir159ab* phenotype; revert: reversion of *mir159ab* phenotype. The segregation ratios of phenotypes are suggested based on the genotypes indicated in the brackets: A: dominant mutation; a: respective wild-type allele.

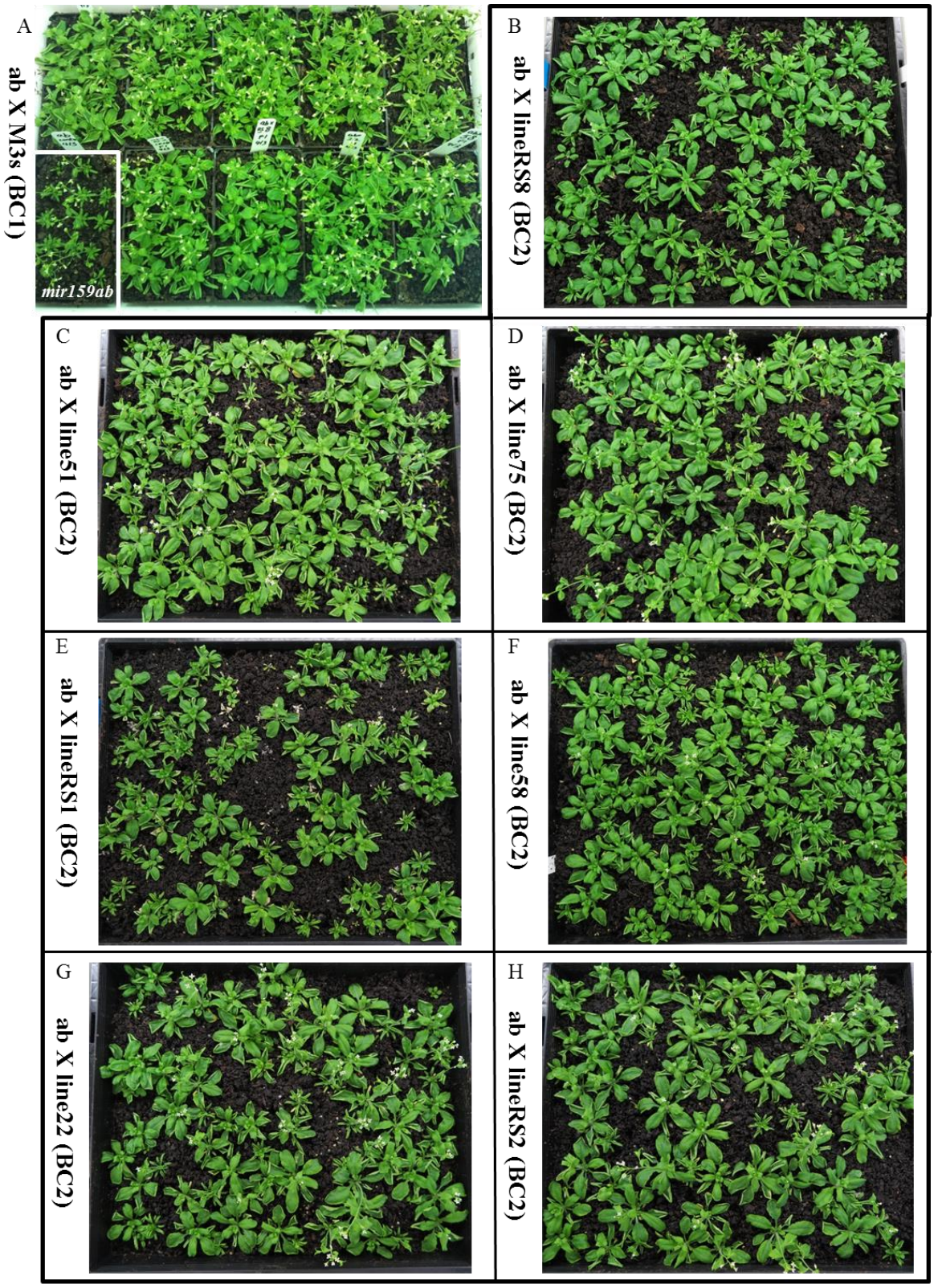

Figure 4.8: Backcrossing of M3 revertants to *mir159ab* suggests many causative mutations are not recessive. (A) Four-week-old BC1s developed revertant phenotypes. Pollen of *mir159ab* was applied to fertilize the ovary of M3 revertants; the resulting BC1 generation was grown alongside *mir159ab* (white boxed) for phenotypic comparison. (B-H) *mir159ab* phenotype reoccurred in the four-week-old BC2s. BC2

generation were respectively produced by self-pollinated BC1s, each tray presents a BC2 population coming from one backcrossing event. ab: *mir159ab* parent; plant line numbers indicate which M3s were used for backcrossing.

	BC2 Phenotype Segregation				
Crossing	*mir159ab*-like	Revert-like	Ratio(ab:revert)	χ^2	p-value
ab X line22	18	51	1:3	0.0435	0.8348
ab X lineRS1	27	46	>1:3	5.5936	0.01803*
ab X line58	31	65	1:3	2.7222	0.09896
ab X line75	16	46	1:3	0.0215	0.8834
ab X line51	23	47	1:3	2.3048	0.129
ab X lineRS2	17	40	1:3	0.7076	0.4002
ab X lineRS8	22	46	1:3	1.9608	0.1614
ab X line55	7	34	1:3	1.374	0.2411

Table 4.3 Segregation ratio test of BC2 from self-fertilized BC1 of *mir159ab* X M3 revertant. ab: *mir159ab* parent; plant line numbers indicate which M3s were used for backcrossing. The segregation ratio was tested by using the Chi-square statistic: $\chi^2 = \sum_{i=1}^{2} \frac{(o_i+e_i)^2}{e_i}$, here o_i is the observed number and e_i is the expected number. The symbol * indicates that the result was significantly different from the Mendelian segregation ratio at the significant level 0.05. For example, for the crossing event of ab X line22 M3, there were o_1 = 18 *mir159ab*-like and o_2= 45 revertant-like BC2's, if the segregation followed the Mendelian law, there should be e_1 = (18+51) × $\frac{1}{4}$ *mir159ab*-like BC2's and e_2 = (18+51) × $\frac{3}{4}$ revertant-like BC2's, then χ^2= 0.0435 which follows a χ^2 distribution with one degree of freedom, and the p-value is p ($\chi^2 > 0.0435$) = 0.8348. This large p-value does not indicate that the segregation significantly differ from the Mendelian segregation at the significant level 0.05.

4.3 Discussion

4.3.1 Many EMS-induced dominant mutations suppress *mir159ab* rosette defects

Two M1 plants displayed revertant phenotypes, likely due to dominant mutations based on the heterozygous status of EMS-induced mutations in the M1 generation (Sasaki et al., 2012). Then, as determined by DNA sequencings (data not shown), both *MYB33* and *MYB65* sequences were found not to be mutated in these mutants (courtesy of Rob Allen), raising the possibility that other dominant mutations are mediating MYB function.

In the M2 generation, a high-frequency phenotypic reversion of *mir159ab* rosette defects was observed. The *MYB33* and *MYB65* mRNA levels were decreased in all the tested revertants, implying that the mutations were in genes related to *MYB33*/*65* expression. The observations that the heterozygous BC1 progenies generated by crossing eight M3s individually with the *mir159ab* plants all displayed revertant phenotypes, and the BC2s derived from every self-fertilized BC1 all displayed segregation ratio supporting the dominant trait of these mutations, indicated the dominant nature of these causative mutations. Theoretically, these dominant mutants could have been detected in the M1 generation, but they were not observable during the M1 screening. A hypothesized reason for this could be the "dilution effect" of *Arabidopsis* embryonic shoot apical meristem, namely the effect of phenotypic suppression in one mutant cell among 8–9 meristematic initial cells can be easily masked by more abundant unaffected initial cells that also generate leaf organs in the later development stage (Furner and Pumfrey, 1992; Irish and Sussex, 1992)

Interestingly, the phenotypic reversions were observed at unusual high frequency. In the M1 screening, two revertants out of 1200 *mir159ab* plants were identified (0.17%), which agrees with the expected M1 mutation frequency of ~10^{-2} to 10^{-3} (Kovalchuk et al., 2000; Van der Auwera et al., 2008). However, more than one third of the M2 populations displayed revertant phenotypes, a much higher frequency than the expected for M2 EMS mutations (~0.1% of the M2 population; Yi and Richards 2009). Such a high reversion frequency may suggest the existence of many genes intervening in the *MYB33/65* expression, and hence the miR159-*MYB33/65* module may be hypothesized to be extensively networked in the rosettes. Additionally, the phenomenon of unusual high EMS revertant frequencies have been observed by Yi and Richards (2008, 2009) and Sasaki et al. (2012) respectively, when they were studying the EMS-induced phenotypic suppression of two other *Arabidopsis* mutants, *bal* (displaying dwarf stature and curled leaves) and *dms4-1*(displaying dwarf stature, pale and serrated leaves, and abnormal phyllotaxy). In both cases, the localized hypermutations correlated to specific causative genes (*SNC1* in the *bal*; *DMS4* in the *dms4-1*) were identified, and hence the enhanced mutagenesis of a few specific genes in these *Arabidopsis* mutants was suggested to be a reason of high frequencies of these phenotypic reversion events (Yi and Richards, 2009; Sasaki et al., 2012). Moreover, since the *SNC1* and *DMS4* genes were found not the general targets of enhanced mutagenesis in the wild-type or wild-type-appearing plants, their hypermutation phenomena identified in respective *bal* and *dms4-1 mutant* backgrounds raised the possibility that the parental mutant backgrounds displaying morphological defects can provide a selection advantage for cells carrying a phenotypic-recovering mutation within the meristematic tissues, as proposed by Comai and Cartwright (2005). This may also increase the chance for specific mutations being enriched in the progeny population. With these regards,

findings in this study may be rationalised by an alternative scenario: some causative genes that can mediate *MYB* expression/function (other than miR159) have been hypermutated via the EMS treatment, so that *mir159ab* phenotype is reverted much more frequently. Moreover, owing to the cells carrying causative mutations could partially re-establish a wild-type phenotype, they might have the selective advantage to outcompete the other cells in the meristematic region, resulting in more frequent recovery of *mir159ab* defects in the self-fertilized M2 generation than expected.

4.3.2 EMS-mutations are found upstream of *MYB33/65* expression, but not downstream of their activity

As one of the most conserved plant miRNA, miR159-*MYB* module has been extensively studied (Palatnik et al., 2007; Alonso-Peral, 2010; Li and Millar, 2013; Rubio-Somoza et al., 2013). However, currently no evidence reported connects *MYB* expression with any other genes in *Arabidopsis* rosettes. This is perhaps due to the great miR159 abundance and its efficient silencing of *MYB* expression (Fahlgren et al., 2007; Allen et al., 2010). Here, by EMS revertant screening of *mir159ab*, an unexpected large number of semi-revertants were identified. Consistently, both the *MYB33* and *MYB65* steady-state mRNA levels were reduced in almost every tested revertant population (Figure 4.8). These data support the tightly correlated redundant relationship of these two *GAMYB* members in the rosette tissue, and moreover it implied these revertant mutations should lie in genes upstream of *MYB33/65*, which could be unknown transcription factors regulating *MYB33/65* expression, agreeing with one of our expectations illustrated in Figure 4.1, B.

These results may be associated with the possibility that the miR159-*MYB* module is being phytohormonally regulated. For instance, during seed germination ABA has been found to influence the miR159 regulation of *MYB33* and *MYB101* via two potent regulators of ABA responses, the transcription factors ABI3 and ABI5 (Reyes and Chua, 2007). Supporting this, the disrupted balance of miR159/*MYB* abundance was indeed observed during the seed germination of an ABA-treated *Arabidopsis* mutant, *abh1* (*ABA hypersensitive 1*, Kim et al., 2008). Additionally, GA, with antagonistic roles to ABA, has also been shown to modulate miR159 levels during anther development (Achard et al., 2004), as well as induce the expression of *GAMYB* or *GAMYB*-like genes (Gubler et al., 2002; Woodger et al., 2003; Aya et al., 2009). It is hence a plausible scenario that under the loss-of-function *mir159ab* background, the EMS-induced mutation on relevant phytohormonal regulator(s), could regulate the *MYB33/65* expression in the rosette tissue. This may be important for inducing a *MYB*-related biological effect in rosettes, contributing to the phytohormonal signaling response when miR159 silencing is compromised under certain growth condition(s) or by certain stimuli. Besides that, some of these EMS-induced mutations might pinpoint causal genes of other regulatory network(s) that could coordinate the miR159 regulation of *MYB33/65* expression. Since the connection between the miR159-*MYB* pathway and a phytohormonal or other regulatory network(s) has never been strongly suggested in rosettes (as discussed in the introduction section), any insights into these possibilities will enrich our understanding of the role of miR159-*MYB* module in this tissue. Additionally, we should not ignore the possibility that among upstream factors modulating *MYB33/65* expression, one could be the activation of *MIR159c*. To test this, we can compare the mature miR159c level in each revertant with that in the *mir159ab* plant.

Noticeably, there is no EMS-mutant being identified downstream of MYB33/65 activity. This implied the possibility that if there are downstream gene(s) that can mediate the MYB33/65 function, the number of them is probably much smaller than the number of upstream genes regulating *MYB33/65* expression. Hence the EMS mutagenesis performed in this study might not be sufficient for screening out the causal gene(s) downstream of *MYB33/65*. However, the other possibility cannot be ignored: rare downstream genes can independently determine the MYB33/65 activity, instead they may coordinate with each other or function redundantly in mediating the rosette morphology, thus cannot be isolated via the EMS mutagenesis approach. If the latter possibility is real, it also provides the alternative explanation for the finding that *CP1* expression is not a major contributor to the *mir159ab* phenotype, by suggesting the likelihood of other genes being acting redundantly to the CP1 activity.

4.3.3 Selection of mapping populations and identification of causative mutations are the next critical steps

Certainly, the EMS-revertants will provide critical materials for analysing the *MYB33/65* role in rosettes, but the large number of revertant candidates raised the question about how to select the proper candidates for next step of mapping. Considering some gene(s) may be hypermutated or belong to paralogous family and function similarly, the selection can be aimed to search for revertants carrying mutations in different loci. To this end, the practice of crossing the M3 revertants with each other to generate progenies for an allelism test could be performed, as the working model suggested by Daszkowska-Golec et al. (2013). In this way, we may gain more insight of the relationship among these mutations, and narrow down the number of mapping

populations by selecting the revertant candidates carrying mutations in different loci. Additionally, crossing independent mutants to one another may result in a progeny phenotype closer to wild-type.

With respect to the dominant nature of the causative mutations in many revertants, the SNP-Ratio mapping scheme suggested by Heike et al. (2012) may be adopted to identify the mutations: namely another two rounds of backcrossing should be performed. Starting from crossing M3s respectively back to unmutagenized *mir159ab* parents, BC1 generations carrying heterozygous mutants will be produced. These heterozygous BC1 can then be crossed back again to the *mir159ab* parents to generates the new BC1-1 population. By selecting only revertant individuals in the F1 generation derived from self-fertilized BC1-1s, the causative mutation is supposed to be enriched with a 1:1 segregation ratio in the pool of F1 revertants, whereas any non-causative mutation will segregate with a ratio of 1:3 (refer to Heike et al., 2012 for details). This allows the following SOLiD sequencing, SNP calling, and SNP/non-SNP ratio calculation, by which the causative mutations should be distinguished from the non-causative ones (Heike et al., 2012). Again, since both the high reversion frequency of *mir159ab* defect and the dominant nature of mutations in many examined revertants are extremely unusual phenomena, any results obtained from candidate selection and sequencing methods should be cautiously discussed in the future, to make clear suggestions about how extensively is the miR159-*MYB* networked in the rosette tissue, and moreover what is the function of it.

Chapter 5

Application and efficacy analysis of miRNA *SP*s for inhibiting miRNA functions in *Arabidopsis*

5.1 Introduction

Plant miRNAs are important gene regulators for maintaining a proper embryonic, vegetative and floral development (Mallory and Vaucheret, 2006; Jones-Rhoades et al., 2006). This is because many plant miRNAs have been verified to negatively regulate a set of functionally related targets, which are primarily comprised of gene encoding transcription factors (Chen, 2005), such as the *AUXIN RESPONSE FACTOR*s regulated by miR167 or miR390 (Allen et al., 2005; Wu et al., 2006), the *NAC-LIKE TRANSCRIPTION FACTOR*s regulated by miR164 (Rhoades et al., 2002; Laufs et al., 2004), and the *GROWTH-REGULATING FACTOR*s regulated by miR396 (Jones-Rhoades and Bartel, 2004; Wang et al., 2011b). Additionally, they also mediate the regulation of other genes encoding regulatory factors, such as the *ARGONAUTE 1* and *ARGONAUTE 2* regulated by miR168 and miR403 respectively, which play roles in miRNA metabolism (Allen et al., 2005); and the *PHOSPHATE 2* regulated by miR399, which plays a role in the maintenance of phosphate homeostasis (Allen et al., 2005; Chiou et al., 2006). In addition, a number of these miRNA-target relationships are strongly conserved, present in most land plants (Jones-Rhoades et al., 2006; Li et al., 2011b; Jones-Rhoades, 2012), which also emphasizes the important role of miRNA-mediated gene expression in plant regulatory systems. However, functions of many conserved plant miRNAs remain unclear.

As a prerequisite for functional analysis of these plant miRNAs, a best approach is to generate loss-of-function *mirna* outcomes. To this end, the mutagenesis approaches, such as T-DNA-insertional method or EMS, have been used to generate loss-of-function *mirna* mutants. However, currently only a few such mutants have been isolated (e.g.

mir159a/b, Allen et al., 2007; *mir164a/b/c*, Sieber et al., 2007; *mir319a*, Nag et al., 2009), because mutagenizing these *MIRNA* genes and identifying the single mutagenized *mirna* mutant can be difficult. First, many *MIRNA* genes are small or medium sized, hence they are less likely to be mutated by a T-DNA insert or other mutagen than many bigger-sized protein-coding genes (Ma et al., 2010; Todesco et al., 2010). Second, the plant miRNA families frequently contain many genes that can produce mature miRNA members near-identical or identical in sequence, such as the *Arabidopsis* miR169 family consisting of at least 14 members deriving from 14 genomic loci. These miRNA family members are likely to have overlapping expression domains, and may function redundantly to buffer against the loss of any single miRNA locus (Nogueira et al., 2006; Sieber et al., 2007; Yan et al., 2012). Therefore, all members of a miRNA family may need to be simultaneously knocked out to generate a loss-of-function *mirna* outcome. Due to this, even if a single mutant for every *MIRNA* locus could be isolated, it would be extremely time-consuming to obtain a loss-of-function *mirna* mutant carrying mutations in all the *MIRNA* loci of a miRNA family.

For this reason, the transgenic expression of miRNA decoy in a bid to generate loss-of-function *mirna* outcomes has become a focus. MiRNA decoys are transgenes designed to carry target sites highly complementary to particular miRNA families, so that transcripts of decoys can act by competing for miRNA binding, sequestrating the miRNA family of interest from their endogenous targets, (Todesco et al., 2010, Ivashuta et al., 2011, Yan et al., 2012; Reichel et al., 2015). Since the specificity of a miRNA decoy is mainly determined by the degree of its complementarity to the miRNA, it should be able to target all members of a miRNA family and overcome problems of

functional redundancy among these miRNA family members (Reichel et al., 2015). They have been explored for inhibiting miRNAs' activities in mammalian system. Such as the transgene *Tough Decoy* (*TuD*), which deposits two complementary target sites into an optimised DNA backbone that provides the secondary structure accessible for a miRNA binding (Haraguchi et al., 2009; Haraguchi et al., 2012); and the miRNA *SPONGES* (*SP*s), which carries many target sites complementary to a miRNA of interest, either in a non-protein coding DNA sequence or in the 3' UTR of a reporter gene, to increase the opportunity for a miRNA binding to the *SP* transcripts (Ebert et al., 2007). Both methods achieved effective miRNA inhibitions and are applied in functional analysis of mammalian miRNAs.

In plants, the decoy transgenes constructed for miRNA inhibition are known as "*Target Mimic*" and "*Short Tandem Target Mimic*" (*STTM*) (Todesco et al., 2010; Yan et al., 2012). Similar to the *TuD* method, these *Mimic* transgenes are designed to position one or two miRNA target sites within certain DNA backbones. Both of them realized efficient inhibition of several miRNAs in *Arabidopsis*. Supporting this is a collection of phenotypic defects observed for *Target Mimic* and *STTM* transformants, such as the reduced leaf initiation rates of *MIM156* plants, serrated leaves of *MIM160* plants, twisted and downwardly rolled leaves of *MIM167* plants, and loss of leaf asymmetry displayed by *STTM165/166* plants (Todesco et al., 2010; Yan et al., 2012). However, also found by Todesco et al. (2010), out of 71 analysed miRNA families, inhibiting the function of only 14 with *Target Mimic* method led to morphological abnormalities. Moreover, some of these *Target Mimic* transgenes were demonstrated to be weak miRNA decoys, when their inhibition effects were compared with that of the modified *Mimic* method "*STTM*" (Yan et al., 2012). Thus it is intriguing to investigate if there is

an alternative inhibition method to verify and complement these *Mimic* methods (we considered *STTM* as a modified version of the *Target Mimic* method, hereby the name *Mimic* is used to collectively describe these two methods in following sections, if not otherwise specified). With this respect, the application of miRNA *SP* method, namely constructing the transgene carrying as many as 15 target sites complimentary to a miRNA of interest, was explored to inhibit miRNAs' activities in *Arabidopsis* in this study, and the factors that may influence the inhibition efficacy of a plant miRNA *SP* were also analysed.

5.2 Results

5.2.1 Construction of miRNA *SP*s against ten conserved plant miRNAs.

To investigate whether the miRNA *SP*s can be widely applied for analysing the function of plant miRNAs, ten *SP* constructs were designed against ten plant miRNAs, with the same principles designing the animal miRNA *SP*s (Figure 5.1, A). The selected ten miRNAs are conserved miRNAs identified in many species including *Arabidopsis*, and most of these miRNAs have been suggested to play roles in plant development (Figure 5.1, B). Their respective targets have been verified by a series of previous studies, but the miRNA biological functions for some of them have not been verified by a loss-of-function approach. If the *SP* constructs can efficiently inhibit the activities of these miRNAs, this may provide a useful method for their functional analysis.

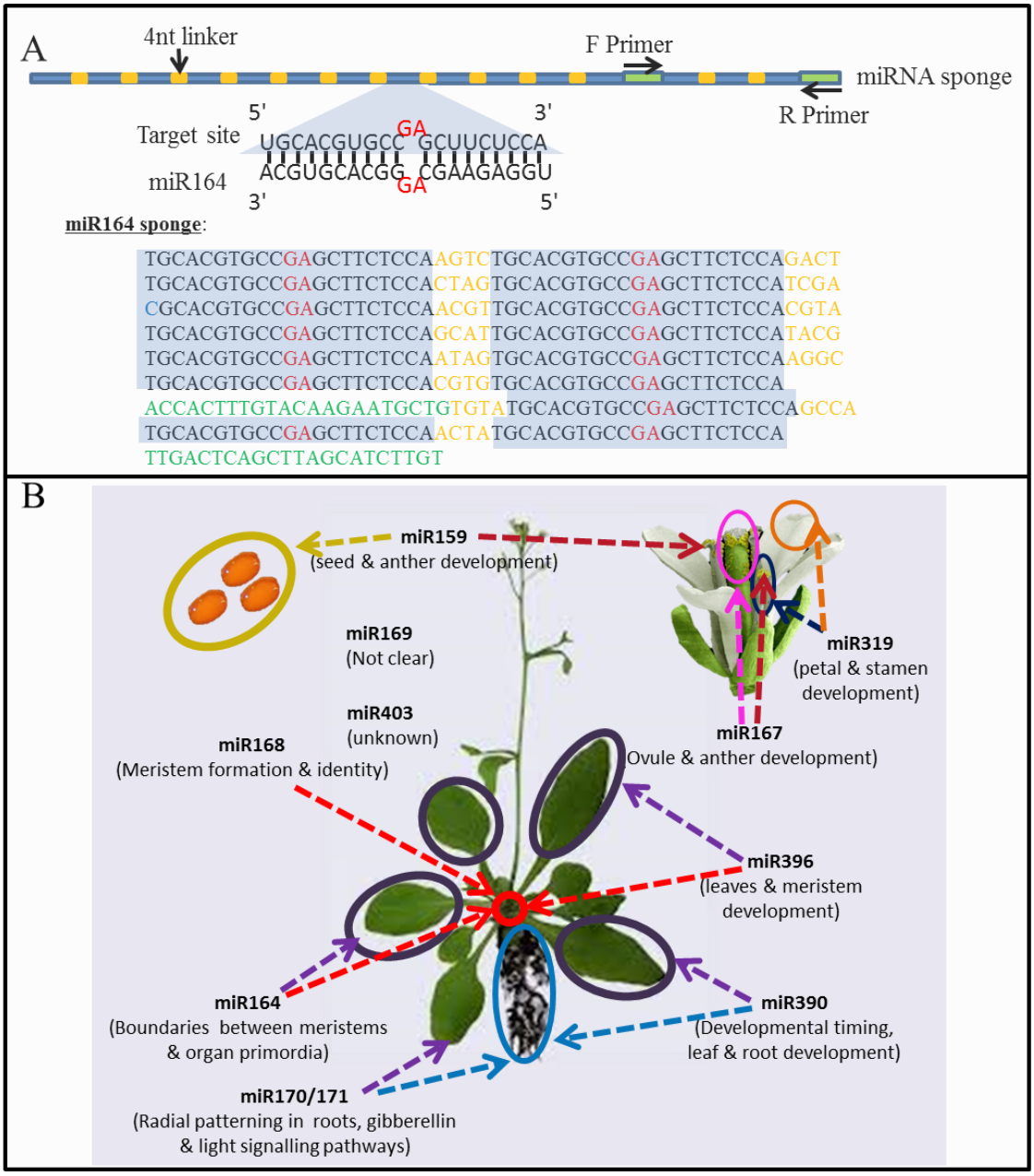

Figure 5.1: Construction of plant miRNA *SP*s. (A) Diagram of the *SP* construction. Exemplified by *SP164*, every *SP* consists of fifteen target sites (blue blocked), with a 4nt-linker between each neighbouring target sites (orange coloured). Two 22nt "primer" sequences are sandwiched in around the 3'end, to facilitate qRT-PCR analysis (green coloured). The sequence of target site is fully complementary to the miRNA of interest, with 2 nt central mismatches (red coloured) against the position 10 and 11 of the miRNA (from the 5' end), while the linker sequences were randomly picked if not specified. (B) Cartoon illustrating functions of the ten conserved miRNAs indicated in *Arabidopsis*.

5.2.2 Plant miRNA *SPs* have various inhibition efficacies

To constitutively express the *SP* transgenes, they were fused downstream of the constitutive *Cauliflower Mosaic Virus* (CaMV) 35S promoter, and transformed into wild-type *Arabidopsis* (Col-0). 45~60 primary transformants (T1) of each *SP* were planted and phenotypic analysis was performed when they were four-week-old (Figure 5.2, courtesy of Marlene Reichel for constructing the *SP165/166*). To assess the inhibitory effects of these *SP*s, the "inhibition efficacy" was defined based on the percentage of the primary transformants displaying abnormal developmental phenotypes.

5.2.2.1 The expression of *SP165/166* and *SP159* induced rosette defects with high efficacies

First, 49 out of 57 (inhibition efficacy: 86%) *SP165/166* transformants generated rosettes with either trumpet-shaped leaves (severe morphological abnormalities) or adaxialized organs (mild morphological abnormalities) (Figure 5.2). This observation is in agreement with previous studies inhibiting miR165/166 function, which shows the disruption of the miR165/166 activity resulting in leaves of adaxial characters around their circumference (Kidner and Martienssen, 2004; Mallory et al., 2004a; Todesco et al. 2010). Moreover, the severity of rosette abnormality present on *SP165/166* transformants resembles the inhibition outcome using the modified *Mimic* method "*STTM*" (Yan et al., 2012), whereas the *SP* method shows even higher efficacy (detailed comparisons refer to our recent paper: Reichel et al., 2015).

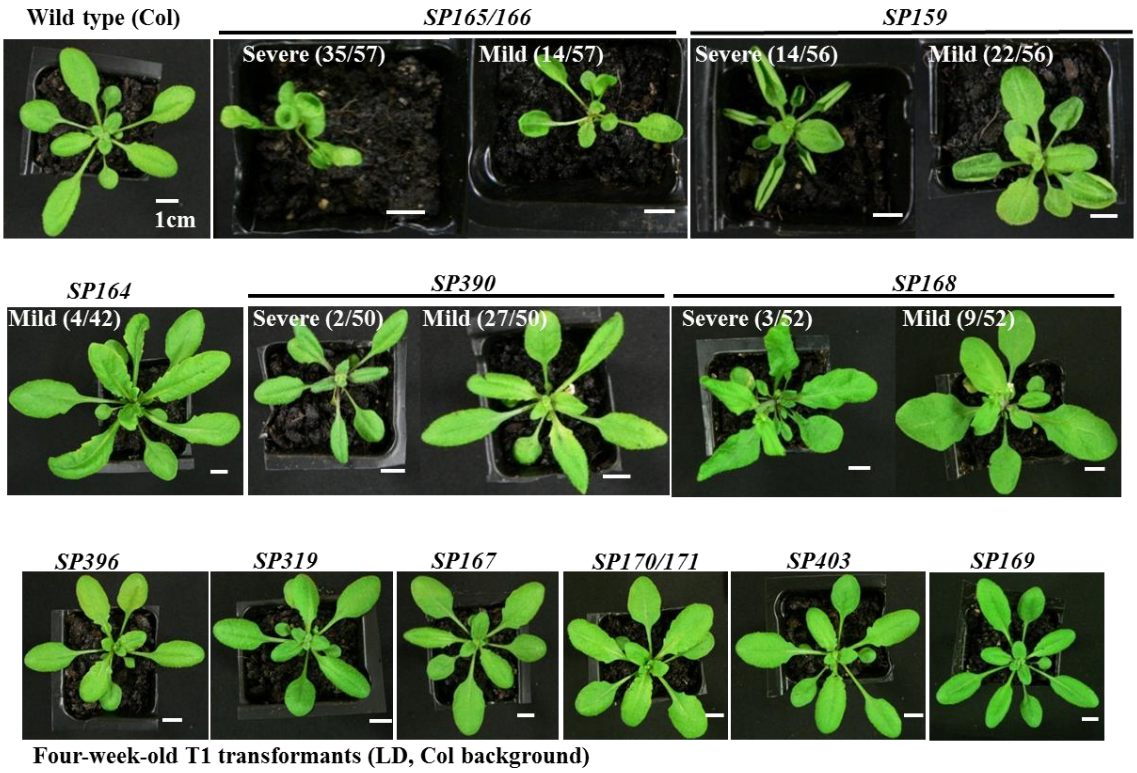

Figure 5.2: Eleven *35S-SP* transgenes induced rosette morphological abnormalities at varying efficacies. The abnormalities are classified as "severe", if the rosettes are smaller in size, and the leaf blades are fully folded (*SP165/166*), fully curled (*SP159*), obviously narrow (*SP390*) or ruffled (*SP168*). While the other similar but milder abnormalities are classified as "mild". The serrated leaf of *SP164* transformants is a marginal phenotype observed in a few plants, and so be considered as "mild". The embedded fractional number indicates the proportions of the primary transformants (T1) falling into the classified phenotype group (e.g. 35/57, among 57 transformants analysed, 35 plants developed the phenotype illustrated in the picture). For every transgene, 45~60 primary transformants (T1) were grown under long-day condition (16h light/8h dark, 21^{o}C), and photographed at four-week-old. The phenotypic results were also verified by growing plants under short-day condition (8h light/16h dark, 21^{o}C).

Next, 36 out of 56 (inhibition efficacy: 65%) *SP159* primary transformants generated rosettes with reduced rosette size and either fully curled leaves (severe morphological abnormalities) or partially curled leaves (mild morphological abnormalities) (Figure 5.2). These phenotypes also resembled the developmental defects displayed by loss-of-function *mir159ab* mutant (Allen et al., 2007). Therefore, these data indicated that both *SP165* and *SP159* could induce characteristic loss-of-function *mirna* defects, suggesting they could respectively inhibit the functions of these two plant miRNAs, and moreover with high inhibition efficiencies.

5.2.2.2 The expression of *SP390* induced *ago7*-like phenotype with a moderate efficacy

Interestingly, more than half of the *SP390* transformants developed narrow and pointing leaves. This phenotype has not been shown by other miRNA inhibition methods, but resembles the descriptions for the leaves of gain-of-function plants expressing miR390-resistent target *AUXIN RESPONSE FACTOR 3* (*ARF3*, Fahlgren et al., 2006); and the loss-of-function *ago7* mutant (Montgomery et al., 2008), with the respect that the protein ARGONAUTE7 (AGO7) is the specific co-operator of miR390 (Montgomery et al., 2008; Endo et al., 2013). The observation that 29 out of 50 (58%) *SP390* primary transformants displaying narrow and pointing leaves indicated that *SP390* had a good inhibition efficacy.

However, when the *SP390* transformants were grown alongside the loss-of-function *ago7* mutant (*ago7-1*), the leaf defect developed on *SP390* plants were found obviously milder than that of *ago7* mutant, because the latter plants appeared narrower and more

elongated, and despite the symptom of *SP390* transformant intensified with the rosette growth, it would not be as severe as that of *ago7-1* (Figure 5.3). Thus, it is possible that the *SP390* may not strongly inhibit miR390 function in most of the transgenic plants. In supporting of this, among *SP390* transformants with narrow-pointing leaves, only few plants appeared much smaller in rosette size and more compacted in leaf form (classified as "severe morphological abnormalities" in Figure 5.2).

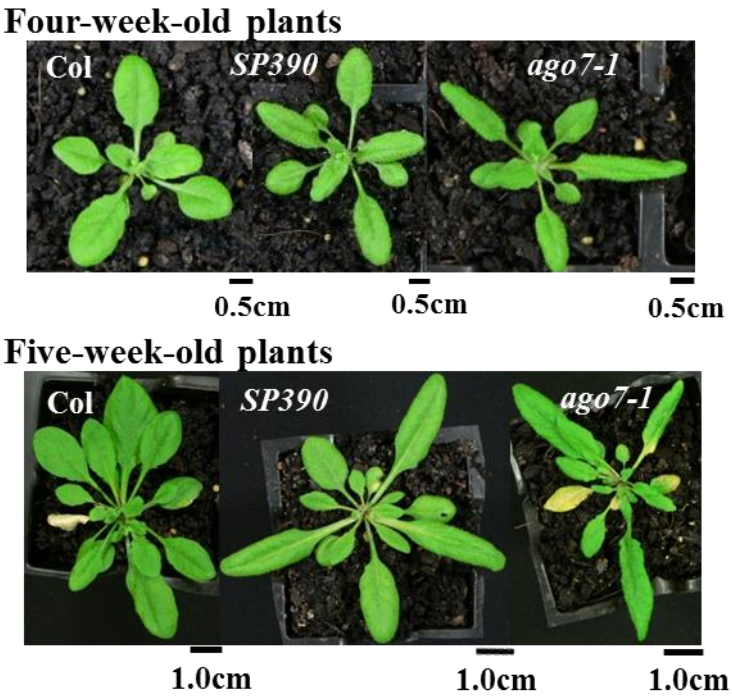

Figure 5.3: **Phenotypic analysis of *SP390*.** Primary transformants of *SP390* is compared with Col and ago7-1 plants under long-day condition (16h light/8h dark, 21^{o}C). Plants are photographed at four-week-old (top panel) and five-week-old (bottom panel) to show the development of *SP390* defect.

Furthermore, to investigate if the narrow-pointing leaf trait of *SP390* transformants could be stably inherited, the seeds (T2) of self-fertilized T1 transformants were harvested, and further phenotypic and molecular analyses were done on T2 transformants. Here, the T2 transformants developed phenotypes that segregated: rosettes with wild-type like leaves and rosettes with narrow-pointing leaves (these phenotypes resembled the T1 phenotypes, data not shown). In rosettes with the narrow-pointing leaves, the target genes of miR390, *ARF3* and *ARF4* (*AUXIN RESPONSE FACTORs* targeted by *TAS3* ta-siRNAs, which are produced by miR390-AGO7 mediated cleavage; Adenot et al., 2006; Montgomery et al., 2008), were detected to be up-regulated by qRT-PCR analysis (Figure 5.4). This verified that the miR390 function was perturbed in the T2 transformants of *SP390*.

In summary, the data indicates that *SP390* expression inhibits miR390 function, resulting in the formation of narrow-pointing leaves, which resembles that of the loss-of-function *ago7* mutant. However, the *SP390* phenotype was not as strong as *ago7-1*, and the inhibition efficacy (58%) was lower than that of *SP165/166* and *SP159*.

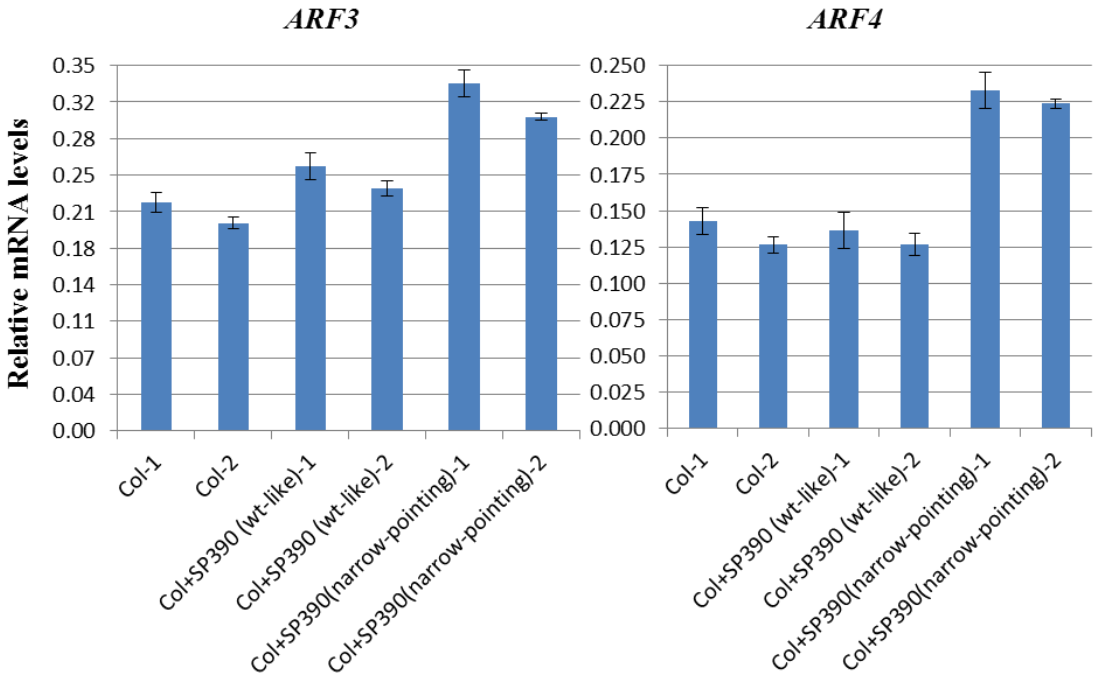

Figure 5.4: qRT-PCR analysis of *ARF3* and *ARF4* transcript levels in the rosettes of the progenies of the primary transformants (T2). The RNA samples were extracted from classified individual rosettes of 5-week-old. The phenotypic classifications are indicated in the brackets, wt-like: wild-type phenotype. Col rosettes were used as wild-type control for phenotypic and molecular comparison. Two rosettes of each phenotype were used to appraise the variation of RNA levels in each phenotypic class. All mRNA levels were normalized to that of housekeeping gene *CYCLOPHILIN* (At2g29960). The Measurements are the average of three technical replicates with error bars representing the SD.

5.2.2.3 The expression of *SP164* and *SP168* induced mild rosette defects with low efficacies

Next, *SP164* and *SP168* were found to induce developmental abnormalities but with much lower efficacies. For *SP164* transformants, serration occurred around the leaf circumference (Figure 5.2), which is similar to what has been observed in *MIM164* plants (Todesco et al., 2010) or the loss-of-function *mir164abc* triple mutant (Sieber et al., 2007). However, the frequency of this phenotype in *SP164* primary transformants was low, that is only four of 42 *SP164* T1 plants displayed the serration defect (less than 10%), which illustrated the low inhibitory efficacy of *SP164*. Additionally, the floral defects observed in a loss-of-function *mir164abc* triple mutant (Sieber et al., 2007), which includes unfused carpels, an increased number of petals and sepals, was not apparent in *SP164* transformants. This suggests that *SP164* did not completely inhibit miR164 function. For *SP168*, a number of transformants developed ruffled and less compacted rosette leaves (Figure 5.2). Again the efficacy appeared weak, as only 12 out of 52 (23%) primary transformants displayed this phenotype. Interestingly, this phenotype has not been observed in a *mir168a* loss-of-function mutant under normal growth condition (Vaucheret, 2009), indicating there may be a further redundancy with miR168b.

To verify inhibitory effects of *SP*s displaying low efficacies, transcript levels of relative target genes were measured (Figure 5.5). Consistent with the developmental changes in *SP164* transformants, these plants had higher transcript levels of target *CUC1*/*CUC2* (*CUP-SHAPED COTYLEDON*) than that of Col control (Figure 5.5, C-D), implying these genes had been de-regulated. Likewise, in *SP168* transformants, there was an

increase of target *AGO1* transcript level, suggesting the de-regulation of *AGO1* (Figure 5.5, E). Therefore, these data support the notion of the inhibitory capability of *SP164* and *SP168*, even though they appeared less efficient in inducing phenotypic defects.

To my knowledge, the AGO1 protein is the major effector of most miRNAs and *TAS3* ta-siRNA functions, and usually the homeostasis of the AGO1 protein and mRNA is well maintained via several fine-tuned adjustments, to ensure a proper balance of other miRNAs and their targets abundance (Vaucheret et al., 2006; Mallory and Vaucheret, 2009; Vaucheret, 2009). It is thus intriguing to analyse if the de-regulation of *AGO1* in *SP168* transformants can influence other miRNA-target pathways. To investigate, mRNA levels of *CUC1* (target of miR164) and *ARF3* (target of *TAS3* ta-siRNAs) were further qRT-PCR quantified. The result showed that the *CUC1* and *ARF3* mRNAs in *SP168* transformants increased ~6 and ~1.6 fold respectively (Figure 5.5, G and F), which is comparable to the mRNA fold change of *CUC1* in *SP164* transformants (~7.5 fold, Figure 5.5, C) and *ARF3* in *SP390* transformants (~1.7 fold, Figure 5.5, A). Thus the results suggested the *SP168* could strongly inhibit the function of miR168 to cause perturbations of other miRNA and *TAS3* ta-siRNA pathways. This perturbation of other miRNA pathway may also help to explain the observed defect of *SP168* rosettes.

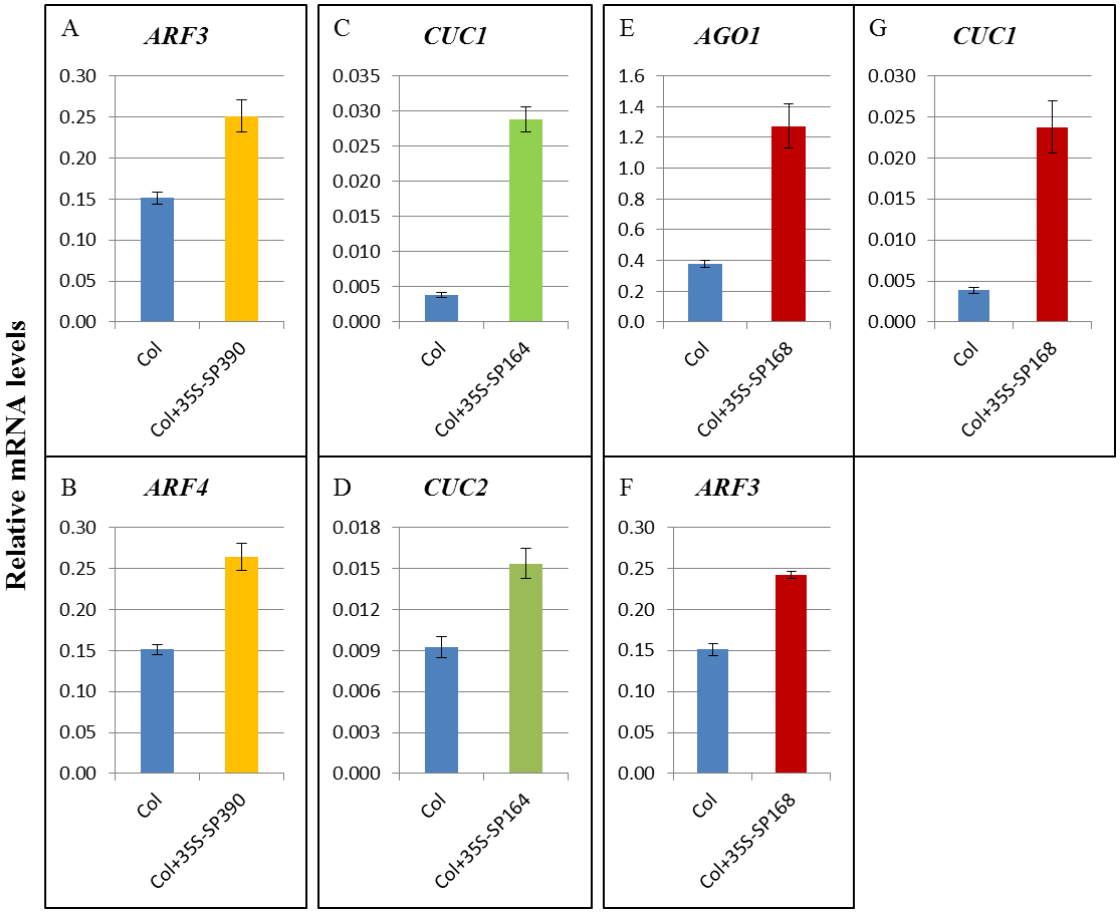

Figure 5.5: Molecular analysis of relative targets in Col transformants of *SP390*, *SP164* and *SP168*. (A-B) mRNA levels of *ARF3* and *ARF4* in *SP390* transformants. (C-D) mRNA levels of *CUC1* and *CUC2* in *SP164* transformants. (E-G) mRNA levels of *AGO1*, *ARF3* and *CUC1* in *SP168* transformants. For each *SP* construct, the RNA samples were extracted from approximate 120 seedlings of the corresponding primary transformants (T1), at 12-day-old. All mRNA levels were normalized with *CYCLOPHILIN*. Measurements are the average of three technical replicates with error bars representing the SD.

5.2.2.4 Many *SP*s failed to induce predicted morphological defects

Lastly, expression of six *SP*s failed to result in any detectable abnormalities (i.e. *SP169*, *SP170/171*, *SP396*, *SP167*, *SP319* and *SP403*), despite inhibitions of three of these miRNA pathways (miR169, miR170/171, miR396) are predicted to result in developmental abnormalities (Todesco et al., 2010; Rodriguez et al., 2012), while the inhibitions of two other miRNA pathways (miR167 and miR319) are predicted to trigger floral defects (Wu et al., 2006; Nag et al., 2009). Therefore, the data suggest that not all *SP*s have strong efficacies to inhibit the miRNAs they are targeting.

5.2.3 The steady-state RNA levels of *SP*s did not correlate with their inhibition efficacies

To investigate why the *SP*s displayed different inhibition efficacies, the potential factors that may influence the *SP*-miRNA interaction were carefully scrutinized. First, it was investigated if the *SP* inhibition efficacies have a correlation to the RNA levels of different *SP*s, by qRT-RCR analysis of each *SP* in their respective T1 transformants. It was found that, though all *SP*s were under the control of 35S promoter, the RNA levels of different *SP*s varied significantly, by even more than an order of magnitude (Figure 5.6). More importantly, the RNA levels did not correlate with their inhibition efficacy. For instance, the abundance of *SP159* was low despite it having a relatively strong efficacy. By comparison, some of the highly abundant *SP*s, such as *SP164* and *SP319*, had low or no inhibition efficacies. This indicates that the steady-state RNA levels of the *SP*s are not strictly indicative of efficacies. However, the question remained, that is for *SP*s with lowly abundant RNA levels, such as *SP170/171*, *SP396* and *SP403*, in which

predicted developmental abnormalities did not arise, can increasing their abundance increase their inhibitory effects?

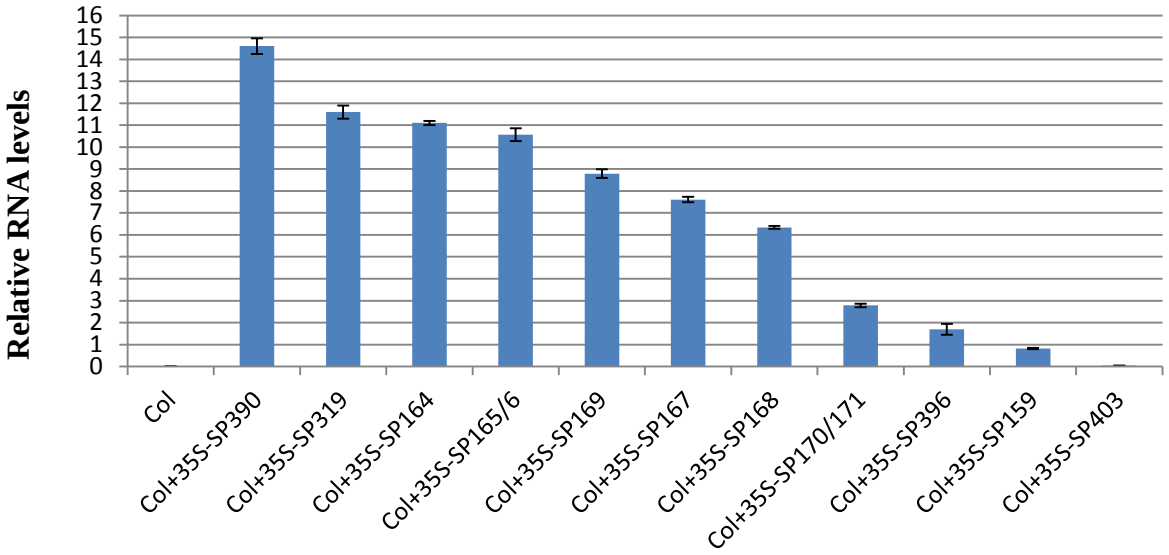

Figure 5.6: Quantification of *SP* transcripts in 12-day-old seedlings of Col transformants (Col+*35S-SP*s). For every *SP* construct, the RNA sample was extracted from 70~90 seedlings of the corresponding primary transformants (T1), when the plants were 12-day-old. All *SP* RNA levels were normalized with *CYCLOPHILIN*. Measurements are the average of three technical replicates with error bars representing the SD.

5.2.4 Increased *SP* RNA levels in *rdr6* did not enhance the *SP* inhibition efficacies

*SP*s are composed of repetitive sequences, which raise the possibility that the plant RNAi transitivity pathway is triggered to silence these *SP* transgenes (Axtell et al., 2006). To examine this possibility, *SP* transgenes that resulted in only low steady-state *SP* RNA levels, were transformed into a RNAi-transitivity-defective mutant, *rdr6* (*RNA-DEPENDENT POLYMERASE 6*, Peragine et al., 2004). Additionally, *SP319* (highly expressed, ineffective *SP*) and *SP159* (lowly expressed, high efficacy) were also transformed into *rdr6* for comparison.

For each *SP*, the transcript levels were compared between the *rdr6* and Col primary transformants (Figure 5.7, A). As shown, in the *rdr6* background, the RNA levels of *SP319*, *SP170/171* and *SP159* increased significantly, ~2.5, ~3 and ~9 fold respectively, while the RNA levels of *SP396* and *SP403* were similar between Col and *rdr6*. Therefore, it appeared that the plant RNAi transitivity pathway can impact the abundance of some *SP* transcripts, but there must be other unknown factors impacting *SP* transcript abundance as well. Then, the phenotypic analysis was performed on the *rdr6* transformants of *SP159*, *SP319* and *SP170/171*, to see if their inhibition efficacies were enhanced accordingly with the increases in their RNA abundance (Figure 5.7, B). However, similar to Col transformants, no obvious developmental defects were observed in *rdr6* transformants of either *SP319* or *SP170/171*, except the narrow-pointing leaves of *rdr6* background.

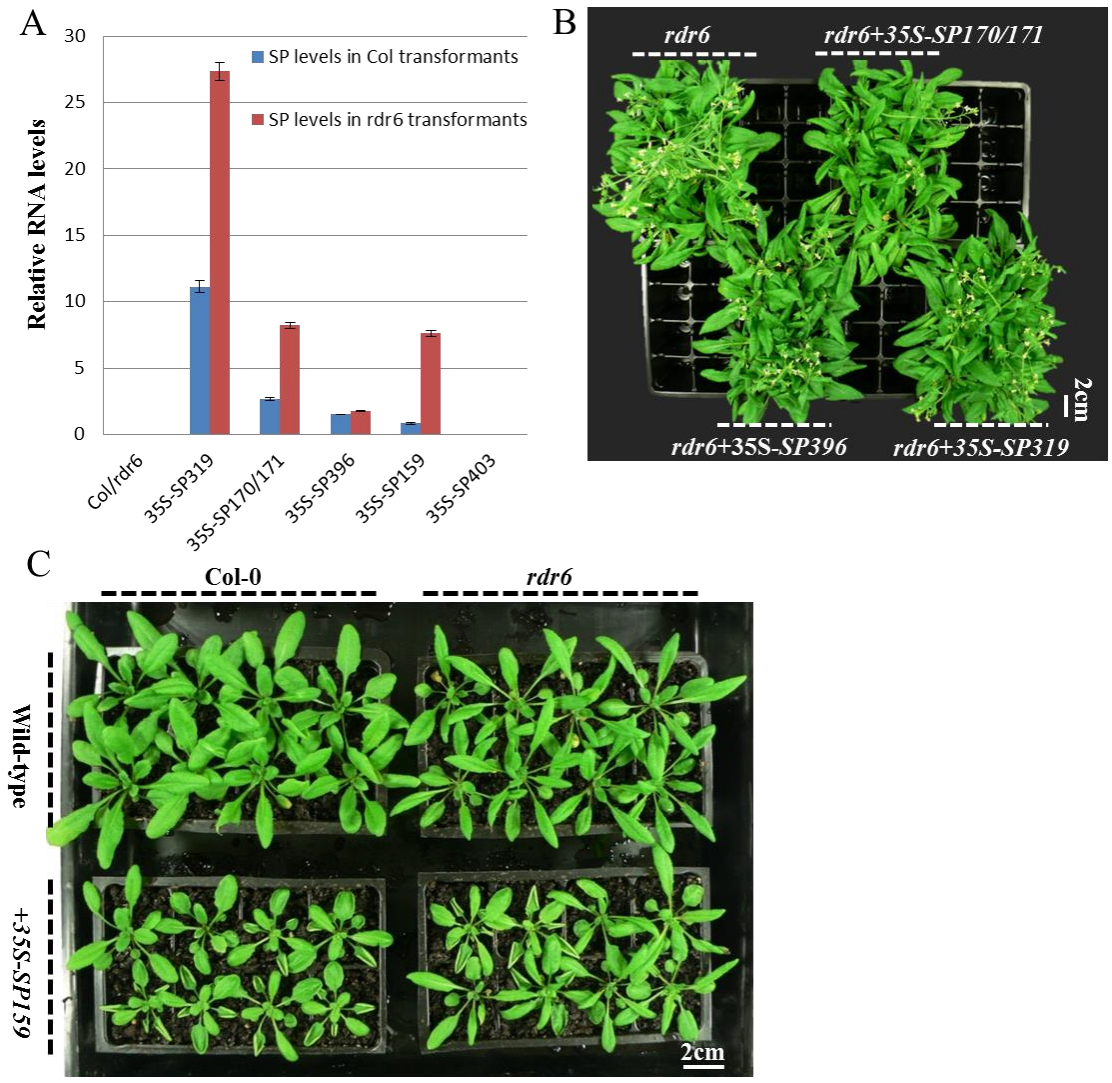

Figure 5.7: Different *SP* transcript levels in Col and *rdr6* transformants induced similar rosette phenotypes. (A) Comparison of *SP* RNA levels between Col and *rdr6* transformants. RNA samples were prepared from 50~70 seedlings of 12-day-old T1 transformants of each *SP* construct. All *SP* RNA levels were normalized with *CYCLOPHILIN*. Measurements are the average of three technical replicates with error bars representing the SD. (B) The aerial view of five-week-old *rdr6* transformants of *SP170/171*, *SP396* and *SP319*. (C) Phenotypic comparison of four-week-old Col and *rdr6* transformants of *SP159*.

In contrast, the *rdr6* transformants of *SP159* developed *mir159ab*-like leaf-curl phenotype, at high frequency. Thus the respective Col and *rdr6* transformants of *SP159* were then grown side by side, to compare the *SP* inhibition efficacies under different backgrounds (Figure 5.7, C). The results showed that, first, the severity of leaf-curl phenotypes were similar for both transformants; then moreover, the frequencies of leaf-curl events were also similar for both transformants: according to the observation, 40 out of 59 *rdr6* transformants displayed the leaf-curl phenotype (67.7%), while 35 out of 54 Col transformants also developed the similar phenotype (64.8%). Hence, the data revealed that even though the *SP159* transcript level was approximately nine folds higher in *rdr6* than in Col background, the *SP* inhibition efficacy was not evidently enhanced in *rdr6,* which indicated that the maximum inhibition efficacy of *SP159* might already be achieved in Col background. Addtionally, Li et al. (2005) have demonstrated that the miR159 level in leaves of *rdr6* mutant *Arabidopsis* did not differ from that in wild-type plants, hence the abundance of miR159 does not appear to be affected by the *rdr6* background. Taken together, these data supported the above finding that *SP* RNA abundance is not a strong factor determining *SP* efficacy.

5.2.5 No correlation between predicted RNA secondary structure and *SP* efficacy

Then, the alternative possibility was investigated: if the sequence context surrounding or within the miRNA-binding sites (target sites in *SP*s) could influence the miRNA-*SP* interaction, by affecting *SP* accessibility for a miRNA binding (Lone et al., 2007; Gu et al., 2012). First of all, the secondary structures of all eleven *SP*s were predicted using the RNAfold web server (http://rna.tbi.univie.ac.at/cgi-bin/RNAfold.cgi), which turned

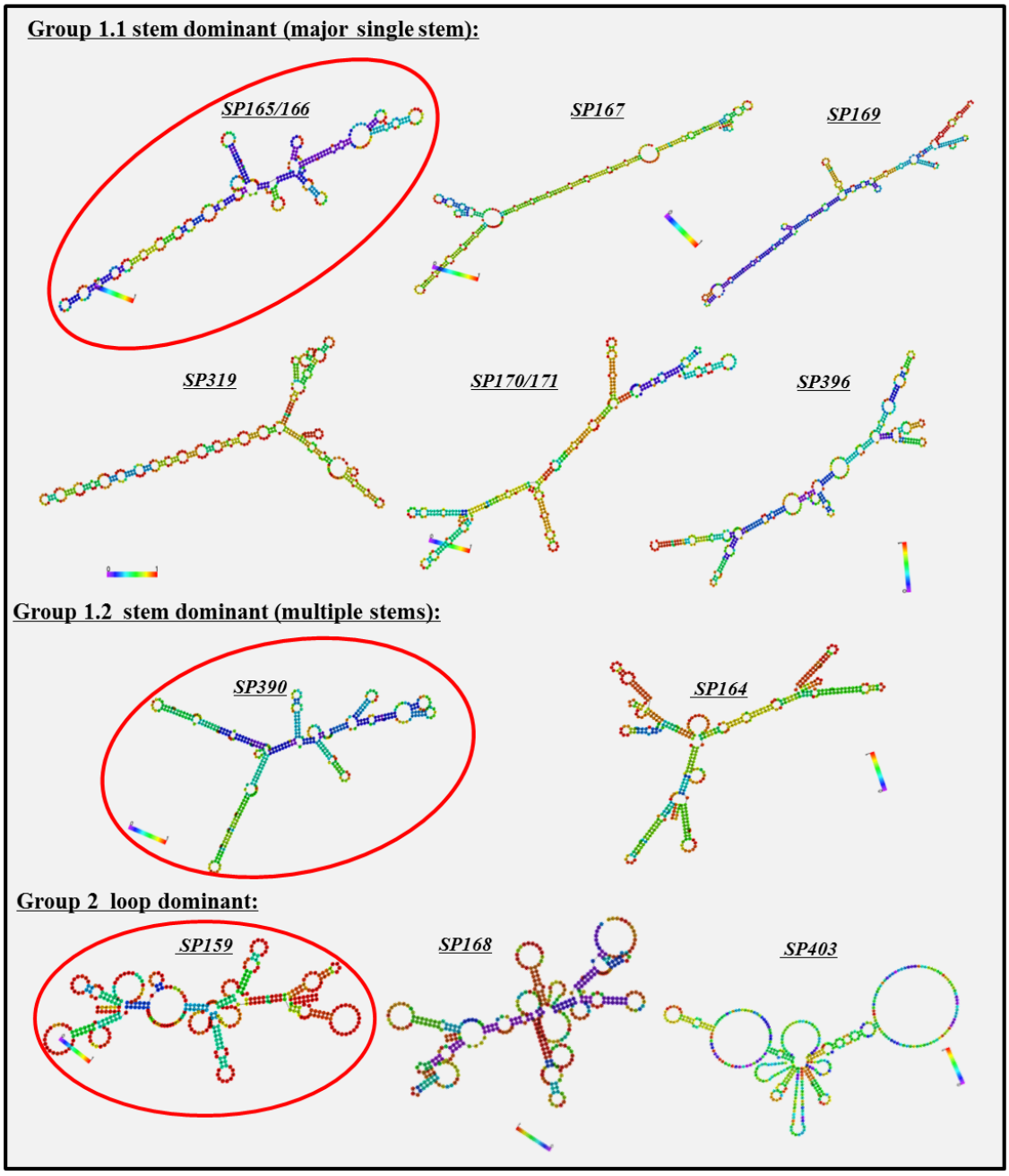

Figure 5.8: Bioinformatically predicted secondary structures of eleven *SP*s. The structures were statistically predicted using the RNAfold web server (ViennaRNA Web Services: http://rna.tbi.univie.ac.at/cgi-bin/RNAfold.cgi), coloured scale bars indicate base-pair probabilities; *SP*s with good inhibition efficacies were red circled.

out to vary from case to case (Figure 5.8). To simply classify, the sponges were assigned into two groups with regard to the overall structure similarity. Group one has the sponges predominantly composed of long stems, either a single stem or with branches (Figure 5.8, group 1.1 and 1.2). Group two has the sponges predominantly composed of loops (Figure 5.8, group 2). Then, it was found that the predicted structures of *SP*s with good inhibition efficacies varied drastically, which could be allocated into all classified groups, such as the efficient *SP165/166* is predicted to have a long single stem, appearing similar to the predicted structure of *SP319*, while the latter is the inefficient *SP*. Also, both the *SP159* and *SP168* are predicted to carry multiple loops, suggesting their target sites is likely readily exposed, and hence is likely highly accessible to the respective miRNA binding (Lone et al., 2007; Li et al., 2012a; Gu et al., 2012), but the inhibition efficacy of *SP168* (23%) was found much lower than that of *SP159* (65%). Therefore, according to the RNA folding analysis, there is no preferential secondary structure predicted to associate with a good *SP* inhibition efficacy.

5.2.6 Optimizing the predicted accessibility of target sites did not increase the *SP* inhibition efficacy

Target site accessibility represents the difficulty of opening miRNA target region (target site) for its binding with a miRNA (Gu et al., 2012). To test whether the target site accessibility can influence the *SP* inhibition efficacy, experiments were designed to alter the accessibility of the *SP* target sites, and check if the *SP* inhibition efficacy can be changed. Owing to the complexity of analysing accessibilities of 15 target sites in one *SP*, I chose to focus on the relationship between the accessibility of single target site and its inhibition efficacy. Since the *MIM159* and *MIM156* transgenes utilizing a single

target site have been shown to effectively inhibit miR159 and miR156 activities respectively (Franco-Zorrilla et al., 2007; Todesco et al., 2010), the *MIM159* and *MIM156* target sites were chosen.

Previous analysis has shown that, to make the plant miRNA target site more accessible, not only the target site is less structured than the flanking region (Li et al., 2012a), but also synonymous codons are often utilized in flanking regions, to making the region less structured and easier to open (Gu et al., 2012). Thereby, the accessibility optimization was attempted by placing the target site in a completely unpaired loop region of a "stem-loop" transgene (termed *Loop159* and *Loop156*, Figure 5.9). To compare, the target site was alternatively placed into the tightly-paired stem region of a "stem-loop" transgene (termed *Stem159* and *Stem156*, Figure 5.9). To maximise the chance that these structures will form *in vivo*, I aimed to design these constructs with high base-pairing probability; and to minimise the chance of these constructs being cleaved by *DICER*-cleavage activity (Song et al., 2010), the predicted long stem region of each construct was interrupted with two small stem-loop branches (Figure 5.9). Also, for these transgenes, both the GC content and the thermodynamic stability ($\Delta G_{(s)}$, Figure 5.9), which had been suggested might influence the accessibility and the inhibition effect (Gu et al., 2012; Yan et al., 2012), were kept as close as possible for *Loop159* and *Stem159*, and for *Loop156* and *Stem156*.

For comparison, the target sites were placed into the backbone of "*TuD*" miRNA decoy, which had been chosen to achieve efficient miRNA inhibition in mammalian cells (Haraguchi et al., 2009), and hence is supposed to provide flanking structural features that make the target site easily accessible (termed *TuD159* and *TuD156*, Figure 5.9).

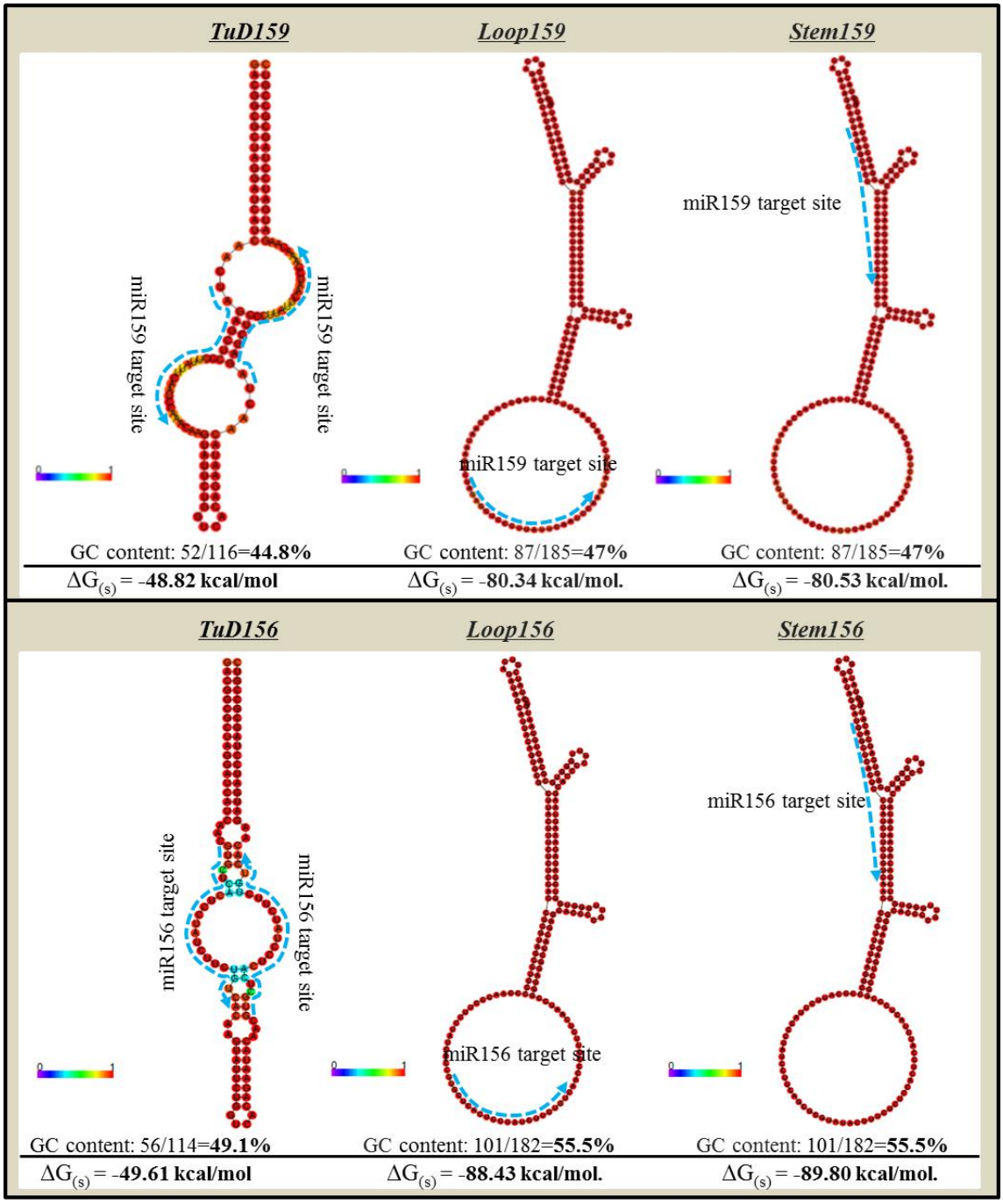

Figure 5.9: Construction of miR159/miR156 target sites into *TuD* backbone and *stem-loop* backbone. The secondary structures were predicted by the RNAfold web server (http://rna.tbi.univie.ac.at/cgi-bin/RNAfold.cgi). The dashed blue curved arrow represents the miRNA-binding site (5'-3'). The thermodynamic stability was illustrated by the free energy of the thermodynamic ensemble [ΔG(s)]. Colour bars indicate the base-pairing probability.

Next, the respective transformants were generated to assess the inhibition efficacies of these six constructs. For every construct, ~100 primary transformants were obtained and their phenotypes were scored. In contrast to the expression of *MIM159* that induces *mir159ab*-like phenotypes (Todesco et al., 2010), or expression of *MIM156* that promotes early flowering, with reduced number and size of rosette leaves (Franco-Zorrilla et al., 2007; Todesco et al., 2010), only *TuD159* transformants developed *mir159ab*-like phenotypes, at a low frequency (25%, Figure 5.10, A). Neither the *Loop159* nor the *Loop156* could effectively inhibit the respective miR159 and miR156 activities to result in a morphological defect, even though the *MIM159* and *MIM156* target sites in these transgenes were predicted to be highly accessible. Moreover, the low inhibition efficacy of *TuD159* and ineffective *TuD156* indicated that the *TuD* backbone cannot guarantee efficient miRNA inhibition in plants either.

For each primary transformant population (T1), mRNA levels of the relative miRNA targets were measured by qRT-PCR analysis (Figure 5.10, B). The results showed that the expression of *TuD159* could result in the de-regulation of *MYB33/65* and *CP1* transcript levels, confirming the *TuD159* can inhibit miR159 function to a certain extent. However, this inhibition was weak as gauged by *MYBs* and *CP1* mRNA levels in *mir159ab* (Figure 5.10, B). For the *Loop159* and *Stem159* transformants, mRNA levels of *MYB* and *CP1* were slightly higher (Student's T-Test: $P < 0.05$), suggesting they might be weakly inhibiting miR159 activity, but since these plants were similar to wild-type in appearance, these inhibitions were not phenotypically significant. Similarly, the *SPL3* mRNA level (target of miR156) was not strongly de-regulated in *TuD156*, *Loop156* and *Stem156* transformants (Figure 5.10, B), consistent with these constructs being incompetent in inhibiting miR156 function. Therefore, it appeared that neither

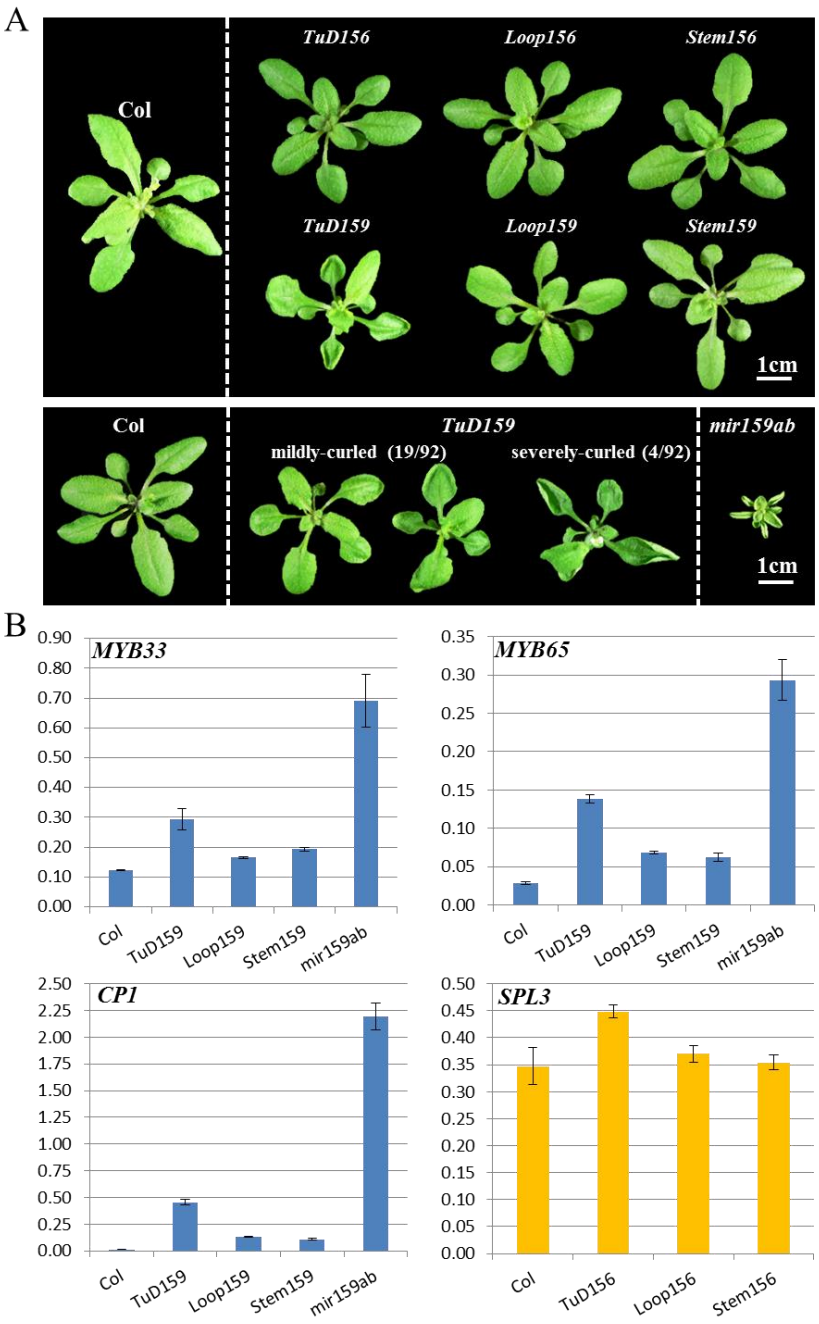

Figure 5.10 Phenotypic and molecular analyses of T1 transformants of *TuD/Loop/Stem-156/159*. (A) Expression of *TuD159* induces leaf-curl phenotype in four-week-old T1 transformants. Top panel: Aerial view of four-week-old Col transformants of *TuD/Loop/Stem-156/159*; bottom panel: close-up of the *TuD159* transformants. The embedded number indicates the proportion of T1 transformants falling into the classified group. (B) qRT-PCR analysis of relative mRNA levels in these T1 transformants. RNA samples were extracted from 70~100 T1 rosettes of 12-day-old. All mRNA levels were normalized with *CYCLOPHILIN*. Measurements are the average of three technical replicates with error bars representing the SD.

utilizing the "*TuD*" backbone with assumed good target site accessibility, nor designing an artificial construct in which the miRNA target site is predicted to be highly accessible, could result in an efficient miRNA inhibition in *Arabidopsis*.

5.2.7 Modified target sites with favourable free energy for miRNA hybridization could not change the *SP* inhibition efficacy

A third possible reason for poor *SP* efficacy is that the *SP* transcript is still cleaved by the target miRNA, and hence is unable to efficiently sequester the miRNA (Ivashuta et al., 2011). Supporting this, Li et al. (2014a) has recently reported the robust cleavage activity of miR159, where a miR159-*MYB* target duplex with two central mismatches can still result in cleavage of the target. Based on this, *SP*s were modified in an attempt to circumvent this possibility, by introducing extra unpaired nucleotides in the central region of the miRNA-*SP* duplex region. More specifically, two central mismatches of the *SP* target site (termed 2M; Figure 5.11, A) were introduced with an additional one nucleotide bulge (termed 2M+1B, Figure 5.11, B), to further obstruct the miRNA-mediated target cleavage. This was compared to a *MIM* binding site, where there are no central mismatches, but only an unpaired 3 nt bulge (termed 3B; Figure 5.11, C) (Franco-Zorrilla et al., 2007). Owing to both *SP390* and *SP164* were proved effective miRNA decoys displaying moderate or low inhibition efficacies, the modifications were made on these two *SP*s, to test if the modified target sites could enhance the *SP* inhibition efficacies.

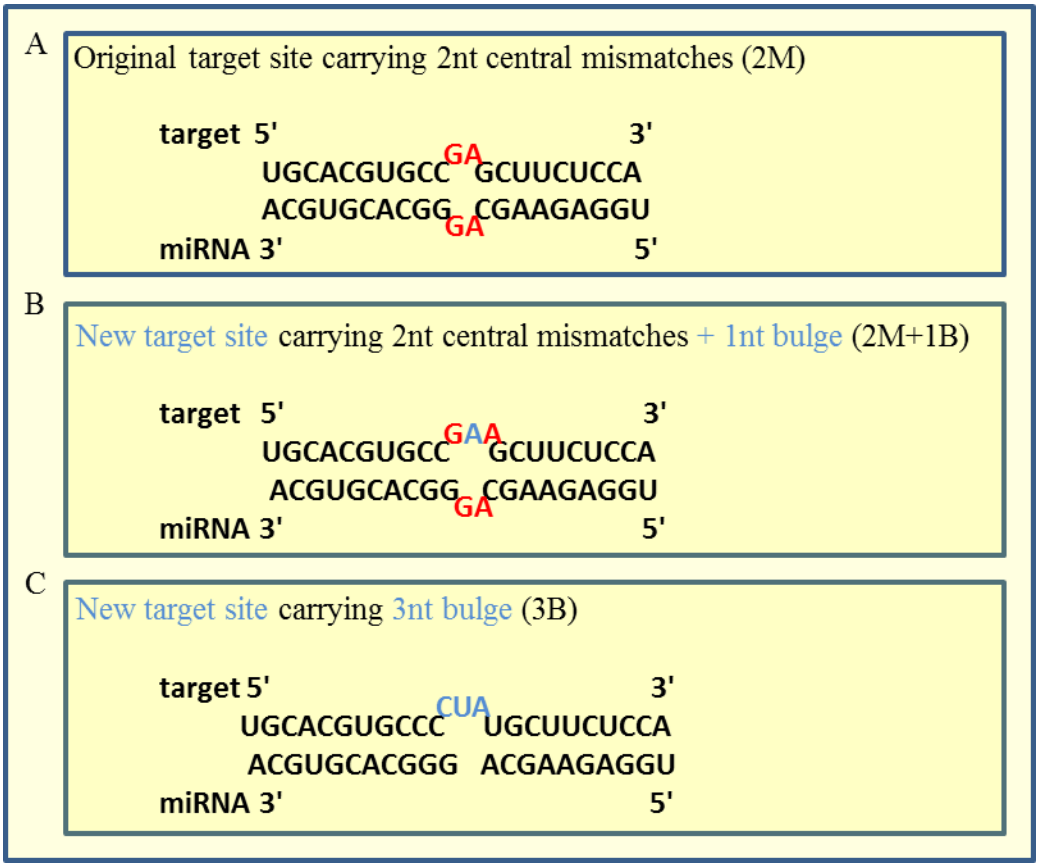

Figure 5.11: Modification of the sponge target site with central unpaired nucleotides. The *SP164* were taken as an example. (A) The original target site carrying 2nt central mismatches [termed *SP164(2M)*]. (B) Modified target site carrying 2nt central mismatches plus an additional 1nt bulge [termed *SP164(2M+1B)*]. (C) Modified target sites carrying a 3 nt central bulge [termed *SP164(3B)*]. Red-coloured sequences indicate the original mismatches; blue coloured sequences indicate the newly introduced bulges.

Additionally, the free energy (ΔG) of miRNA-target hybridization was calculated for all these *SP* target sites. As shown in Table 5.1 and 5.2, the ΔG of all target site versions satisfied the energetic requirement for a strong miRNA-target interaction (at least 72% compare to the perfect match; Schwab et al., 2005). Among them, the 3B target site has the strongest ΔG, whereas the 2M+1B target site had the weakest. This difference may help to analyse whether ΔG of miRNA-target hybridization was a factor influencing the *SP* inhibition efficacy.

miR164a TGGAGAAGCAGGGCACGTGCA	**Mfold web server (Zuker, 2003)**	**RNAhybrid web server (Rehmsmeier, 2004)**	**Hybridization (Rehmsmeier, 2004)**
Perfect match			
TGCACGTGCCCTGCTTCTCCA	-49.1 kcal/mol	-49.4 kcal/mol	Target 5' 3' UGCACGUGCCCUGCUUCUCCA ACGUGCACGGGACGAAGAGGU miRNA 3' 5'
Sponge with 2 mismatches (2M)			
TGCACGTGCCGAGCTTCTCCA (**Original sponge**)	-40.0 kcal/mol (81.5%)	-43.6 kcal/mol (88.3%)	Target 5' GA 3' UGCACGUGCC GCUUCUCCA ACGUGCACGG CGAAGAGGU miRNA 3' GA 5'
additional 1nt bulge (2M+1B)			
TGCACGTGCCGaAGCTTCTCCA	-40.0 kcal/mol (81.5%)	-39.8 kcal/mol (80.6%)	Target 5' GAA 3' UGCACGUGCC GCUUCUCCA ACGUGCACGG CGAAGAGGU miRNA 3' GA 5'
with 3nt bulge (3B)			
TGCACGTGCCCctaTGCTTCTCCA	-43.8 kcal/mol (89.2%)	-44.1kcal/mol (89.3%)	Target 5' CUA 3' UGCACGUGCCC UGCUUCUCCA ACGUGCACGGG ACGAAGAGGU miRNA 3' 5'

Table 5.1: Energetic analysis of miR164a interaction with *SP164* target sites. Red coloured sequences indicate the central mismatches (uppercase) and bulges (lowercase). For each miRNA-target site hybridization, the free energy (ΔG) was calculated by two independent web servers: Mfold web server (http://mfold.rna.albany.edu//?q=DINAMelt/Two-state-melting) and RNAhybrid web server (http://bibiserv.techfak.uni-bielefeld.de/rnahybrid/submission.html). The ΔG of miRNA-perfect match is calculated, to assess the percentage for ΔG of each miRNA-target site compared to it. The base pairings listed on the right column were predicted by RNAhybrid web server (http://bibiserv.techfak.uni-bielefeld.de/rnahybrid/submission.html).

miR390a AAGCTCAGGAGGGATAGCGCC	Mfold web server (Zuker, 2003)	RNAhybrid web server (Rehmsmeier, 2004)	Hybridization (Rehmsmeier, 2004)
Perfect match			
GGCGCTATCCCTCCTGAGCTT	-47.9 kcal/mol	-48.9 kcal/mol	Target 5' 3' GGCGCUAUCCCUCCUGAGCUU CCGCGAUAGGGAGGACUCGAA miRNA 3' 5'
Sponge with 2nt mismatches (2M)			
GGCGCTATCCGGCCTGAGCTT (**Original sponge**)	-39.8kcal/mol (83.1%)	-41.1 kcal/mol (84.0%)	Target 5' GG 3' GGCGCUAUCC CCUGAGCUU CCGCGAUAGG GGACUCGAA miRNA 3' GA 5'
additional 1nt bulge (2M+1B)			
GGCGCTATCCGaGCCTGAGCTT	-39.2kcal/mol (81.8%)	-40.1 kcal/mol (82.0%) (worse)	Target 5' GAG 3' GGCGCUAUCC CCUGAGCUU CCGCGAUAGG GGACUCGAA miRNA 3' GA 5'
with 3nt bulge (3B)			
GGCGCTATCCCctaTCCTGAGCTT	-42.6kcal/mol (88.9%)	-43.6 kcal/mol (89.2%) (better)	Target 5' CUA 3' GGCGCUAUCCC UCCUGAGCUU CCGCGAUAGGG AGGACUCGAA miRNA 3' 5'

Table 5.2: Energetic analysis of miR390a interaction with *SP390* target sites. Red coloured sequences indicate the central mismatches (uppercase) and bulges (lowercase). For each miRNA-target site hybridization, the free energy (ΔG) was calculated by two independent web servers: Mfold web server (http://mfold.rna.albany.edu//?q=DINAMelt/Two-state-melting) and RNAhybrid web server (http://bibiserv.techfak.uni-bielefeld.de/rnahybrid/submission.html). The ΔG of miRNA-perfect match is calculated, to assess the percentage for ΔG of each miRNA-target site compared to it. The base pairings listed on the right column were predicted by RNAhybrid web server (http://bibiserv.techfak.uni-bielefeld.de/rnahybrid/submission.html).

~200 Primary transformants per transgene were obtained and compared for *SP164(2M)*, *SP164(2M+1B)* and *SP164(3B)*. Likewise, ~200 primary transformants per transgene were obtained and compared for *SP390(2M)*, *SP390(2M+1B)* and *SP390(3B)*. All *SP*s induced similar defects at similar frequencies and severities. For the *SP*s targeting miR164, approximately 10% of primary transformants had defects; whereas for the *SP*s targeting miR390, approximately 55% of primary transformants had defects.

To complement these observations, the transcript levels of the target genes of miR390 and miR164 were measured by qRT-PCR (Figure 5.12). The data revealed that all *SP*s resulted in similar de-regulation of their respective target genes. First, in all three *SP390* transformant populations (T1), the *ARF3/4* mRNA levels were increased by 1-1.5 fold (ANOVA test, *ARF3*: P = 0.008455; *ARF4*: P = 0.001188), supporting the notion that all three *SP390* versions have similar inhibition effects. Likewise, *CUC* mRNA levels increased by either 3-4 fold (*CUC1*, ANOVA test: P= 0.01025) or 1.5-2 fold (*CUC2*, ANOVA test: P= 0.04268) in transformants of all three *SP164* versions, supporting the notion that all three *SP164* versions also have similar inhibition efficacies. Together, the data suggests that modifying the target sites within *SP*s did not have a drastic impact on their efficacies, and also that strengthening the ΔG of miRNA-target hybridization does not guarantee an enhanced inhibition efficacy (refer to the comparison between the 3B and 2M+1B target site versions).

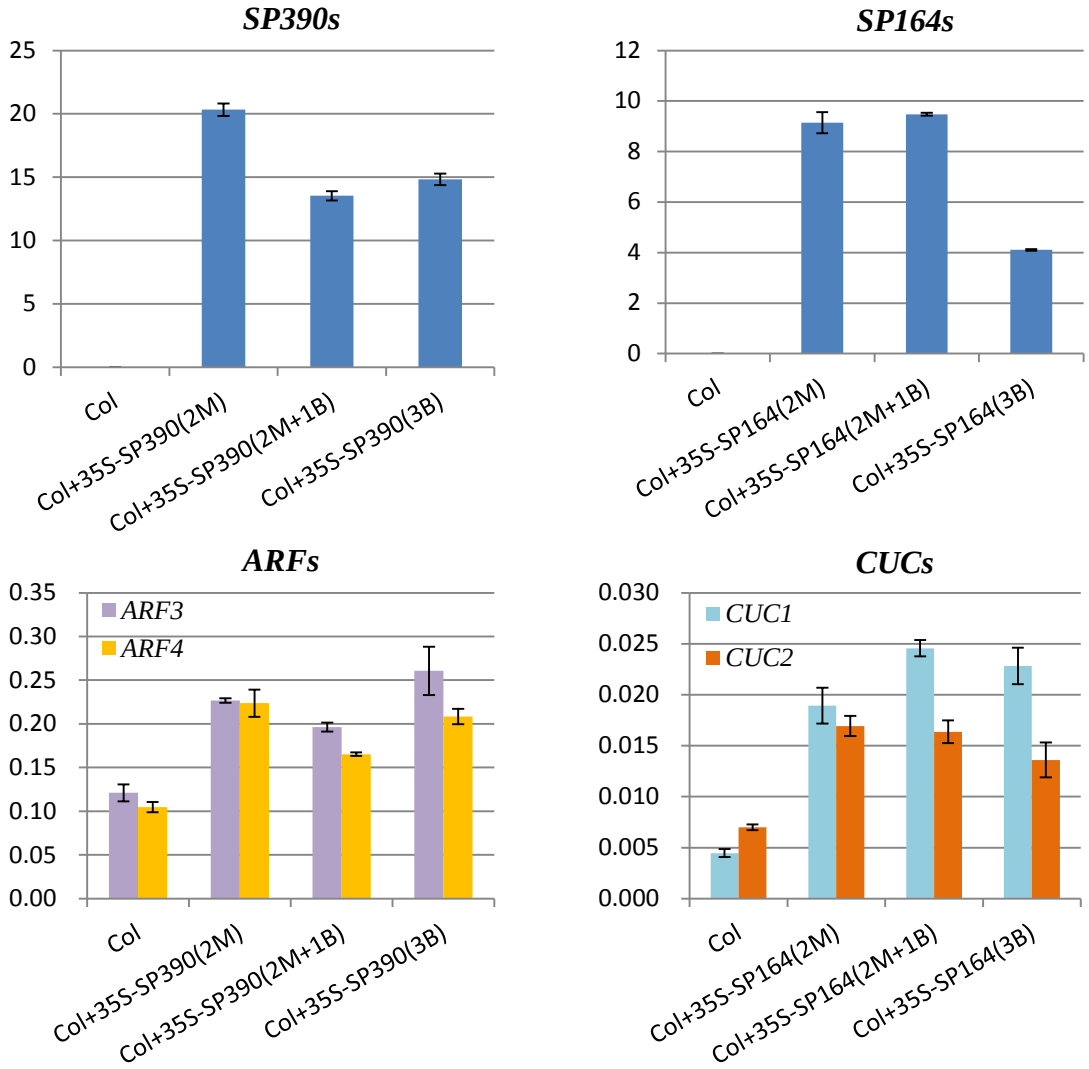

Figure 5.12: Molecular analysis of different *SP390*s and *SP164*s transformants. For every construct, the RNA samples were extracted from ~100 12-day-old T1 transformants. All mRNA levels were normalized with *CYCLOPHILIN*. Measurements are the average of three technical replicates with error bars representing the SD.

5.2.8 Generation of LhG4/*pOP6-SP*s system to inhibit miRNA function in a tissue/cell specific manner (this work has been published in Reichel et al., 2015)

In plants, many miRNAs are functioning in specific spatial and temporal manners, in order to achieve precise target gene regulation for required developmental outcomes, namely regulating specific tissue or even cell development (Vá lóczi et al., 2006; Wu et al., 2009, Wong et al., 2011). Therefore, inhibiting miRNA in a tissue/temporal-specific manner may reveal the specific developmental role that a miRNA play. To this end, an LhG4/pOP6 transactivation system was utilized to investigate this possibility (Figure 5.13, A).

5.2.8.1 Generation of the LhG4/*pOP6-SP*s system

This system is composed of two components (Figure 5.13, A). First, a transactivator LhG4, which has been incorporated into an enhancer trap line, becomes under control of an endogenous promoter resulting in a very precise tissue/temporal expression pattern (Rutherford et al., 2005). Secondly, a *pOP6-SP* transgene to be transformed into this enhancer trap line, where the LhG4 transactivator can bind onto the pOP6 promoter and activate expression of its downstream gene(s). To generate the *pOP6-SP* expression clones, a multisite gateway method was utilized: The *SP*s were synthesized with the attL1 and attL2 flanks, so that they could be recombined with the attL4-*pOP6*-attR1, the attR2-*GFP*-attL3 entry clones, and the attR3-*ccdb*-attR4 destination clone, via a single LR reaction, to form the *pOP6-SP-GFP* expression clones (Figure 5.13, C; Karimi et al., 2007).

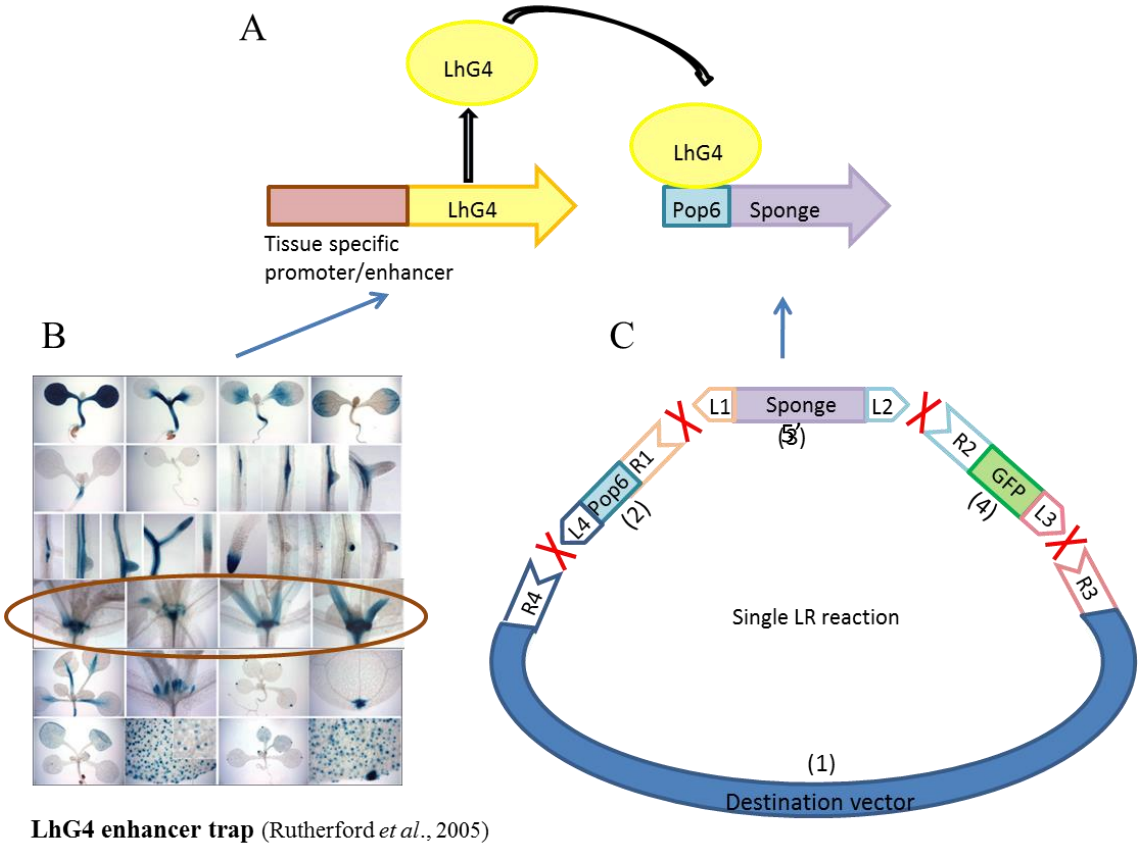

Figure 5.13: Construction of LhG4/*POP6-SP* transactivation system. (A) Cartoon depicting LhG4/*POP6*-based transactivation of sponge expression. When LhG4 is fused downstream of a tissue specific promoter or enhancer, it will be expressed in the corresponding tissue where it can activate the pOP6 promoter and hence the *SP* expression. (B) The *Arabidopsis* enhancer traps verified by GUS-staining of *pOP6-GUS* transgene (Rutherford et al., 2005). Tested LhG4 lines in this study were brown circled (C) Preparation of *pOP6-SP-GFP* clone via a MultiSite LR reaction. The entry vector 3 was designed to carry the *SP* sequence with the attL1 and attL2 sites in order as shown. The other three are commercial vectors carrying the attR3-*ccdb*-attR4 (vector 1), the attL1-*pOP6*-attL2 (vector 2) and the attR2-*GFP*-attL3 (vector 4) fragments respectively (http://gateway.psb.ugent.be/vector/show/pEN-R2-F-L3/search/index/), so that the compatible attL and attR sites (indicated by the same number) can be recombined in the predefined orientation via a single LR clonase reaction, to form the *pOP6-SP-GFP* expression clone (Karimi et al., 2007)

5.2.8.2 Using *SP165/166* to inhibit miR165/166 activity in a tissue specific manner

To test if the LhG4/*pOP6-SP* system can inhibit miRNAs in a tissue specific manner, the *SP165/166* was utilized, as this *SP* gave a very characteristic phenotype (Figure 5.2). The miR165 have been suggested to play essential roles in the establishment of leaf polarity and the development of the shoot apical meristem (SAM), by accumulating in the abaxial domain of developing leaf primordia, but being sequestered by the *AGO10* protein in the SAM area (Zhu et al., 2011; Zhang and Zhang 2012). Thereby, what developmental defects can be triggered by inhibiting miR165/166 function in the SAM and relative leaf areas are intriguing but unknown. To investigate, the enhancer LhG4 line, termed HET:59a, that activates the expression of *pOP6-GUS* predominantly in the SAM and midrib of the leaves was utilized (indicated in Figure 5.13, B, Rutherford et al., 2005).

Primary HET:59a transformants of *pOP6-SP165/166-GFP* and *pOP6-GUS-GFP* were generated [termed *pOP6-SP165/166-GFP*(HET:59a) and *pOP6-GUS-GFP*(HET:59a)], they were then grown side by side for comparison. First of all, to verify the expression pattern, the GFP fluorescence was checked under the microscopy, but no signals could be detected. However, when the Histochemical GUS staining was performed along the growth of the *pOP6-GUS-GFP*(HET:59a), the expression of *GUS* was found restricted around the SAM area for approximately two-week during early vegetative growth (Figure 5.14, A), and then gradually penetrated into the midrib of the developing leaves when the plant became older (Figure 5.14, B). Thus, the GUS staining results indicated that the *pOP6*-transgene constructs were able to deliver the expected expression pattern.

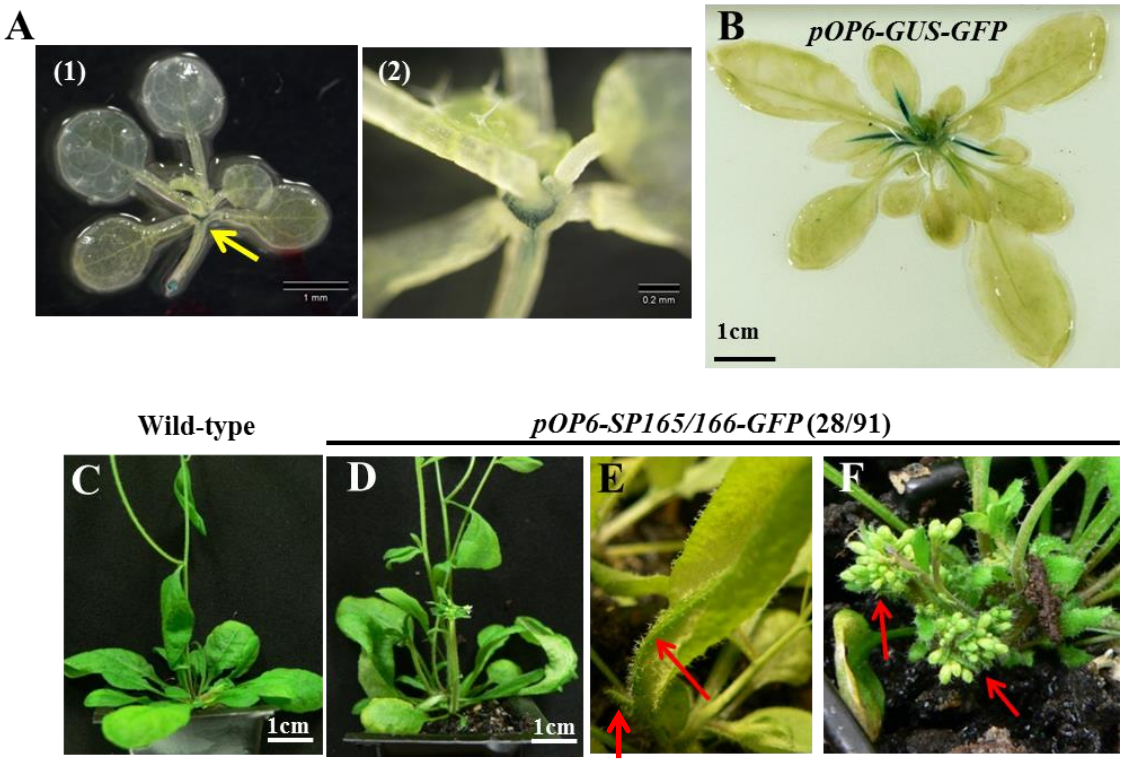

Figure 5.14: Expression of *pOP6-SP165* transgene induced phenotypic abnormalities in LhG4 enhancer trap line: HET:59a. (A-B) Histochemical GUS staining of 17-day-old seedlings and 40-day-old rosettes of *pOP6-GUS-GFP* (HET:59a) control plants. (C-D) Phenotypic comparison of 5-week-old *pOP6-GUS-GFP*(HET:59a) (wild-type) and *pOP6-SP165/166*(HET:59a) plants. (E-F) Close-ups of defects in leaves and floral organs of 5-week-old *pOP6-SP165/166* (HET:59a) transformants. Yellow arrow indicates the GUS-stained region. Red arrow indicates the identified defect.

Next, phenotypes of the *pOP6-SP165/166-GFP*(HET:59a) were recorded along with the plant growth. It turned out that the expression of *pOP6-SP165/166-GFP* induced obvious phenotypic defects, in approximately one third of the HET:59a transformants, which were consistently presented on the leave midrib and SAM tissues (Figure 5.14, C-F). Interestingly, unlike the *35S-SP165/166* induced trump-shaped leaves, the *pOP6-SP165/166-GFP*(HET:59a) displayed an aberrant outgrowth of adaxial-like tissue on the abaxial side of the leaf midrib, with trichomes growing on them (figure 5.14, E). This illustrated the specific effect of inhibiting the miR165 function in the leaf midrib. Meanwhile the *pOP6-SP165/166-GFP*(HET:59a) also developed 'fasciated' florescence meristems with flowers crowded around the proximal area, which was likely due to the inhibition of miR165 function in "SAM" area, as indicated by the GUS-staining in the SAM of the *pOP6-GUS-GFP*(HET:59a) line (Figure 5.14, A and B).

In summary, the *pOP6-SP165/166-GFP* could be conveniently generated via the multisite gateway method, and be utilized to inhibit the miR165/166 function in specific tissues upon transformation into the LhG4 enhancer trap lines (Rutherford et al., 2005). This may provide a simple approach to realize the tissue or even cell specific miRNA inhibition, with the utilization of effective *SP* or *Mimic* transgenes. As a minor modification, the *GFP* gene could be removed from the pOP6 constructs, as the GFP signal may not be strong enough to be detected.

5.3 Discussion

5.3.1 Inhibition efficacy assessment revealed significantly varying *SP* inhibitory effects for different plant miRNAs

Though the "miRNA sponge" is well known as an efficient miRNA decoy for inhibiting animal miRNA activities (Ebert et al., 2007), rare research has shown its capability in inhibiting plant miRNAs. In this study, ten miRNA *SP*s were allocated to ten conserved plant miRNAs, and the inhibition efficacy (the percentage of the miRNA-decoy-induced phenotype) was defined for quantitatively assessing the *SP* inhibitory effect in *Arabidopsis*. With this efficacy assessment, it was found that the efficiencies of *SP*s in inhibiting different plant miRNAs remarkably varied. More specifically, based on previous methods that indicated loss-of-function *mirna* outcomes (i.e. transgenic expression of miRNA-resistant target transgene, transgenic expression of miRNA *Mimic* decoy, and generation of *mirna* mutant), the expected loss-of-function *mirna* phenotypes for examined ten miRNAs were summarised (Table 5.3). It is clear to see that the defects induced by some *SPs* agreed with the expectations (i.e. *SP159*, *SP390*, *SP168*, *SP164*), which supports the inhibition activities of plant miRNA *SP*s. However, via inhibition efficacy assessment it was found that efficacies of different *SP*s varied drastically, from 10% to 65% (Table 5.3), even if *SP*s that did not induce observable defects were excluded. An explanation to this could be that some miRNA(s) play important role(s) in plant development (e.g. miR168), the inhibition of which would result in a substantial loss of plant viability. Thus, for transformants of *SP*s targeting these miRNAs, only plants showing mild or no inhibition of miRNA activities could be recovered, resulting in seemingly reduced *SP* efficacies. However, this possibility would not explain the low efficacies of several *SP*s, such as *SP164* and *SP319*, since the corresponding *mir164abc* and *mir319a* knockout mutants have been obtained and

developed distinct viable phenotypic defects (Sieber et al., 2007; Nag et al., 2009).. Therefore, it is likely that there may be other factors that influence miRNA-*SP* interactions. Finding these factors may be the key to modify *SP*s into more effective versions so that they can be widely applied for inhibiting miRNA activities in plants.

miRNA	Expected loss-of-function *mirna* phenotype	Observed phenotype in *SP* transformants (efficacy)
miR159	Upwardly curled leaves, reduction of rosette size (*mir159ab*) [3]	65%
miR390	Narrow, pointed leaves (*ago7-1*) [3]	58%
miR168	Narrow, twisted leaves and early flowering (*mir168a* grown in a glasshouse) [3]	23%
miR164	Serrated leaves[2]	10%
miR169	Reduced rosette sizes[2]	N
miR170/171	Round leaves of pale green colour, reduced fertility[2]	N
miR396	Larger leaves[1]	N
miR167	Smaller leaves and sterile flowers[1]	N
miR319	Short petals and stamens (*mir319a*) [3]	N
miR403	Unknown	N

Table 5.3: Summary of the expected and observed loss-of-function *mirna* phenotypes for ten examined miRNAs. The expected phenotypes were summarized from previous miRNA functional analyses performed in *Arabidopsis* using established methods: (1) miRNA-resistant target transgene; (2) miRNA *Mimic* decoy; (3) *mirna* mutant (the mutant is specified in brackets). The observed phenotype meeting the corresponding expectation is illustrated by a percentage of the primary transformants displaying this expected phenotype (efficacy). "N" indicates no obvious morphological abnormality could be observed.

5.3.2 Using *SP390* and *SP168* to inhibit the miR390 and miR168 respectively

Inhibiting miR390 and miR168 activities via *SP* method induced distinct morphological defects (Figure 5.2), which had not been reported by using current *Mimic* methods (Todesco et al., 2010; Yan et al., 2012). Thus, the *SP390* and *SP168* may be used as the alternative miRNA decoys for functional analyses of miR390 and miR168 respectively.

First, unlike the other miRNAs, the miR390-mediated gene regulation is majorly implemented through its incorporation into AGO7 protein, instead of AGO1 (Montgomery et al., 2008; Endo et al., 2013). The questions could be raised as whether the miR390 activity and function are exclusively implemented through AGO7 and whether AGO7 only implement miR390 activity and function, considering other miRNAs can be incorporated into AGO7 as well (Montgomery et al., 2008) and a certain amount of miR390 could be loaded into other AGO proteins (Mi et al., 2008). To date, studies of the gain-of-function *ARF3/ARF4* transgenic plants (the targets of ta-siRNAs derived from miR390-mediated cleavage of *TAS3* transcript, Adenot et al., 2006) have suggested roles of the miR390-AGO7 association in developmental timing and patterning (Hunter et al., 2006; Fahlgren et al., 2006). However, these data cannot precisely illustrate the contribution of miR390 activity in plant phase change process; on account of that *ARF* targets are also under the control of other protein regulators, termed ASYMMETRIC LEAVES (i.e. AS1 and AS2, Iwasaki et al., 2013). To circumvent this complexity in functionally analyzing the miR390, the miRNA decoy that can effectively inhibit miR390 activity is required. In this study, more than half of the *SP390* transformants developed narrow and pointing leaves, which is similar to the rosette defect of *ago7* mutants, but appeared milder (Figure 5.3). Thus the resulted phenotypic defect supports *SP390* to be such a miRNA decoy. For investigating the possibility of functional discrepancy between miR390-mediated and AGO7-mediated

gene expression, the transformation of *SP390* into the *ago7-1* mutant may be performed to examine if severer or additional morphological defect(s) could be revealed.

Then, the expression of *SP168* inhibited the miR168 function, resulting in an increase of the *AGO1* mRNA level, accompanied with ruffled and less compacted rosette leaves. This morphological defect might be explained by the combinational effects of up-regulated targets of multiple miRNAs and *TAS3* ta-siRNA, as indicated by the increases of *ARF3* and *CUC1* mRNA levels in the *SP168* transformants (Figure 5.5). However, this defect has not been observed for growing a loss-of-function *mir168a* single mutant under normal condition (Vaucheret, 2009), which may be due to a further redundancy with miR168b. Thus prior to applying *SP168* for any functional analysis of miR168, the *SP168*-induced defect required to be justified, perhaps by generating a *mir168ab* double mutant with Col background.

5.3.3 The RNA level of a miRNA *SP* with high inhibition efficacy is not necessarily high

To find out why the *SP*s displayed varying inhibition efficacies, factors that might influence the miRNA-*SP* interaction were carefully scrutinized. To start with, it was investigated if the *SP* RNA level is one of the influential factors. Interestingly, the qRT-PCR analysis suggested that even under the control of the same 35S promoter, the steady-state RNA levels of different *SP*s varied significantly (Figure 5.6). Moreover, the *SP159* displaying high inhibition efficacy was found in a relatively low abundance whereas high abundance of some other *SP*s, such as *SP164* and *SP319*, did not make them efficient miRNA decoys. These results illustrated that the *SP* inhibition efficacy is

not strongly correlated to its abundance. Then, the transformation of *35S-SP159* into a *rdr6-15* mutant, where the RNA level of *SP159* was increased approximately nine folds than that in Col background, did not significantly enhance the inhibition efficacy of *SP159* (Figure 5.7). This further suggested the *SP* with good efficacy is not necessarily highly expressed, and it appears that the expression threshold for a *SP* to effectively inhibit a miRNA may not be very high, thus once this threshold was satisfied, enhancing *SP* expression further could not enhance the *SP* inhibition efficacy.

5.3.4 Correlation between the *SP* inhibition efficacy and target site accessibility could not be found via bioinformatics-based RNA secondary structural analysis

Structural and sequence features surrounding/within the *SP* target sites may affect *SP* target sites accessibility for miRNA binding and thus influence miRNA-*SP* interaction (Kertesz et al., 2007; Lone et al., 2007). In this study, analysis was performed to investigate if there is a correlation between the *SP* inhibition efficacy and target sit accessibility. This was mainly based on bioinformatic prediction of RNA secondary structures, using the RNAfold web server (http://rna.tbi.univie.ac.at/cgi-bin/RNAfold.cgi). First, a brief comparison of the RNAfold-predicted secondary structures of all eleven *SP*s (including the *SP165/166*, Figure 5.8) did not identify any preferential structural feature that was associated with the *SP*s displaying good inhibition efficacies. Then, to optimize the target site accessibility, maximizing the openness of the target region for miRNA binding was attempted. Namely, the *MIM159* and *MIM156* target sites were placed respectively into an unpaired loop structure of the transgene (i.e. *Loop159* and *Loop156*, Figure 5.9), so that these target sites are supposed to be readily accessible for miRNA binding (Li et al.,

2012a; Gu et al., 2012). However these optimized transgene constructs turned out to be ineffective in inhibiting miRNA activities, which induced similar inhibition outcomes to the transgenes embedding target site in a predicted tightly-paired stem region. Therefore, the data suggest that target sites that current bioinformatics predicts to have highly accessible secondary structures may not be able to enhance the inhibition efficacy of a decoy transgene. In addition, the low inhibition efficacy of *TuD159* and ineffective *TuD156* outcomes indicate that the optimized *TuD* backbone of mammalian miRNA decoy cannot guarantee the efficient miRNA inhibition in plant system either.

It is worth noting that these structures are predicted by the RNAfold web server. They may have high base-pairing probability according to the bioinformatic prediction method (i.e. *Loop159, stem159, Loop156 and stem156*); however, whether they can form as predicted *in vivo* is questionable. A possible explanation is that some RNA-binding proteins and or/RISC components may modulate the target accessibility *in vivo* altering their secondary structure (Long et al. 2007). Therefore, it would be good to have a method that can examine the transgene RNA structure *in vivo*, for which the *in vivo* DMS assay may be utilized (Kwok et al., 2013), to further address the relationship between the structural feature of a *SP* decoy and its inhibition efficacy.

5.3.5 Alteration of central sequences in the *SP* target site cannot strongly influence the *SP* inhibition efficacy

According to Li et al (2014a), at least some plant miRNAs can mediate the cleavage of their complementary targets that have 2-nt central mismatches against the miRNA. This raises the likelihood that some *SP* inhibitory effect might be compromised by the

efficient plant-miRNA-cleavage activity, given that all *SP*s carry target sites with 2-nt central mismatches against their corresponding miRNAs. As a modification, the *SP* target sites were either introduced with an additional 1 nt-central bulge, or a 3 nt-central bulge, aiming to further obstruct the miRNA cleavage. However, the modified *SP* versions produced similar phenotypic and molecular outcomes to the original ones. These results suggest that *SP* inhibition efficacy cannot be simply changed by an alteration of the central area of the target sites.

Note that the 3 nt-bulged target site had the most favourable ΔG for miRNA-target site interaction (Table 5.1 and 5.2). This may help to explain a previous observation: when a 2 nt-mismatched miRNA decoy was compared with a 3 nt-bulged miRNA decoy, the latter was found to deliver stronger inhibition effect on the miR171 function (Ivashuta et al., 2011). However, the ΔG did not seem to be a clear factor that is indicative of the *SP* inhibition efficacy in this study, as similar phenotypic and molecular inhibition outcomes were found for *SP164(3B)* and *SP164(2M),* and also for *SP390(3B)* and *SP390(2M).* According to these data, one may conclude that once the energetic threshold for miRNA-target site interaction is satisfied (72% compare to the perfect match; Schwab et al., 2005), a more favourable (i.e. lower) ΔG cannot strongly enhance the *SP* inhibition efficacy. Taken together, a slight change of the central-cleavage region of a target site may not strongly influence the overall *SP* inhibition efficacy when many target sites are arranged in tandem into a *SP* construct.

To sum up, when applied to plant miRNAs, the *SP*s induced significantly varying inhibition efficacies. *SP* inhibitory effects were robust, altering a general parameter

influencing the miRNA-target interaction would not strongly influence the *SP* inhibition outcome. Future discovery of novel effectors that specifically influence a plant miRNA activity may help to address the different miRNA inhibition outcomes. With respect to the observation that expression of miRNA decoys could lead to the degradation of their target miRNAs, and the severity of phenotypic effect induced by a *SP* appeared negatively correlated with the corresponding miRNA steady-state level (Yan et al., 2012; Reichel et al., 2015), it is not clear if the different degradation rates of miRNAs is a cause, or just the consequence of different *SP* efficacies, which deserves attention. We should also acknowledge the possibility that some miRNAs may not play any essential role in regulating plant morphology and hence inhibiting their activity may not result in any strong morphological defects (Flynt and Lai, 2008). This may explain the failure of the *SP* and previously studied *Mimic*s methods in inducing any observable defect when they were used to inhibit some miRNAs in *Arabidopsis* (also see chapter 6 for detailed discussion). To test this possibility, perhaps the steady-state miRNA level could be measured in transformants of *SP*s that failed to induce any phenotypic defect, to assess the availability of the respective miRNA. A hypothesis for this is that if the expression of a *SP* could induce the degradation of the cognate miRNA without affecting the plant phenotype, it may suggest the incompetence of this miRNA in inducing any morphological defect. Finally, as a suggestion for future research, the inhibition efficacies of *SP*s drastically varied from miRNA to miRNA, and recently no transgenic method can be used as "magic bullet" for effective inhibition of all plant miRNAs, hence these miRNA decoys should be used cautiously and analysed case by case.

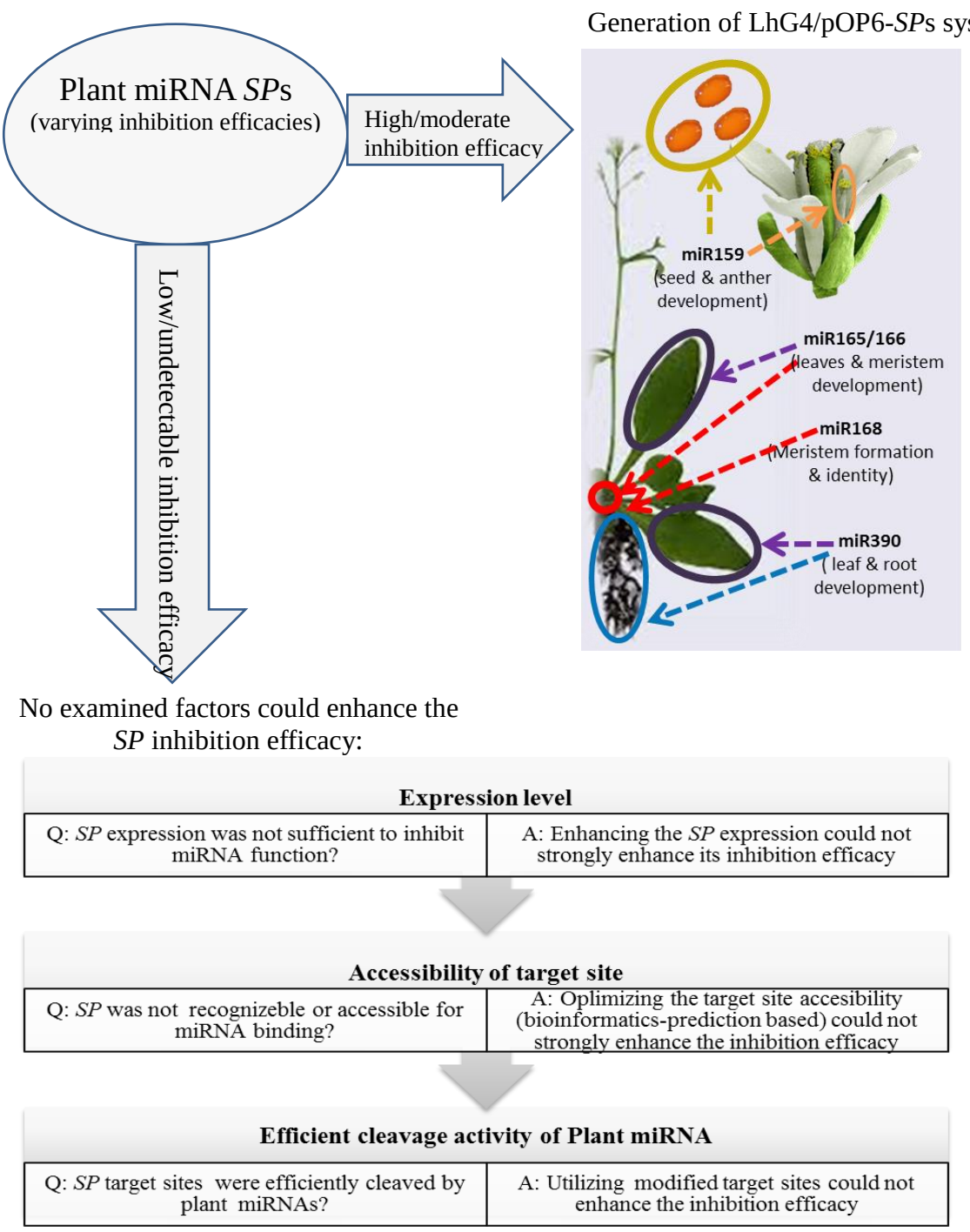

Figure 5.16: Summary diagram of exploring the *SP* method to inhibit *Arabidopsis* miRNAs. When applied to inhibit 11 conserved plant miRNAs, the *SP*s presented varying inhibition efficacies, some of them showed high (e.g. *SP159* and *SP165/166*) or moderate (e.g. *SP390* and *SP168*) inhibition efficacies, which could be used to generate the LhG4/*pOP6-SP*s for functional analyses of the corresponding miRNAs in a tissue specific manner, as their functions have been suggested to promote varying tissue developments. While some other *SP*s showed low or undetectable inhibition efficacies, for which the potential influential factors were investigated, however none of these factors could strongly influence the *SP* inhibition efficacies, thus these *SP*s may not be used to do the functional studies of relative miRNAs.

Chapter 6

General Discussion

6.1 *CP1* can act as a molecular marker that facilitates the estimation of MYB33/65 protein expression in *Arabidopsis* rosettes

Previously, a microarray-based transcriptomic comparison between *mir159ab* and wild-type Col plants has identified *CYSTEINE PROTEINASE1* (*CP1*) as the most up-regulated gene in the *mir159ab* mutant (Alonso-Peral et al., 2010). Consistently, the *CP1* transcript level increased when *MYB33* expression was de-regulated in a *mMYB33* transgenic *Arabidopsis* (*mMYB33* carries the *MYB33* coding region with synonymous mutations of the miR159 binding site and become resistant to miR159 silencing; Palatnik et al., 2003; Alonso-Peral et al., 2010). Thus, *CP1* was considered a gene downstream of *MYB33* and *MYB65*. Supporting this is bioinformatic analysis that predicts six *MYB* or *MYB*-related binding sites in the promoter region of the *CP1* gene (http://*Arabidopsis*.med.ohio-state.edu/). Additionally, proteinases are associated with programmed cell death (PCD) processes during the later stages of seed germination (reviewed in Fath et al., 2000), raising the possibility that *MYB33/65* promotes PCD-related processes during seed germination via activation of *CP1* (Alonso-Peral et al., 2010). This evidence may support the notion that *CP1* is a major *MYB33/65* downstream gene and causative of *mir159ab* phenotypic defects. However, in this study, the generation of a loss-of-function *mir159ab.cp1* triple mutant failed to suppress any phenotypic defects of the *mir159ab* rosette (Chapter 4). This indicates that *CP1* is not the sole causative gene of the *mir159ab* phenotype in the rosette, however, the possibility of other genes being functionally redundant to *CP1* in contributing to the *mir159ab* phenotype cannot be excluded.

By generating *mir159ab* mutants that carry different combinations of *MYB33* and *MYB65* wild-type alleles, the *CP1* transcript level was found to positively correlate with

MYB33 and *MYB65* expression and also the severity of *MYB33/65*-induced rosette defects (Chapter 3). This suggests a tight correlation between *CP1* transcription and *MYB33/65* expression/activity, implying it can be used as a reliable molecular marker indicating MYB expression levels in rosettes. In terms of measuring MYB33/65 protein, this provides the best alternative to western blot analysis, where no reliable antibody against MYB33 or MYB65 has been generated. Such measurements are important in assessing the MYB33/65 protein levels, as the existence of miR159-mediated translational inhibition of these *MYB* transcripts implies measuring *MYB33/65* mRNA levels give little to no indication of MYB protein levels (Li et al., 2014a).

The application of the *CP1* molecular maker of MYB33/65 is indeed critical to complement the phenotypic observations reminiscent of *mir159ab* defects. This is because the leaf-curl phenotype is a common rosette defect which is not necessarily derived from MYB33/65 activity, as illustrated by the expression of VSSs in Chapter 4, and thus the molecular verification of the *MYB* expression is required. However, we should note that the tight *CP1* regulation by *MYB33/65* was only demonstrated in rosettes, whether it can faithfully reflect the *MYB* activity in other tissues requires further investigation. For instance, in *Arabidopsis* seeds and anthers, where the miR159 activity is weak, *MYB33/65* are expressed playing important roles in promoting PCD of seed aleurone and anther tapetum (Millar and Gubler, 2005; Alonso-Peral et al., 2010). Hence, the use of *CP1* as a molecular marker of MYB expression may also be important here.

6.2 The uniqueness of miR159-*MYB* module in rosettes: miR159 is constitutively expressed to confer robust silencing of MYB33/65 expression

Using the *Arabidopsis* system, a developmental time-course found that strong miR159 activity mediates constitutive and ubiquitous silencing of *MYB33/65* expression throughout rosette development (Chapter 3). This is in sharp contrast to other miRNA families that are involved in rosette development (e.g. miR165/166, miR396, miR156 and miR172), on account of that those miRNAs all regulate their respective targets in specific spatiotemporal manners, to enable correct rosette development (Zhu et al., 2011; Poethig, 2009; Wu et al., 2009; Wang et al., 2011b). Thus, the uniqueness of miR159-mediated silencing of *MYB33/65* expression in rosettes suggests that it is unlikely to play an essential role in promoting rosette development under normal growth condition.

Then, further analysis revealed that the miR159-*MYB* module is functionally active in rosettes, in terms of regulating the rosette morphology. This is because disrupting miR159 function in an inducible manner resulted in activation of *MYB33/65* expression and the leaf-curl defect of rosettes (Chapter 3). It raised the possibility that the constitutive silencing of *MYB33/65* can be perturbed by the inhibition of miR159 function during rosette development, leading to altered rosette morphology. Such circumstances may occur in response to an environmental stress(es), in which miR159 function is attenuated, leading to MYB33/65 expression and possibly contributing to the plant response against the environmental stress(es). Interestingly, miR159 can inhibit *MYB* expression at the translational level (Li et al., 2014), hence miR159-mediated *MYB* inhibition may be reversible, offering the flexibility for a quick target mRNA reactivation (Flynt and Lai, 2008), enabling a rapid plant response to an abrupt and

temporal stress. Therefore, investigating which stress(es) can repress miR159 activity, enabling the activation of *MYB33/65* pathway is critical for elucidating the possible functional role of this module in the rosette.

However, as mentioned in Chapter 3, a search using the GENEVESTIGATOR platform (https://www.genevestigator.com/gv/) and *Arabidopsis* eFP Browser (http://bar.utoronto.ca/efp/cgi-bin/efpWeb.cgi), found that the *CP1* transcription remains low under all the investigated growth conditions, suggesting that miR159 cannot be strongly perturbed by a common environmental stress. Highlighting this, the attempts of using a variety of abiotic stresses or even viral infection, the latter of which should generally perturb miRNA biogenesis and function, failed to strongly perturb miR159-mediated silencing in rosettes (Chapter 3). These experiments imply that miR159 mediated silencing of *MYB33/65* to be extremely robust. It may be possible that to strongly perturb miR159-mediated silencing in rosettes, a stress that specifically interacts with miR159 is required. Although the existence of such environmental stress has not been discovered in this study, Alonso-Peral et al. (2012) has found that the efficient miR159 silencing of *MYB33/65* in rosettes did not occur in the seeds of *Arabidopsis*, namely miR159 appeared to have a very weak silencing efficacy in seeds, which raises the possibility of an unknown mechanism/factor regulating miR159 efficacy. This mechanism is apparently inactive in rosette tissue under normal growth condition, but whether it can be induced to repress the miR159 activity by environmental stress may address the above possibility and hence deserves further investigation. Additionally, the recent finding that some genetic programs are specifically activated when multiple stresses were applied to the plant simultaneously (Prasch and Sonnewald 2013), raises the possibility that strong perturbation of miR159

activity may only occur in the response to the simultaneous application of multiple stresses. Since the simultaneous abiotic and biotic stresses frequently occur in nature, it is possible that multiple simultaneous stresses have a synergistic impact regarding the perturbation of miR159 activity.

6.3 Is the miR159-*MYB* module extensively networked in *Arabidopsis* rosettes?

Recently, the miR159-*MYB* module has been reported in a floral regulatory network (Rubio-Somoza and Weigel, 2013). Here, the miR159-*MYB* and miR319-*TCP* nodes coordinate to regulate the miR167-*ARF* node in flower tissue, which is critical for floral organ maturation (Rubio-Somoza and Weigel, 2013). However, whether this network is important in rosettes is unclear, as under what conditions the *MYB* target genes are expressed in rosettes is unknown as shown by this thesis, and miR319 is very lowly expressed in rosette tissues (Warthmann et al., 2008; Neg et al., 2009). Additionally, a role for the miR159-*MYB* pathway in GA signaling has also been suggested (Achard et al., 2004), but uncertainty remains, as neither Reyes and Chua (2007) nor Alonso-Peral et al. (2010) could detect any change of miR159 abundance or *MYB* transcript levels upon GA application during seedling germination or rosette development respectively. Therefore, whether and how is the miR159-*MYB* module networked with other pathways in rosettes are still largely unknown and remain to be clarified.

Here, via an EMS-based *mir159ab* revertant screen, the repressors of the *mir159ab* rosette defects were identified at an extremely high frequency, and molecular analysis revealed that many EMS-mutants have attenuated *MYB33/65* transcription. Considering that EMS treatment primarily results in loss-of-function mutations, the *MYB33/65* genes are potentially downstream of many transcription factors that promote *MYB33/65*

transcription, and once EMS-mutated they would result in reductions of *MYB33/65* transcription. However, an alternative possibility that may argue against the existence of factors promoting *MYB* transcription should not be ignored, that is *MYB33/65* may only be strongly transcribed in specific rosette cells, thus a "dilution effect" of *MYB* transcription may be resulted whenever an EMS-mutation can induce an increase of rosette size (revertant phenotype): namely the transcription of *MYB33/65* in specific cells might remain unchanged, but the expanded rosette tissue surrounding these cells would make the *MYB* mRNA levels seemingly reduced when the whole EMS-mutant rosette was analysed. This concern comes from the previous observation that the stronger expression of a *mMYB33*:*GUS* transgene was detected in and around the shoot meristem region and on the proximal periphery of young developing leaves (Millar and Gubler, 2005). However, in contrast, my time-course of GUS-staining found no such difference (Chapter 3), suggesting the previous observation may be due to position effects of the transgene or the staining quality regarding the penetration of the GUS staining buffer. To clarify the uncertainty, the quantitative GUS staining assay (Jefferson, 1987) may be performed on finely sectioned *mMYB33-GUS* leaves of multiple *mMYB33*-GUS lines, to assess the *MYB* transcription level in different leaf areas.

6.4 Other potential roles of miR159 silencing in rosette tissues

6.4.1 A role for miR159 in controlling floral transition from the vegetative phase?

Previously, overexpression of miR159 in the Landsberg *erecta* ecotype of *Arabidopsis* had been found to delay short-day (SD) photoperiod flowering time (Achard et al., 2004). This agreed with the findings that overexpression of miR159 in rice (*Oryza sativa cv.* Nipponbare) caused a delayed head formation (Tsuji et al., 2006) and overexpression of miR159 in Gloxinia (*Sinningia speciosa*, an ornamental plant) also

caused delayed flowering (Li et al., 2013). These data support a role of miR159 in controlling the floral transition from the vegetative phase.

However, overexpressing miR159 in *Arabidopsis* Columbia did not affect flowering time, which was possibly due to the difference in ecotypes (Schwab et al., 2005; Teotia and Tang, 2014). Additionally, the mechanism regarding whether the miR159 control of flowering time is mediated through *MYB* pathway is not well established (excellent review provided by Teotia and Tang, 2014). Although miR159 overexpression resulted in down-regulation of target *MYB*s in flowers of *Arabidopsis* and rice (Achard et al., 2004; Tsuji et al., 2006), neither the generation of a *myb33.myb65* mutant in *Arabidopsis* nor a *gamyb* mutant in rice affected the plant flowering time under the tested growth conditions (Kaneko et al., 2004; Alonso-Peral et al., 2010; Teotia and Tang, 2014). Hence, the role and mechanism of the miR159-*MYB* module in controlling flowering time remains unclear.

6.4.2 miR159 does not appear to act as a backup to prevent leaky transcription of other MYB target genes

Another possible role of miR159 in rosettes is to serve as a backup to transcriptional control, repressing any leaky transcription of other *MYB* target genes. This is owing to the fact that besides *MYB33* and *MYB65*, bioinformatics has predicted five more *GAMYB*-like genes that can be regulated by miR159 (i.e. *MYB81*, *MYB97*, *MYB101*, *MYB104*, *MYB120*, Reinhart et al., 2002), and miR159-mediated cleavage of *MYB81*, *MYB101* and *MYB120* mRNAs have been experimentally verified by 5’RACE (Palatnik et al., 2007; Reyes and Chua, 2007; Allen et al., 2010). Though these *MYB* genes are transcribed predominantly in anthers and pollens where the transcription of miR159a/b

appears absent (Allen et al., 2007; Slotkin et al., 2009), the expression of miRNA-resistant versions of these *MYB*s, such as *mMYB101* and *mMYB120*, were found to result in rosette defects resembling that of *mir159ab* (i.e. dwarfed rosettes with upwardly curled leaves, Allan et al., 2010; Li and Millar, 2013). It is likely that MYB101 and MYB120 are operating via the same pathway as MYB33/65, as *CP1* is strongly up-regulated in miR159-resistant *mMYB101* and *mMYB120* transformants (Li and Millar, 2013; unpublished data from our lab). Therefore, since the expression of these anther/pollen expressed *MYB* genes can lead to deleterious rosette growth, it is possible that they have retained their miR159 binding site in order to prevent them from being expressed in rosettes, which may occur under stress conditions that result in leaky transcription.

To address this possibility, the *mir159ab.myb33.myb65* quadruple mutant was subjected to a number of stresses; if leaky anther/pollen MYB expression occurs in the rosette, phenotypic characteristic of *mir159ab*-like rosette defects (e.g. upwardly curled leaves) should become apparent with a concomitant increase in *CP1* mRNA levels. However, under the stress conditions examined in this study (e.g. high or low temperature, high light and drought), the *CP1* mRNA level remained unchanged in the *mir159ab.myb33.myb65* quadruple mutant and no morphological/growth difference could be detected between the quadruple mutant and wild-type Col plant (Chapter 3). This suggests that the leaky transcription of *MYB* genes in the rosettes is not induced by these common stresses. Therefore, these experiments do not support a role for miR159 acting as a backup to prevent expression of these anther/pollen-MYB genes in the rosettes, but it does not rule out that other stresses or combinations of stresses could induce such a scenario.

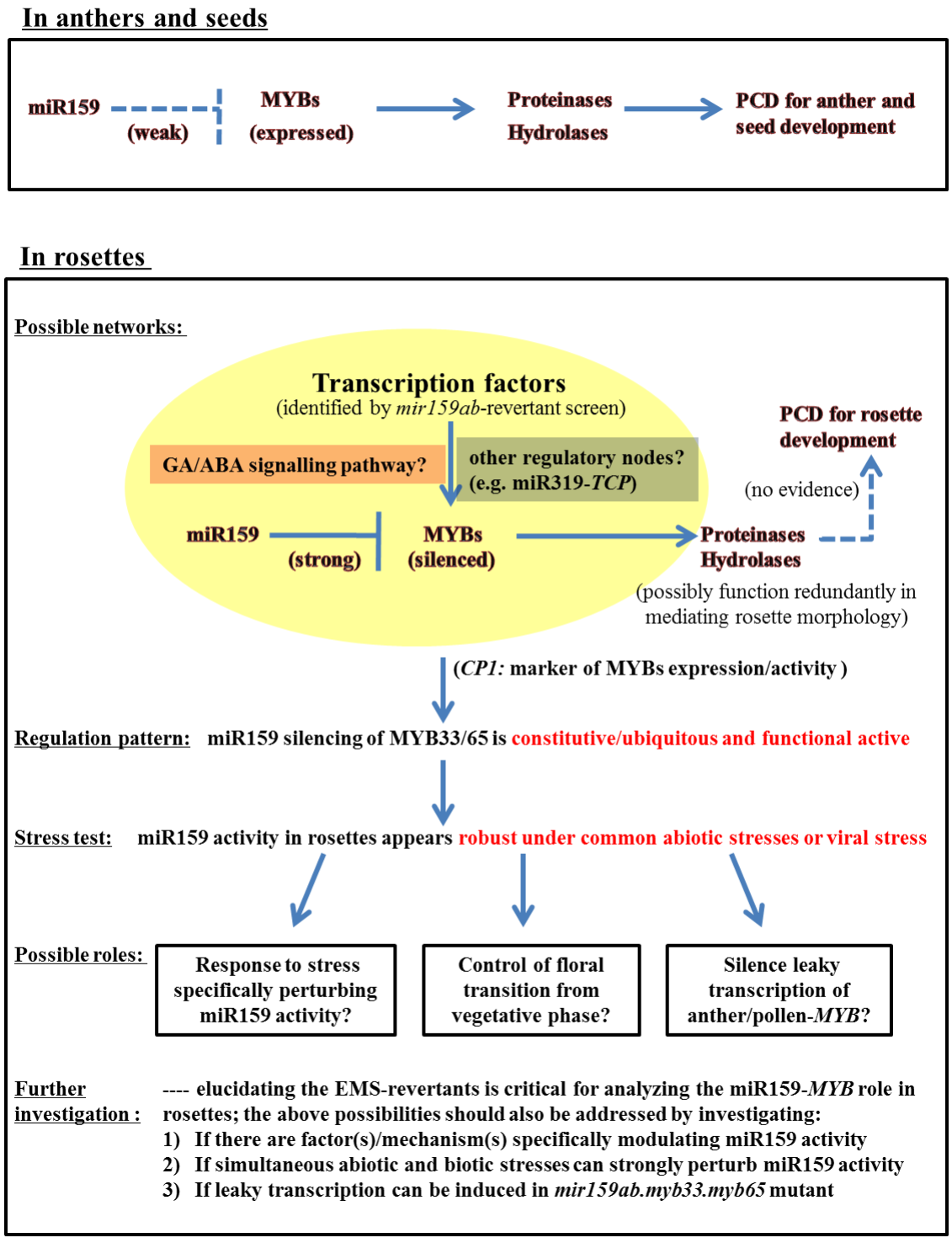

Figure 6.1: Summary diagram of the findings and possibilities regarding the role of the miR159-*MYB* module in plants. (See text for explanation)

6.5 Inhibiting plant miRNA function through miRNA decoys

It is well known that plant miRNA-target relationships rely on their high complementarity (Schwab et al. 2005), thus *SP* transgenes designed to carry highly complementary miRNA target site(s) would be predicted to be highly competitive against endogenous miRNA target sites. Moreover, the transcription of these *SP* transgenes is driven by the CaMV 35S promoter, which is likely to be much stronger than the promoters of many endogenous target genes that encode transcription factors. Hence, these *SP* transgenes would be expected to easily outcompete the endogenous targets for interacting with the respective miRNA, resulting in strong miRNA inhibition. However, this study revealed that *SP* transgenes inhibited different *Arabidopsis* miRNA activities with different efficacies (Chapter 5). These data suggest that different miRNAs have variable sensitivities to *SP* transgenes.

Explanations for the varying miRNA sensitivities to the *SP*s may lie in the factor(s) that can specifically influence a miRNA-target interaction in plants. There could be many possible factors impacting miRNA-target interaction. First, specific nucleotide mismatches between a miRNA and its endogenous target site may favour their interaction, over a *SP*-miRNA interaction. Evidence for such a possibility comes from the finding for human Argonaute2-mediated miRNA-target interactions (De et al., 2013), where the highly complementary target RNAs have been demonstrated to accelerate the release of miRNAs from Argonaute2 by several orders of magnitude, while the introduction of specific mismatches between the miRNA 3′ end and the target sites can attenuate this releasing process, enhancing the miRNA-target interaction in AGO2. According to this, it may also be hypothesized that instead of efficiently sequestering the *Arabidopsis* miRNAs, the highly complementary *SP* transgenes are promoting the

release of miRNAs from *Arabidopsis* AGO1, which may in turn be recycled for regulation of the endogenous targets that carry the required mismatches. Supporting this, using the plant system (dual-luciferase based sensor system in *Nicotiana benthamiana*, Liu et al., 2014), it was found that miRNA binding sites with a few mismatches to the 3′ end of the miRNA are often equally or more effective than miRNA binding site with full complementarity to the miRNA, in term of the efficacy of miRNA-mediated silencing. Therefore, target-miRNA mismatches could be a factor influencing *SP* efficacy and deserves an attention.

Alternatively, different miRNA may have different tolerances to central mismatches between miRNA-*SP* pairs, so that some miRNAs may be able to cleave the *SP* transcripts, enabling miRNA-RISC recycling, while other miRNAs may be unable to cleave the *SP* transcripts and become sequestered. As a precedent for this, Li et al (2014a) has found that miR159 can mediate cleavage of target sites with 2 nt central mismatches. However, it is worth noting that the *SP159* with 2 nt central mismatches worked comparatively well regarding the inhibition of miR159 function, lowering the likelihood of this possibility. As a third possibility, RNA binding proteins may exist to bind to a specific secondary structure of an endogenous target and facilitate miRNA recognition of that target (Flynt and Lai, 2008), but the artificially designed *SP* transgenes do not contain this secondary structure, resulting in them being inefficient miRNA decoys. No doubt, more possibilities can be enumerated, and the point is that plant miRNA-target interactions appeared complex, perturbations of which through these SP transgenes still have many uncertainties. Moreover, based on the analyses in Chapter 5, it appeared that the inhibition efficacy of a *SP* cannot be changed by a simple alteration of its structural or sequence property. These illustrate the limitation of

applying *SP* transgenes in generating loss-of-function *mirna* outcomes in plants, and whether a *SP* can be applied for a miRNA inhibition should be analysed case by case cautiously.

To complement the transgenic miRNA decoy method, the expression of miRNA-resistant target transgenes may be the choice of many studies. This method has been widely used to analyse the function of many plant miRNAs (Garcia, 2008), such as a miR164-resistant *CUC2* transgene that defined the role of miR164 in the development of leaf margins (Nikovics et al., 2006); a miR396-resistant *GRF9* transgene that found the role of miR396 in establishment of leaf polarity (Wang et al., 2011). However, it is worth noting that some miRNA-target relationships may not have discernible morphological consequences, even though they are beneficial for plant growth (Flynt and Lai, 2008). In such instances, the utility of miRNA-resistant targets may still trigger phenotypic defects that exaggerate the importance of miRNA-mediated silencing. This is due to the transgenic method being accompanied with transgene position effects, which can lead to a range of expression levels of miRNA-resistant transgenes, even when the transgene is transcribed under its endogenous promoter (Li and Millar, 2013). In contrast, the failure of the corresponding miRNA decoy expression to induce any discernible phenotypic defect may actually reflect that the miRNA is not involved in plant morphogenesis (Zhao et al., 2007; Garcia, 2008; Todesco et al., 2010). Therefore, if a miRNA decoy failed to generate an obvious developmental defect, and expression of the corresponding miRNA-resistant target transgene did result in a developmental defect, both results should be taken into careful considerations. If the data obtained from expression of miRNA-resistant target suggested a role the miRNA plays in either developmental or stress response, perhaps a useful follow up analysis is to transform the

miRNA decoy into plants that have a sensitized genetic background[e.g. some relative mutants that can easily manifest a relevant developmental defect, such as transforming the *SP396* into leaf polarity mutants *asymmetric leaves1* (*as1*)], or subjecting the miRNA decoy transformants under relative environmental stresses for functional validation.

6.6 Conclusions

Based on their conservation, many plant miRNA-target relationships are under strong evolutionary pressure, where the relationship has been finely modulated to play specific and essential roles in plant development. However, our knowledge of how these miRNAs are incorporated into plant regulatory networks is still very limited. Illustrated by this thesis, through the molecular and functional analyses of miR159-*MYB* module in the *Arabidopsis* rosette, the miR159-mediated silencing of MYB33/65 expression was found constitutive, ubiquitous and functionally active during rosette growth. In addition, miR159-mediated silencing of MYB33/65 in the rosette appeared extremely robust; under no examined conditions could this silencing be perturbed. Finally, the pathway appeared extensively networked in rosettes based on the large number of *mir159ab* revertants recovered in a suppression screen. These intriguing findings have increased our understanding of this module in rosettes, but raises further questions about its functional role. Finding the answer could be very difficult, as all attempts to disrupt the miR159 function in rosettes did not result in an obvious morphological outcome. Hopefully, in near future, elucidating the mutations identified in the EMS-based *mir159ab* revertant screen will provide more information of the miR159-*MYB* role in rosettes. Likewise, by using the methods (e.g. *CP1* marker) and mutants (e.g. *mir159ab.myb33.myb65*) described in this thesis, the relative functional analysis could

be greatly facilitated. Last but not least, via exploiting miRNA *SP*s for inhibiting miRNA functions in *Arabidopsis*, many broader questions in relation to how the miRNA-target interactions are modulated in plants have also been raised. Identifying these modulating factors by modifying the miRNA decoys into versions resembling different structural/sequence features of miRNA endogenous targets, may be an approach to address these questions and hence should be considered for further investigation.

References

Abrahante, J. E., Daul, A. L., Li, M., Volk, M. L., Tennessen, J. M., Miller, E. A & Rougvie, A. E. (2003). The Caenorhabditis elegans hunchback-like gene lin-57/hbl-1 controls developmental time and is regulated by microRNAs. *Dev Cell* **4**, 625–37.

Achard, P., Herr, A., Baulcombe, D. C. & Harberd, N. P. (2004). Modulation of floral development by a gibberellin-regulated microRNA. *Development* **131**, 3357–65.

Addo-Quaye, C., Snyder, J. A., Park, Y. B., Li, Y.-F., Sunkar, R. & Axtell, M. J. (2009). Sliced microRNA targets and precise loop-first processing of MIR319 hairpins revealed by analysis of the Physcomitrella patens degradome. *RNA* **15**, 2112–21.

Adenot, X., Elmayan, T., Lauressergues, D., Boutet, S., Bouché, N., Gasciolli, V. & Vaucheret, H. (2006). DRB4-dependent TAS3 trans-acting siRNAs control leaf morphology through AGO7. *Curr Biol* **16**, 927–32.

Allen, E., Xie, Z., Gustafson, A. M. & Carrington, J. C. (2005). microRNA-directed phasing during trans-acting siRNA biogenesis in plants. *Cell* **121**, 207–21.

Allen, E., Xie, Z., Gustafson, A. M., Sung, G.-H., Spatafora, J. W. & Carrington, J. C. (2004). Evolution of microRNA genes by inverted duplication of target gene sequences in Arabidopsis thaliana. *Nat Genet* **36**, 1282–90.

Allen, R. S., Li, J., Alonso-Peral, M. M., White, R. G., Gubler, F. & Millar, A. A. (2010). MicroR159 regulation of most conserved targets in Arabidopsis has negligible phenotypic effects. *Silence* **1**, 18.

Allen, R. S., Li, J., Stahle, M. I., Dubroué, A., Gubler, F. & Millar, A. A. (2007). Genetic analysis reveals functional redundancy and the major target genes of the Arabidopsis miR159 family. *Proc Natl Acad Sci U S A* **104**, 16371–6.

Allen, R. S., Nakasugi, K., Doran, R. L., Millar, A. a & Waterhouse, P. M. (2013). Facile mutant identification via a single parental backcross method and application of whole genome sequencing based mapping pipelines. *Front Plant Sci* **4**, 362.

Alonso-Peral, M. M., Li, J., Li, Y., Allen, R. S., Schnippenkoetter, W., Ohms, S., White, R. G. & Millar, A. A. (2010). The microRNA159-regulated GAMYB-like genes inhibit growth and promote programmed cell death in Arabidopsis. *Plant Physiol* **154**, 757–71.

Alonso-Peral, M. M., Sun, C. & Millar, A. A. (2012). MicroRNA159 can act as a switch or tuning microRNA independently of its abundance in Arabidopsis. *PLoS One* **7**, e34751.

Arazi, T., Talmor-Neiman, M., Stav, R., Riese, M., Huijser, P. & Baulcombe, D. C. (2005). Cloning and characterization of micro-RNAs from moss. *Plant J* **43**, 837–48.

Aukerman, M. J. & Sakai, H. (2003). Regulation of Flowering Time and Floral Organ Identity by a MicroRNA and Its APETALA2 -Like Target Genes The Plant Cell. *Plant Cell* **15**, 2730–41.

Aung, K., Lin, S., Wu, C., Huang, Y., Su, C. & Chiou, T. (2006). pho2 , a Phosphate Overaccumulator , Is Caused by a Nonsense Mutation in a MicroRNA399 Target Gene. *Plant Physiol* **141**, 1000–11.

Austin, R. S., Vidaurre, D., Stamatiou, G., Breit, R., Provart, N. J., Bonetta, D., Zhang, J., Fung, P., Gong, Y. & other authors. **(2011).** Next-generation mapping of Arabidopsis genes. *Plant J* **67**, 715–25.

Axtell, M. J. & Bartel, D. P. (2005). Antiquity of MicroRNAs and Their Targets in Land Plants. *Plant Cell* **17**, 1658–73.

Axtell, M. J. & Bowman, J. L. (2008). Evolution of plant microRNAs and their targets. *Trends Plant Sci* **13**, 343–9.

Axtell, M. J. (2008). Evolution of microRNAs and their targets: are all microRNAs biologically relevant? *Biochim Biophys Acta* **1779**, 725–34.

Aya, K., Ueguchi-Tanaka, M., Kondo, M., Hamada, K., Yano, K., Nishimura, M. & Matsuoka, M. (2009). Gibberellin modulates anther development in rice via the transcriptional regulation of GAMYB. *Plant Cell* **21**, 1453–72.

Backman, T. W. H., Sullivan, C. M., Cumbie, J. S., Miller, Z. a, Chapman, E. J., Fahlgren, N., Givan, S. a, Carrington, J. C. & Kasschau, K. D. (2008). Update of ASRP: the Arabidopsis Small RNA Project database. *Nucleic Acids Res* **36**, 982–5.

Baek, D., Villén, J., Shin, C., Camargo, F. D., Gygi, S. P. & Bartel, D. P. (2008). The impact of microRNAs on protein output. *Nature* **455**, 64–71.

Baker, C. C., Sieber, P., Wellmer, F. & Meyerowitz, E. M. (2005). The early extra petals1 Mutant Uncovers a Role for MicroRNA miR164c in Regulating Petal Number in Arabidopsis. *Curr Biol* **15**, 303–15.

Bartel, D. P. (2004). MicroRNAs : Genomics , Biogenesis , Mechanism , and Function Genomics : The miRNA Genes. *Cell* **116**, 281–97.

Bartel, D. P., Lee, R. & Feinbaum, R. (2004). MicroRNAs : Genomics , Biogenesis , Mechanism , and Function Genomics : The miRNA Genes. *Cell* **116**, 281–97.

Baulcombe, D. (2004). RNA silencing in plants. *Nature* **431**, 356-63

Baumberger, N. & Baulcombe, D. C. (2005). Arabidopsis ARGONAUTE1 is an RNA Slicer that selectively recruits microRNAs and short interfering RNAs. *Proc Natl Acad Sci U S A* **102**, 11928–33.

Bazzini, A. A., Hopp, H. E., Beachy, R. N. & Asurmendi, S. (2007). Infection and coaccumulation of tobacco mosaic virus proteins alter microRNA levels, correlating with symptom and plant development. *Proc Natl Acad Sci U S A* **104**, 12157–62.

Bevan, M., Mayer, K., White, O., Eisen, J. A., Preuss, D., Bureau, T., Salzberg, S. L. & Mewes, H. (2001). Sequence and analysis of the Arabidopsis genome. *Curr Opin Plant Biol* **4**, 105–10.

Bhattacharyya, S. N., Habermacher, R., Martine, U., Closs, E. I. & Filipowicz, W. (2006). Relief of microRNA-mediated translational repression in human cells subjected to stress. *Cell* **125**, 1111–24.

Blevins, T., Rajeswaran, R., Shivaprasad, P. V, Beknazariants, D., Si-ammour, A., Park, H., Vazquez, F., Robertson, D., Jr, F. M. & other authors. (2006). Four plant Dicers mediate viral small RNA biogenesis and DNA virus induced silencing. *Nucleic Acids Res* **34**, 6233–46.

Bohmert, K., Camus, I., Bellini, C., Bouchez, D., Caboche, M. & Benning, C. (1998). AGO1 defines a novel locus of Arabidopsis controlling leaf development. *EMBO J* **17**, 170–80.

Bollman, K. M. (2003). HASTY, the Arabidopsis ortholog of exportin 5/MSN5, regulates phase change and morphogenesis. *Development* **130**, 1493–1504.

Bonnet, E., Wuyts, J., Rouzé, P. & Van de Peer, Y. (2004). Detection of 91 potential conserved plant microRNAs in Arabidopsis thaliana and Oryza sativa identifies important target genes. *Proc Natl Acad Sci U S A* **101**, 11511–6.

Bortolamiol, D., Pazhouhandeh, M., Marrocco, K., Genschik, P. & Ziegler-Graff, V. (2007). The Polerovirus F box protein P0 targets ARGONAUTE1 to suppress RNA silencing. *Curr Biol* **17**, 1615–21.

Botella, M. A. (2012). Two strawberry miR159 family members display developmental-specific expression patterns in the fruit receptacle and cooperatively regulate Fa-GAMYB. *New Phytol* **195**, 47–57.

Brodersen, P., Sakvarelidze-Achard, L., Bruun-Rasmussen, M., Dunoyer, P., Yamamoto, Y. Y., Sieburth, L. & Voinnet, O. (2008). Widespread translational inhibition by plant miRNAs and siRNAs. *Science* **320**, 1185–90.

Buhtz, A., Springer, F., Chappell, L., Baulcombe, D. C. & Kehr, J. (2008). Identification and characterization of small RNAs from the phloem of Brassica napus. *Plant J* **53**, 739–49.

Buxdorf, K., Hendelman, A., Stav, R., Lapidot, M., Ori, N. & Arazi, T. (2010). Identification and characterization of a novel miR159 target not related to MYB in tomato. *Planta* **232**, 1009–22.

Chapman, E. J., Prokhnevsky, A. I., Gopinath, K., Dolja, V. V & Carrington, J. C. (2004). Viral RNA silencing suppressors inhibit the microRNA pathway at an intermediate step. *Genes Dev* **18**, 1179–86.

Chellappan, P., Vanitharani, R. & Fauquet, C. M. (2005a). MicroRNA-binding viral protein interferes with Arabidopsis development. *Proc Natl Acad Sci U S A* **102**, 10381–6.

Chellappan, P., Vanitharani, R., Ogbe, F. & Fauquet, C. M. (2005b). Effect of Temperature on Geminivirus-Induced RNA Silencing in Plants. *Plant Physiol* **138**, 1828–41.

Chen, M., Meng, Y., Gu, H. & Chen, D. (2010). Functional characterization of plant small RNAs based on next-generation sequencing data. *Comput Biol Chem* **34**, 308–12.

Chen, X. (2004). A microRNA as a translational repressor of APETALA2 in Arabidopsis flower development. *Science* **303**, 2022–5.

Chen, X. (2005). MicroRNA biogenesis and function in plants. *FEBS Lett* **579**, 5923–31.

Chen, X. (2010). Plant microRNAs at a glance. *Semin Cell Dev Biol* **21**, 781.

Chiou, T.-J., Aung, K., Lin, S.-I., Wu, C.-C., Chiang, S.-F. & Su, C.-L. (2006). Regulation of phosphate homeostasis by MicroRNA in Arabidopsis. *Plant Cell* **18**, 412–21.

Chitwood, D. H., Guo, M., Nogueira, F. T. S. & Timmermans, M. C. P. (2007). Establishing leaf polarity: the role of small RNAs and positional signals in the shoot apex. *Development* **134**, 813–23.

Colbert, T., Till, B. J., Tompa, R., Reynolds, S., Steine, M. N., Yeung, A. T., Mccallum, C. M., Comai, L., Henikoff, S. & other authors. **(2001).** High-Throughput Screening for Induced Point Mutations. *Plant Physiol* **126**, 480–4.

Comai, L. & Cartwright, R. a. **(2005).** A toxic mutator and selection alternative to the non-Mendelian RNA cache hypothesis for hothead reversion. *Plant Cell* **17**, 2856–8.

Csorba, T., Lózsa, R., Hutvágner, G. & Burgyán, J. (2010). Polerovirus protein P0 prevents the assembly of small RNA-containing RISC complexes and leads to degradation of ARGONAUTE1. *Plant J* **62**, 463–72.

Cuperus, J. T., Fahlgren, N. & Carrington, J. C. (2011). Evolution and functional diversification of MIRNA genes. *Plant Cell* **23**, 431–42.

Daszkowska-Golec, A., Chorazy, E., Maluszynski, M. & Szarejko, I. (2013). Towards the Identification of New Genes Involved in ABA-Dependent Abiotic Stresses Using Arabidopsis Suppressor Mutants of abh1 Hypersensitivity to ABA during Seed Germination. *Int J Mol Sci* **14**, 13403–32.

De, N., Young, L., Lau, P. W., Meisner, N. C., Morrissey, D. & MacRae, I. J. (2013). Highly complementary target RNAs promote release of guide RNAs from human argonaute2. *Mol Cell* **50**, 344–355.

D áz-Pend ón, J. a & Ding, S.-W. (2008). Direct and indirect roles of viral suppressors of RNA silencing in pathogenesis. *Annu Rev Phytopathol* **46**, 303–26.

Diederichs, S. & Haber, D. a. (2007). Dual role for argonautes in microRNA processing and posttranscriptional regulation of microRNA expression. *Cell* **131**, 1097–108.

Ding, L., Kim, S. Y. & Michaels, S. D. (2013). FLOWERING LOCUS C EXPRESSOR family proteins regulate FLOWERING LOCUS C expression in both winter-annual and rapid-cycling Arabidopsis. *Plant Physiol* **163**, 243–52.

Ding, S. W. & Voinnet, O. (2007) Antiviral immunity directed by small RNAs. *Cell* **130**, 413-26.

Dong, M., Yang, D., Lang, Q., Zhou, W., Xu, S. & Xu, T. (2013). Microarray and degradome sequencing reveal microRNA differential expression profiles and their targets in Pinellia pedatisecta. *PLoS One* **8**, e75978.

Du, Z., Chen, A., Chen, W., Westwood, J. H., Baulcombe, D. C. & Carr, J. P. (2014). Using a viral vector to reveal the role of microRNA159 in disease symptom induction by a severe strain of Cucumber mosaic virus. *Plant Physiol* **164**, 1378–88.

Dubos, C., Stracke, R., Grotewold, E., Weisshaar, B., Martin, C. & Lepiniec, L. (2010). MYB transcription factors in Arabidopsis. *Trends Plant Sci* **15**, 573–81.

Dugas, D. V & Bartel, B. (2004). MicroRNA regulation of gene expression in plants. *Curr Opin Plant Biol* **7**, 512–20.

Dunoyer, P. & Voinnet, O. (2005). The complex interplay between plant viruses and host RNA-silencing pathways. *Curr Opin Plant Biol* **8**, 415–23.

Dunoyer, P., Lecellier, C., Parizotto, E. A., Himber, C. & Voinnet, O. (2004). Probing the MicroRNA and Small Interfering RNA Pathways with Virus-Encoded Suppressors of RNA Silencing. *Plant Cell* **16**, 1235–50.

Ebert, M. S. & Sharp, P. a. (2010). MicroRNA sponges: progress and possibilities. *RNA* **16**, 2043–50.

Ebert, M. S., Neilson, J. R. & Sharp, P. A. (2007). MicroRNA sponges : competitive inhibitors of small RNAs in mammalian cells. *Nat Methods* **4**, 721–26.

Endo, Y., Iwakawa, H. & Tomari, Y. (2013). Arabidopsis ARGONAUTE7 selects miR390 through multiple checkpoints during RISC assembly. *EMBO Rep* **14**, 652–8.

Fagard Mathilde, Boutet Ste ́phanie, Morel Jean-Benoit, Bellini Catherine, and V. H. (2000). AGO1, QDE-2, and RDE-1 are related proteins required for post-transcriptional gene silencing in plants, quelling in fungi, and RNA interference in animals. *Pric Natl Acad Sci USA* **97**, 11650–4.

Fahlgren, N., Howell, M. D., Kasschau, K. D., Chapman, E. J., Sullivan, C. M., Cumbie, J. S., Givan, S. a, Law, T. F., Grant, S. R. & other authors. **(2007).** High-throughput sequencing of Arabidopsis microRNAs: evidence for frequent birth and death of MIRNA genes. *PLoS One* **2**, e219.

Fahlgren, N., Jogdeo, S., Kasschau, K. D., Sullivan, C. M., Chapman, E. J., Laubinger, S., Smith, L. M., Dasenko, M., Givan, S. A & other authors. **(2010).** MicroRNA gene evolution in Arabidopsis lyrata and Arabidopsis thaliana. *Plant Cell* **22**, 1074–89.

Fahlgren, N., Montgomery, T. A, Howell, M. D., Allen, E., Dvorak, S. K., Alexander, A. L. & Carrington, J. C. (2006). Regulation of AUXIN RESPONSE FACTOR3 by TAS3 ta-siRNA affects developmental timing and patterning in Arabidopsis. *Curr Biol* **16**, 939–44.

Feller, A., Machemer, K., Braun, E. L. & Grotewold, E. (2011). Evolutionary and comparative analysis of MYB and bHLH plant transcription factors. *Plant J* **66**, 94–116.

Filipowicz, W. (2005). RNAi: the nuts and bolts of the RISC machine. *Cell* **122**, 17–20.

Floyd, S.K. & Bowman, J. L. (2004). Gene regulation: ancient microRNA target sequences in plants. *Nature* **428**, 485–6.

Flynt, A. S. & Lai, E. C. (2008). Biological principles of microRNA-mediated regulation: shared themes amid diversity. *Nat Rev Genet* **9**, 831–42.

Franco-Zorrilla, J. M., Valli, A., Todesco, M., Mateos, I., Puga, M. I., Rubio-Somoza, I., Leyva, A., Weigel, D., Garc á, J. A. & Paz-Ares, J. (2007). *Target Mimic*ry provides a new mechanism for regulation of microRNA activity. *Nat Genet* **39**, 1033–7.

Fujii, H., Chiou, T.-J., Lin, S.-I., Aung, K. & Zhu, J.-K. (2005). A miRNA involved in phosphate-starvation response in Arabidopsis. *Curr Biol* **15**, 2038–43.

Fukunaga, R. & J. A. Doudna, (2009). dsRNA with 5' overhangs contributes to endogenous and antiviral RNA silencing pathways in plants. *EMBO J* **28**: 545-55.

Furner, I. A. N. J. & Pumfrey, J. E. (1992). Cell fate in the shoot apical meristem of Arabidopsis thaliana. *Development* **115**, 755–64.

Fusaro, A. F., Matthew, L., Smith, N. A., Curtin, S. J., Dedic-hagan, J., Ellacott, G. A., Watson, J. M., Wang, M., Brosnan, C. & other authors. **(2006).** RNA interference-inducing hairpin RNAs in plants act through the viral defence pathway. *EMBO Rep* **7**, 1168–75.

German, M. a, Pillay, M., Jeong, D.-H., Hetawal, A., Luo, S., Janardhanan, P., Kannan, V., Rymarquis, L. a, Nobuta, K. & other authors. **(2008).** Global identification of microRNA-target RNA pairs by parallel analysis of RNA ends. *Nat Biotechnol* **26**, 941–6.

Gu, W., Wang, X., Zhai, C., Xie, X. & Zhou, T. (2012). Selection on synonymous sites for increased accessibility around miRNA binding sites in plants. *Mol Biol Evol* **29**, 3037–44.

Gubler, F., Chandler, P. M., White, R. G., Llewellyn, D. J. & Jacobsen, J. V. **(2002).** Gibberellin Signaling in Barley Aleurone Cells . Control of SLN1 and GAMYB Expression. *Plant Physiol* **129**, 191–200.

Gubler, F., Kalla, R., Robertqa, K. & Jacobsen, J. V. (1995). Gibberellin-regulated expression of a myb gene in barley aleurone cells: evidence for Myb transactivation of a high-pI alpha-amylase gene promoter. *Plant Cell* **7**, 1879–91.

Guddeti, S., Zhang, D. C., Li, A. L., Leseberg, C. H., Kang, H., Li, X. G., Zhai, W. X., Johns, M. A & Mao, L. (2005). Molecular evolution of the rice miR395 gene family. *Cell Res* **15**, 631–8.

Guo, A.-Y., Zhu, Q.-H., Gu, X., Ge, S., Yang, J. & Luo, J. (2008). Genome-wide identification and evolutionary analysis of the plant specific SBP-box transcription factor family. *Gene* **418**, 1–8.

Guo, H., Xie, Q., Fei, J. & Chua, N. (2005). MicroRNA Directs mRNA Cleavage of the Transcription Factor NAC1 to Downregulate Auxin Signals for Arabidopsis Lateral Root Development. *Plant Cell* **17**, 1376–86.

Guo, W.-J., Ho, T.-H. & David Ho, T.-H. (2008). An abscisic acid-induced protein, HVA22, inhibits gibberellin-mediated programmed cell death in cereal aleurone cells. *Plant Physiol* **147**, 1710–22.

Gupta, O. P., Permar, V., Koundal, V., Singh, U. D. & Praveen, S. (2011). MicroRNA regulated defense responses in Triticum aestivum L. during Puccinia graminis f.sp. tritici infection. *Mol Biol Rep* **39**, 817–24.

Gutierrez, L., Bussell, J. D., Pacurar, D. I., Schwambach, J., Pacurar, M. & Bellini, C. (2009). Phenotypic plasticity of adventitious rooting in Arabidopsis is controlled by complex regulation of AUXIN RESPONSE FACTOR transcripts and microRNA abundance. *Plant Cell* **21**, 3119–32.

Ha, M., Pang, M., Agarwal V., Chen, Z. J. (2008). Interspecies Regulation of MicroRNAs and Their Targets. *Biochim Biophys Acta* **1779**, 735–742.

Han, M.-H., Goud, S., Song, L. & Fedoroff, N. (2004). The Arabidopsis double-stranded RNA-binding protein HYL1 plays a role in microRNA-mediated gene regulation. *Proc Natl Acad Sci U S A* **101**, 1093–8.

Haraguchi, T., Ozaki, Y. & Iba, H. (2009). Vectors expressing efficient RNA decoys achieve the long-term suppression of specific microRNA activity in mammalian cells. *Nucleic Acids Res* **37**, e43.

Haraguchi, T., Nakano, H., Tagawa, T., Ohki, T., Ueno, Y., Yoshida, T. & Iba, H. (2012). A potent 2′-O-methylated RNA-based microRNA inhibitor with unique secondary structures. *Nucleic Acids Res* **40**, e58.

Harvey, J. J. W., Lewsey, M. G., Patel, K., Westwood, J., Heimstädt, S., Carr, J. P. & Baulcombe, D. C. (2011). An antiviral defense role of AGO2 in plants. *PLoS One* **6**, e14639.

Heike Lindner, Michael T. Raissig, Christian Sailer, Hiroko Shimosato-Asano, R. B. and U. G. (2012). SNP-Ratio Mapping (SRM): Identifying Lethal Alleles and Mutations in Complex Genetic Backgrounds by Next-Generation Sequencing. *Genetics* **191,** 1381-6.

Henikoff, S. & Comai, L. (2003). Single-nucleotide mutations for plant functional genomics. *Annu Rev Plant Biol* **54**, 375–401.

Hewezi, T. & Baum, T. J. (2012). Complex feedback regulations govern the expression of miRNA396 and its GRF target genes. *Plant Signal Behav* **7**, 749–51.

Hibio, N., Hino, K., Shimizu, E., Nagata, Y. & Ui-Tei, K. (2012). Stability of miRNA 5'terminal and seed regions is correlated with experimentally observed miRNA-mediated silencing efficacy. *Sci Rep* **2**, 996.

Ho T, Wang L, Huang L, Li Z, Pallett DW, Dalmay T, Ohshima K, Walsh JA, W. H. (2010). Nucleotide bias of DCL and AGO in plant anti-virus gene silencing. *Protein Cell* **1**, 847–58.

Hunter, C., Willmann, M. R., Wu, G., Yoshikawa, M., de la Luz Gutiérrez-Nava, M. & Poethig, S. R. (2006). Trans-acting siRNA-mediated repression of ETTIN and ARF4 regulates heteroblasty in Arabidopsis. *Development* **133**, 2973–81.

Irish, V. F. & Sussex, I. A. N. M. (1992). A fate map of the Arabidopsis embryonic shoot apical meristem. *Development* **115**, 745–53.

Ishige, F., Takaichi, M., Foster, R., Chua, N. & Oeda, K. (1999). A G-box motif (GCCACGTGCC) tetramer confers high-level constitutive expression in dicot and monocot plants. *Plant J* **18**, 443–8.

Ivashuta, S., Banks, I. R., Wiggins, B. E., Zhang, Y., Ziegler, T. E., Roberts, J. K. & Heck, G. R. (2011). Regulation of gene expression in plants through miRNA inactivation. *PLoS One* **6**, e21330.

Iwasaki, M., Takahashi, H., Iwakawa, H., Nakagawa, A., Ishikawa, T., Tanaka, H., Matsumura, Y., Pekker, I., Eshed, Y. & other authors. **(2013).** Dual regulation of ETTIN (ARF3) gene expression by AS1-AS2, which maintains the DNA methylation level, is involved in stabilization of leaf adaxial-abaxial partitioning in Arabidopsis. *Development* **140**, 1958–69.

Jay, F., Wang, Y., Yu, A., Taconnat, L., Pelletier, S., Colot, V., Renou, J.-P. & Voinnet, O. (2011). Misregulation of AUXIN RESPONSE FACTOR 8 underlies the developmental abnormalities caused by three distinct viral silencing suppressors in Arabidopsis. *PLoS Pathog* **7**, e1002035.

Jeong, D.-H., Schmidt, S. a, Rymarquis, L. a, Park, S., Ganssmann, M., German, M. a, Accerbi, M., Zhai, J., Fahlgren, N. & other authors. **(2013).** Parallel analysis of RNA ends enhances global investigation of microRNAs and target RNAs of Brachypodium distachyon. *Genome Biol* **14**, R145.

Jiang, D., Yin, C., Yu, A., Zhou, X., Liang, W., Yuan, Z., Xu, Y., Yu, Q., Wen, T. & Zhang, D. (2006). Duplication and expression analysis of multicopy miRNA gene family members in Arabidopsis and rice. *Cell Res* **16**, 507–18.

Jin Hee Kim, Hye Ryun Woo, Jeongsik Kim, Pyung Ok Lim, In Chul Lee, S. H. C. & Daehee Hwang, H. G. N. (2009). Trifurcate Feed-Forward Regulation of Age-Dependent Cell Death Involving miR164 in Arabidopsis. *Science* **323**, 1053–7.

Jones-Rhoades, M. W. & Bartel, D. P. (2004). Computational identification of plant microRNAs and their targets, including a stress-induced miRNA. *Mol Cell* **14**, 787–99.

Jones-Rhoades, M. W. (2012). Conservation and divergence in plant microRNAs. *Plant Mol Biol* **80**, 3–16.

Jones-Rhoades, M. W., Bartel, D. P. & Bartel, B. (2006). MicroRNAS and their regulatory roles in plants. *Annu Rev Plant Biol* **57**, 19–53.

Jouannet, V., Moreno, A. B., Elmayan, T., Vaucheret, H., Crespi, M. D. & Maizel, A. (2012). Cytoplasmic Arabidopsis AGO7 accumulates in membrane-associated siRNA bodies and is required for ta-siRNA biogenesis. *EMBO J* **31**, 1704–13.

Kaneko, M., Inukai, Y., Ueguchi-tanaka, M., Itoh, H., Izawa, T. & Kobayashi, Y. (2004). Loss-of-function mutations of the rice GAMYB gene impair alpha-amylase expression in aleurone and flower development. *Plant Cell* **16**, 33–44.

Karimi, M., Bleys, A., Vanderhaeghen, R. & Hilson, P. (2007). Building blocks for plant gene assembly. *Plant Physiol* **145**, 1183–91.

Kasschau, K. D., Fahlgren, N., Chapman, E. J., Sullivan, C. M., Cumbie, J. S., Givan, S. a & Carrington, J. C. (2007). Genome-wide profiling and analysis of Arabidopsis siRNAs. *PLoS Biol* **5**, e57.

Kasschau, K. D., Xie, Z., Allen, E., Llave, C., Chapman, E. J., Krizan, K. a. & Carrington, J. C. (2003). P1/HC-Pro, a Viral Suppressor of RNA Silencing, Interferes with Arabidopsis Development and miRNA Function. *Dev Cell* **4**, 205–17.

Kawashima, C. G., Matthewman, C. a, Huang, S., Lee, B.-R., Yoshimoto, N., Koprivova, A., Rubio-Somoza, I., Todesco, M., Rathjen, T. & other authors. **(2011).** Interplay of SLIM1 and miR395 in the regulation of sulfate assimilation in Arabidopsis. *Plant J* **66**, 863–76.

Kawashima, C. G., Yoshimoto, N., Maruyama-Nakashita, A., Tsuchiya, Y. N., Saito, K., Takahashi, H. & Dalmay, T. (2009). Sulphur starvation induces the expression of microRNA-395 and one of its target genes but in different cell types. *Plant J* **57**, 313–21.

Kertesz, M., Iovino, N., Unnerstall, U., Gaul, U. & Segal, E. (2007). The role of site accessibility in microRNA target recognition. *Nat Genet* **39**, 1278–84.

Khraiwesh, B., Zhu, J.-K. & Zhu, J. (2012). Role of miRNAs and siRNAs in biotic and abiotic stress responses of plants. *Biochim Biophys Acta* **1819**, 137–48.

Kidner, C. A. & Martienssen, R. A. (2004). Spatially restricted microRNA directs leaf polarity through ARGONAUTE1. *Nature* **428**, 81–4.

Kidner, C. A. & Martienssen, R. A. (2005). The developmental role of microRNA in plants. *Curr Opin Plant Biol* 38–44.

Kidner, C. A. & Martienssen, R. A. **(2005).** The role of ARGONAUTE1 (AGO1) in meristem formation and identity. *Dev Biol* **280**, 504–17.

Kim, J., Jung, J., Reyes, J. L., Kim, Y., Kim, S., Chung, K., Kim, J. A., Lee, M., Lee, Y. & other authors. **(2006).** *Plant J* **42**, 84–94.

Kim, S., Yang, J.-Y., Xu, J., Jang, I.-C., Prigge, M. J. & Chua, N.-H. (2008). Two cap-binding proteins CBP20 and CBP80 are involved in processing primary MicroRNAs. *Plant Cell Physiol* **49**, 1634–44.

Kim, V. N. (2005). MicroRNA biogenesis: coordinated cropping and dicing. *Nat Rev Mol Cell Biol* **6**, 376–85.

Kim, Y., Schumaker, K. S. & Zhu, J.-K. (2006). EMS mutagenesis of Arabidopsis. *Methods Mol Biol* **323**, 101–3.

Kovalchuk, I., Kovalchuk, O. & Hohn, B. (2000). Genome-wide variation of the somatic mutation frequency in transgenic plants. *EMBO J* **19**, 4431–8.

Koyama, T., Mitsuda, N., Seki, M., Shinozaki, K. & Ohme-Takagi, M. (2010). TCP transcription factors regulate the activities of ASYMMETRIC LEAVES1 and miR164, as well as the auxin response, during differentiation of leaves in Arabidopsis. *Plant Cell* **22**, 3574–88.

Kozomara, A. & Griffiths-jones, S. (2014). miRBase : annotating high confidence microRNAs using deep sequencing data. *Nucleic Acids Res* **42**, 68–73.

Kurihara, Y. & Watanabe, Y. (2004). Arabidopsis micro-RNA biogenesis through Dicer-like 1 protein functions. *Proc Natl Acad Sci U S A* **101**, 12753–8.

Kwok, C. K., Ding, Y., Tang, Y., Assmann, S. M. & Bevilacqua, P. C. (2013). Determination of in vivo RNA structure in low-abundance transcripts. *Nat Commun* **4**, 2971.

Lakatos, L., Csorba, T., Pantaleo, V., Chapman, E. J., Carrington, J. C., Liu, Y.-P., Dolja, V. V, Calvino, L. F., López-Moya, J. J. & Burgyán, J. (2006). Small RNA binding is a common strategy to suppress RNA silencing by several viral suppressors. *EMBO J* **25**, 2768–80.

Lanet, E., Delannoy, E., Sormani, R., Floris, M., Brodersen, P., Crété, P., Voinnet, O. & Robaglia, C. (2009). Biochemical evidence for translational repression by Arabidopsis microRNAs. *Plant Cell* **21**, 1762–8.

Lang, Q., Zhou, X., Zhang, X., Drabek, R., Zuo, Z., Ren, Y., Li, T., Chen, J. & Gao, X. (2011). Microarray-based identification of tomato microRNAs and time course analysis of their response to Cucumber mosaic virus infection. *J Zhejiang Univ Sci B* **12**, 116–25.

Laubinger, S., Zeller, G., Henz, S. R., Buechel, S., Sachsenberg, T., Wang, J.-W., Rätsch, G. & Weigel, D. (2010). Global effects of the small RNA biogenesis machinery on the Arabidopsis thaliana transcriptome. *Proc Natl Acad Sci U S A* **107**, 17466–73.

Laufs, P., Peaucelle, A., Morin, H. & Traas, J. (2004). MicroRNA regulation of the CUC genes is required for boundary size control in Arabidopsis meristems. *Development* **131**, 4311–22.

Lee, E.-J., Matsumura, Y., Soga, K., Hoson, T. & Koizumi, N. (2007). Glycosyl hydrolases of cell wall are induced by sugar starvation in Arabidopsis. *Plant Cell Physiol* **48**, 405–13.

Lee, R. C., Feinbaum, R. L. & Ambros, V. (1993). The C. elegans heterochronic gene lin-4 encodes small RNAs with antisense complementarity to lin-14. *Cell* **75**, 843–54.

Lee, S., Jung, K.-H., An, G. & Chung, Y.-Y. (2004a). Isolation and characterization of a rice cysteine protease gene, OsCP1, using T-DNA gene-trap system. *Plant Mol Biol* **54**, 755–65.

Lee, Y., Kim, M., Han, J., Yeom, K.-H., Lee, S., Baek, S. H. & Kim, V. N. (2004b). MicroRNA genes are transcribed by RNA polymerase II. *EMBO J* **23**, 4051–60.

Li, B., Duan, H., Li, J., Deng, X. W., Yin, W. & Xia, X. (2013a). Global identification of miRNAs and targets in Populus euphratica under salt stress. *Plant Mol Biol* **81**, 525–39.

Li, C. & Lu, S. (2014). Genome-wide characterization and comparative analysis of R2R3-MYB transcription factors shows the complexity of MYB-associated regulatory networks in Salvia miltiorrhiza. *BMC Genomics* **15**, 277.

Li, F. & Ding, S.-W. (2006). Virus counterdefense: diverse strategies for evading the RNA-silencing immunity. *Annu Rev Microbiol* **60**, 503–31.

Li, F., Zheng, Q., Vandivier, L. E., Willmann, M. R., Chen, Y. & Gregory, B. D. (2012a). Regulatory impact of RNA secondary structure across the Arabidopsis transcriptome. *Plant Cell* **24**, 4346–59.

Li, H., Xu, L., Wang, H., Yuan, Z., Cao, X., Yang, Z., Zhang, D., Xu, Y. & Huang, H. (2005). The Putative RNA-Dependent RNA Polymerase RDR6 Acts Synergistically with ASYMMETRIC LEAVES1 and 2 to Repress BREVIPEDICELLUS and MicroRNA165 / 166 in Arabidopsis Leaf Development. *Plant Cell* **17**, 2157–71.

Li, J. & Millar, A. a. **(2013).** Expression of a microRNA-resistant target transgene misrepresents the functional significance of the endogenous microRNA: target gene relationship. *Mol Plant* **6**, 577–80.

Li, J., Reichel, M. & Millar, A. A. **(2014a).** Determinants beyond Both complementarity and Cleavage Govern MicroR159 Efficacy in Arabidopsis. *PLoS Genet* **10**, e1004232.

Li, J., Reichel, M., Li, Y. & Millar, A. A. **(2014b).** The functional scope of plant microRNA-mediated silencing. *Trends Plant Sci* **19**, 750–6.

Li, N., Zhang, D.-S., Liu, H.-S., Yin, C.-S., Li, X., Liang, W., Yuan, Z., Xu, B., Chu, H.-W. & other authors. **(2006).** The rice tapetum degeneration retardation gene is required for tapetum degradation and anther development. *Plant Cell* **18**, 2999–3014.

Li, T., Li, H., Zhang, Y.-X. & Liu, J.-Y. (2011a). Identification and analysis of seven H2O2-responsive miRNAs and 32 new miRNAs in the seedlings of rice (Oryza sativa L. ssp. indica). *Nucleic Acids Res* **39**, 2821–33.

Li, W., Cui, X., Meng, Z., Huang, X., Xie, Q., Wu, H., Jin, H., Zhang, D. & Liang, W. (2012b). Transcriptional regulation of Arabidopsis MIR168a and argonaute1 homeostasis in abscisic acid and abiotic stress responses. *Plant Physiol* **158**, 1279–92.

Li, F., Pignatta, D., Bendix, C., Brunkard, J. O., Cohn, M. M., Tung, J. & Sun, H. (2012c). MicroRNA regulation of plant innate immune receptors. *Proc Natl Acad Sci U S A* **109**, 1790–5.

Li, X., Bian, H., Song, D., Ma, S., Han, N., Wang, J. & Zhu, M. (2013b). Flowering time control in ornamental gloxinia (Sinningia speciosa) by manipulation of miR159 expression. *Ann Bot* **111**, 791–9.

Li, Y., Li, C., Ding, G. & Jin, Y. (2011b). Evolution of MIR159/319 microRNA genes and their post-transcriptional regulatory link to siRNA pathways. *BMC Evol Biol* **11**, 122.

Li, Y.-F., Zheng, Y., Addo-Quaye, C., Zhang, L., Saini, A., Jagadeeswaran, G., Axtell, M. J., Zhang, W. & Sunkar, R. (2010). Transcriptome-wide identification of microRNA targets in rice. *Plant J* **62**, 742–59.

Lim, L. P., Lau, N. C., Garrett-Engele, P., Grimson, A., Schelter, J. M., Castle, J., Bartel, D. P., Linsley, P. S. & Johnson, J. M. (2005). Microarray analysis shows that some microRNAs downregulate large numbers of target mRNAs. *Nature* **433**, 769–773.

Lin, S., Johnson, S. M., Abraham, M., Vella, M. C., Pasquinelli, A., Gamberi, C., Gottlieb, E., Slack, F. J. & Haven, N. (2003). The C . elegans hunchback Homolog , hbl-1 , Controls Temporal Patterning and Is a Probable MicroRNA Target 2500 Speedway. *Dev Cell* **4**, 639–50.

Liu, H., Tian, X. I. N., Li, Y., Wu, C. & Zheng, C. (2008). Arabidopsis thaliana Microarray-based analysis of stress-regulated microRNAs in Arabidopsis thaliana. *RNA* **14**, 836–43.

Liu, P.-P., Montgomery, T. a, Fahlgren, N., Kasschau, K. D., Nonogaki, H. & Carrington, J. C. (2007). Repression of AUXIN RESPONSE FACTOR10 by microRNA160 is critical for seed germination and post-germination stages. *Plant J* **52**, 133–46.

Liu, Q., Wang, F. & Axtell, M. J. (2014). Analysis of complementarity requirements for plant MicroRNA targeting using a Nicotiana benthamiana quantitative transient assay. *Plant Cell* **26**, 741–53.

Liu, Q., Yao, X., Pi, L., Wang, H., Cui, X. & Huang, H. (2009). The ARGONAUTE10 gene modulates shoot apical meristem maintenance and establishment of leaf polarity by repressing miR165/166 in Arabidopsis. *Plant J* **58**, 27–40.

Llave, C., Xie, Z., Kasschau, K. D. & Carrington, J. C. (2002). Cleavage of Scarecrow-like mRNA targets directed by a class of Arabidopsis miRNA. *Science* **297**, 2053–6.

Lobbes, D., Rallapalli, G., Schmidt, D. D., Martin, C. & Clarke, J. (2006). SERRATE: a new player on the plant microRNA scene. *EMBO Rep* **7**, 1052–8.

Long, D., Lee, R., Williams, P., Chan, C. Y., Ambros, V. & Ding, Y. (2007). Potent effect of target structure on microRNA function. *Nat Struct Mol Biol* **14**, 287–94.

Lu, C. & Fedoroff, N. (2000). A mutation in the Arabidopsis HYL1 gene encoding a dsRNA binding protein affects responses to abscisic acid, auxin, and cytokinin. *Plant Cell* **12**, 2351–66.

Lund, E., Güttinger, S., Calado, A., Dahlberg, J. E. & Kutay, U. (2004). Nuclear export of microRNA precursors. *Science* **303**, 95–8.

Lewis, B. P., Burge, C. B. & Bartel, D. P. (2005). Conserved seed pairing, often flanked by adenosines, indicates that thousands of human genes are microRNA targets. *Cell* **120**, 15–20.

Lynn, K., Fernandez, a, Aida, M., Sedbrook, J., Tasaka, M., Masson, P. & Barton, M. K. (1999). The PINHEAD/ZWILLE gene acts pleiotropically in Arabidopsis development and has overlapping functions with the ARGONAUTE1 gene. *Development* **126**, 469–81.

M. Koornneeff, L.W.M. Dellaert, J. H. van der V. (1982). EMS- and radiation-induced mutation frequencies at individual loci in Arabidopsis thaliana (L.) Heynh. *Mutat Res* **93**, 109–23.

Ma, Z., Coruh, C. & Axtell, M. J. (2010). Arabidopsis lyrata small RNAs: transient MIRNA and small interfering RNA loci within the Arabidopsis genus. *Plant Cell* **22**, 1090–103.

Ma, Z., Hu, X., Cai, W., Huang, W., Zhou, X., Luo, Q., Yang, H., Wang, J. & Huang, J. (2014). Arabidopsis miR171-Targeted Scarecrow-Like Proteins Bind to GT cis-Elements and Mediate Gibberellin-Regulated Chlorophyll Biosynthesis under Light Conditions. *PLoS Genet* **10**, e1004519.

Mallory, A. C. & Vaucheret, H. (2006). Functions of microRNAs and related small RNAs in plants. *Nat Genet* **38 Suppl**, S31–6.

Mallory, A. C. & Vaucheret, H. (2009). ARGONAUTE 1 homeostasis invokes the coordinate action of the microRNA and siRNA pathways. *EMBO Rep* **10**, 521–6.

Mallory, A. C., Dugas, D. V., Bartel, D. P. & and Bartel, B. (2004b). MicroRNA Regulation of NAC-Domain Targets Is Required for Proper Formation and Separation of Adjacent Embryonic, Vegetative, and Floral Organs. *Development* **14**, 1035–1046.

Mallory, A. C., Reinhart, B. J., Bartel, D., Vance, V. B. & Bowman, L. H. (2002). A viral suppressor of RNA silencing differentially regulates the accumulation of short interfering RNAs and micro-RNAs in tobacco. *Proc Natl Acad Sci U S A* **99**. 15228–33

Mallory, A. C., Reinhart, B. J., Jones-Rhoades, M. W., Tang, G., Zamore, P. D., Barton, M. K. & Bartel, D. P. (2004a). MicroRNA control of PHABULOSA in

leaf development: importance of pairing to the microRNA 5’ region. *EMBO J* **23**, 3356–64.

Marin, E., Jouannet, V., Herz, A., Lokerse, A. S., Weijers, D., Vaucheret, H., Nussaume, L., Crespi, M. D. & Maizel, A. (2010). miR390, Arabidopsis TAS3 tasiRNAs, and their AUXIN RESPONSE FACTOR targets define an autoregulatory network quantitatively regulating lateral root growth. *Plant Cell* **22**, 1104–17.

Martinez, N. J. & Gregory, R. I. (2013). Argonaute2 expression is post-transcriptionally coupled to microRNA abundance. *RNA* **19**, 605–12.

Martinez, N. J., Ow, M. C., Barrasa, M. I., Hammell, M., Sequerra, R., Doucette-Stamm, L., Roth, F. P., Ambros, V. R. & Walhout, A. J. M. (2008). A C. elegans genome-scale microRNA network contains composite feedback motifs with high flux capacity. *Genes Dev* **22**, 2535–49.

Maunoury, N. & Vaucheret, H. (2011). AGO1 and AGO2 act redundantly in miR408-mediated Plantacyanin regulation. *PLoS One* **6**, e28729.

McCallum, C. M., Comai, L., Greene, E. a & Henikoff, S. (2000). Targeted screening for induced mutations. *Nat Biotechnol* **18**, 455–7.

McConnell, J. R., Emery, J., Eshed, Y., Bao, N., Bowman, J. & Barton, M. K. (2001). Role of PHABULOSA and PHAVOLUTA in determining radial patterning in shoots. *Nature* **411**, 709–13.

Mecchia, M. A, Debernardi, J. M., Rodriguez, R. E., Schommer, C. & Palatnik, J. F. (2013). MicroRNA miR396 and RDR6 synergistically regulate leaf development. *Mech Dev* **130**, 2–13.

Meng, Y., Huang, F., Shi, Q., Cao, J., Chen, D., Zhang, J., Ni, J., Wu, P. & Chen, M. (2009). Genome-wide survey of rice microRNAs and microRNA-target pairs in the root of a novel auxin-resistant mutant. *Planta* **230**, 883–98.

Meng, Y., Shao, C., Wang, H. & Chen, M. (2012a). Are all the miRBase-registered microRNAs true? A structure- and expression-based re-examination in plants. *RNA Biol* 249–53.

Meng, Y., Shao, C., Wang, H. & Jin, Y. (2012b). *Target Mimic*s: an embedded layer of microRNA-involved gene regulatory networks in plants. *BMC Genomics* **13**, 197.

Meyers, B. C., Axtell, M. J., Bartel, B., Bartel, D. P., Baulcombe, D., Bowman, J. L., Cao, X., Carrington, J. C., Chen, X. & other authors. **(2008).** Criteria for annotation of plant MicroRNAs. *Plant Cell* **20**, 3186–90.

Mi, S., Cai, T., Hu, Y., Chen, Y., Hodges, E., Ni, F., Wu, L., Li, S., Zhou, H. & other authors. **(2008).** Sorting of small RNAs into Arabidopsis argonaute complexes is directed by the 5’ terminal nucleotide. *Cell* **133**, 116–27.

Millar, A. A. & Gubler, F. (2005). The Arabidopsis GAMYB-Like Genes, MYB33 and MYB65, Are MicroRNA-Regulated Genes That Redundantly Facilitate Anther Development. *Plant Cell* **17**, 705–21.

Montgomery, T. a, Howell, M. D., Cuperus, J. T., Li, D., Hansen, J. E., Alexander, A. L., Chapman, E. J., Fahlgren, N., Allen, E. & Carrington, J. C. (2008). Specificity of ARGONAUTE7-miR390 interaction and dual functionality in TAS3 trans-acting siRNA formation. *Cell* **133**, 128–41.

Morel, J., Godon, C., Mourrain, P., Béclin, C., Boutet, S., Feuerbach, F., Proux, F. & Vaucheret, H. (2002a). Fertile Hypomorphic ARGONAUTE (ago1) Mutants Impaired in Post-Transcriptional Gene Silencing and Virus Resistance. *Plant Cell* **14**, 629–39.

Mullen, T. E. & Marzluff, W. F. (2008). Degradation of histone mRNA requires oligouridylation followed by decapping and simultaneous degradation of the mRNA both 5′ to 3′ and 3′ to 5′. *Genes Dev* **22**, 50–65.

Murray, F., Kalla, R., Jacobsen, J. & Gubler, F. (2003). A role for HvGAMYB in anther development. *Plant J* 481–91.

Nabanita De, Lisa Young, Pick-Wei Lau, Nicole-Claudia Meisner, David V. Morrissey, and I. J. M. (2013). Highly Complementary Target RNAs Promote Release of Guide RNAs from Human Argonaute2. *Mol Cell* **50**, 344–55.

Nag, A. & Jack, T. (2010). Sculpting the flower; the role of microRNAs in flower development. *Curr Top Dev Biol* **91**, 349–78.

Nag, A., King, S. & Jack, T. (2009). miR319a targeting of TCP4 is critical for petal growth and development in Arabidopsis. *Proc Natl Acad Sci U S A* **106**, 22534–9.

Nakano, M., Nobuta, K., Vemaraju, K., Tej, S. S., Skogen, J. W. & Meyers, B. C. (2006). Plant MPSS databases: signature-based transcriptional resources for analyses of mRNA and small RNA. *Nucleic Acids Res* **34**, D731–5.

Naqvi, A. R., Haq, Q. M. R. & Mukherjee, S. K. (2010). MicroRNA profiling of tomato leaf curl New Delhi virus (tolcndv) infected tomato leaves indicates that de-regulation of mir159/319 and mir172 might be linked with leaf curl disease. *Virol J* **7**, 281.

Navarro, L., Dunoyer, P., Jay, F., Arnold, B., Dharmasiri, N., Estelle, M., Voinnet, O. & Jones, J. D. G. (2006). A Plant miRNA Contributes to Antibacterial Resistance by Repressing Auxin Signaling. *Science* **312**, 436-9.

Navarro, L., Jay, F., Nomura, K., He, S. Y. & Voinnet, O. (2008). Suppression of the microRNA pathway by bacterial effector proteins. *Science* **321**, 964–7.

Nobuta, K., Mccormick, K., Nakano, M. & Meyers, B. C. (2010). Bioinformatics Analysis of Small RNAs in Plants Using Next Generation Sequencing Technologies. *Methods Mol Biol***592**, 89–106.

Nogueira, F. T. S., Sarkar, a K., Chitwood, D. H. & Timmermans, M. C. P. (2006). Organ polarity in plants is specified through the opposing activity of two distinct small regulatory RNAs. *Cold Spring Harb Symp Quant Biol* **71**, 157–64.

Ohshima, K., Akaishi, S., Kajiyama, H., Koga, R. & Gibbs, A. J. (2010). Evolutionary trajectory of turnip mosaic virus populations adapting to a new host. *J Gen Virol* **91**, 788–801.

Pacurar, D. I., Pacurar, M. L., Pacurar, A. M., Gutierrez, L. & Bellini, C. (2014). A Novel Viable Allele of Arabidopsis CULLIN1 Identified in a Screen for Superroot2 Suppressors by Next Generation Sequencing-Assisted Mapping. *PLoS One* **9**, e100846.

Palatnik, J. F., Allen, E., Wu, X., Schommer, C., Schwab, R., Carrington, J. C. & Weigel, D. (2003). Control of leaf morphogenesis by microRNAs. *Nature* **425**, 257–63.

Palatnik, J. F., Wollmann, H., Schommer, C., Schwab, R., Boisbouvier, J., Rodriguez, R., Warthmann, N., Allen, E., Dezulian, T. & other authors. **(2007).** Sequence and expression differences underlie functional specialization of Arabidopsis microRNAs miR159 and miR319. *Dev Cell* **13**, 115–25.

Park, M. Y., Wu, G., Gonzalez-Sulser, A., Vaucheret, H. & Poethig, R. S. (2005). Nuclear processing and export of microRNAs in Arabidopsis. *Proc Natl Acad Sci U S A* **102**, 3691–6.

Park, W., Li, J., Song, R., Messing, J. & Chen, X. (2002). CARPEL FACTORY, a Dicer homolog, and HEN1, a novel protein, act in microRNA metabolism in Arabidopsis thaliana. *Curr Biol* **12**, 1484–95.

Pasquinelli, A. E. & Ruvkun, G. (2002). Control of developmental timing by micrornas and their targets. *Annu Rev Cell Dev Biol* **18**, 495–513.

Pazhouhandeh, M., Dieterle, M., Marrocco, K., Lechner, E., Berry, B., Brault, V., Hemmer, O., Kretsch, T., Richards, K. E. & other authors. **(2006).** F-box-like domain in the polerovirus protein P0 is required for silencing suppressor function. *Proc Natl Acad Sci U S A* **103**, 1994–9.

Penfield, S., Li, Y., Gilday, A. D., Graham, S. & Graham, I. A. (2006). Arabidopsis ABA INSENSITIVE4 Regulates Lipid Mobilization in the Embryo and Reveals Repression of Seed Germination by the Endosperm. *Plant Cell* **18**, 1887–99.

Peragine, A., Yoshikawa, M., Wu, G., Albrecht, H. L. & Poethig, R. S. (2004). SGS3 and SGS2/SDE1/RDR6 are required for juvenile development and the production of trans-acting siRNAs in Arabidopsis. *Genes Dev* **18**, 2368–79.

Plisson, C., Drucker, M., Blanc, S., German-Retana, S., Le Gall, O., Thomas, D. & Bron, P. (2003). Structural characterization of HC-Pro, a plant virus multifunctional protein. *J Biol Chem* **278**, 23753–61.

Poethig, R. S. (2009). Small RNAs and developmental timing in plants. *Curr Opin Genet Dev* **19**, 374–8.

Prasch, C. M. & Sonnewald, U. (2013). Simultaneous application of heat, drought, and virus to Arabidopsis plants reveals significant shifts in signaling networks. *Plant Physiol* **162**, 1849–66.

Promoter, H. G., Gubler, F., Kalla, R. & Robertqa, K. (1995). Gibberellin-regulated expression of a myb gene in barley aleurone cells: evidence for Myb transactivation of a high-pI alpha-amylase gene promoter. *Plant Cell* **7**, 1879–91.

Qi, Y., Denli, A. M. & Hannon, G. J. (2005). Biochemical specialization within Arabidopsis RNA silencing pathways. *Mol Cell* **19**, 421–8.

Qi, Y., He, X., Wang, X.-J., Kohany, O., Jurka, J. & Hannon, G. J. (2006). Distinct catalytic and non-catalytic roles of ARGONAUTE4 in RNA-directed DNA methylation. *Nature* **443**, 1008–12.

Qu, F., Ye, X. & Morris, T. J. (2008). Arabidopsis DRB4, AGO1, AGO7, and RDR6 participate in a DCL4-initiated antiviral RNA silencing pathway negatively regulated by DCL1. *Proc Natl Acad Sci U S A* **105**, 14732–7.

Rajagopalan, R., Vaucheret, H., Trejo, J. & Bartel, D. P. (2006). A diverse and evolutionarily fluid set of microRNAs in Arabidopsis thaliana. *Genes Dev* **20**, 3407–25.

Rajewsky, N. & Socci, N. D. (2004). Computational identification of microRNA targets. *Dev Biol* **267**, 529–35.

Rehmsmeier, M., Steffen, P. & Ho, Matthias and Giegerich, R. (2004). Fast and effective prediction of microRNA/target duplexes. *RNA* **10**, 1507–17.

Reichel, M., Li, Y., Li, J. & Millar, A. A. **(2015).** Inhibiting plant microRNA activity: molecular SPONGEs, *Target Mimic*s and STTMs all display variable efficacies against target microRNAs. *Plant Biotechnol J* **13**, 915-26..

Reinhart, B. J., Slack, F. J., Basson, M., Pasquinelli, a E., Bettinger, J. C., Rougvie, a E., Horvitz, H. R. & Ruvkun, G. (2000). The 21-nucleotide let-7 RNA regulates developmental timing in Caenorhabditis elegans. *Nature* **403**, 901–6.

Reinhart, B. J., Weinstein, E. G., Rhoades, M. W., Bartel, B. & Bartel, D. P. (2002). MicroRNAs in plants. *Genes Dev* **16**, 1616–26.

Reyes, J. L. & Chua, N.-H. (2007). ABA induction of miR159 controls transcript levels of two MYB factors during Arabidopsis seed germination. *Plant J* **49**, 592–606.

Rhoades, M. W., Reinhart, B. J., Lim, L. P., Burge, C. B., Bartel, B. & Bartel, D. P. (2002b). Prediction of plant microRNA targets. *Cell* **110**, 513–20.

Rodriguez, R. E., Mecchia, M. a, Debernardi, J. M., Schommer, C., Weigel, D. & Palatnik, J. F. (2010). Control of cell proliferation in Arabidopsis thaliana by microRNA miR396. *Development* **137**, 103–12.

Rolland, F., Baena-Gonzalez, E. & Sheen, J. (2006). Sugar sensing and signaling in plants: conserved and novel mechanisms. *Annu Rev Plant Biol* **57**, 675–709.

Rubio-Somoza, I. & Weigel, D. (2011). MicroRNA networks and developmental plasticity in plants. *Trends Plant Sci* **16**, 258–64.

Rubio-Somoza, I. & Weigel, D. (2013). Coordination of flower maturation by a regulatory circuit of three microRNAs. *PLoS Genet* **9**, e1003374.

Rubio-Somoza, I., Cuperus, J. T., Weigel, D. & Carrington, J. C. (2009). Regulation and functional specialization of small RNA-target nodes during plant development. *Curr Opin Plant Biol* **12**, 622–7.

Rutherford, S., Brandizzi, F., Townley, H., Craft, J., Wang, Y., Jepson, I., Martinez, A. & Moore, I. (2005). Improved transcriptional activators and their use in mis-expression traps in Arabidopsis. *Plant J* **43**, 769–88.

Sanei, M. & Chen, X. (2015). Mechanisms of microRNA turnover. *Curr Opin Plant Biol* **27**, 199–206.

Sasaki, T., Naumann, U., Forai, P., Matzke, A. J. M. & Matzke, M. (2012). Unusual case of apparent hypermutation in Arabidopsis thaliana. *Genetics* **192**, 1271–80.

Schauer, S. E., Jacobsen, S. E., Meinke, D. W., Ray, A. & Sin, S. I. (2002). DICER-LIKE1 : blind men and elephants in Arabidopsis development. *Trends Plant Sci* **7**, 487–91.

Schieferstein R. H. & Loomis W. E. (1956). WAX DEPOSITS ON LEAF SURFACES. *Plant Physiol* **31(3)**, 240–7.

Scholthof, H. B., Alvarado, V. Y., Vega-Arreguin, J. C., Ciomperlik, J., Odokonyero, D., Brosseau, C., Jaubert, M., Zamora, A. & Moffett, P. (2011). Identification of an ARGONAUTE for antiviral RNA silencing in Nicotiana benthamiana. *Plant Physiol* **156**, 1548–55.

Scholthof, H. B., Scholthof, K. B. & Jackson, A. O. (1995). Identification of tomato bushy stunt virus host-specific symptom determinants by expression of individual genes from a potato virus X vector. *Plant Cell* **7**, 1157–72.

Schommer, C., Bresso, E. G., Spinelli, S. V & Palatnik, J. F. (2012). MicroRNAs in Plant Development and Stress Responses. *Signal Commun Plants* **15**, 29–48.

Schommer, C., Palatnik, J. F., Aggarwal, P., Chételat, A., Cubas, P., Farmer, E. E., Nath, U. & Weigel, D. (2008). Control of jasmonate biosynthesis and senescence by miR319 targets. *PLoS Biol* **6**, e230.

Schwab, R., Palatnik, J. F., Riester, M., Schommer, C., Schmid, M. & Weigel, D. (2005). Specific effects of microRNAs on the plant transcriptome. *Dev Cell* **8**, 517–27.

Selbach, M., Schwanhäusser, B., Thierfelder, N., Fang, Z., Khanin, R. & Rajewsky, N. (2008a). Widespread changes in protein synthesis induced by microRNAs. *Nature* **455**, 58–63.

Serrat, X., Esteban, R., Guibourt, N., Moysset, L., Nogués, S. & Lalanne, E. (2014). EMS mutagenesis in mature seed-derived rice calli as a new method for rapidly obtaining TILLING mutant populations. *Plant Methods* **10**, 5.

Shen, B. & Goodman, H. M. (2004). Uridine addition after microRNA-directed cleavage. *Science* **306**, 997.

Shiboleth, Y. M., Haronsky, E., Leibman, D., Arazi, T., Wassenegger, M., Whitham, S. a, Gaba, V. & Gal-On, A. (2007). The conserved FRNK box in HC-Pro, a plant viral suppressor of gene silencing, is required for small RNA binding and mediates symptom development. *J Virol* **81**, 13135–48.

Shivaprasad, P. V., Chen, H.-M., Patel, K., Bond, D. M., Santos, B. A. C. M. & Baulcombe, D. C. (2012). A MicroRNA Superfamily Regulates Nucleotide Binding Site-Leucine-Rich Repeats and other mRNAs. *Plant Cell* **24**, 859–74.

Shukla, L. I., Chinnusamy, V. & Sunkar, R. (2008). The role of microRNAs and other endogenous small RNAs in plant stress responses. *Biochim Biophys Acta* **1779**, 743–8.

Sieber, P., Wellmer, F., Gheyselinck, J., Riechmann, J. L. & Meyerowitz, E. M. (2007). Redundancy and specialization among plant microRNAs: role of the MIR164 family in developmental robustness. *Development* **134**, 1051–60.

Slotkin, R. K., Vaughn, M., Borges, F., Tanurdzić, M., Becker, J. D., Feijó, J. A & Martienssen, R. A. (2009). Epigenetic reprogramming and small RNA silencing of transposable elements in pollen. *Cell* **136**, 461–72.

Song, L., Axtell, M. J. & Fedoroff, N. V. (2010). RNA secondary structural determinants of miRNA precursor processing in Arabidopsis. *Curr Biol* **20**, 37–41.

Song, Q.-X., Liu, Y.-F., Hu, X.-Y., Zhang, W.-K., Ma, B., Chen, S.-Y. & Zhang, J.-S. (2011). Identification of miRNAs and their target genes in developing soybean seeds by deep sequencing. *BMC Plant Biol* **11**, 5.

Stav, R., Hendelman, A., Buxdorf, K. & Arazi, T. (2010). Transgenic expression of tomato bushy stunt virus silencing suppressor P19 via the pOp/LhG4 transactivation system induces viral-like symptoms in tomato. *Virus Genes* **40**, 119–29.

Sunkar, R., Chinnusamy, V., Zhu, J. & Zhu, J.-K. (2007). Small RNAs as big players in plant abiotic stress responses and nutrient deprivation. *Trends Plant Sci* **12**, 301–9.

Sunkar, R., Kapoor, A. & Zhu, J. (2006). Posttranscriptional Induction of Two Cu / Zn Superoxide Dismutase Genes in Arabidopsis Is Mediated by Downregulation of miR398 and Important for Oxidative Stress Tolerance. *Plant Cell* **18**, 2051–65.

Sunkar, R., Li, Y. F. & Jagadeeswaran, G. (2012). Functions of microRNAs in plant stress responses. *Trends Plant Sci* **17**, 196–203.

Szittya, G., Silhavy, D., Molnár, A., Havelda, Z., Lovas, A., Lakatos, L., Bánfalvi, Z. & Burgyán, J. (2003). Low temperature inhibits RNA silencing-mediated defence by the control of siRNA generation. *EMBO J* **22**, 633–40.

Tétreault, N. & De Guire, V. (2013). MiRNAs: Their discovery, biogenesis and mechanism of action. *Clin Biochem* **46**, 842–5.

Teotia, S. & Tang, G. (2014). To bloom or not to bloom: Role of microRNAs in plant flowering. *Mol Plant* **8**, 359–377.

Thiebaut, F., Rojas, C. a, Almeida, K. L., Grativol, C., Domiciano, G. C., Lamb, C. R. C., Engler, J. D. A., Hemerly, A. S. & Ferreira, P. C. G. (2012). Regulation of miR319 during cold stress in sugarcane. *Plant Cell Environ* **35**, 502–12.

Todesco, M., Rubio-Somoza, I., Paz-Ares, J. & Weigel, D. (2010). A collection of Target Mimics for comprehensive analysis of microRNA function in Arabidopsis thaliana. *PLoS Genet* **6**, e1001031.

Trindade, I., Capitão, C., Dalmay, T., Fevereiro, M. P. & Santos, D. M. Dos. **(2010).** miR398 and miR408 are up-regulated in response to water deficit in Medicago truncatula. *Planta* **231**, 705–16.

Tsuji, H., Aya, K., Ueguchi-Tanaka, M., Shimada, Y., Nakazono, M., Watanabe, R., Nishizawa, N. K., Gomi, K., Shimada, A. & other authors. **(2006).** GAMYB controls different sets of genes and is differentially regulated by microRNA in aleurone cells and anthers. *Plant J* **47**, 427–44.

Uchida, N., Sakamoto, T., Kurata, T. & Tasaka, M. (2011). Identification of EMS-induced causal mutations in a non-reference Arabidopsis thaliana accession by whole genome sequencing. *Plant Cell Physiol* **52**, 716–22.

Válóczi, A., Várallyay, E., Kauppinen, S., Burgyán, J. & Havelda, Z. (2006). Spatio-temporal accumulation of microRNAs is highly coordinated in developing plant tissues. *Plant J* **47**, 140–51.

Van der Auwera, G., Baute, J., Bauwens, M., Peck, I., Piette, D., Pycke, M., Asselman, P. & Depicker, A. (2008). Development and application of novel constructs to score C:G-to-T:A transitions and homologous recombination in Arabidopsis. *Plant Physiol* **146**, 22–31.

Van Wees, S. (2008). Phenotypic analysis of Arabidopsis mutants: trypan blue stain for fungi, oomycetes, and dead plant cells. *CSH Protoc* **3**, pdb.prot4982.

Várallyay, E., Válóczi, A., Agyi, A., Burgyán, J. & Havelda, Z. (2010). Plant virus-mediated induction of miR168 is associated with repression of ARGONAUTE1 accumulation. *EMBO J* **29**, 3507–19.

Vaucheret, H. (2009). AGO1 homeostasis involves differential production of 21-nt and 22-nt miR168 species by MIR168a and MIR168b. *PLoS One* **4**, e6442.

Vaucheret, H., Mallory, A. C. & Bartel, D. P. (2006). AGO1 homeostasis entails coexpression of MIR168 and AGO1 and preferential stabilization of miR168 by AGO1. *Mol Cell* **22**, 129–36.

Vaucheret, H., Vazquez, F., Cre, P. & Bartel, D. P. (2004). The action of ARGONAUTE1 in the miRNA pathway and its regulation by the miRNA pathway are crucial for plant development. *Genes Dev* 1187–97.

Vaucheret, H. (2006). Post-transcriptional small RNA pathways in plants: Mechanisms and regulations. *Genes Dev* **20**, 759–771.

Voinnet, O. (2005). Induction and suppression of RNA silencing: insights from viral infections. *Nat Rev Genet* **6**, 206–20.

Voinnet, O. (2009). Origin, biogenesis, and activity of plant microRNAs. *Cell* **136**, 669–87.

Wang, C.-Y., Chen, Y.-Q. & Liu, Q. (2011a). Sculpting the meristem: the roles of miRNAs in plant stem cells. *Biochem Biophys Res Commun* **409**, 363–6.

Wang, L., Gu, X., Xu, D., Wang, W., Wang, H., Zeng, M., Chang, Z., Huang, H. & Cui, X. (2011b). miR396-targeted AtGRF transcription factors are required for coordination of cell division and differentiation during leaf development in Arabidopsis. *J Exp Bot* **62**, 761–73.

Wang, X.-J., Reyes, J. L., Chua, N.-H. & Gaasterland, T. (2004). Prediction and identification of Arabidopsis thaliana microRNAs and their mRNA targets. *Genome Biol* **5**, R65.

Wang, Y., Sun, F., Cao, H., Peng, H., Ni, Z., Sun, Q. & Yao, Y. (2012). TamiR159 directed wheat TaGAMYB cleavage and its involvement in anther development and heat response. *PLoS One* **7**, e48445.

Warthmann, N., Das, S., Lanz, C. & Weigel, D. (2008). Comparative analysis of the MIR319a microRNA locus in Arabidopsis and related Brassicaceae. *Mol Biol Evol* **25**, 892–902.

Williams, L., Grigg, S. P., Xie, M., Christensen, S. & Fletcher, J. C. (2005). Regulation of Arabidopsis shoot apical meristem and lateral organ formation by microRNA miR166g and its AtHD-ZIP target genes. *Development* **132**, 3657–68.

Wong, C. E., Zhao, Y.-T., Wang, X.-J., Croft, L., Wang, Z.-H., Haerizadeh, F., Mattick, J. S., Singh, M. B., Carroll, B. J. & Bhalla, P. L. (2011). MicroRNAs in the shoot apical meristem of soybean. *J Exp Bot* **62**, 2495–506.

Woodger, F. J., Millar, A., Murray, F., Jacobsen, J. V. & Gubler, F. (2003). The Role of GAMYB Transcription Factors in GA-Regulated Gene Expression. *J Plant Growth Regul* **22**, 176–84.

Wu, G. & Poethig, R. S. (2006). Temporal regulation of shoot development in Arabidopsis thaliana by miR156 and its target SPL3. *Development* **133**, 3539–47.

Wu, G., Park, M. Y., Conway, S. R., Wang, J.-W., Weigel, D. & Poethig, R. S. (2009). The sequential action of miR156 and miR172 regulates developmental timing in Arabidopsis. *Cell* **138**, 750–9.

Wu, H.-J., Wang, Z.-M., Wang, M. & Wang, X.-J. (2013). Widespread long noncoding RNAs as endogenous target mimics for microRNAs in plants. *Plant Physiol* **161**, 1875–84.

Wu, H.-W., Lin, S.-S., Chen, K.-C., Yeh, S.-D. & Chua, N.-H. (2010). Discriminating mutations of HC-Pro of zucchini yellow mosaic virus with differential effects on small RNA pathways involved in viral pathogenicity and symptom development. *Mol Plant Microbe Interact* **23**, 17–28.

Wu, M.-F., Tian, Q. & Reed, J. W. (2006). Arabidopsis microRNA167 controls patterns of ARF6 and ARF8 expression, and regulates both female and male reproduction. *Development* **133**, 4211–8.

Xie, Z., Allen, E., Fahlgren, N., Calamar, A., Givan, S. A. & Carrington, J. C. (2005). Expression of Arabidopsis MIRNA Genes. *Plant Physiol* **138**, 2145–54.

Xie, Z., Kasschau, K. D. & Carrington, J. C. (2003). Negative Feedback Regulation of Dicer-Like1 in Arabidopsis by microRNA-Guided mRNA Degradation. *Curr Biol* **13**, 784–9.

Xie, Z., Khanna, K. & Ruan, S. (2010). Expression of microRNAs and its regulation in plants. *Semin Cell Dev Biol* **21**, 790–7.

Xu, L., Yang, L., Pi, L., Liu, Q., Ling, Q., Wang, H., Poethig, R. S. & Huang, H. (2006). Genetic interaction between the AS1-AS2 and RDR6-SGS3-AGO7 pathways for leaf morphogenesis. *Plant Cell Physiol* **47**, 853–63.

Yan, J., Gu, Y., Jia, X., Kang, W., Pan, S., Tang, X., Chen, X. & Tang, G. (2012). Effective small RNA destruction by the expression of a Short Tandem Target Mimic in Arabidopsis. *Plant Cell* **24**, 415–27.

Yang, J., Zhang, N., Mi, X., Wu, L., Ma, R., Zhu, X., Yao, L., Jin, X., Si, H. & Wang, D. (2014). Identification of miR159s and their target genes and expression analysis under drought stress in potato. *Comput Biol Chem* **53**, 204–13.

Yi, H. & Richards, E. J. (2008). Phenotypic instability of Arabidopsis alleles affecting a disease Resistance gene cluster. *BMC Plant Biol* **8**, 36.

Yi, H. & Richards, E. J. (2009). Gene duplication and hypermutation of the pathogen Resistance gene SNC1 in the Arabidopsis bal variant. *Genetics* **183**, 1227–34.

Yifhar, T., Pekker, I., Peled, D., Friedlander, G., Pistunov, A., Sabban, M., Wachsman, G., Alvarez, J. P., Amsellem, Z. & Eshed, Y. (2012). Failure of the tomato trans-acting short interfering RNA program to regulate AUXIN RESPONSE FACTOR3 and ARF4 underlies the wiry leaf syndrome. *Plant Cell* **24**, 3575–89.

Yoon, E. K., Yang, J. H., Lim, J., Kim, S. H., Kim, S. K. & Lee, W. S. (2009). Auxin regulation of the microRNA390-dependent transacting small interfering RNA pathway in Arabidopsis lateral root development. *Nucleic Acids Res* **38**, 1382–1391.

Yu, B., Yang, Z., Li, J., Minakhina, S., Yang, M., Padgett, R. W., Steward, R. & Chen, X. (2005). Methylation as a crucial step in plant microRNA biogenesis. *Science* **307**, 932–5.

Zeng, X., Zhu, L., Chen, Y., Qi, L., Pu, Y., Wen, J., Yi, B., Shen, J., Ma, C. & other authors. **(2011).** Identification, fine mapping and characterisation of a dwarf mutant (bnaC.dwf) in Brassica napus. *Theor Appl Genet* **122**, 421–8.

Zhang, L., Chia, J.-M., Kumari, S., Stein, J. C., Liu, Z., Narechania, A., Maher, C. a, Guill, K., McMullen, M. D. & Ware, D. (2009). A genome-wide characterization of microRNA genes in maize. *PLoS Genet* **5**, e1000716.

Zhang, X., Yuan, Y., Pei, Y., Lin, S., Tuschl, T. & Patel, D. J. (2006). Cucumber mosaic virus -encoded 2b suppressor inhibits Arabidopsis Argonaute1 cleavage activity to counter plant defense. *Genes Dev* 3255–68.

Zhang, W., Gao, S., Zhou, X., Chellappan, P., Chen, Z., Zhou, X., Zhang, X., Fromuth, N., Coutino, G. & other authors. **(2011).** Bacteria-responsive microRNAs regulate plant innate immunity by modulating plant hormone networks. *Plant Mol Biol* **75**, 93–105.

Zhang, Z. & Zhang, X. (2012). Argonautes compete for miR165/166 to regulate shoot apical meristem development. *Curr Opin Plant Biol* **15**, 652–8.

Zhao, M., Tai, H., Sun, S., Zhang, F., Xu, Y. & Li, W.-X. (2012). Cloning and characterization of maize miRNAs involved in responses to nitrogen deficiency. *PLoS One* **7**, e29669.

Zhou, Z. S., Zeng, H. Q., Liu, Z. P. & Yang, Z. M. (2012). Genome-wide identification of Medicago truncatula microRNAs and their targets reveals their differential regulation by heavy metal. *Plant Cell Environ* **35**, 86–99.

Zhu, H., Hu, F., Wang, R., Zhou, X., Sze, S.-H., Liou, L. W., Barefoot, A., Dickman, M. & Zhang, X. (2011). Arabidopsis Argonaute10 specifically sequesters miR166/165 to regulate shoot apical meristem development. *Cell* **145**, 242–56.

Zimmermann, P., Hirsch-hoffmann, M., Hennig, L. & Gruissem, W. (2004). GENEVESTIGATOR . Arabidopsis Microarray Database and Analysis Toolbox. *Bioinformatics* **136**, 2621–32.

Zuker, M. (2003). Mfold web server for nucleic acid folding and hybridization prediction. *Nucleic Acids Res* **31**, 3406–15.

Zuo, J., Niu, Q. W. & Chua, N. H. (2000). Technical advance: An estrogen receptor-based transactivator XVE mediates highly inducible gene expression in transgenic plants. *Plant J* **24**, 265–73.

Appendix

File 1: Sequences of miRNA inhibitors (Black: target site, Red: central mismatch, Purple: flank, Green: primer sequence. The free energies of the thermodynamic ensemble [ΔG(s)], were calculated by RNAfold web server (http://rna.tbi.univie.ac.at/cgi-bin/RNAfold.cgi), to indicate thermodynamic stabilities.)

***SP159*:**

TAGAGCTCCCCACAATCCAAAAGTCTAGAGCTCCCCACAATCCAAAGACT

TAGAGCTCCCCACAATCCAAACTAGAAGAGCTCCCCACAATCCAAATCGA

TAGAGCTCCCCACAATCCAAAACGTTAGAGCTCCCCACAATCCAAACGTA

TAGAGCTCCCCACAATCCAAAGCATAAGAGCTCCCCACAATCCAAATACG

TAGAGCTCCCCACAATCCAAAATAGTAGAGCTCCCCACAATCCAAAAGGC

TAGAGCTCCCCACAATCCAAACGTGAAGAGCTCCCCACAATCCAAA

ACCACTTTGTACAAGAATGCTGTGTATAGAGCTCCCCACAATCCAAAGCCA

TAGAGCTCCCCACAATCCAAAACTATAGAGCTCCCCACAATCCAAA

TTGACTCAGCTTAGCATCTTGT

Linker: Random

The free energy of the thermodynamic ensemble [ΔG(s)] is **-84.98** kcal/mol.

***SP164*:**

TGCACGTGCCGAGCTTCTCCAAGTCTGCACGTGCCGAGCTTCTCCAGACT

TGCACGTGCCGAGCTTCTCCACTAGTGCACGTGCCGAGCTTCTCCATCGA

CGCACGTGCCGAGCTTCTCCAACGTTGCACGTGCCGAGCTTCTCCACGTA

TGCACGTGCCGAGCTTCTCCA GCATTGCACGTGCCGAGCTTCTCCATACG

TGCACGTGCCGAGCTTCTCCA ATAGTGCACGTGCCGAGCTTCTCCAAGGC

TGCACGTGCCGAGCTTCTCCACGTGTGCACGTGCCGAGCTTCTCCA

ACCACTTTGTACAAGAATGCTGTGTATGCACGTGCCGAGCTTCTCCAGCCA

TGCACGTGCCGAGCTTCTCCAACTATGCACGTGCCGAGCTTCTCCA

TTGACTCAGCTTAGCATCTTGT

Linker: Random

The free energy of the thermodynamic ensemble [ΔG(s)] is **-156.00** kcal/mol.

***SP167*:**

TAGATCATGCAAGCAGCTTCAAGTCTAGATCATGCAAGCAGCTTCAGACC
TAGATCATGCAAGCAGCTTCACTACTAGATCATGCAAGCAGCTTCATCGC
CCAGATCATGCAAGCAGCTTCAACGCTAGATCATGCAAGCAGCTTCACGTC
TAGATCATGCAAGCAGCTTCAGCACTAGATCATGCAAGCAGCTTCATACC
TAGATCATGCAAGCAGCTTCAATACCCAGATCATGCAAGCAGCTTCAAGGC
TAGATCATGCAAGCAGCTTCACGTCTAGATCATGCAAGCAGCTTCA
ACCACTTTGTACAAGAATGCTGTGTCTAGATCATGCAAGCAGCTTCAGCCC
TAGATCATGCAAGCAGCTTCAACTCCCAGATCATGCAAGCAGCTTCA
TTGACTCAGCTTAGCATCTTGT

Linker: XXXC

The free energy of the thermodynamic ensemble [ΔG(s)] is **-116.35** kcal/mol.

***SP168*:**

GTTCCCGACCTAAACCAAGCGAAGTCGTTCCCGACCTAAACCAAGCGAGACT
GTTCCCGACCTAAACCAAGCGACTAGGTTCCCGACCTAAACCAAGCGATCGA
GTTCCCGACCTAAACCAAGCGAACGTGTTCCCGACCTAAACCAAGCGACGTA
GTTCCCGACCTAAACCAAGCGAGCATGTTCCCGACCTAAACCAAGCGATACG
GTTCCCGACCTAAACCAAGCGAATAGGTTCCCGACCTAAACCAAGCGAAGGC
GTTCCCGACCTAAACCAAGCGACGTGGTTCCCGACCTAAACCAAGCGA
ACCACTTTGTACAAGAATGCTGTGTAGTTCCCGACCTAAACCAAGCGAGCCA
GTTCCCGACCTAAACCAAGCGAACTAGTTCCCGACCTAAACCAAGCGA
TTGACTCAGCTTAGCATCTTGT

Linker: Random

The free energy of the thermodynamic ensemble [ΔG(s)] is **-76.05** kcal/mol.

***SP169*:**

TCGGCAAGTCTGCCTTGGCTGTGTCTCGGCAAGTCTGCCTTGGCTGTACT
TCGGCAAGTCTGCCTTGGCTGTTAGTCGGCAAGTCTGCCTTGGCTGTCGA
TCGGCAAGTCTGCCTTGGCTGTCGTTCGGCAAGTCTGCCTTGGCTGTGTA
TCGGCAAGTCTGCCTTGGCTGTCATTCGGCAAGTCTGCCTTGGCTGTACG
CCGGCAAGTCTGCCTTGGCTGTTGACGGCAAGTCGAACTTGGCTCATGGA
CGGCAAGTCGAACTTGGCTCATGTGCAGGCAAGTCTGCCTTGGCTA
ACCACTTTGTACAAGAATGCTGTGTACAGGCAAGTCTGCCTTGGCTATCCA
CAGGCAAGTCTGCCTTGGCTATCTACAGGCAAGTCTGCCTTGGCTA
TTGACTCAGCTTAGCATCTTGT

Linker: Random

The free energy of the thermodynamic ensemble [ΔG(s)] is **-162.62** kcal/mol.

***SP170/171*:**

GATATTGACAATGCTCAATCAAATGGATATTGACAATGCTCAATCAGATG
GATATTGACAATGCTCAATCACATGGATATTGACAATGCTCAATCATATG
GATATTGGCGATGCTCAATCAAATGGATATTGGCGATGCTCAATCACATG
GATATTGGCGATGCTCAATCAGATGGATATTGGCGATGCTCAATCATATG
GATATTGGCGATGCTCAATCAAATGGATATTGGCGATGCTCAATCAAATG
GATATTGGCGATGCTCAATCACATGGATATTGGCGATGCTCAATCA
ACCACTTTGTACAAGAATGCTGTGTACGTGATATTGAAACGGCTCAAGATA
CGTGATATTGAAACGGCTCAAGATGGATATTGGCGATGCTCAATCA
TTGACTCAGCTTAGCATCTTGT

Linker: XATG or GATX

The free energy of the thermodynamic ensemble [ΔG(s)] is **-102.44** kcal/mol.

***SP319*:**

AGGGAGTTCCGGTCAGTCCAGTGTCAGGGAGTTCCGGTCAGTCCAGTACT
AAGGAGTTCCGGTCAGTCCAGTTAGAGGGAGTTCCGGTCAGTCCAGTCGA
AGGGAGTTCCGGTCAGTCCAGTCGTAAGGAGTTCCGGTCAGTCCAGTGTA
AGGGAGTTCCGGTCAGTCCAGTCATAGGGAGTTCCGGTCAGTCCAGTACG
AAGGAGTTCCGGTCAGTCCAGTTAGAGGGAGTTCCGGTCAGTCCAGTGGC
AGGGAGTTCCGGTCAGTCCAGTGTGAAGGAGTTCCGGTCAGTCCAG
ACCACTTTGTACAAGAATGCTGTGTA AGGGAGTTCCGGTCAGTCCAGTCCA
AGGGAGTTCCGGTCAGTCCAGTCTAAAGGAGTTCCGGTCAGTCCAG
TTGACTCAGCTTAGCATCTTGT

Linker: TXXX

The free energy of the thermodynamic ensemble [ΔG(s)] is **-136.00** kcal/mol.

***SP390*:**

GGCGCTATCCGGCCTGAGCTTAGTCGGCGCTATCCTATCTGAGCTTGACT
GGCGCTATCCGGCCTGAGCTTCTAGGGCGCTATCCTATCTGAGCTTTCGA
GGCGCTATCCGGCCTGAGCTTACGTGGCGCTATCCTATCTGAGCTTCGTA
GGCGCTATCCGGCCTGAGCTTGCATGGCGCTATCCTATCTGAGCTTTACG
GGCGCTATCCGGCCTGAGCTTATAGGGCGCTATCCTATCTGAGCTTAGGC
GGCGCTATCCGGCCTGAGCTTCGTGGGCGCTATCCTATCTGAGCTT
ACCACTTTGTACAAGAATGCTGTGTAGGCGCTATCCGGCCTGAGCTTGCCA
GGCGCTATCCTATCTGAGCTTACTAGGCGCTATCCGGCCTGAGCTT
TTGACTCAGCTTAGCATCTTGT

Linker: Random

The free energy of the thermodynamic ensemble [ΔG(s)] is **-157.99** kcal/mol.

***SP396*:**

CAGTTCAAGATTGCTGTGGAAAGTCAAGTTCAAGATTGCTGTGGAAGACT
CAGTTCAAGATTGCTGTGGAACTAGAAGTTCAAGATTGCTGTGGAATCGA
CAGTTCAAGATTGCTGTGGAAACGTAAGTTCAAGATTGCTGTGGAACGTA
CAGTTCAAGATTGCTGTGGAAGCATAAGTTCAAGATTGCTGTGGAATACG
CAGTTCAAGATTGCTGTGGAAATAGAAGTTCAAGATTGCTGTGGAAAGGC
CAGTTCAAGATTGCTGTGGAACGTGAAGTTCAAGATTGCTGTGGAA
ACCACTTTGTACAAGAATGCTGTGTACAGTTCAAGATTGCTGTGGAAGCCA
AAGTTCAAGATTGCTGTGGAAACTACAGTTCAAGATTGCTGTGGAA
TTGACTCAGCTTAGCATCTTGT

Linker: Random

The free energy of the thermodynamic ensemble [ΔG(s)] is **-108.91** kcal/mol.

***SP403*:**

CGAGTTTGTGAATGAATCTAAAGTCCGAGTTTGTGAATGAATCTAAGACT
CGAGTTTGTGAATGAATCTAACTAGCGAGTTTGTGAATGAATCTAATCGA
CGAGTTTGTGAATGAATCTAAACGTCGAGTTTGTGAATGAATCTAACGTA
CGAGTTTGTGAATGAATCTAAGCATCGAGTTTGTGAATGAATCTAATACG
CGAGTTTGTGAATGAATCTAAATAGCGAGTTTGTGAATGAATCTAAAGGC
CGAGTTTGTGAATGAATCTAACGTGCGAGTTTGTGAATGAATCTAA
ACCACTTTGTACAAGAATGCTGTGTACGAGTTTGTGAATGAATCTAAGCCA
CGAGTTTGTGAATGAATCTAAACTACGAGTTTGTGAATGAATCTAA
TTGACTCAGCTTAGCATCTTGT

Linker: Random

The free energy of the thermodynamic ensemble [ΔG(s)] is **-83.21** kcal/mol.

SP164 (2M+1B):

TGCACGTGCCGAAGCTTCTCCAAGTCTGCACGTGCCGAAGCTTCTCCAGACT

TGCACGTGCCGAAGCTTCTCCACTAGTGCACGTGCCGAAGCTTCTCCATCGA

CGCACGTGCCGAAGCTTCTCCAACGTTGCACGTGCCGAAGCTTCTCCACGTA

TGCACGTGCCGAAGCTTCTCCAGCATTGCACGTGCCGAAGCTTCTCCATACG

TGCACGTGCCGAAGCTTCTCCAATAGTGCACGTGCCGAAGCTTCTCCAAGGC

TGCACGTGCCGAAGCTTCTCCACGTGTGCACGTGCCGAAGCTTCTCCA

ACCACTTTGTACAAGAATGCTGTGTATGCACGTGCCGAAGCTTCTCCAGCCA

TGCACGTGCCGAAGCTTCTCCAACTATGCACGTGCCGAAGCTTCTCCA

TTGACTCAGCTTAGCATCTTGT

Linker: Random

The free energy of the thermodynamic ensemble [ΔG(s)] is **-179.41** kcal/mol

SP164(3B):

TGCACGTGCCCCTATGCTTCTCCAAGTCTGCACGTGCCCCTATGCTTCTCCAGACT

TGCACGTGCCCCTATGCTTCTCCACTAGTGCACGTGCCCCTATGCTTCTCCATCGA

CGCACGTGCCCCTATGCTTCTCCAACGTTGCACGTGCCCCTATGCTTCTCCACGTA

TGCACGTGCCCCTATGCTTCTCCAGCATTGCACGTGCCCCTATGCTTCTCCATACG

TGCACGTGCCCCTATGCTTCTCCAATAGTGCACGTGCCCCTATGCTTCTCCAAGGC

TGCACGTGCCCCTATGCTTCTCCACGTGTGCACGTGCCCCTATGCTTCTCCA

ACCACTTTGTACAAGAATGCTGTGTATGCACGTGCCCCTATGCTTCTCCAGCCA

TGCACGTGCCCCTATGCTTCTCCAACTATGCACGTGCCCCTATGCTTCTCCA

TTGACTCAGCTTAGCATCTTGT

Linker: Random

The free energy of the thermodynamic ensemble [ΔG(s)] is **-139.58** kcal/mol.

SP390(2M+1B):

GGCGCTATCCGAGCCTGAGCTTAGTCGGCGCTATCCGAGCCTGAGCTTGACT

GGCGCTATCCGAGCCTGAGCTTCTAGGGCGCTATCCGAGCCTGAGCTTTCGA

GGCGCTATCCGAGCCTGAGCTTACGTGGCGCTATCCGAGCCTGAGCTTCGTA

GGCGCTATCCGAGCCTGAGCTTGCATGGCGCTATCCGAGCCTGAGCTTTACG

GGCGCTATCCGAGCCTGAGCTTATAGGGCGCTATCCGAGCCTGAGCTTAGGC

GGCGCTATCCGAGCCTGAGCTTCGTGGGCGCTATCCGAGCCTGAGCTT

ACCACTTTGTACAAGAATGCTGTGTAGGCGCTATCCGAGCCTGAGCTTGCCA

GGCGCTATCCGAGCCTGAGCTTACTAGGCGCTATCCGAGCCTGAGCTT

TTGACTCAGCTTAGCATCTTGT

Linker: Random

The free energy of the thermodynamic ensemble [ΔG(s)] is **-177.93** kcal/mol.

SP390(3B):

GGCGCTATCCCCTATCCTGAGCTTAGTCGGCGCTATCCCCTATCCTGAGCTTGACT

GGCGCTATCCCCTATCCTGAGCTTCTAGGGCGCTATCCCCTATCCTGAGCTTTCGA

GGCGCTATCCCCTATCCTGAGCTTACGTGGCGCTATCCCCTATCCTGAGCTTCGTA

GGCGCTATCCCCTATCCTGAGCTTGCATGGCGCTATCCCCTATCCTGAGCTTTACG

GGCGCTATCCCCTATCCTGAGCTTATAGGGCGCTATCCCCTATCCTGAGCTTAGGC

GGCGCTATCCCCTATCCTGAGCTTCGTGGGCGCTATCCCCTATCCTGAGCTT

ACCACTTTGTACAAGAATGCTGTGTAGGCGCTATCCCCTATCCTGAGCTTGCCA

GGCGCTATCCCCTATCCTGAGCTTACTAGGCGCTATCCCCTATCCTGAGCTT

TTGACTCAGCTTAGCATCTTGT

Linker: Random

The free energy of the thermodynamic ensemble [ΔG(s)] is **-132.85** kcal/mol.

TuD159:

GACGGCGCTAGGATCATCAACTAGAGCTCCCTTATTCAATCCAAACAAGTATTCTGGTCA
CAGAATACAACTAGAGCTCCCTTATTCAATCCAAACAAGATGATCCTAGCGCCGTC

The free energy of the thermodynamic ensemble [ΔG(s)] is **-48.82** kcal/mol

Loop159:

CCTATCGTCAGATAGCATGATTATTCCCGCATACTCAATACATCCCTTTATCACACCTTCGC
CACCCAATAATCCTAGAGCTCCCTTATTCAATCCAAATACTTCCCACCACTTGGTGTGATA
AAGGCACCCCGTTGGGTGGATGTATTGAGTATGCGCACCCCGTTGGGTGGGAATAATCAT
GG

The free energy of the thermodynamic ensemble [ΔG(s)] is **-80.34** kcal/mol

Stem159:

CCTATCGTCAGATAGCATTAGAGCTCCCTTATTCAATCCAAATCCCTTTATCACACCTTCGC
CACCCAATAATCCAGTTTAATCCCAGTCACTATCACATACTTCCCACCACTTGGTGTGATA
AAGGCACCCCGTTGGGTGGATTTGGATTGAATAAGCACCCCGTTGGGTGGGAGCTCTAAT
GG

The free energy of the thermodynamic ensemble [ΔG(s)] is **-80.53** kcal/mol

***TuD156*:**

GACGGCGCTAGGATCATCAACGTGCTCACTCCTATCTTCTGTCACAAGTATTCTGGTCACA
GAATACAACGTGCTCACTCCTATCTTCTGTCACAAGATGATCCTAGCGCCGTC

The free energy of the thermodynamic ensemble [ΔG(s)] is **-49.61** kcal/mol

***Loop156*:**

CCTATCGTCAGATAGCATTACAGTGCGCTTACTTTCTCTCCACCTCGTAGCCTCCCCCAAC
CCTTCCTATCTCCGTGCTCACTCCTATCTTCTGTCAACCCCTTCTCAATCCGGGAGGCTAC
GAGCACCCCGTTGGGTGGTGGAGAGAAAGTAAGCACCCCGTTGGGTGCGCACTGTAATG
G

The free energy of the thermodynamic ensemble [ΔG(s)] is **-88.43** kcal/mol

***Stem156*:**

CCTATCGTCAGATAGCATGTGCTCACTCCTATCTTCTGTCAACCCCTTCTCAGGCCCCCAT
TCCTACCCTATCCTTCAGCGCGTATACTTTCTCTCCACTCCATCTACTCCCGGCCTGAGAA
GGGCACCCCGTTGGGTGGTTGACAGAAGATAGCACCCCGTTGGGTGGAGTGAGCACATG
G

The free energy of the thermodynamic ensemble [ΔG(s)] is **-89.80** kcal/mol

File 2: Primer table

Name	Template	Sequence 5'-3'	Purpose
LB3	pCSA110/pDAP101	TAGCATCTGAATTTCATAACCAATCTCGATACA	T-DNA genotyping of *mir159a* and *mir159b*
159a-5	At1g73687	ACAAACAATGTCAGACCCTTCCCATGTCT	T-DNA genotyping of *mir159a*
159a-3	At1g73687	AGTCAGTGCATATGGCAGCAAAGATTGCA	T-DNA genotyping of *mir159a*
159b-5	At1g18075	GGTTTTTCACTTTTGTTCTCCTCCTCCCT	T-DNb genotyping of *mir159b*
159b-3	At1g18075	CATCCATGTTTATACACCTGCAACAGACA	T-DNb genotyping of *mir159b*
MYB33-5	At5g06100	TTACACGAGCACTGACAGTG	T-DNA genotyping of *myb33*
MYB33-3	At5g06100	TCAAGGAGATCAGAGTGTGG	T-DNA genotyping of *myb33*
JL202	pAC161	CATTTTATAATAACGCTGCGGACATCTAC	T-DNA genotyping of *myb33*
MYB65-5	At3g11440	TTACCTGGTCGAACAGATAATGAG	T-DNA genotyping of *myb65*
MYB65-3	At3g11440	AACCACCAAGTCATGTAAGC	T-DNA genotyping of *myb65*
LBb1	pAC106/pROK2	GCGTGGACCGCTTGCTGCAACT	T-DNA genotyping of *myb65* and *cp1*
CP1-5	At4g36880	CCCAAATGTTTATCGAGCGTC	T-DNA genotyping of *cp1*
CP1-3	At4g36880	CAAGGAACTTGCGGTAATTACC	T-DNA genotyping of *cp1*
CYCLO-F	At2g29960	TGGACCAGGTGTACTTTCAATGG	qRT-PCR of reference gene *CYCLOPHILIN*
CYCLO-R	At2g29960	CCACTGTCTGCAATTACGACTTTG	qRT-PCR of reference gene *CYCLOPHILIN*
UBQ10-F	At4g05320	GATCCAGGATAAGGAGGGCAT	qRT-PCR of reference gene *UBIQUITIN10*
UBIQ10-R	At4g05320	TCCTTCTGGATATTGTAATCAGCC	qRT-PCR of reference gene *UBIQUITIN10*
MYB33-F	At5g06100	TCGTCATCTCCTCCACACTCTG	qRT-PCR of uncleaved *MYB33*
MYB33-R	At5g06100	CCTCGGATTTAGTTTGGGATAC	qRT-PCR of uncleaved *MYB33*
MYB65-F	At3g11440	AAGACGACTCCGTCACCTCCAC	qRT-PCR of uncleaved *MYB65*
MYB65-R	At3g11440	ATCAACAAACTGTGCTTCGCAC	qRT-PCR of uncleaved *MYB65*
CP1-F	At4g36880	ACGCTCGATAAACATTTGGG	qRT-PCR of *CP1*
CP1-R	At4g36880	CAAGCAAACAATCTTTCTTTGAA	qRT-PCR of *CP1*
BXL2-F	At1g02640	TTCAAGCTTCTACTCTTGGAGTCA	qRT-PCR of *BXL2*
BXL2-R	At1g02640	AATCCGAGGCCATACAATTC	qRT-PCR of *BXL2*
P0-F	P0 coding sequence	CATAACCAACTACTCTTTACC	qRT-PCR of *P0*
P0-R	P0 coding sequence	CAGCGTGATGCAAAGTAATG	qRT-PCR of *P0*
TuMV-F	COAT PROTEIN gene of TuMV	GATTACGAACTGACGGAGGACA	qRT-PCR of *TuMV*
TuMV-R	COAT PROTEIN gene of TuMV	CATCATCACCCACATTCCGTTT	qRT-PCR of *TuMV*
PHB-F	At2g34710	CCAGCAGGACTCCTTTCTATA	qRT-PCR of uncleaved *PHB*
PHB-R	At2g34710	TTGCGCGAAATAGCGACTATG	qRT-PCR of uncleaved *PHB*
CUC1-F	At3g15170	TCTGCCGGTTCTGCAATTG	qRT-PCR of uncleaved *CUC1*
CUC1-R	At3g15170	CATCGGTATGAGCAGCAGAGTT	qRT-PCR of uncleaved *CUC1*
CUC2-F	At5g53950	CAGCCGT AGCACCAACACAA	qRT-PCR of uncleaved *CUC2*
CUC2-R	At5g53950	GTCTAAGCCCAAGGCCCCGTAGTA	qRT-PCR of uncleaved *CUC2*
ARF3-F	At2g33860	TGGTCCCAAGAGAAGCAGG	qRT-PCR of uncleaved *ARF3*
ARF3-R	At2g33860	TCCACCATCCGAACAAGTG	qRT-PCR of uncleaved *ARF3*
ARF4-F	At5g60450	GCCGCTGAAGATTGTTTTGCTC	qRT-PCR of uncleaved *ARF4*
ARF4-R	At5g60450	AGTAGATGCCTCCTTGGTTGACC	qRT-PCR of uncleaved *ARF4*
TCP4-F	At3g15030	TGGTTTGATCCTCACCATCATCAC	qRT-PCR of uncleaved *TCP4*
TCP4-R	At3g15030	GATTCCGGGGATTGCTGATTGGTG	qRT-PCR of uncleaved *TCP4*
AGO1-F	At1g48410	AAGGAGGTCGAGGAGGGTATGG	qRT-PCR of uncleaved *AGO1*
AGO1-R	At1g48410	CAAATTGCTGAGCCAGAACAGTAGG	qRT-PCR of uncleaved *AGO1*
SPL3-F	At2g33810	CCAAAGCTCCTCATGTTCGG	qRT-PCR of uncleaved *SPL3*
SPL3-R	At2g33810	CTCGTTGTGTCCAGCTAAGC	qRT-PCR of uncleaved *SPL3*
SPONGE-F	Sponge transgene	ACCACTTTGTACAAGAATGCTG	qRT-PCR of miRNA *SPONGE*
SPONGE-R	Sponge transgene	ACAAGATGCTAAGCTGAGTCAA	qRT-PCR of miRNA *SPONGE*